International School for Advanced Studies
SISSA/ISAS

Loop and non-perturbative effects in the dark matter phenomenology

Thesis submitted for the degree of
Doctor Philosophiae

Candidate:
Andrzej Hryczuk

Supervisor:
Prof. Piero Ullio

Trieste, September 2012

To the memory of
Stanisław Lipiński

Abstract

In this thesis we analyze the importance of the one-loop corrections and the non-perturbative Sommerfeld enhancement on the dark matter thermal relic density and indirect detection signals. We discuss general properties of these effects and present a detailed study of their impact in the Minimal Supersymmetric Standard Model.

For the Sommerfeld effect (SE) we have developed a general formalism to compute the enhancement factors for a multi-state system of fermions, in all possible spin configurations and with generic long-range interactions. We show how to include such SE effects in an accurate calculation of the thermal relic density for WIMP dark matter candidates. We apply the method to the MSSM and perform a numerical study of the relic abundance of neutralinos with arbitrary composition and including the SE due to the exchange of the W and Z bosons, photons and Higgses. Additionally, we perform an analogous analysis in the case of large co-annihilation effects with a scalar particle, presenting also the appropriate formulas for a general scenario of this kind, with a set of particles with arbitrary masses and (off-)diagonal interactions.

We find non-negligible corrections in whole sfermion co-annihilation regimes and a very strong effect for the heavy Wino-like neutralino. We also provide a numerical package for computing the neutralino relic density including the Sommerfeld effect in a general MSSM setup.

We turn then to a specific scenario, where the dark matter is made of Wino-like particles, and study the indirect detection signals including both our full computation of one-loop level electroweak corrections and the Sommerfeld effect. We discuss how to incorporate them simultaneously and present the results for the full present-day annihilation cross-section. Having well under control the particle physics properties of the model, we concentrate on what exclusion limits and detection prospects we can obtain for this model taking into account various astrophysical uncertainties. Our results on the indirect detection signals show a significant impact of higher order effects and moreover the importance of cross correlation between various search channels.

Acknowledgements

First and foremost, I would like to thank my supervisor, Prof. Piero Ullio. Over my whole time at SISSA, Piero has given me the guidance I needed, at the same time granting the freedom of developing my own research interests. His broad knowledge and dedication to truly scientific attitude have left a lasting imprint on me.

I thank also Prof. Roberto Iengo for very fruitful collaboration and teaching me how important it is to constantly seek for a deeper understanding of all we do in physics.

Many thanks to Ilias Cholis for his invaluable help in introducing me to the cosmic ray physics and to Maryam Tavakoli for discussions and joint work.

SISSA provided the best possible environment for the completion of this thesis, which I am grateful for. This is an effect of effort and commitment of many people: professors, young researchers and also administrative staff. Above all students, who are creating an unforgettable atmosphere. Thanks to you all!

My family deserves particular thanks. My parents, who valued education above all else, and my family for continuous support. A very special thanks to Ania whose encouragements and loving support has been the most precious gift.

Finally, I want to express my gratitude to all those brave and steadfast, but nowadays sadly so often forgotten people, thanks to whom I, as well as many other young Poles, was able to go abroad to expand my education.

Contents

1 Introduction **1**
- 1.1 Evidence for particle dark matter . . . 3
  - 1.1.1 "Missing matter" in galaxy clusters . . . 3
  - 1.1.2 The Bullet cluster . . . 5
  - 1.1.3 Rotation curves of spiral galaxies . . . 6
  - 1.1.4 Cosmological scale evidences . . . 6
- 1.2 Candidates . . . 9
  - 1.2.1 Weakly Interacting Massive Particles . . . 11
  - 1.2.2 Non-WIMPs . . . 12
- 1.3 Thermal history of the Universe . . . 14
  - 1.3.1 Relic density calculations . . . 15
- 1.4 Detection methods . . . 19
  - 1.4.1 Direct detection . . . 19
  - 1.4.2 Indirect detection . . . 21

2 The Minimal Supersymmetric Standard Model **25**
- 2.1 The Standard Model and its problems . . . 25
  - 2.1.1 Gauge interactions and the field content . . . 25
  - 2.1.2 Open questions in the SM . . . 27
- 2.2 Supersymmetry . . . 31
- 2.3 Field content of the MSSM . . . 37
  - 2.3.1 The superpotential and R-parity . . . 38
  - 2.3.2 SUSY breaking and soft parameters . . . 39
  - 2.3.3 The spectrum . . . 40
- 2.4 Supersymmetric dark matter . . . 42
  - 2.4.1 Neutralino . . . 43
  - 2.4.2 Sneutrino . . . 47
  - 2.4.3 Gravitino . . . 48
  - 2.4.4 Axino . . . 49

3 Electroweak corrections to DM annihilation **51**
- 3.1 The importance of the electroweak corrections . . . 52
  - 3.1.1 The helicity suppression and its lifting by gauge boson emission . . . 52
  - 3.1.2 TeV scale dark matter . . . 54
- 3.2 One-loop computation for the Wino dark matter . . . 56

3.2.1 The scale of the coupling . . . 58
3.2.2 Wino-Wino annihilation . . . 60
3.2.3 Chargino-Chargino annihilation . . . 66
3.2.4 The one-loop corrections to $\chi^+\chi^- \to ZZ, Z\gamma, \gamma\gamma$ . . . 68

4 The Sommerfeld effect **71**
4.1 The origin of the Sommerfeld enhancement . . . 71
4.2 Enhancement due to a dark force . . . 73
4.3 Field theory derivation for general multi-state case . . . 77
4.3.1 Fermion initial state . . . 78
4.3.2 Scalar and scalar-fermion initial state . . . 87
4.4 Applications to the MSSM . . . 88
4.4.1 Sommerfeld enhanced scenarios of the MSSM . . . 89
4.4.2 Relic density with the Sommerfeld effect . . . 91
4.4.3 Results for the relic density . . . 92
4.5 Kinetic decouping and the SE . . . 102

5 Indirect detection of Wino dark matter **105**
5.1 The EW and Sommerfeld corrections . . . 106
5.1.1 The results for the cross-sections . . . 108
5.1.2 Fluxes at production . . . 112
5.2 Cosmic ray propagation . . . 120
5.2.1 The solar modulation . . . 123
5.3 Indirect detection signals . . . 124
5.3.1 Propagation models and uncertainties . . . 126
5.3.2 Antiprotons . . . 128
5.3.3 Positrons . . . 131
5.3.4 Gamma-rays . . . 134
5.3.5 Neutrinos . . . 142
5.3.6 Antideuterons . . . 143
5.3.7 Summary . . . 144

6 Conclusions **147**

Chapter 1

Introduction

The Universe is amazing. It is enough to look once at the starry sky to become aware of how enormous and rich it is. Not surprisingly, it is even more striking when one gets to know that what we are looking on, the luminous matter, is just a small portion of what there really *is*. On the other hand, it is remarkable how relatively few laws are needed to describe much of its behaviour.

What seems to be a fascinating possibility is that this dark side of the Universe, which we have no means to directly probe yet, can lead us to deeper and more complete understanding of what we see on Earth. Indeed, although we already know a lot about fundamental properties of matter and interactions experienced in our everyday life, there are still some puzzling issues which indicate that we do not have a complete picture yet. Recent discovery of the Higgs (or at least Higgs-like) boson at the LHC [1, 2] gives us even more confidence in thinking that our theoretical framework correctly describes the world at all energy scales currently accessible to particle physics experiments. However, it did not shed much light onto these puzzling properties of our theory, which we still do not fully understand. From a theory point of view the open issues of the Standard Model (SM) of particle physics give the main hints on where to look for a more fundamental description. When finally found, it is likely to also open a new window on the Universe. Such a window would be extremely useful in helping us to understand various astrophysical and cosmological observations, in particular connected to the dark matter.

This is a theoretical particle physicist's perspective. But through a window one can look in both directions. Although we do not know what dark matter (DM) is, what is it made of and most of its properties, we already have a lot of knowledge about it. This comes from numerous observational and experimental data, with constantly increasing precision. Owing to this, the dark matter can be also studied separately and detachedly from addressing the problems of particle physics. When detected and with some of its properties measured, it will on the one hand pose a challenge, but on the other give strong guidance principle on how to complete our particle physics picture. This is the astroparticle physics perspective. Throughout this thesis we are aiming in joining this two points of view, by studying the dark matter phenomenology within the well motivated particle physics framework, the Minimal Supersymmetric Standard Model (MSSM).

However, there are two obstacles one encounters when trying to infer some information

on particle physics from the dark matter phenomenology. Firstly, the data is not yet constraining and precise enough to make on one hand very general and on the other strong statements. This is becoming better and better every year with new experiments using state-of-art technology and detection methods. Second obstacle is on the theory side and is the one we are going to tackle with. There are plenty of ideas what the dark matter can be. Many of them give predictions for experiments which are already running, or have prospects for being tested in the near future. However, the theoretical predictions for concrete models are very often not at the state-of-art level, using calculations only at the lowest level of perturbation theory. In many cases this is satisfactory, since higher order corrections are typically expected to be of per cent level, and thus not affecting much the outcome of a given model. However, for many well motivated scenarios this statement is not true. Loop and also non-perturbative effects can significantly alter the phenomenology and accordingly the general picture of a wide class of dark matter models.

The work described in this thesis aims in extending our knowledge of the importance of such effects in general and give concrete examples of computations in some specific cases. We start the discussion from introducing the dark matter paradigm and summarizing what we know about it. Then in Section 1.2 we present general ideas of what the DM can be made of and in the remaining parts of Chapter 1 describe its production mechanisms and detection methods.

The particle physics framework is introduced in Chapter 2. We briefly summarize the Standard Model of particle physics and discuss its open issues. Then we argue why supersymmetry is an appealing idea to address them and following in Section 2.3 we specify the model we will work in, i.e. the MSSM. Finally, we discuss the possible dark matter candidates in this framework in Section 2.4.

Chapter 3 presents the importance of the electroweak radiative corrections. Firstly, we summarize what is the current status of the subject and then describe our computation of the full one-loop corrections in the Wino dark matter model and comment on more general applications.

In Chapter 4 we describe the non-perturbative Sommerfeld effect and its role in the dark matter physics. This effect can strongly affect the annihilation cross-section leading to dramatically different phenomenology in some classes of models. Although, in the literature it is mostly described to enter due to existence of some new "dark" force, in our work we adopt much less speculative approach and study its impact coming from the electroweak gauge bosons. In Section 4.3 we derive a formalism applicable in a general multi-state scenario, where the dark matter can be degenerated in mass with other particles, being both fermions and bosons. As a result we can apply this method to such general setups like the MSSM. We perform studies of this model in several distinct cases and present the results in Section 4.4.

Both of these effects, electroweak radiative and Sommerfeld corrections, have impact on the dark matter searches. The most important place where they cannot be neglected is the indirect detection. Taking advantage of our detailed analysis of the Wino model, in Chapter 5 we study the full multi-channel indirect detection signals for this scenario, and show the impact of the higher order effects. Furthermore, thanks to the good understanding of the particle physics properties of this model, we are able to make some observations

about the astrophysical uncertainties associated with different search channels.

Finally, we give our conclusions in Chapter 6.

1.1 Evidence for particle dark matter

There is no doubt that "dark matter" exists in our Universe. "Dark" in the sense that we do not observe it in the electromagnetic waves. In fact it is not at all surprising: after all many astrophysical objects are to faint to be seen at any wavelength. One thus may expect that inferring the mass of a large astrophysical object like a galaxy cluster from its luminosity should in principle give a different result than the one obtained from its dynamical properties. Of course, this kind of measurements come with a substantial uncertainties and a small "missing mass" would be impossible to extract. However, observations told us something which certainly was unexpected, and eventually lead to radical changes in our understanding of astrophysics. In 1933 Fritz Zwicky [3] measured velocity dispersions of some of the galaxies of the Coma cluster and then estimated its mass with the use of the virial theorem. The results showed that the ratio of mass to the total luminosity obtained this way was more than two orders of magnitude larger than the mass to the luminosity ratio locally. This discrepancy was surprising, as such a large value by any means could not be explained with the standard astrophysical objects. This led Zwicky to suggest, that at least in the observed cluster, there exists some non-luminous matter component which holds the cluster together. Similar "missing mass" was also subsequently found in the Virgo cluster [4].

Not surprisingly, however, those measurements were initially not considered robust enough to accept such a extraordinary interpretation. In fact, Zwicky's work did not get much attention of the astronomical community until several decades later. The change came with the development of observational techniques and new measurements on various scales ranging from galaxy and cluster up to cosmological ones. Nowadays, the existence of dark matter is not only widely accepted by astrophysicists, but also influences a lot line of research of the modern particle physics.

Of course, existence of dark matter is indeed an extraordinary claim, and as such it needs extraordinary evidence. We will shortly summarize these evidences below, emphasizing mostly the ones demonstrating the particle nature of dark matter, as opposed to the mere modification of gravity.[1]

1.1.1 "Missing matter" in galaxy clusters

The estimation of the mass of a galaxy clusters have progressed considerably since the time of Zwicky and now we are in possession of much more precise measurements. Furthermore, in addition to the observation of the peculiar velocities of the galaxies inside a cluster two

[1] All the evidence we have so far are based on the gravitational interactions. It is thus in principle possible, and in fact also studied a lot, that instead of adding new matter component our theory of gravity needs to be modified (see e.g. [5] for a review). Those ideas are however rather unmotivated theoretically and facing problems in explaining simultaneously all observed phenomena. It is fair to say that by know the dark matter hypothesis is the only well-established one.

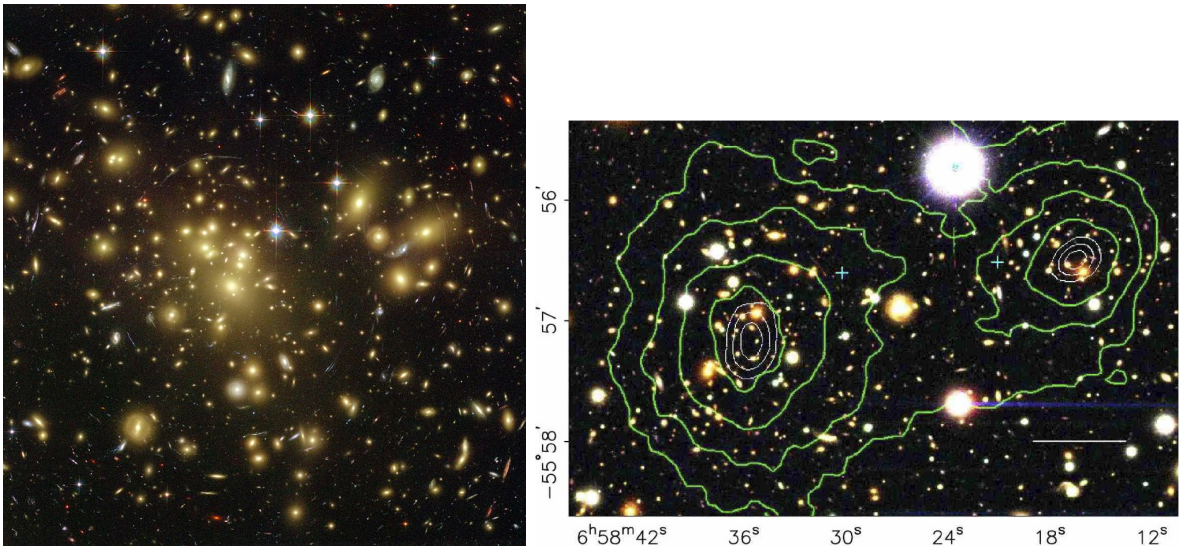

Figure 1.1: An example of gravitational lenses. *Left:* strong lensing from the Abell 1689 galaxy cluster captured by the HST. Image taken from [6]. *Right:* contours of the mass distribution in the Bullet cluster inferred from the weak gravitational lensing of the background sources [7].

other techniques were developed and used thoroughly: gravitational lensing and thermal X-rays emission.

In general relativity (GR) the light follows the null geodesics, which are determined by the stress-energy tensor. In particular, presence of a gravitational field caused by a massive object bends these trajectories and thus inflicts deflection of light. This gives rise to two effects: the so-called *strong* and *weak* gravitational lensing. The first one is straightforward. If some mass concentration is present between the observer and a distant object, then it acts as a lens and produces fake images in the form of spherical arcs. A fine and famous example of this effect was captured by the Hubble Space Telescope (HST) while looking through the center of one of the most massive clusters called Abell 1689, as given on Fig. 1.1.

Weak gravitational lensing is a bit more subtle. The distortions of the background object coming from lensing are often to small to be observed. However, even then a net statistical effect can be seen. What one measures is the deformation of shapes, e.g. elongations of spherical objects, or the systematic alignment of background objects around the foreground mass. Weak lensing is thus intrinsically statistical measurement, but it is very useful in determining the mass of the foreground lensing objects without assumptions on their composition or dynamical state.

The second method, thermal X-ray emission, relies on the fact that the intercluster medium consist mostly of very hot gas, with the temperature between $10^7\,\mathrm{K}$ and $10^8\,\mathrm{K}$. By measuring its X-ray emission one can deduce the total mass distribution, assuming that gas is in approximate hydrostatic equilibrium with the overall cluster gravitational field. If the gas is the only component, the relation of its temperature T and the mass M

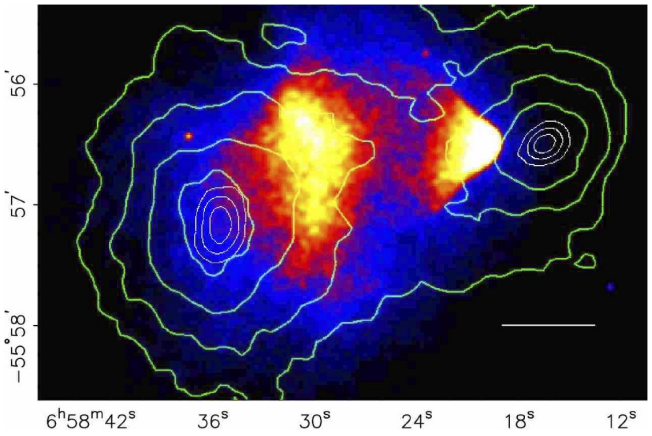

Figure 1.2: Observation of the Bullet cluster [7]. A clear shock profile is visible in the X-rays. The green contours present the gravitational potential inferred from the weak gravitational lensing, which was not strongly affected by the collision. This gives a strong evidence for a collisionless particle nature of dark matter.

inside a given radius R is given by [8]:

$$T \sim 1.5\,\mathrm{keV}\frac{M(R)}{10^{14}M_{\odot}}\,\frac{1\mathrm{Mpc}}{R}. \tag{1.1}$$

Again, the observed value of the temperature of about 10 keV is about 6 times larger and inconsistent with this assumption, leading to the conclusion of existence of an additional matter component.

1.1.2 The Bullet cluster

Probably the most compelling piece of astrophysical evidence for the particle dark matter is the observation of the collision of two clusters by Clowe et al. [7], i.e. the so-called Bullet cluster (1E 0657-558).[2] The main baryonic component, the intercluster gas observed in X-rays, was strongly affected by the electromagnetic interactions and created the clear shock profile, see Fig. 1.2. What was so striking, was that most of the mass, which was inferred from weak gravitational lensing, didn't trace the gas, but rather visible objects. It follows, that most of the mass is not in the intercluster gas and furthermore, that the additional "dark" component is collision-less. Comparing Fig. 1.2 with Fig. 1.1b showing the same cluster but in the optical band, one can clearly see that the gravitational potential, presented as green contours, traces the collisionless part, and not the interacting gas. This lead to the conclusion expressed in the title of the paper: *A direct empirical proof of the existence of dark matter.*

This observation is not only a direct indication of existence of dark matter but also of its particle, collisionless behaviour. In fact, authors of this work claim that at a statistical

[2]Strictly speaking the Bullet is the smaller of the two, which crosses the larger with a very high velocity. The name comes from the characteristic conical shock, see Fig. 1.2.

significance of about 8σ, the spatial offset of the center of the total mass from the center of the baryonic mass peaks cannot be explained with an alteration of the gravitational force law.

1.1.3 Rotation curves of spiral galaxies

On the galactic scale the strong case for the dark matter follows from observation of the rotation curves in spiral galaxies.[3] It was pointed out quite early by Rubin and collaborators [11] that the true galaxies exhibit unexpected, nearly flat behaviour at large distances r. In Newtonian gravity (being of course a sufficient approximation of GR at these scales) one can easily compute the rotational velocity v_r for a given mass distribution $M(r)$, giving

$$v_r(r) = \sqrt{\frac{G_N M(r)}{r}}, \tag{1.2}$$

where G_N is the gravitational constant. Therefore, for constant $M(r)$, i.e. outside the visible part of the galaxy, the velocity should fall down as $r^{-1/2}$. This is however not what we see in observations. As an example, on Fig. 1.3a we present a rotation curve from NGC 6503 galaxy with highlighted various contributions. As evident, the simplest explanation to the apparent approximate flatness is the inclusion of a dark matter component called the "halo". The precise shape of the rotation curves is an important ingredient in determining the halo profile: flat rotation curve would point to $\rho \sim r^{-2}$, i.e. the so-called isothermal profile. In reality however, the observations give different slopes for different galaxies, with only some being very close to flat (for a recent and comprehensive review of the rotation curves in spiral galaxies see e.g. [12]).

1.1.4 Cosmological scale evidences

Our understanding of cosmology made a huge progress in recent decades, leading to now a well-established and widely accepted cosmological model, known as the concordance model or sometimes even called the standard model of cosmology (for a modern review see e.g. [15]). Observations from various distances (redshifts), especially the Cosmic Microwave Background (CMB), large scale structures (LSS), clusters of galaxies and supernovae, point to a precise model within this framework, called the ΛCDM, see Fig. 1.4. The name comes from the content of the Universe, which in general can constitute of matter Ω_m, curvature Ω_k and the cosmological constant Ω_Λ.[4] The different relative values of these three parameters result in different models, which can be illustrated on a triangle, Fig. 1.4a. Observations strongly suggest that the Universe has a flat geometry. As a consequence, the curvature contribution vanishes and the total energy density of the Universe is equal to the critical density, i.e. $\Omega_{\rm tot} = 1$. When additional constraints are

[3] Another, although not so clean evidence comes form the velocity dispersion measurements for pressure supported galaxies, see e.g. [9] for elliptical galaxies and [10] for dwarf spheroidals.

[4] Energy densities in cosmology are typically given in terms of the critical density $\rho_c = 1.879 \times 10^{-29} h^2\,\mathrm{g/cm^3}$, i.e. $\Omega_i = \rho_i/\rho_c$, where $h = 0.702 \pm 0.014$ is the Hubble constant in units of $100\,\mathrm{km\,s^{-1}Mpc^{-1}}$.

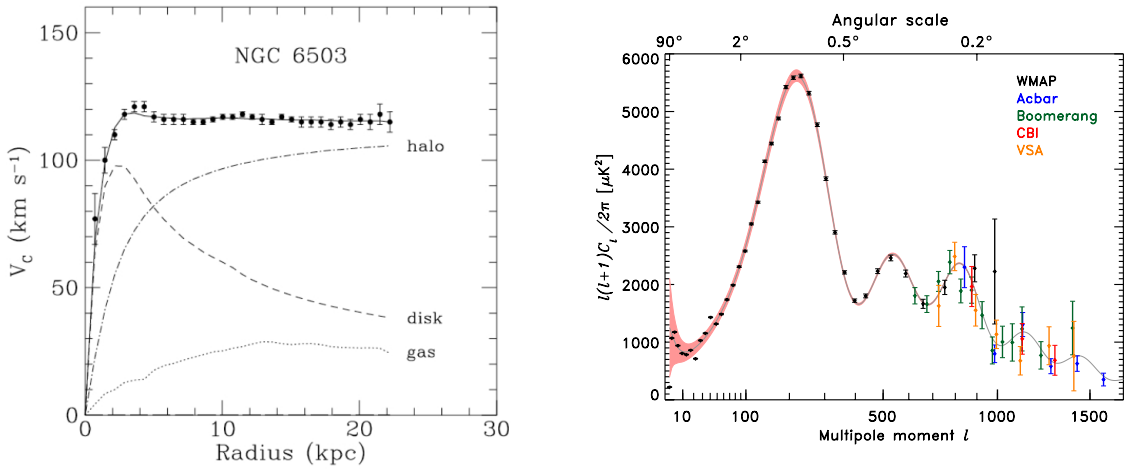

Figure 1.3: *Left:* an example of a galaxy rotation curve with separate contributions from the galactic disk, gas and the dark matter halo. Figure from [13]. *Right:* CMB power spectrum anisotropies [14]. The solid line gives the ΛCDM model fit to the data from various experiments.

superimposed one can see that the favoured model is the one with $\Omega_m \approx 1/4$, $\Omega_k \approx 0$ and $\Omega_\Lambda \approx 3/4$, where the matter is mostly composed of the cold non-baryonic component, i.e. cold dark matter (CDM).

From the dark matter perspective, the most important ingredient of the cosmological model is the CMB and in particular measurements of its anisotropies. The CMB is an imprint of the first moment in the history of the Universe when it became transparent to light. After the temperature dropped below about 0.4 eV, protons and electrons recombine to form neutral atoms making the photons' scattering on the plasma no longer efficient enough. They decoupled and started to propagate freely. We observe those "relic" photons as a nearly uniform radiation coming from all the directions in space, with the perfect spectrum of a black body radiation with the temperature of 2.725 K. The anisotropies of this radiation are very small, with $\Delta T/T \sim 10^{-4}$–10^{-5}, which is truly a remarkable fact. Moreover, their presence is considered to be of crucial importance for the large scale structures formation. The reason is that these minute temperature differences trace the density inhomogeneities at the moment of last scattering, which are seeds for later collapse and clustering around the more dense regions.

In fact, these anisotropies carry a lot of information about the composition of the Universe at that time, i.e about 300 000 years ater the Big Bang, corresponding to redshifts around $z \sim 1100$. In order to extract it one makes an expansion in spherical harmonics:

$$\frac{\Delta T}{T}(\theta,\phi) = \sum_{l=2}^{\infty}\sum_{m=-l}^{m=l} a_{lm}Y_{lm}(\theta,\phi), \tag{1.3}$$

and calculates the variance

$$C_l \equiv \langle |a_{lm}|^2 \rangle = \frac{1}{1+2l}\sum_{m=-l}^{m=l} |a_{lm}|^2. \tag{1.4}$$

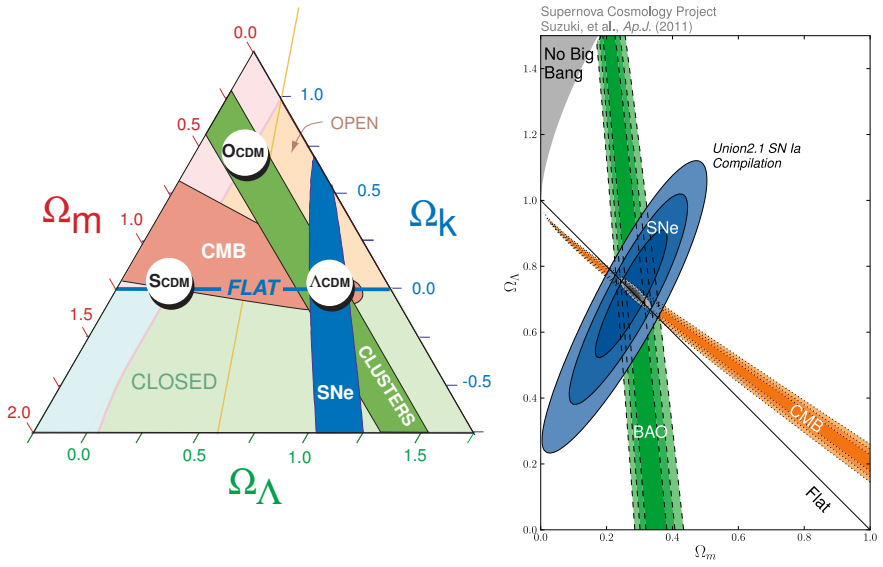

Figure 1.4: *Left:* the cosmic triangle [16]: *Right:* The same but on a $(\Omega_m, \Omega_\Lambda)$ plane, showing the "concordance" of the various independent observations [17].

The plot of $l(l+1)C_l/(2\pi)$ both from experimental data and the fit in the 6-parameter ΛCDM model is shown of Fig. 1.3b. It shows a characteristic sound waves peaks and an overall fall for large l from diffusion damping (also called Silk damping). The acoustic oscillations arise because of a competition in the photonbaryon plasma: the pressure of the photons tends to erase anisotropies, whereas the gravitational attraction of the baryons makes them tend to collapse. These acoustic peeks contain information about the cosmological parameters. The measured angular scale (position) of the first peak gives the total energy $\Omega_{\rm tot}$, since it appears at the harmonic of the sound horizon and thus depends on the curvature of the Universe. Recent results of the WMAP collaboration give [18] (all uncertainties indicate the 68% confidence levels):

$$\Omega_{\rm tot} = 1.0023^{+0.0056}_{-0.0054} \, . \tag{1.5}$$

The odd peaks come from the compressions of the photon-baryon fluid, while the even peaks from rarefactions. Therefore, the more baryons, the fluid feels the potential well stronger, and the larger the ratio of the amplitudes of the odd to even peaks. In particular, the ratio of the first to second peak leads to the determination[5] of the energy density in the baryons:[6]

$$\Omega_b h^2 = 0.02255 \pm 0.00054 \, . \tag{1.6}$$

In the presence of additional matter component not coupled to photons the potential well is steeper but the effective mass of the photon-baryon fluid is not altered. This

[5]Note, however, that the quoted numbers are obtained from the full fit of the ΛCDM model and therefore do not come directly from the acoustic peaks only.

[6]A completely independent measurement of the baryon energy density follows also from the Big Bang Nucleosynthesis (BBN), which leads to a consistent value. For a review of the results see [19].

effects in boosting the odd peaks and allows to use the relation between the third and two previous ones to infer the energy density of this additional component:

$$\Omega_{\rm CDM} h^2 = 0.1126 \pm 0.0036 \ . \tag{1.7}$$

This provides a strong evidence for the dark matter, more abundant than the baryons by roughly a factor of 5, a completely independent from the evidences from astrophysical observations. Moreover, it already gives some information about the properties of such new dark particle.

To conclude this section, let us just mention the last cosmological scale observation, also leading to the consistent picture. As mentioned above, the anisotropies of the CMB trace the density anisotropies which are then imprinted in the large scale structures of our Universe. This can be seen observationally by the distributions of galaxies in large surveys like recent Sloan Digital Sky Survey (SDSS) [20] containing more than 930 000 galaxies. The results of the three-dimensional power spectrum again show characteristic pattern, coming from the baryon acoustic oscillations (BAO). It is compatible with the sound waves seen in CMB and lead to cross-check of the cosmological parameters. Consistent results show that the overall LSS formation picture, with large CDM component, provides a good explanation of the complexity of large scales of the observed Universe. Although the full description of structure formation, covering also the non-linear regime, is still not available and thus the theory still possess some unresolved issues (e.g. "missing satelites" [21] or "cusp" [22] problems in the comparison of numerical simulations with the observational data), the recent enormous progress in the field gives more and more confidence in the general picture.

1.2 Candidates

One of the major challenges of modern particle physics is to understand the nature of dark matter and hopefully incorporate it in the more fundamental and complete theory. The efforts go in two directions: detecting and then measuring properties of dark matter particles, which we shortly discuss in Sec. 1.4 and on the theory side to deduce its properties from a particle physics perspective. The latter gives also some hope that solving the dark matter problem will be also connected with the resolving the shortcomings of the Standard Model and giving an indication where to look for a more fundamental theory. Needless to say, in the literature there exists many kinds of models for particle dark matter with huge number of their realizations. In this section we are going to summarize the main properties that a particle should have in order to be a viable candidate for dark matter and then give some examples (of arguably the most promising) classes of models.

What we already know about dark matter can be summarized by the following *5 golden rules*:

1. **DM is optically dark**

   By definition, being "dark", it does not contribute significantly to the background radiation at any frequency [23]. This condition is however much stronger, because it

means also that dark matter cannot couple to photons at the CMB epoch and even more importantly it does not cool by photon radiation (otherwise it would dissipate energy and collapse in the same way as the baryonic matter).

2. **DM is collision-less**

   This can be most straightforwardly seen from the Bullet cluster, as discussed above, but in fact more stringent constraints come from the ellipticity of the halo and even dissipation of sub-halos or growth rates of super-massive black holes (see e.g. [24] and references therein).

3. **DM is in a classical fluid limit**

   No discrete effects in the halos are observed. In fact, large granularities would affect the stability of astrophysical systems by introducing a time dependent gravitational potential, see e.g. [25]. Classical, because no quantum effects are seen in observations, for a boson giving lower bound on the mass of about $m_{DM} \gtrsim 10^{-22}$ eV. In the fermion case analogous, though much weaker bound exists, called the Tremaine-Gunn bound [26]. It follows from the condition of not exceeding the possible phase space density allowed by the Pauli exclusion principle.

4. **DM is stable**

   If it could decay with a lifetime shorter than the age of the Universe, it would not survive to present day and could not solve small scale missing matter issues. This sets a rough bound for the lifetime $\tau \gtrsim$ few $\times\, t_{\text{Universe}}$. Moreover, in the case it can decay to visible states it could be already detected in the cosmic rays and the condition for the lifetime is typically much more restrictive.

5. **DM is cold**

   "Cold" means here non-relativistic at the moment of structure formation onset, i.e. matter-radiation equality at redshifts $z \sim 10^6$. The reason is that relativistic particles tend to free-stream and smooth the initial density perturbations, which would lead to different large scale structures than observed in the present day Universe [27]. For example, neutrinos have a free-streaming length of

   $$\lambda_{FS} \approx 40\,\text{Mpc}\left(\frac{30\,\text{eV}}{m_\nu}\right), \tag{1.8}$$

   which would need a top-down hierarchy in the large structure formation, i.e. first large structures are formed and then collapsed to smaller ones. This is however disfavoured by observations, since the galaxies are known to be much older than superclusters. In fact, referring also to additional arguments, one can show that the amount of allowed "hot" dark matter satisfies $\Omega_{HDM} < 0.0062\,(95\%\,\text{CL})$ [18].

In a single sentence all this can be summarized by the statement, that observations favour the non-baryonic, cold dark matter. However, as usual, some of the conditions described above may be relaxed and still one can obtain a viable candidate. For example

interaction with photons via electric or magnetic dipole moment [28] are still allowed. Another example is the idea that dark matter composed of axions can form a Bose-Einstein condensate [29], clearly not being a classical fluid. Decaying dark matter was also heavily studied recently, especially in the context of possible indirect detection signals. Most models however preserve those golden rules, which act as a useful guideline for model building.

To illustrate how this works for a particular model, it is useful to use as an example historically one of the first candidates, a neutrino. Neutrinos are the only possible potential candidates among the known particles: they are stable, do not couple to photons, interact only very weekly and it is now well-established that they have mass. Therefore, they definitely contribute to the total DM component. However, as already mentioned, relic neutrinos do not give cold dark matter. The reason is that they are too light, with the upper limit on the mass of the heaviest one, $m_\nu < 2$ eV [30]. It follows, that neutrinos are still relativistic at their decoupling, which happens for temperatures at the MeV scale. Additionally, to constitute the whole DM they would need to be very dense in the phase space and as fermions they would start to be in conflict with the Tremaine-Gunn bound. As a consequence, although neutrinos contribute to the total dark matter density, they cannot be the main component.

1.2.1 Weakly Interacting Massive Particles

Two reasons draw most of the attention to the very broad class of models in which the dark matter is weakly interacting, i.e. a WIMP. Firstly, as we will discuss below in Sec. 1.3.1, the thermal relic density for such a particle is approximately given by:

$$\Omega_{\rm DM} h^2 \approx 0.1 \, \frac{3 \times 10^{-26} {\rm cm}^3 {\rm s}^{-1}}{\langle \sigma v \rangle} \, , \tag{1.9}$$

i.e. a generic particle with the self-interaction cross-section of the typical weak scale process of tens of pb (corresponding to $\langle \sigma v \rangle$ of the order of $10^{-26}\,{\rm cm}^3/{\rm s}$) leads rather naturally to a thermal relic density in agreement with observations. This property was dubbed a "WIMP Miracle". Secondly, from a more practical point of view, WIMPs' generic properties allow for a concrete detection methods, which one can use to search for dark matter experimentally (see Sec. 1.4).

Many models fall in this category, with the two most widely studied cases being: lightest supersymmetric particles (LSPs) and Kaluza-Klein particles present in some models with extra dimensions.

LSPs

In supersymmetric scenarios with R-parity conservation the lightest supersymmetric particle is stable and thus can potentially give a very well theoretically motivated dark matter candidate. In the minimal supersymmetric extensions of the SM there are three possible candidates of this type: sneutrino (scalar partner of a neutrino), neutralino (fermionic partner to gauge and Higgs bosons) and gravitino (fermionic partner of graviton). We will discuss them in detail in Sec. 2.4.

Kaluza-Klein particles

Models of Universal Extra Dimensions (UED) [31, 32] or Warped GUTs (e.g. Randall-Sundrum [33]) predict existence of infinite tower of massive states, Kaluza-Klein particles (KK), from which the lightest one can play the role of dark matter. For example, in the simplest UED models the extra fifth dimension is compactified on a sphere of radius R. Then from the 4D point of view one sees a tower of KK states with the mass of the n^{th} state proportional to n/R. The stability of the lightest one is ensured by the conservation of momentum in the extra dimension, which in the 4D picture translates to conservation of the KK number. In the early Universe those new states are produced thermally with the cross-section being naturally at a weak scale [34, 35]. Although Kaluza-Klein particles are typically hard to detect experimentally, some signals can still be potentially observed, most probably in collider and indirect searches [36].

1.2.2 Non-WIMPs

Apart from WIMPs, there exist also other types of candidates. Although not motivated by the thermal origin, they often possess additional strong motivation, coming from cosmology or particle physics. Two prominent examples of such kind are axions and Q-balls.

Axions

One of the naturalness issues of the SM is the so-called Strong-CP problem: why CP is seen to be conserved in strong interactions, although the QCD Lagrangian contains a term which breaks it explicitly? This term arises via non-perturbative effects and is connected to the non-trivial topological structure of the QCD. It has a form

$$\mathcal{L}_\theta = \bar{\theta}\frac{g^2}{64\pi^2}\epsilon^{\mu\nu\alpha\beta}G^a_{\mu\nu}G^a_{\alpha\beta}, \tag{1.10}$$

where $G^a_{\mu\nu}$ is the field stress tensor. The coefficient $\bar{\theta}$ gets contributions from the initial non-perturbative θ-angle and the argument of the quark mass matrix determinant (due to weak interactions the quark mass matrix becomes complex and because of the chiral anomaly the re-absorption of phases done by the chiral rotation contributes to $\mathcal{L}_\theta$). One can easily check that this term indeed breaks CP, P and T, and thus it seems that the only possibility is that the $\bar{\theta}$ coefficient vanishes. To quantify this problem, note that this term would lead to a non-zero electric dipole moment of the neutron, of the order of $d_n \approx 10^{-16}|\bar{\theta}|\,\mathrm{e\,cm}$. From the measurements one gets then condition that $|\bar{\theta}| \lesssim 3\times10^{-10}$ (or $|\bar{\theta}-\pi| \lesssim 3\times10^{-10}$). There comes the naturalness issue: since it gets contributions from two completely different parts of the theory, how comes that they cancel so effectively?

Several solutions to this issue were proposed, among which the most compelling one is the dynamical mechanism of driving $\bar{\theta}$ to zero, by promoting it to a dynamical field a. The mechanism used by Peccei and Quinn [37] was to consider a to be a pseudo-Goldstone boson of a new spontaneously broken $U(1)_{PQ}$ symmetry. The resulting particle, named axion by Wilczek [38], is a very weakly interacting pseudoscalar, with a mass related (in the simplest models inversely proportional) to the scale of PQ symmetry breaking f_a. This

scale has to be high enough to evade all the experimental constraints. For the scenarios where axion can be a viable dark matter candidate it gives $10^9\,\mathrm{GeV} \lesssim f_a \lesssim 10^{12}\,\mathrm{GeV}$, with the precise values being model dependent. This translates to a bound on the mass (again model dependent) $10^{-2}\,\mathrm{eV} \gtrsim m_a \gtrsim 10^{-6}\,\mathrm{eV}$.

Even with such a strong experimental constraints, axion remains a viable and interesting dark matter candidate. Its main unique feature is the production mechanism, called the *misalignment production*. The idea is that when the temperature of the Universe exceeds the PQ symmetry breaking scale the θ angle is displaced from its minimum. When the temperature drops down, at around 1 GeV potential for the axion field starts to be effective and the fields starts to "roll down" to its minimum. It starts to oscillate coherently, behaving like a condensate of axions at rest. This mechanism can give a correct thermal relic density for a still allowed values of the axion mass m_a.[7]

Q-balls

Another interesting possibility are the so-called Q-balls [40]. A Q-ball is a coherent state of a complex scalar field, a non-topological soliton, whose existence and stability arises due to the conservation of some global U(1) quantum number. For example, the usual baryon (lepton) number may play the role of such conserved quantity for the Q-balls built of squarks (sleptons), i.e. the supersymmetric scalar partners of quarks (leptons). In particular, Q-balls are generically present in the Affleck-Dine baryogenesis [41] scenarios, as it was shown in [42]. They are very heavy, containing at least 10^{22} particles and rather difficult to detect. Q-balls can be produced in right amount in the early universe and survive to the present day and thus can be considered as a viable dark matter candidate [43]. Production mechanisms include phase transitions, fragmentation of the scalar condensate at the end of inflation and the so-called solitosynthesis (analogue of nucleosynthesis). Additional interesting features of this scenario is that by predicting rather warm dark matter it can accommodate for the solution of the cosmological "cusp" and "missing satellites" problems [44]. In the end it is rather safe to say that although the Q-ball dark matter is without doubt an interesting idea, it is also certainly a bit exotic and therefore not in the mainstream of the field.

Baryonic dark matter

For completeness, let us mention the sometimes invoked possibility that the dark matter is in fact of the baryonic origin, but is contained in the Massive Astrophysical Compact Halo Objects (MACHOs). This possibly could evade detection at any wavelengths if these objects are optically dark (like e.g. planets, black holes, neutron stars, etc). However, this kind of models have typically substantial problems with the CMB and BBN constraints. One example of possibly working scenario could be the primordial black holes (PBH) [45].

From the observational point of view various surveys were conducted with the aim of searching for MACHOs. The bottom line of all those searches is the following (for a

[7] Thermal population of axions has a very low relic density. However, another potentially important production exists, namely the decay of the cosmic strings coming from $U(1)_{PQ}$ breaking in the early Universe. For a recent axion review see e.g. [39].

short summary see e.g. [46]): MACHOs are excluded as a main DM component of the Milky Way halo in the entire range of masses above $10^{-7}M_{\odot}$. Another attempt to save the Universe from the non-baryonic dark matter is seen to fail.

1.3 Thermal history of the Universe

In the standard cosmological model, the Universe after the inflationary period consists of extremely hot plasma, containing all possible kinds of existing particles.[8] Although it is not truly in a thermodynamic equilibrium, it can be approximated as such for the most of its history. Therefore, we can trace its evolution with temperature playing the role of time. In this parametrization various epochs are much more clearly visible, since it is the temperature which sets the energy scale for a given moment, determining which processes take place efficiently and which are not effective any more. In particular, as the temperature decreases, the interactions rates between different particles in the thermal bath are typically decreasing as well. If the interaction rate for a given particle species drops below the rate of the expansion of the Universe, then the interactions are too rare to be important, and this particle *freezes-out*. After that, it is decoupled from the thermal bath and evolves independently with constant comoving number density, i.e. number density normalized to the entropy density.

The interaction rate Γ is given by the product of the number density n and the thermally averaged cross-section $\langle\sigma v\rangle$, while the expansion is governed by the Hubble rate H. This gives an estimation of the freeze-out temperature $T_{f.o.}$:

$$n\langle\sigma v\rangle|_{T_{f.o.}} = H|_{T_{f.o.}}\,, \tag{1.11}$$

which for a WIMP happens typically for $T_{f.o.} \approx m/20$. More precise treatment involves solving (numerically) the set of Boltzmann equations governing the evolution of the individual number densities under simultaneous effects of expansion, scatterings and annihilations, see Sec. 1.3.1 below.

This provides a very natural mechanism for production of particles in the early Universe, which is in fact seen to give predictions consistent with the abundance of light elements from the BBN. Furthermore, after decoupling the only possible depleting effect would be the decay, therefore if the freezed-out particle is stable it will survive up to the present day. It is the most promising and natural scenario for the generation of the observed dark matter density. The Universe is however something more than just the dark matter, thus in the following we will shortly sketch its whole history from the Big Bang till now [47]:

- $T = 10^{19}$ GeV (10^{-43} s): Planck epoch. Quantum gravity desperately needed.
- $T \sim 10^{15}$ GeV (10^{-36} s): the most typical period for inflation. A conjectured, model-dependent phase of exponential expansion, which flattens and isotropizes the

[8] With masses not larger than the highest temperature of the plasma, which in the inflationary models is the so-called reheating temperature T_{RH}.

observed patch of Universe, giving answers to several important issues, like e.g. why CMB is so uniform even though (without inflation) we were never in causal contact with most of the observed regions.

- $T \sim 10^{15}$–10^{3} GeV (10^{-36}–10^{-11} s): lepto- and baryogenesis? Supersymmetry breaking? Not yet well understood.
- $T = 10^{3}$–5 GeV (10^{-11}–10^{-7} s): typical WIMP freezes-out and dark matter relic abundance created.
- $T = 100$ GeV (10^{-10} s): electroweak phase transition.
- $T \approx 0.3$ GeV (10^{-5} s): QCD phase transition. Gluons and quarks confine inside baryons.
- $T = 0.1$–10 MeV (10^{2}–10^{-2} s): Big Bang Nucleosynthesis.
- $T = 1$ MeV (1 sec): neutrinos decouple and form relic population (still too elusive to be found with present technology).
- $T = 1$ eV (10^{4} yr): matter-radiation equivalence and onset of structure formation.
- $T = 0.4$ eV (10^{5} yr): recombination and last scattering, CMB is formed.
- $T = 0.4$–10^{-4} eV (10^{5}–14×10^{9} yr): formation of galaxies, stars, planets, etc.
- $T = 10^{-4}$ eV (14×10^{9} yr): present day.

1.3.1 Relic density calculations

In this section we will discuss in detail the thermal production mechanism and show for a generic particle how to compute its relic density by solving the Boltzmann equation. We will follow quite closely the approach of Ref. [48], which is the one appropriate for situations strongly affected by co-annihilations [49, 50] and will be needed in our computations of the relic density with the Sommerfeld effect (see Sec. 4.4.2).

To be general, let's assume that we have set of N particles χ_1, χ_2, ... χ_N, each with mass m_i (the ordering is such that $m_1 \leqslant m_2 \leqslant \cdots \leqslant m_N$) and number of internal degrees of freedom h_i. Moreover, we assume that they are sharing a conserved quantum number so that: *i)* if kinematically allowed, inelastic scatterings on SM thermal bath particles can turn each of these states into another, and *ii)* χ_1 is stable (and is our DM particle).

If the mass splitting between the heaviest and the lightest is comparable with $T_{f.o.} \approx m_1/20$, roughly speaking the freeze-out temperature for a WIMP, all these states have comparable number densities at decoupling and actively participate in the process of thermal freeze-out.

The evolution is governed by the expansion of the Universe and interactions with the thermal bath. The latter depends not only on the temperature and the number densities,

but also on their phase space distributions. For a given particle i, its phase space density f_i satisfies the continuity relation:

$$\mathcal{L}[f_i] = \mathcal{C}[f_i], \tag{1.12}$$

where $\mathcal{L}$ is the Liouville operator describing the evolution of the phase space volume, in general relativity given by:

$$\mathcal{L}_{GR} = p^\alpha \frac{\partial}{\partial x^\alpha} - \Gamma^\alpha_{\beta\gamma} p^\beta p^\gamma \frac{\partial}{\partial p^\alpha} \,. \tag{1.13}$$

The right hand side of (1.12) describes all possible processes resulting in producing or destroying particle i, by the so-called collision operator $\mathcal{C}$. Since some of these processes involve also other particles from the thermal bath, $\mathcal{C}$ depends also on their corresponding phase space densities, which in general leads to a set of coupled Boltzmann equations for their number densities $n_i = \int d^3p f_i(p)$. For a given particle species i it has the form:

$$\begin{aligned} \frac{dn_i}{dt} + 3\,H\,n_i = & - \sum_{j=1}^{N} \langle \sigma_{ij} v_{ij} \rangle \left(n_i n_j - n_i^{eq} n_j^{eq} \right) \\ & - \sum_{j \neq i} \left[\langle \sigma_{Xij} v_{ij} \rangle \left(n_i n_X - n_i^{eq} n_X^{eq} \right) - \langle \sigma_{Xji} v_{ij} \rangle \left(n_j n_X - n_j^{eq} n_X^{eq} \right) \right] \\ & - \sum_{j \neq i} \left[\Gamma_{ij} \left(n_i - n_i^{eq} \right) - \Gamma_{ji} \left(n_j - n_j^{eq} \right) \right], \end{aligned} \tag{1.14}$$

where n_i^{eq} is the thermal equilibrium number density and

$$\sigma_{ij} = \sum_X \sigma \left(\chi_i \chi_j \to X \right), \tag{1.15}$$

$$\sigma_{Xij} = \sum_Y \sigma \left(\chi_i X \to \chi_j Y \right), \tag{1.16}$$

$$\Gamma_{ij} = \sum_X \Gamma \left(\chi_i \to \chi_j X \right), \tag{1.17}$$

are the annihilation cross-section, the inelastic scattering cross-section and decay rate, respectively. The "relative velocity" v_{ij} is defined as

$$v_{ij} = \frac{\sqrt{(p_i \cdot p_j)^2 - m_i^2 m_j^2}}{E_i E_j}, \tag{1.18}$$

where p_i is the four-momentum and E_i the energy of particle i. The thermal averaging for processes of the type $\chi_i + \chi_j \to X$ (in the dilute limit two-body initial state processes dominate) is given by:

$$\langle \sigma_{ij} v_{ij} \rangle = \frac{1}{n_i^{eq}\, n_j^{eq}} \sum_X \int \frac{d^3p_i}{2\,E_i} \frac{d^3p_j}{2\,E_j} \frac{d^3p_X}{2\,E_X} \delta^4(p_i + p_j - p_X) f_i^{eq}(p_i) f_j^{eq}(p_j) \left| A_{ij \to X} \right|^2, \tag{1.19}$$

where the sum here is on the set X of allowed SM final states and $d^3p_X/2\,E_X$ stands symbolically for the integration over the phase space in the final state. Normally in X only two-body final states are considered, since they are clearly the dominant ones.

This set of coupled Boltzmann equations traces all the number densities n_i. However, we do not need all this information to compute the relic density. Indeed, after freeze-out all heavier states decay into the lightest one and one usually solves a single equation written for the sum of the number densities, $n = \sum_i n_i$, which can be obtained from (1.14):

$$\frac{dn}{dt} + 3\,H\,n = -\langle\sigma_{\rm eff} v\rangle \left[n^2 - (n^{eq})^2\right] \,, \tag{1.20}$$

where we have defined the effective thermally averaged annihilation cross section:

$$\langle\sigma_{\rm eff} v\rangle = \sum_{i,j} \langle\sigma_{ij} v_{ij}\rangle \frac{n_i^{eq}}{n^{eq}} \frac{n_j^{eq}}{n^{eq}} \,, \tag{1.21}$$

written as a weighted sum over the thermally averaged (co-)annihilation cross-sections.

There are two main assumptions which allow to rewrite the system of coupled Boltzmann equations as the single equation for n, in analogy to the case one writes for one single WIMP, with the usual term of dilution by volume on the l.h.s. and the depletion and replenish terms on the r.h.s.:

- The factorization of the individual terms in Eq. (1.14) and the sum of Eq. (1.21) is possible if one assumes that the shape of phase space densities for each particle χ_i follows the shape of the corresponding thermal equilibrium phase space density, namely $f_i(p_i, t) = c(t) \cdot f_i^{eq}(p_i, t)$ (with the coefficient c depending on time but not on momentum). This is the case if the so-called kinetic equilibrium is maintained, i.e. if scattering processes of the kind $\chi_i + X_l \to \chi_k + X_m$ (with k equal to i or different from it) on SM thermal bath states X_l and X_m have a rate which is larger than the Universe expansion rate H.

  Kinetic equilibrium is a legitimate assumption, because kinetic decoupling usually takes place much later than chemical freeze-out. The reason is that although the amplitudes for scattering and annihilation processes are usually comparable, since the two can be related via crossing symmetry, the scatterings are much more frequent than annihilations. This is due to the fact that around the time of freeze-out $T_{f.o.} \ll m_1$ and WIMPs are very rare in the thermal bath. On the other hand scatterings are stimulated by thermal bath states themselves, which are relativistic and hence whose number density is not suppressed.

- The second assumption which is implicit in Eq. (1.20) is that one takes $n_i/n \simeq n_i^{eq}/n^{eq}$. This quantity in the Maxwell-Boltzmann approximation for equilibrium phase space densities, i.e. $f_i^{eq}(p_i, t) = h_i/(2\pi)^3 \exp(-E_i/T)$, is proportional to the number of internal degrees of freedom h_i and is exponentially suppressed with the mass splittings. Analogously to the first assumption, this approximation is valid in case inelastic scatterings are active for the whole phase in which the depletion term is relevant.

Once the particle physics of χ_is is known, we can compute all the cross-sections, plug them into (1.21) and then solve the Boltzmann equation with the initial condition that at early times the number densities n_i trace the equilibrium ones. This can be done very accurately by using fully numerical computations, typically using existing codes like DarkSUSY [51] or micrOMEGAs [52]. Note also, that the treatment outlined above does not involve any approximations in the way thermally averaged annihilation cross-sections are computed.

In order to get some more insight on the possible result, it is useful to look at a simplified case. Let's assume that there is only one WIMP and thus no co-annihilation effects are present. It is convenient to write then the Boltzmann equation in the variables: $Y = n/s$, where s is the total entropy density, and $x = m/T$. Then Eq. (1.20) can be rewritten in a form:

$$\frac{dY}{dx} = \frac{1}{3H}\frac{ds}{dx}\langle\sigma v\rangle\left(Y_{eq}^2 - Y^2\right). \tag{1.22}$$

Now let us make an approximation that the thermally averaged cross-section can be expanded with respect to the velocity and truncated on the second term:

$$\langle\sigma v\rangle = a + bv^2 + \mathcal{O}(v^4) \approx a + 6\,b/x\,. \tag{1.23}$$

This is justified, since the WIMP has to be non-relativistic at the time of freeze-out in order to constitute a cold dark matter. Then the Boltzmann equation can be written as:

$$\frac{dY}{dx} = -\left(\frac{45}{\pi}G_N\right)^{-1/2}\frac{g_*^{1/2}m}{x^2}(a + 6(b/x))(Y^2 - Y_{\rm eq}^2), \tag{1.24}$$

with

$$g_*^{1/2} = \frac{h_{eff}}{g_{eff}^{1/2}}\left(1 + \frac{T}{3h_{eff}}\frac{dh_{eff}}{dT}\right), \tag{1.25}$$

$$g_{eff} = \frac{30\rho}{\pi^2 T^4}\,, \tag{1.26}$$

$$h_{eff}(T) = \frac{45s}{2\pi^2 T^3}\,, \tag{1.27}$$

and ρ being the total energy density. Within this approximation, in a radiation dominated Universe with an adiabatic expansion, it is possible to find an analytical solution, giving the freeze-out happening at [50, 47]:

$$x_f \simeq \log\left(\frac{5}{4}\sqrt{\frac{45}{8}}\frac{h}{2\pi^3}\frac{m_\chi m_{Pl}(a + 6\,b/x_f)}{\sqrt{g_*(x_f)x_f}}\right), \tag{1.28}$$

and the relic density being equal to

$$\Omega_\chi h^2 \approx \frac{1.07\times 10^9}{m_{Pl}}\frac{x_f}{\sqrt{g_*(x_f)}}\frac{1}{a + 3\,b/x_f}\,. \tag{1.29}$$

For an S-wave annihilation, if one plugs in the numbers of a typical WIMP of a mass $\mathcal{O}(100\ \mathrm{GeV})$ one indeed gets $x_f \simeq 20$–30 and the relic density:

$$\Omega_\chi h^2 \approx 0.1\ \frac{3 \times 10^{-26}\mathrm{cm}^3\mathrm{s}^{-1}}{\langle \sigma v \rangle}\ . \tag{1.30}$$

This is the advocated famous "WIMP Miracle": a particle of a typical cross-section governed by weak interactions and mass on a weak scale gives correct thermal relic density. This result should be however taken with a grain of salt. Not only it depends on several assumptions and is related to the simplified case without co-annihilations, but also inspected in more detail is seen to be rather fine-tuned in in many concrete realizations. For instance, the low-energy supersymmetry typically predicts too large or too small relic density, unless one goes to narrow regions of parameter space [53]. This tension can be eased if one allows for the dark matter mass to approach TeV scale, but this weakens a bit the motivation of a WIMP as a manifestation of new weak scale physics. Nevertheless, this simple computations shows why so much effort is devoted to studies of the weakly interacting massive particles.

1.4 Detection methods

The prospects for experimental searches for the dark matter very strongly rely on its nature. If it is (nearly) decoupled from our visible SM sector we can probe it only via gravitational effects. In this case it is extremely hard to measure any of its properties. On the other hand, if the dark matter has anything to do with the new physics suggested by the open issues in the SM, other detection channels are possible. In the case of a WIMP, its properties make viable either direct detection (DD) via scattering on a nucleus or indirect detection (ID) searching for a WIMP-induced component in cosmic rays, in the photon background at frequencies ranging from the radio to gamma-ray band, or in the neutrino flux from the Sun or other astrophysical objects.

1.4.1 Direct detection

The mechanism of thermal generation of WIMP dark matter relies on the weak-interaction strength of their pair annihilation into thermal bath particles, most likely light SM states. Using crossing symmetry one expects also scattering processes on the same states to be of similar order. In particular, s-channel annihilation to quarks leads to t-channel scattering of a WIMP on a quark.

Direct detection is a method of exploiting this process for looking for a dark matter signal and if found, determining the DM particle mass and scattering cross-section.[9] However, the expected signal is very small and additionally one has to make a lot of effort in order to discriminate the background.

The quantity measured is the recoil energy E_r of the nucleus after the WIMP scatters off. It can be easily related to the kinematical properties of the impinging WIMP, using

[9] For a recent review see e.g. [54] and references therein.

non-relativistic kinematics: $E_r = q^2/2m_\chi$, where $q^2 = 2\mu^2 v^2(1-\cos\theta)$ is the momentum transfer, $\mu = m_\chi m_N/(m_\chi + m_N)$ is the reduced mass with nucleon mass m_N, θ is the scattering angle in the center of mass frame and v the WIMP velocity relative to the target nucleus. The typical value of the recoil energy is relatively small, of the order of $\mathcal{O}(10\text{ keV})$. The scattering rate on a nucleus with atomic number A is given by:

$$\frac{dR}{dE_r} = \frac{\rho_0}{m_\chi}\frac{N_A}{A}\int_{v_{min}}^{v_{esc}} d^3v\, v\, f(\vec{v})\frac{d\sigma_{\chi N}}{dE_r}\,, \tag{1.31}$$

where v_{min} is the minimal relative velocity corresponding to angle $\theta = \pi$, $v_{esc} \sim 544$ km/s is the local galactic escape velocity and N_A is the Avogadro number. The function $f(\vec{v})$ is the velocity distribution function of WIMPs and is not know well. Together with local dark matter density ρ_0, it brings a considerable uncertainty for making predictions on the event rate for a given DM model.

The scattering cross-section $\sigma_{\chi N}$ can be determined from the DM interactions with quarks and gluons, and the nuclear matrix elements. For a typical WIMP candidate, a Majorana fermion, there are two types of interactions: spin-independent and spin-dependent (corresponding to interactions mediated by scalar or pseudo-vector, respectively). The latter one is usually subdominant, since it means that a WIMP scatters only on the unpaired nucleon in the nucleus, while the former happens coherently for all the nucleons. Therefore, the most stringent experimental bounds are obtained for the spin-independent scatterings.

The method described above has been exploited in many experiments, using various detection techniques. The two ones giving strongest constraints up to date are XENON [55] and CDMS-II [56]. The former is a detector operating with 100 kg liquid xenon as a target and measuring the scintillation light from a recoil.[10] The latter is a cryogenic experiment using germanium and silicon crystals inferring the recoil energy from measurements of phonons.[11] The most up to date exclusion limits are given on Fig. 1.5 borrowed from [58].

On the other hand, several groups reported positive signals, possibly coming from dark matter. These are:

- DAMA/LIBRA [63]: the experiment concentrates on the annual modulation signal from DM coming from the cyclic variation of the mean energy of WIMPs in the detector frame due to the orbital motion around the Sun. The collaboration claims to observe an effect with more than 8σ statistical significance. Interestingly, even though this result is known already for a long time, still there exists no other plausible explanation of this signal rather than the scattering of dark matter particles. Especially, that not only the period but also the phase of observed modulation coincides with the motion of Earth around the Sun.

[10] For WIMP masses of the order of $\mathcal{O}(10\text{ GeV})$ the 100 kg version of the experiment has less sensitivity than the previous, 10 kg one, called XENON10 [57]. This is due to higher energy threshold and still not sufficient understanding of scintillation efficiency, the so-called L_{eff}, at very low energies. In the autumn of 2012 a construction of 1 ton version, XENON1T, is planned to start with sensitivity goal of 2×10^{-47} cm^2 for a WIMP mass of about 50 GeV after two years of data-taking [58].

[11] In reality both XENON and CDMS combine two detection channels in order to reject the background, with the second one in both experiments being the measurement of the ionization charge.

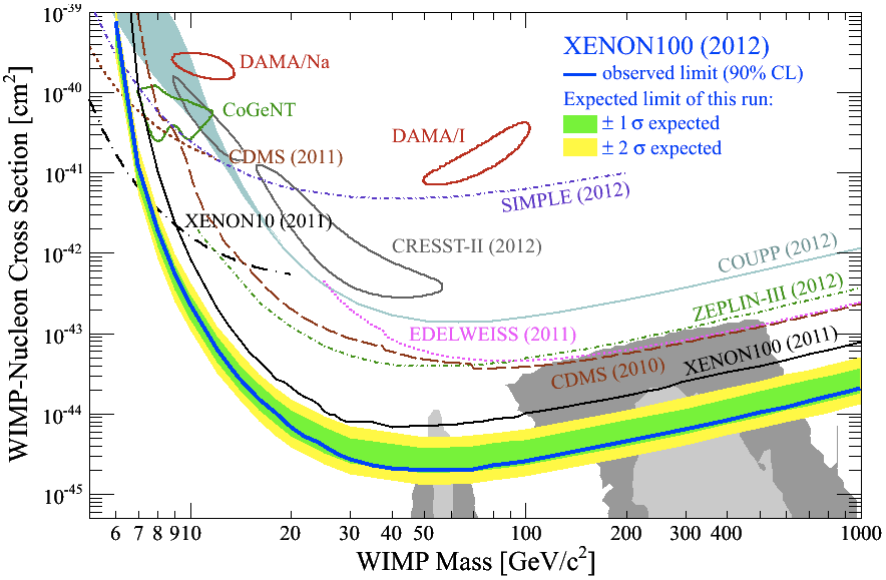

Figure 1.5: Exclusion limits on the $\sigma_{\chi N}$ vs. the WIMP mass from XENON, CDMS, EDELWEISS [59], ZEPLIN-III [60], COUPP [61] and SIMPLE [62] experiments. The contours indicate regions consistent with possible signals found in DAMA, CoGeNT and CRESST. Tha gray shaded region shows part of the parameter space suggested by the supersymmetric theories. Figure from [58].

- CoGeNT [64, 65]: this experiment uses high-purity germanium crystal and measures the ionization charge from nuclear recoils. It takes advantage of a very low threshold of about 0.5 keV which allows to search for nuclear recoil events coming from dark matter particles of relatively low mass, i.e. as low as 5 GeV. It has reported an excess that cannot be associated to any known background source and furthermore recently also found a hint for a annual modulation of the observed signal.

- CRESST [66]: uses $CaWO_4$ crystals as the target, and detects scintillation and also phonons in order to discriminate the background nuclear recoils. It has found an excess of events in the oxygen band, making the results statistically significantly inconsistent with the background-only hypothesis.

All of these experiments point to a region with a WIMP with mass of a few GeV and scattering cross-section ranging from about 10^{-42} to nearly 10^{-39} cm^2, see Fig. 1.5. The results are, however, not consistent with each other and furthermore very difficult to reconcile with the null results of XENON and CDMS. The situation is unclear and at the moment subject to a debate, nevertheless, it constitutes an intriguing hint for a light WIMP scenario.

1.4.2 Indirect detection

Indirect detection aims in measuring the fluxes of photons, neutrinos and various cosmic rays reaching Earth and try to single out the ones coming from dark matter annihilation or decay in the halo. In Chapter 5 we will present the detailed study of the multi-channel indirect detection signals for a specific model, a Wino dark matter, and also discuss

prospects of detection and resolving various uncertainties. At that point we also discuss all necessary physical ingredients, here let us just describe the general concept.

In the same way as for direct detection, this method relies on the assumption that the dark matter annihilate to the SM final states, as happens for a typical WIMP. This present-day annihilation produces both matter and antimatter, which then contributes to the measured cosmic rays. Photons and neutrinos reach us essentially unaltered by the interstellar gas and magnetic fields, while charged particles scatter and propagate in more complicated, diffusive manner. Moreover, in both cases the astrophysical backgrounds are much larger than the would-be dark matter contribution, and unfortunately they are also not fully known. Given all that, to search for a signal one has to study and understand as much as possible about the background and how cosmic rays propagate and additionally look for distinctive signatures. An example of the latter is a monochromatic gamma-ray line, which is not expected to be generated by any astrophysical processes, and therefore is considered to be a smoking-gun signature of dark matter.

Furthermore, the signal coming from DM annihilation depends not only on its particle physics properties and propagation model, but also on the DM distribution in the halo of our Galaxy, or other targets for the indirect detection. This distribution is again not yet fully understood. The data we have from observations, coming mainly from the dynamical properties of galaxies, are by itself not sufficient to determine the dark matter density profile.

Therefore, the profile is rather inferred from N-body simulations and then compared with observations (for a review see e.g. [67]). In principle these simulations are straightforward, since only (Newtonian) gravity matters, but technically are rather challenging and very CPU time consuming. Only recently they reached accuracy needed for resolving substructures in individual collapsed structures and in fact now one can resolve about 10^5 substructures in a Milky-Way size halo. Today simulations are running with up to 10^9 particles and with spatial resolution better than 0.1% of the virialized region. Nevertheless, still to make comparisons with observations one often is forced to make extrapolations well below the current resolution scale.

What is striking is that the results show a universal density profile for objects of different scales, from dwarf spheroidals and spiral galaxies up to even clusters. It can be approximated be a Navarro-Frenk-White (NFW) profile [68]:

$$\rho_{NFW}(r) = \frac{\rho_s}{(r/r_s)\,(1+r/r_s)^2}\,, \tag{1.32}$$

where r_s is the so-called scale radius, with typical values for Milky-Way size halo ranging from about 15 to 25 kpc.

On the other hand, in the inner part of the halo, well below r_s, different simulations give several different results. Indeed, most resulting halos were seen to be marginally shallower than what follows from the NFW profile. To improve this, one can use a generalized version of the NFW:

$$\rho(r) = \frac{\rho_s}{(r/r_s)^{\alpha}\,(1+r/r_s)^{\frac{\beta-\gamma}{\alpha}}}\,, \tag{1.33}$$

and let the α, β and especially γ parameters to vary or adopt an Einasto profile [69, 70]:

$$\rho_{Ein}(r) = \rho_s e^{-\frac{2}{\alpha}[(r/r_s)^\alpha - 1]} \ , \tag{1.34}$$

where again α is a free parameter, with typical values ranging from 0.1 to 0.25. In fact, nowadays there is a rather general consensus on that the results of simulations using only CDM, i.e. without any baryons, are described best by the Einasto profile. However, if baryons cool and collapse into CDM potential well adiabatically, they would tend to make the DM profile steeper, resembling more the NFW.

Another possibility studied in the literature is the Burkert profile [71]:

$$\rho_B(r) = \frac{1}{\left[1 + (r/r_s)\right]\left[1 + (r/r_s)^2\right]} \ . \tag{1.35}$$

It is distinct from the other two, because it has a core. This is what also might happen in reality when one includes baryons whose infall can induce the shallowing of the central DM slope, if there is a substantial angular momentum transfer between baryons and dark matter. In fact, the complex interplay between the dark matter and baryons is not yet understood, and this is what is limiting the extrapolations from simulations to the actual distribution of the DM in the central regions of galaxies.

From the above discussion it is clear that lack of full knowledge about the dark matter profile introduces another uncertainty in the indirect searches. However, this is important mainly when looking at the Galactic center, where the differences between the profiles are the most pronounced.

Chapter 2

The Minimal Supersymmetric Standard Model

The one of the best motivated WIMP candidates comes from the supersymmetric extensions of the standard model. In this chapter we will firstly review the necessary ingredients of the SM and then its shortcomings. In Sec. 2.2 we introduce supersymmetry and in Sec. 2.3 the Minimal Supersymemtric Standard Model (MSSM). The dark matter in this framework is then discussed in the last Section 2.4.

2.1 The Standard Model and its problems

The Standard Model is one of the most successful theories ever written.[1] It was tested to a very high precision in numerous experiments [30] and describes all known elementary particles and their interactions except gravity. It comprises two parts, both invented in the 1960's: quantum chromodynamics (QCD) [76, 77, 78] and the electroweak theory of Weinberg [79], Salam and Glashow [80, 81].

The Standard Model is a renormalizable quantum field theory in which both matter and interactions are described in terms of four-dimensional fields in flat Minkowski spacetime. Excitations of these fields manifest themselves as particles. It is also a gauge theory: the fundamental interactions are described by the fields' transformations under the standard model group gauge G_{SM}.

In the following we present a short overview of the main features of the SM relevant for this work. In particular we concentrate on the open questions and their possible explanation within the framework of its supersymmetric extensions.

2.1.1 Gauge interactions and the field content

The SM gauge group is a direct product of three simple groups $G_{SM} = SU(3)_C \times SU(2)_L \times U(1)_Y$, where the strong interactions are symmetric under $SU(3)_C$ transformations while the electroweak interactions under the $SU(2)_L \times U(1)_Y$. The generators of these subgroups correspond to the fields carrying the interactions. The color $SU(3)_C$ is associated

[1] Numerous textbooks and reviews of the Standard Model exist. See for example [72, 73, 74, 75].

Fields	$(SU(3)_C,\, SU(2)_L,\, U(1)_Y)$	Particles	Spin
$\begin{pmatrix} u \\ d \end{pmatrix}_L, \begin{pmatrix} c \\ s \end{pmatrix}_L, \begin{pmatrix} t \\ b \end{pmatrix}_L$	$\left(\mathbf{3}, \mathbf{2}, +\frac{1}{3}\right)$	Quarks	$\frac{1}{2}$
$u_R^\dagger,\, c_R^\dagger,\, t_R^\dagger$	$\left(\overline{\mathbf{3}}, \mathbf{1}, -\frac{4}{3}\right)$		
$d_R^\dagger,\, s_R^\dagger,\, b_R^\dagger$	$\left(\overline{\mathbf{3}}, \mathbf{1}, +\frac{2}{3}\right)$		
$\begin{pmatrix} \nu_e \\ e \end{pmatrix}_L, \begin{pmatrix} \nu_\mu \\ \mu \end{pmatrix}_L, \begin{pmatrix} \nu_\tau \\ \tau \end{pmatrix}_L$	$(\mathbf{1}, \mathbf{2}, -1)$	Leptons	$\frac{1}{2}$
$e_R^\dagger,\, \mu_R^\dagger,\, \tau_R^\dagger$	$(\mathbf{1}, \mathbf{1}, +2)$		
g	$(\mathbf{8}, \mathbf{1}, 0)$	Gauge bosons	1
W	$(\mathbf{1}, \mathbf{3}, 0)$		
B	$(\mathbf{1}, \mathbf{1}, 0)$		
H	$(\mathbf{1}, \mathbf{2}, +1)$	Higgs	0

Table 2.1: The field content of the Standard Model. All the fields correspond to given particles, except for the Higgs field H which is partially reabsorbed into longitudinal components of the massive gauge bosons and from a complex scalar doublet only one neutral boson h remains. See text for more details.

to 8 gluons, while $SU(2)_L$ and $U(1)_Y$ give W^i, $i = 1, 2, 3$ and B bosons, respectively. The subscript L refers to *Left*, indicating that the theory is chiral: left- and right-chiral fermion fields transform differently. The generators can be written as Hermitian matrices satisfying the commutation relations of the corresponding Lie algebras:

$$\begin{aligned} [T^a, T^b] &= i f^{abc} T^c \qquad \text{for } SU(3)_C \quad a = 1, \ldots, 8\,, \\ [I^i, I^j] &= i \epsilon^{ijk} I^k \qquad \text{for } SU(2)_L \quad a = 1, 2, 3\,, \end{aligned} \tag{2.1}$$

where the structure constants are given by the totally antisymmetric tensors f^{abc} and ϵ^{ijk}. Moreover, the generators are normalized such that $\mathrm{Tr}\left\{T^a T^b\right\} = \frac{1}{2}\delta^{ab}$. Obviously, since $U(1)_Y$ is Abelian it has only one generator and the corresponding commutation relation is trivial.

This group structure allows for an easy classification of the matter content of the theory. Indeed, every SM particle can be classified according to its symmetry properties under $SU(3)_C$ and $SU(2)_L$ transformations, or in other words by their representations. Additionally, every particle has an assigned $U(1)_Y$ charge Y, related to the electromagnetic charge by the Gell-Man–Nishijima relation:

$$Q = I^3 + \frac{Y}{2}\,. \tag{2.2}$$

The complete field content of the SM is listed in Tab. 2.1, where the fermions come with three copies, called families for quarks and generations for leptons.

Gauge symmetry prevents gauge fields to be massive: a mass term for them is forbidden if the symmetry is preserved. On the other hand we know from experiment that for weak gauge bosons this is not the case. Therefore, the $SU(2)_L \times U(1)_Y$ symmetry has

to be broken. In the SM this is done *spontaneously*, i.e. by a non-vanishing vacuum expectation value (VEV) of a scalar field. This, so-called Brout-Englert-Higgs mechanism [82, 83, 84, 85], gives masses to the gauge bosons and fermions of the standard model (through the Yukawa interactions with the Higgs field) and predicts an existence of a neutral scalar boson, called the Higgs boson.[2]

Photon, on the other hand, is massless. Thus the $SU(2)_L \times U(1)_Y$ symmetry is not broken completely, but to an $U(1)_{em}$, called electromagnetic. The gauge bosons are no longer mass eigenstates and they mix to form $W^{\pm}$, Z and a photon:

$$W^{\pm} = \frac{1}{\sqrt{2}}(W^1 \mp i\, W^2), \quad \begin{pmatrix} Z \\ \gamma \end{pmatrix} = \begin{pmatrix} \cos\theta_W & -\sin\theta_W \\ \sin\theta_W & \cos\theta_W \end{pmatrix} \begin{pmatrix} W^3 \\ B \end{pmatrix}. \tag{2.3}$$

Here, the θ_W is the weak mixing angle, called the Weinberg angle, and is defined as $\cos\theta_W = g_2/\sqrt{g_2^2 + g'^2}$ with g_2 being the coupling constant of the $SU(2)_L$ and g' of the $U(1)_Y$ gauge theory. It is also related to the masses of the weak gauge bosons, via $\cos\theta_W = M_W/M_Z$. These masses arise due to non-vanishing Higgs VEV $v \approx 246$ GeV and are given by $M_W = (v/2)g_2$ and $M_Z = (v/2)\sqrt{g_2^2 + g'^2}$.

2.1.2 Open questions in the SM

The standard model is certainly not the ultimate theory, despite its great successes. The most important reason is gravity. It is not incorporated in the SM and in fact cannot be. Our understanding of gravitational interactions is still classical and relies on the fact that the space-time is curved and dynamical. This is very challenging to fit into quantum theory on a static flat Minkowski space.

Indeed, no theory of quantum gravity exists yet, but nevertheless we know that it is inevitable. At all the energy scales currently accessible experimentally, gravity is very weak. However, its importance clearly grows with energy, such that around the scale of the Plank mass $m_{Pl} = 10^{19}$ GeV it cannot be neglected any more. As a consequence, at this point a new, more complete theory is needed to replace our low energy description.

This obliges us to look on a Standard Model as an effective theory, valid only up to some energy scale Λ. At higher energies it should be replaced by a new, possibly still effective, theory. It is conceivable that this new physics is also related to the other open questions of the SM, so that they can provide hints where to look. In the following we will briefly summarize those issues which are most important for this work.

Naturalness problems

Introducing a maximal energy scale to the theory, i.e. a cut-off Λ, leads to its appearance in various observables in the form of contributions from quantum corrections. If the cut-off is physical, it cannot be sent to infinity and taken care of by the renormalization procedure. Therefore, in general one obtains observable corrections that can depend on the

[2] The very recent result from ATLAS [1] and CMS [2] experiments at LHC show an existence of a new boson with Higgs-like properties and a mass of $(126.0 \pm 0.4 \pm 0.4)$ GeV and $(125.3 \pm 0.4 \pm 0.5)$ GeV, respectively. Most likely the last particle of the Standard Model has been finally found.

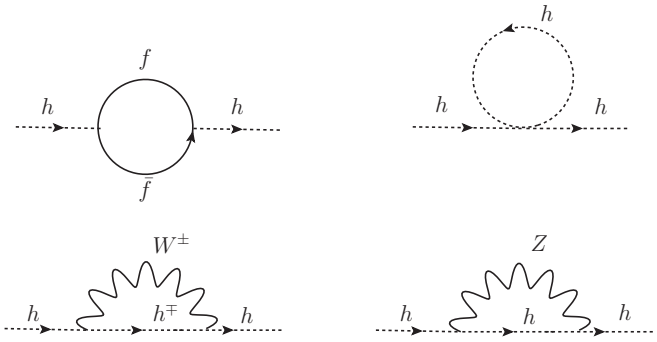

Figure 2.1: The diagrams giving the dominant one-loop corrections to the mass of the Higgs boson h.

cut-off through $\Lambda^m \log^n \Lambda$, where $n, m \in \mathbb{Z}$. Among those, the logarithmic contributions are always not that relevant numerically, even for Λ being replaced by the Planck scale. On the other hand the ones with $n = 0$, $m \geqslant 1$ are puzzling. Those type of corrections are found in the contributions to the mass of scalar particles. In particular, the only scalar of the SM, the Higgs boson h gets a one-loop correction of the form:

$$\Delta m_h^2 = \frac{3\Lambda^2}{8\pi^2 v^2}\left[4m_t^2 - 2m_W^2 - m_Z^2 - m_h^2\right] + \mathcal{O}\left(\log\frac{\Lambda}{v}\right), \tag{2.4}$$

where the contributions of other quarks than a t were neglected, due to the smallness of their Yukawa couplings (or equivalently masses). Diagrams giving this type of corrections are given on Fig. 2.1. This quadratic correction tend to push the mass of the Higgs boson to the highest scale of the theory. On the other hand, electroweak precision data favour the physical Hiigs boson mass m_h^{ph} to be at the EW scale [86] and in fact, now we know that $m_h^{\text{ph}} = m_h + \Delta m_h \approx 125$–$126$ GeV. Therefore, in order to satisfy these constraints and obtain the physical mass of the Higgs boson as observed, an important cancellation between positive and negative contributions to correction (2.4) is needed.

This is a viable solution, but leads to the famous naturalness issue, the so-called *hierarchy problem*: why does the EW scale is so small compared to the cut-off one (typically considered to be the GUT[3] or Planck scale)? Or, more technically, why the parameters of the model need to be so precisely *fine-tuned*, so that this cancellation occurs? Although this might be just a coincidence, a more "natural" reason would be that there exists some sort of mechanism that eliminates or strongly suppresses these quadratic corrections. Such a mechanism can be provided by a symmetry. For example, in the SM fermions and gauge bosons do not get these kind of contributions, due to chiral and gauge symmetry, respectively. This symmetry might be supersymmetry, which we will discuss in Sec. 2.2.

Another neutralness issue present in the Standard Model is the Strong-CP problem already discussed Sec. 1.2.2. Also there a large fine-tuning is necessary, unless some mechanism for driving the $\bar{\theta}$ to zero is present.

[3]Grand Unified Theories (GUTs) aim to unify the fundamental interactions by embedding G_{SM} into a higher dimensional group. This happens typically at roughly 10^{16} GeV.

In principle, the naturalness issues are not "true problems" of the theory. They do not pose any logical difficulties, nor disagreement with experiment. However, they are puzzling open questions and may serve as hints for the new physics.

Cosmological problems

From the point of view of this thesis, the most crucial drawback of the SM is the lack of viable dark matter candidate. As we discussed previously, none of the known particles can satisfy the constraints coming from various astrophysical and cosmological observations. This itself is enough to claim that SM is incomplete and needs to be extended. Fortunately, most of the theoretically motivated extensions give such candidates, as discussed in Sec. 1.2.

Apart from the dark matter, the SM itself cannot explain the baryon-antibaryon asymmetry. If there was no initial asymmetry between them or no new physics beyond the SM, during the evolution of the Universe nearly all the baryons would annihilate. This is clearly not what we observe. More quantitatively, defining the baryon number asymmetry normalized to the photon number density by:

$$\eta_b \equiv \frac{n_b - n_{\bar{b}}}{n_\gamma}, \tag{2.5}$$

one gets a constraint from the BBN [87]:

$$4.7 \times 10^{-10} \leqslant \eta_b \leqslant 6.5 \times 10^{-10}. \tag{2.6}$$

Independently, the value of baron asymmetry can be inferred from CMB [18], giving consistent result. If there was no initial asymmetry at the Big Bang, it had to be generated dynamically by some processes occurring before the BBN epoch, called *baryogenesis*.

The necessary and sufficient conditions under which baryogenesis happens in the early Universe, were pointed out in 1967 by Sakharov [88]. Those are:

1. baryon number violation,
2. C and CP violation,
3. departure from thermal equilibrium.

Although at the qualitative level all these conditions are present inside the Standard Model[4], quantitatively the SM itself fails to produce even such small asymmetry as in (2.6). The reason is that the amount of the CP-violation in the SM is too small [91] and moreover, the departure from the thermal equilibrium is not sufficient. The latter could happen if the EW phase transition was a first order one, but because of the lower bound on the Higgs mass [92], it cannot be strong enough. In conclusion, in order to obtain the observed value of η_b, it is necessary to go beyond the SM.

[4]The chiral anomaly of EW interactions together with sphaleron configurations leads to baryon and lepton number violation, C is maximally violated by the weak interactions, while CP is broken due to the Cabibbo-Kobayashi-Maskawa mixing [89, 90] and the departure from thermal equilibrium can be due to a strongly first order electroweak phase transition in the early Universe.

Neutrino masses

On contrary to what the Standard Model predicts, we now know that neutrinos are massive. This is a major issue for the original SM, but luckily it can be very easily extended in order to take neutrino masses into account. It is sufficient to add a new right-handed neutrino ν_R for every generation and introduce a Dirac mass term. The only conceptual problem with this solution is that the resulting ν_R would be *sterile*, i.e. it would not interact at all with other SM particles (except for gravitationally). Nevertheless, it is again a viable and very minimal solution.

However, treating neutrino masses as another hint where to look for extension of the SM, one encounters a handful of interesting and potentially important ideas. For example, if neutrinos are Majorana particles, i.e. that they are their own antiparticles, the smallness of their masses can be elegantly explained via the see-saw mechanism [93]. This idea can be also embedded in more general frameworks and leads to thermal leptogenesis as a very promising mechanism for producing primordial baryon asymmetry [94].

Others

Finally, there are also some other additional open questions, which we will now mention very briefly:

- Charge quantization: why the hydrogen atom is neutral? After all, the $U(1)$ charges of quarks and leptons could be totally unrelated, but somehow the sum of the electromagnetic charges of three valence proton quarks is exactly opposite to the electron charge.

- Anomaly cancellation: moreover, why the $U(1)$ charges of the SM are quantized in such a way, that all the gauge anomalies cancel out? This is indeed surprising and may suggest that G_{SM} is in fact a subgroup of a higher dimensional group, e.g. $SO(10)$, in which the cancellation is automatic.

- Gauge coupling unification: the evolution of the SM gauge couplings with the energy computed using the renormalization group equation techniques shows the tendency to bring them very close to each other at some very high scale. This happens at some point roughly from 10^{12} up to 10^{16} GeV. However, this unification is not exact within the SM itself. Note, that such an unification is essential for GUT models where the G_{SM} comes from some higher dimensional simple group. Since adding additional matter fields changes this evolution and may correct the unification picture, also this may suggest that SM is incomplete.

- The flavour puzzle: why the flavour sector seems so complicated and without any guiding principle? The enourmous hierarchies in leptons and quark masses or the completely different mixing patterns in the quark vs. lepton sectors call for a deeper understanding, again necessarily going beyond the SM.

2.2 Supersymmetry

The most straightforward way to tackle the open problems of the SM is to extend it by some new fields (to account for neutrino masses, dark matter, unification etc.) related by additional symmetries (naturalness issues, flavour puzzle). One may thus pose a question: what are the all types of symmetries that can be consistently incorporated into SM?

Although, the question is very general, surprisingly it has a very concrete answer. On very general grounds, the SM is a relativistic local QFT containing a mass gap. In 1967 Coleman and Mandula proved a famous theorem [95], that in this framework the most general symmetry is always a direct product of the Poincaré group and an internal group. This means that the only conserved quantities can be the Poincaré generators and a finite number of Lorentz scalars associated with a Lie algebra of some compact Lie group (e.g. gauge symmetry).[5] This puts strong constraints on possible extensions of the SM.

However, the Coleman-Mandula theorem can be bypassed, as was shown by Haag, Łopuszański and Sohnius in 1975 [96]. The reason is that it restricts only symmetries given by Lie algebras, and not graded algebras. In particular they showed, the $\mathbb{Z}_2$ graded Lie algebra, called *Lie superalgebra*, is the only one of this kind compatible with all the symmetries of the S-matrix. The reason is that its generators are not scalars but rather spinors and instead of commutation relations it involves anti-commutators. The symmetry related to this superalgebra is called *supersymmetry* (SUSY).

In conclusion, the most general symmetries consistent with the Poincaré invariance are the internal symmetries and supersymmetry. This is in a way remarkable fact: the SM exploits *nearly* all possible symmetry structures, and for other reasons we already know that it is incomplete. Maybe including supersymmetry[6] is an answer to both these issues?

Indeed, it seems plausible. The most prominent fact about SUSY theories is that it naturally solves the hierarchy problem. The reason is that, since the supersymmetry generators Q_α are spinors, from the conservation of angular momentum it follows:

$$Q_\alpha|\text{fermion}\rangle = |\text{boson}\rangle \quad \text{and vice versa.} \tag{2.7}$$

It means that every fermionic state has its bosonic suerpartner, and vice versa. For the hierarchy problem it has an important consequence that the radiative corrections to the Higgs mass are exactly cancelled by diagrams with SUSY partners of the SM particle fields in the loops (fermion contributions come with opposite sign to the boson ones and the supersymmetry enforces the couplings to be the same).

It is apparent, that the field content of the SM does not contain enough particles to relate them among each other by the relation (2.7). Especially that a particle and its

[5] Note however, that this theorem only constrains the symmetries of the S-matrix itself. Spontaneously broken symmetries, which do not show up directly on the S-matrix level, are not affected. Moreover, it only applies to Lie algebras and not Lie groups, for instance it does not hold for discrete symmetries or globally for Lie groups.

[6] Theory can have more than one supersymmetry, i.e. where there is more than one type of SUSY generator. The number of generators is by convention denoted by $\mathcal{N}$ and can be equal to $\mathcal{N} = 1, 2, 4$ or 8. In this work we will be interested only in $\mathcal{N} = 1$ SUSY, since this is the one most interesting for phenomenology. Higher supersymmetries can be relevant for building and understanding of more fundamental theories, like the string theory. For an introduction to this topic see e.g [97].

superparnter need to have the same quantum numbers, except the spin. Therefore, in order to extend it by SUSY one needs also to extend the field content. From our point of view, what is extremely important is that, as we will show in Sec. 2.4, this also can provide a very promising dark matter candidate.

Finally, adding new fields changes also the coupling running, as discussed previously. In particular, it can be shown that the minimal supersymmetric extension of the SM, the MSSM, can lead to a much better unification than in the SM itself, see e.g. [98]. From that point of view GUTs seem to favour SUSY over non-supersymmetric theories.

All of the above constitutes a strong motivation for studying supersymmetric extensions of the SM. Below we will introduce shortly the formalism (and notation) used in the construction of the MSSM, discussed in more detail in Sec. 2.3.

The Supersymmetry algebra

The SUSY algebra is given by the following (anti-)commutation relations [99]:

$$\begin{aligned}
\{Q_\alpha, Q_\beta\} &= \{\bar{Q}_{\dot{\alpha}}, \bar{Q}_{\dot{\beta}}\} = 0 \,, \\
\{Q_\alpha, \bar{Q}_{\dot{\beta}}\} &= 2(\sigma^\mu)_{\alpha\dot{\beta}} P_\mu \,, \\
[Q_\alpha, P_\mu] &= [\bar{Q}_{\dot{\alpha}}, P_\mu] = 0 \,, \\
[Q_\alpha, M_{\mu\nu}] &= -\frac{1}{2}(\sigma_{\mu\nu})_\alpha{}^\beta Q_\beta \,, \\
[\bar{Q}_{\dot{\alpha}}, M_{\mu\nu}] &= -\frac{1}{2}(\bar{\sigma}_{\mu\nu})_{\dot{\alpha}}{}^{\dot{\beta}} \bar{Q}_{\dot{\beta}} \,.
\end{aligned} \tag{2.8}$$

The generators Q_α and its conjugate $\bar{Q}_{\dot{\alpha}}$ are fermionic operators and Weyl spinors belonging to the $(1/2, 0)$ and $(0, 1/2)$ representations of the Lorentz group, i.e. left- and right-handed, respectively. Matrices $\sigma_{\mu\nu} = \frac{1}{4}(\sigma_\mu \bar{\sigma}_\nu - \sigma_\nu \bar{\sigma}_\mu)$ are the generators of the special linear group $SL(2, \mathbb{C})$, where $\sigma^\mu \equiv (\mathbf{1}, \sigma^i)$ and $\bar{\sigma}^\mu \equiv (\mathbf{1}, -\sigma^i)$. Finally, P^μ are the generators for space-time translations and $M_{\mu\nu}$ for Lorentz transformations.

Essentially all the properties of SUSY follow from (2.8). The one which is most striking is that a particle X and its superpartner $\tilde{X}$ must have the same mass:

$$m_X^2 |X\rangle = P^2 |X\rangle = P^2 \left(Q|\tilde{X}\rangle\right) = Q\left(P^2|\tilde{X}\rangle\right) = Q m_{\tilde{X}}^2 |\tilde{X}\rangle = m_{\tilde{X}}^2 |X\rangle \,, \tag{2.9}$$

where in the third equality we have used the fact that the SUSY generators commute with the momentum operator P, see Eq. (2.8). This is of course completely ruled out by experiment, since no sparticles have been observed so far. This leads to a conclusion, that if SUSY is there, in inevitably has to be broken (at least at the scale of currently accessible energies). Luckily however, this does not spoil its nice features. Although one might be worried that this brings back again the hierarchy problem, it can be shown that it is not necessarily the case. Indeed, even when SUSY is (softly) broken the hierarchy problem is resolved, as long as the scale of the SUSY breaking is not much larger than TeV [100]. It follows that some fine-tunning is still needed, but considerably less than in the Standard Model.

Superspace and superfields

Having introduced the concept of supersymmetry, now we will turn to its specific realizations in the context of extensions of the SM. An efficient and very elegant way to construct Lagrangians invariant under $\mathcal{N} = 1$ SUSY relies on the so-called superfield and superspace formalism. Superspace extends the four-dimensional Minkowski space by two additional anti-commuting (i.e. Grassmann) dimensions. Thus, the point in this space is described by six coordinates, the usual x^μ four Minkowski space-time coordinates and two additional fermionic ones: θ_α and $\bar{\theta}^{\dot{\alpha}}$. They obey the anti-commutation relations:

$$\{\theta^\alpha, \theta^\beta\} = \{\bar{\theta}^{\dot{\alpha}}, \bar{\theta}^{\dot{\beta}}\} = \{\theta^\alpha, \bar{\theta}^{\dot{\beta}}\} = 0. \tag{2.10}$$

A global SUSY transformation can be constructed from the superalgebra, and has a form:

$$G(x^\mu, \theta, \bar{\theta}) = \exp\left[-i\left(x^\mu P_\mu - \theta Q - \bar{\theta}\bar{Q}\right)\right]. \tag{2.11}$$

From the way how two subsequent transformations add,

$$G(x^\mu, \theta, \bar{\theta})G(y^\mu, \zeta, \bar{\zeta}) = G(x^\mu + y^\mu + i\zeta\sigma^\mu\bar{\theta} - i\theta\sigma^\mu\bar{\zeta}, \theta + \zeta, \bar{\theta} + \bar{\zeta}), \tag{2.12}$$

one can deduce the differential representation of the SUSY generators. They are defined as:

$$Q_\alpha = \frac{\partial}{\partial\theta^a} - i\left(\sigma^\mu\right)_{\alpha\dot{\alpha}}\bar{\theta}^{\dot{a}}\partial_\mu\,, \tag{2.13}$$

$$\bar{Q}_{\dot{\alpha}} = \frac{\partial}{\partial\bar{\theta}^{\dot{\alpha}}} - i\theta^\alpha\left(\sigma^\mu\right)_{\alpha\dot{\alpha}}\partial_\mu\,. \tag{2.14}$$

In analogy to gauge theories one also here defines covariant derivatives D_α and $\bar{D}_{\dot{\alpha}}$. Their form follows from the requirement that they have to commute with the SUSY generators, i.e.:

$$\{D_\alpha, Q_\beta\} = \{D_\alpha, \bar{Q}_{\dot{\beta}}\} = \{\bar{D}_{\dot{\alpha}}, Q_\beta\} = \{\bar{D}_{\dot{\alpha}}, \bar{Q}_{\dot{\beta}}\} = 0\,. \tag{2.15}$$

This, together with Eqs. (2.14) and (2.14), gives:

$$D_\alpha = \frac{\partial}{\partial\theta^a} + i\left(\sigma^\mu\right)_{\alpha\dot{\alpha}}\bar{\theta}^{\dot{a}}\partial_\mu\,, \tag{2.16}$$

$$\bar{D}_{\dot{\alpha}} = -\frac{\partial}{\partial\bar{\theta}^{\dot{\alpha}}} - i\theta^\alpha\left(\sigma^\mu\right)_{\alpha\dot{\alpha}}\partial_\mu\,. \tag{2.17}$$

We are now ready to introduce the main "physical" object, i.e. the superfield. A superfield is a field defined on the superspace. It does not correspond to a single particle, but rather it is a function whose components are members of a single *supermultiplet*. In fact, a general superfield contains 32 degrees of freedom (dof), with half being bosonic and half fermionic. Relations (2.10) ensure that the additional coordinates are nilpotent and therefore the superfield can be expanded in a finite series as:

$$\begin{aligned}\Phi(x, \theta, \bar{\theta}) &= \phi(x) + \theta\psi(x) + \bar{\theta}\bar{\chi}(x) + \theta\theta F(x) + \bar{\theta}\bar{\theta}H(x) + \theta\sigma_\mu\bar{\theta}A^\mu(x) \\ &+ (\theta\theta)\bar{\theta}\bar{\lambda}(x) + (\bar{\theta}\bar{\theta})\theta\xi(x) + (\theta\theta)(\bar{\theta}\bar{\theta})D(x).\end{aligned} \tag{2.18}$$

The components of this expansion are: the scalar fields ϕ, F, H and D, the vector field A^μ and the Weyl spinors ψ, $\bar{\chi}$, $\bar{\lambda}$ and ξ. The superfield defined above is in a reducible representation of the supersymmetry algebra. To obtain irreducible representations one imposes some constraints on Φ. In particular, to construct a supersymmetric field theory of particles up to spin 1 (i.e. without gravity) one needs two type of superfields: chiral (containing matter fields) and vector (with gauge fields).

The (left-)chiral superfield is defined by imposing the condition:

$$\bar{D}_{\dot{\alpha}}\Phi = 0. \tag{2.19}$$

This condition gets rid of 24 degrees of freedom, and the chiral superfield is left with 8 dof. It contains two complex scalar fields ϕ and F and one Weyl fermion ψ and it can be expanded as:

$$\begin{aligned}\Phi(x,\theta,\bar{\theta}) &= \phi(x) + i\theta\sigma^\mu\bar{\theta}\partial_\mu\phi(x) + \frac{1}{4}(\theta\theta)(\bar{\theta}\bar{\theta})\Box\phi(x) \\ &+ \sqrt{2}\theta\psi(x) - \frac{i}{\sqrt{2}}(\theta\theta)\partial_\mu\psi(x)\sigma^\mu\bar{\theta} + (\theta\theta)F(x).\end{aligned} \tag{2.20}$$

Note, that on-shell the Weyl fermion has 2 dof and it might seem that the number of bosonic and fermionic dof do not match. However, then the equations of motion for the field F become trivial and on-shell $F = 0$. Therefore, it is called an auxiliary field.

The SUSY gauge transformations with generators T^a and gauge coupling g transform a chiral superfield as

$$\Phi \to e^{-2\,i\,g\Lambda}\Phi\ , \tag{2.21}$$

where $\Lambda = \Lambda^a T^a$ and $\Lambda^a(x,\theta,\bar{\theta})$ are chiral superfields.

A product of two chiral superfields is a chiral superfield. On the other hand, the product of a chiral and a conjugated chiral superfield gives a vector superfield. The vector superfield V is obtained from a superfield (2.18) by imposing the reality condition:

$$V = V^\dagger. \tag{2.22}$$

This condition removes half of the degrees of freedom and leads to an explicit form:

$$\begin{aligned}V(x,\theta,\bar{\theta}) &= C(x) + i\,\theta\chi(x) - i\,\bar{\theta}\bar{\chi}(x) + \theta\sigma^\mu\bar{\theta}A_\mu(x) \\ &+ \frac{i}{2}\theta\theta\left[M(x) + i\,N(x)\right] - \frac{i}{2}(\bar{\theta}\bar{\theta})\left[M(x) - i\,N(x)\right] \\ &+ i(\theta\theta)\bar{\theta}\left[\bar{\lambda}(x) + \frac{i}{2}\bar{\sigma}^\mu\partial_\mu\chi(x)\right] - i(\bar{\theta}\bar{\theta})\theta\left[\lambda(x) + \frac{i}{2}\sigma^\mu\partial_\mu\bar{\chi}(x)\right] \\ &+ \frac{1}{2}(\theta\theta)(\bar{\theta}\bar{\theta})\left[D(x) - \frac{1}{2}\partial^\mu\partial_\mu C(x)\right]\ ,\end{aligned} \tag{2.23}$$

where C, M, N and D are (real) scalar fields, χ and λ are complex Weyl fermions and A_μ is a real vector field. A vector superfield defined in this way still contains redundant degrees of freedom. This can be realized by noticing that the transformation:

$$V \to V + i(\Lambda - \bar{\Lambda}), \tag{2.24}$$

where Λ is a generic chiral superfield, implies the A_μ component change of the form of Abelian gauge transformation. Therefore, it is a straightforward generalization of the gauge symmetry. In general, non-Abelian SUSY gauge transformation has the form

$$e^{2gV} \to e^{-2\,i\,g\bar{\Lambda}} e^{2gV} e^{2\,i\,g\Lambda} , \tag{2.25}$$

again where $V = V^a T^a$.

To reduce the number of components even more one chooses a partial gauge fixing, typically of the Wess-Zumino form [101]. This, at the cost of losing manifest supersymmetry, fixes $C = M = N = 0$ and $\chi = 0$ and we end up with the gauge field A_μ, its fermionic superpartner λ (called the gaugino), and the auxiliary field D:

$$V(x,\theta,\bar{\theta}) = \theta\sigma^\mu\bar{\theta}A_\mu(x) + i(\theta\theta)\bar{\theta}\bar{\lambda}(x) - (\bar{\theta}\bar{\theta})\theta\lambda(x) + \frac{1}{2}(\theta\theta)(\bar{\theta}\bar{\theta})D(x). \tag{2.26}$$

SUSY invariant actions

At this point we have all the ingredients to write actions which are manifestly invariant under supersymmetry.

Under global SUSY transformation (2.11) both the F-term of the chiral superfield and the D-term of the vector superfield transform as total derivatives. Thus we immediately find two classes of globally supersymmetric actions constructed from these terms:

$$\int \mathrm{d}^4x \int \mathrm{d}^2\theta \mathcal{L}|_F \qquad \text{and} \qquad \int \mathrm{d}^4x \int \mathrm{d}^2\theta \mathrm{d}^2\bar{\theta} \mathcal{L}|_D \, . \tag{2.27}$$

The first one contains only function of F-terms, that is a function of chiral superfields and provides us with mass terms for the fermions and Yukawa-type interactions. It can be easily seen that it does not contain any derivatives and therefore contributes to the potential. Moreover, due to the condition (2.19), it does contain only Φ and not $\bar{\Phi}$. This term is thus holomorphic and is called a *superpotential* W. Its most general renormalizable form is:

$$W(\{\Phi_i\}) = \sum_i a_i\Phi_i + \frac{1}{2}\sum_{ij} m_{ij}\Phi_i\Phi_j + \frac{1}{3!}\sum_{ijk}\lambda_{ijk}\Phi_i\Phi_j\Phi_k \, , \tag{2.28}$$

where the couplings m_{ij} and λ_{ijk} are totally symmetric under the interchange of i, j, k.

In terms of the component fields (2.20) it gives:

$$\begin{aligned}\int \mathrm{d}^2\theta\, W(\{\Phi_i\}) &= \sum_i a_i F_i + \sum_{ij} m_{ij}\left(\phi_i F_j - \frac{1}{2}\psi_i\psi_j\right) + \sum_{ijk}\frac{\lambda_{ijk}}{2}\left(\phi_i\phi_j F_k - \phi_i\psi_j\psi_k\right) \\ &= \sum_j \frac{\partial W(\phi)}{\partial\phi_j}F_j - \frac{1}{2}\sum_{jk}\frac{\partial^2 W(\phi)}{\partial\phi_j\partial\phi_k}\psi_j\psi_k \, .\end{aligned} \tag{2.29}$$

The kinetic terms of the matter fields come from the second class, i.e. built from D-terms. The simplest (and renormalizable) choice would be $\bar{\Phi}\Phi|_D$.[7] However, in this

[7] More generally, one can replace it by a real function $K(\bar{\Phi}_i, \Phi_j)$, called the Kähler potential. This leads to a non-linear σ-models and is useful for studying effective filed theories, e.g. in string phenomenology.

simplest form it is not invariant under super gauge transformations. To correct this problem, one follows the minimal coupling procedure: promotes the original derivatives to covariant ones:

$$\partial_\mu \to D_\mu = \partial_\mu + i\, g A^a_\mu T^a \ , \tag{2.30}$$

and modifies:

$$\bar{\Phi}\Phi \to \bar{\Phi}\, e^{2gV}\Phi \ . \tag{2.31}$$

Thus this part of the Lagrangian, in the component notation, reads:

$$\mathcal{L}|_D = \sum_i \Big[D_\mu\phi_i D^\mu\phi_i^* + i\,\bar{\psi}_i\bar{\sigma}^\mu D_\mu\psi_i - \sqrt{2}g\left(\bar{\psi}_i\bar{\lambda}\psi_i + \psi_i^*\lambda\psi_i\right) + g\phi_i^* T^a D^a\psi_i + F_i^* F_i \Big] \ . \tag{2.32}$$

Note, that by including covariant derivatives we automatically add also SUSY-gauge interaction terms.

To construct kinetic terms for the gauge bosons and gauginos one defines another chiral superfield built from the original vector one V, by:

$$W_\alpha \equiv \frac{1}{4}\bar{D}\bar{D}\, e^{-2gV} D_\alpha e^{2gV} . \tag{2.33}$$

Since it is a chiral superfield, $\int \mathrm{d}^2\theta\ \mathrm{Tr}(W_\alpha W^\alpha)$ will be SUSY (and clearly also gauge) invariant. Therefore, with proper normalization, the missing part we need to add is:

$$\mathcal{L}_{\text{kin}} = \frac{1}{16g^2}\int \mathrm{d}^2\theta \mathrm{Tr}(W_\alpha W^\alpha). \tag{2.34}$$

Again translating it into component notation we see that it indeed contains kinetic terms for both gauge bosons and gauginos and couplings between them:

$$\mathcal{L}_{\text{kin}} = -\frac{1}{4}F^a_{\mu\nu}F^{\mu\nu\,a} + i\,\bar{\lambda}^a\bar{\sigma}^\mu(D_\mu\lambda)^a + \frac{1}{2}D^a D^a \ . \tag{2.35}$$

In conclusion, the full Lagrangian is:

$$\mathcal{L}_{SUSY} = \int \mathrm{d}^2\theta W(\{\Phi_i\}) + \frac{1}{16g^2}\int \mathrm{d}^2\theta \mathrm{Tr}(W_\alpha W^\alpha) + \int \mathrm{d}^2\theta\mathrm{d}^2\bar{\theta}\bar{\Phi}\, e^{2gV}\Phi + \text{h.c.} \tag{2.36}$$

For completeness, note that for an Abelian vector superfields one can also include another contribution, called the *Fayet-Iliopoulos term* [102] of the form:

$$\mathcal{L}_{FD} = \int \mathrm{d}^4\theta \xi V = \xi D(x), \tag{2.37}$$

where ξ is just a constant. This affects only the potential, shifting the D-term contribution by a coefficient ξ. This term is however not present in the MSSM and thus we will not consider it in more detail.

Superfield	Type	SM fields	Superpartners	$(SU(3)_C, SU(2)_L, U(1)_Y)$
Q	chiral	$\begin{pmatrix} u \\ d \end{pmatrix}_L$	$\begin{pmatrix} \tilde{u} \\ \tilde{d} \end{pmatrix}_L$	$\left(\mathbf{3}, \mathbf{2}, +\frac{1}{3}\right)$
$\bar{U}$		$\bar{u}_R$	$\tilde{u}_R^*$	$\left(\overline{\mathbf{3}}, \mathbf{1}, -\frac{4}{3}\right)$
$\bar{D}$		$\bar{d}_R$	$\tilde{d}_R^*$	$\left(\overline{\mathbf{3}}, \mathbf{1}, +\frac{2}{3}\right)$
L	chiral	$\begin{pmatrix} \nu \\ e \end{pmatrix}_L$	$\begin{pmatrix} \tilde{\nu} \\ \tilde{e} \end{pmatrix}_L$	$(\mathbf{1}, \mathbf{2}, -1)$
$\bar{E}$		$\bar{e}_R$	$\tilde{e}_R^*$	$(\mathbf{1}, \mathbf{1}, +2)$
G^a	vector	g^a	$\tilde{g}^a$	$(\mathbf{8}, \mathbf{1}, 0)$
W^i		W^i	$\tilde{W}^i$	$(\mathbf{1}, \mathbf{3}, 0)$
B		B	$\tilde{B}$	$(\mathbf{1}, \mathbf{1}, 0)$
H_u	chiral	$\begin{pmatrix} h_u^+ \\ h_u^0 \end{pmatrix}_L$	$\begin{pmatrix} \tilde{h}_u^+ \\ \tilde{h}_u^0 \end{pmatrix}_L$	$(\mathbf{1}, \mathbf{2}, +1)$
H_d		$\begin{pmatrix} h_d^0 \\ h_d^- \end{pmatrix}_L$	$\begin{pmatrix} \tilde{h}_d^0 \\ \tilde{h}_d^- \end{pmatrix}_L$	$(\mathbf{1}, \mathbf{2}, -1)$

Table 2.2: The field content of the MSSM. The SUSY partners of the SM fields are denoted with a tilde. The subscripts L and R of the scalar SUSY fields refer to the chirality of the corresponding fermionic partner. To simplify the notation the family and colour indices for the chiral matter fields are suppressed. The index $a = 1, \ldots, 8$ enumerates the vector superfields of $SU(3)_C$ and the index $i = 1, 2, 3$ of $SU(2)_L$. The Higgs sector is extended with respect to the SM in order to preserve supersymmetry in a phenomenologically viable way.

2.3 Field content of the MSSM

The SM is not a supersymmetric theory. In order to exhibit SUSY invariance it has to be extended by additional field content. This can be done in many ways, among which we will discuss the minimal one, called the Minimal Supersymetric Standard Model (MSSM). It is minimal in the sense that it introduces the least possible amount of new fields while preserving supersymmetry and all the desirable features of the SM.

The first step in constructing the MSSM is to decide in what supermultiplets embed the SM fields. Since fermions belong to the fundamental representation of the gauge group, while gauge bosons to an adjoint, it is not possible to put them together inside the same supermultiplet. Therefore, SM quarks and leptons are placed in (separate) chiral multiplets, while gauge bosons in a vector ones. The remaining degrees of freedom are filled by superpartners: additional particles added to the SM. They consist of scalar partners of quarks and leptons, with the corresponding names with added prefix "s" (short for scalar).

In fact, the left- and right-handed pieces of the quarks and leptons have different gauge transformation properties, so each must have its own complex scalar partner. Note, that the L and R in the name of squarks and sleptons denote the chirality of its corresponding

superpartner. It is important to keep in mind that it has nothing to do with the transformation properties of sfermions, but it affects the gauge interactions. In particular, only the left squarks couple to W boson, while right do not.

The vector multiplet apart from gauge bosons need to contain also fermions. They are called gauginos and belong to an adjoint representation of the gauge group. These are the so-called gluinos, charginos and neutralinos.

Finally, to complete the model one needs to specify the Higgs sector. Because Higgs is a scalar it has to reside in another chiral multiplet and be accompanied by a Weyl fermion superpartner, called Higgsino. In fact, it turns out that one Higgs doublet is not enough. There are two way to see this. Firstly, as discussed previously, the superpotential has to be holomorphic. It follows, that it cannot contain both a field and its conjugate. Hence, to provide masses to both up-type and down-type quarks one needs two Higgs doublets.

Second reason is that it is needed to cancel the gauge anomaly. In the case of one Higgs chiral superfield its fermionic component must be a weak isodoublet with non-zero weak hypercharge. This adds a contribution to the triangle gauge anomaly, which in the SM itself is accidentally vanishing. One needs another contribution with opposite hypercharge to cancel it out. Thus, finally the MSSM Higgs sector comprises two scalar Higgs doublets and four Higgsinos: two neutral and two charged. After the EWSB three scalar degrees of freedom are eaten by the longitudinal components of the massive gauge bosons, and we are left with five spin-0 particles: h, H^0, $H^\pm$ and A, where the first two are real scalars and last one is a pseudoscalar.

The full field content of the MSSM is summarized in Tab. 2.2.

2.3.1 The superpotential and R-parity

The most general superpotential invariant under G_{SM} built out of the field content of the MSSM can be written as [103, 104]:

$$W = (Y_u)_{ij} Q_i \epsilon H_u \bar{U}_j - (Y_e)_{ij} L_i \epsilon H_d \bar{E}_j - (Y_d)_{ij} Q_i \epsilon H_d \bar{D}_j + \mu H_d \epsilon H_u \tag{2.38}$$

$$+ \frac{1}{2}\lambda_{ijk} L_i \epsilon L_j \bar{E}_k + \lambda'_{ijk} L_i \epsilon Q_j \bar{D}_k + \kappa_i L_i \epsilon H_u + \frac{1}{2}\lambda''_{ijk} \bar{D}_i \bar{D}_j \bar{U}_k \, . \tag{2.39}$$

Here, we suppressed gauge indices and introduced the ϵ tensors to account for contracting the $SU(2)_L$ indices.

This decomposes into two distinct parts. The first line (2.38) induces fermion Yukawa couplings and masses and the last term, so-called μ-term, is crucial for electroweak symmetry breaking. Therefore, this part is clearly necessary ingredient.

On the other hand, second line (2.39) is phenomenologically dangerous. Its first three terms violate lepton number while the last one violates the baryon one. This leads to very rapid proton decay [105, 106], unless the coefficients are strongly suppressed.

Note, that in the SM proton is stable due to the baryon and lepton number being (accidentally) exact symmetries. As we can see, this is no longer the case in the MSSM, and to solve this problem an additional symmetry has to be invoked. This is chosen to be a discrete symmetry, the so-called R-parity. It introduces to each particle a multiplicative discrete quantum number:

$$P_R = (-1)^{3(B-L)+2s} \tag{2.40}$$

where B is the baryon number, L the lepton number and s the spin of the particle. It can be easily seen that this gives 1 for SM fields and -1 for SUSY particles. This symmetry forbids the dangerous (2.39) terms and is the main reason why MSSM can provide successful dark matter candidate (see Sec. 2.4).

2.3.2 SUSY breaking and soft parameters

Having described the field content and symmetry constraints, a natural continuation would be to discuss the spectrum. The crucial observation has been already made: supersymmetry requires the same masses for particles and its superpartners and therefore it has to be broken.

How does it happen? This is one of the most important open questions in the subject. It is most probable, that the breaking is spontaneous and that it occurs in some hidden sector and is then mediated to our "visible sector" through some messengers. Obviously, this can be done in plenty of ways, among which the most important are: gravity-mediation [107], gauge-mediation [108], anomaly-mediation [109] or by other effects induced by extra dimensions [110].

Although the precise mechanism is unknown, we can still parametrize the effects of supersymmetry breaking in a model independent way. This approach became an inherent ingredient of the MSSM, in which the SUSY breaking is parametrized by introducing more than 100 free parameters. Those, however, should not be considered to be fundamental parameters of the theory: once the breaking mechanism is known, they will be related with (hopefully) much smaller number of more fundamental parameters.[8]

The way to parametrize the breaking is by introducing explicitly SUSY breaking terms into the Lagrangian. The only constraint we put is that those terms are *soft*, i.e. of a mass dimension at least one. This is done in order to ensure that they do not reintroduce quadratic divergences in the theory and thus bring again the hierarchy problem.

The soft parameters can be classified as follows:[9]

- mass terms for the gauginos

$$-\frac{1}{2}(M_1\tilde{B}\tilde{B} + M_2\tilde{W}\tilde{W} + M_3\tilde{g}\tilde{g}) + \text{h.c.}\,, \tag{2.41}$$

- mass parameters for the Higgses

$$-m_{h_u}^2 h_u^\dagger h_u - m_{h_d}^2 h_d^\dagger h_d - (b h_u \epsilon h_d + \text{h.c.})\,, \tag{2.42}$$

[8] In fact from this point of view, supersymmetry as an extension to the SM is a very economical idea. Without SUSY breaking, despite doubling the field content, the only one new parameter is μ, which mixes the two Higgs superfields in the superpotential, see (2.38). It predicts also a handful of relations between various couplings, leading to (in principle) clear pattern for distinguishing it from other beyond the Standard Model (BSM) scenarios. Let us just mention, that this additional parameter is connected with the arising naturalness problem, called the μ-problem [111, 112], which may suggest a direction to go beyond the MSSM.

[9] In principle, additional fermionic terms could also be included, but they can be reabsorbed by appropriate redefinitions of the superpotential and the above soft terms.

- sfermion mass matrices

$$-\tilde{q}_L^\dagger m_{\tilde{Q}}^2 \tilde{q}_L - \tilde{u}_R^* m_{\tilde{U}}^2 \tilde{u}_R - \tilde{d}_R^* m_{\tilde{D}}^2 \tilde{d}_R - \tilde{l}_L^\dagger m_{\tilde{L}}^2 \tilde{l}_L - \tilde{e}_R^* m_{\tilde{E}}^2 \tilde{e}_R \,, \tag{2.43}$$

- trilinear couplings

$$-\left(A_U \tilde{q}_L h_u \tilde{u}_R^* - A_D \tilde{q}_L h_d \tilde{d}_R^* - A_E \tilde{l}_L h_d \tilde{e}_R^*\right) + \text{h.c.} \tag{2.44}$$

Note, that since the F- and D-terms contribute positively to the Higgs potential, one needs the negative soft supersymmetry breaking terms for the Higgs scalars in order to obtain electroweak symmetry breaking.

The number of free parameters introduced in soft terms may be reduced under some reasonable assumptions about the flavour sector. The reason is that the sfermion masses and trilinear couplings are matrices in the family space and thus they induce mixings which can give rise to new flavour changing processes. Additionally, if the complex phases of the soft parameters are not constrained in any way, they generically lead to unobserved CP violation, e.g. in the electric dipole moments [113].

The flavour problem can be evaded if the SUSY breaking is universal, i.e. squarks and slepton masses are flavour blind. This also clearly reduces the number of parameters, since all the sfermion masses are then proportional to the identity matrix. On the other hand additional CP violation can be removed assuming that the soft parameters do not bring any new phases, i.e. reality of gaugino masses and trilinear couplings. Let us again emphasize, that it is conceivable that these properties follow from more fundamental theory, e.g. flavour blindness is a feature of gravity or gauge mediation.

2.3.3 The spectrum

In this section we briefly summarize the MSSM spectrum. The gauge eigenstates of Tab. 2.2 after EWSB acquire mixings and are no longer mass eigenstates. This happens both for SM particles and their superparnters. Note however, that the standard model states are not altered at the tree level (apart from the extended Higgs sector) and therefore below we describe what happens only with the additional particles.

Sfermions

For every fermion in the SM we have two scalar partners appearing in the spectrum. After the EWSB the L and R scalars mix and give two different mass eigenstates. In general the mass matrices have a form:

$$M_{\tilde{f}}^2 = \begin{pmatrix} m_f^2 + m_{LL}^2 & m_f X_f \\ m_f X_f & m_f^2 + m_{RR}^2 \end{pmatrix}, \tag{2.45}$$

where

$$m_{LL}^2 = m_{\tilde{f}_L}^2 + \left(I_f^3 - Q_f s_W^2\right) m_Z^2 \cos 2\beta \,, \tag{2.46}$$

$$m_{RR}^2 = m_{\tilde{f}_R}^2 + Q_f s_W^2 m_Z^2 \cos 2\beta \,, \tag{2.47}$$

$$X_f = A_f - \frac{\mu}{(\tan\beta)^{2I_f^3}}, \tag{2.48}$$

and $\tan\beta \equiv v_d/v_u$, i.e. is the ratio of the VEV of two Higgs fields, which satisfy $(v_u+v_d)^2 = v^2$. After diagonalization one gets two mass eigenstates for every sfermion pair:

$$m^2_{\tilde{f}_{1,2}} = m^2_f + \frac{1}{2}\left[m^2_{LL} + m^2_{RR} \mp \sqrt{(m^2_{LL} - m^2_{RR})^2 + 4m^2_f X^2_f}\right]. \tag{2.49}$$

Especially interesting case is the stop squark in which this mixing can be very large, if the $X_t = A_t - \mu/\tan\beta$ is large. The reason is that then the lighter of the pair can be as light as the t quark (or even lighter) and much lighter than all the other sfermions. This is important for the neutralino dark matter in the stop co-annihilation region, see Sec. 2.4.1.

Gauginos and Higgsinos

The fermionic sector is composed of the superpartners to gauge bosons and Higgses. The charged ones, i.e. two Winos and two Higgsinos, mix to form charginos, while the neutral Wino, Bino and Higgsions form neutralinos.

- The charginos mass terms in the Lagrangian are given by

$$(\tilde{W}^-, \tilde{h}_u^-) M_{\tilde{\chi}^\pm} \begin{pmatrix} \tilde{W}^+ \\ \tilde{h}_d^+ \end{pmatrix} + \text{h.c}, \tag{2.50}$$

  with a tree level mass matrix:

$$M_{\tilde{\chi}^\pm} = \begin{pmatrix} M_2 & \sqrt{2}m_W s_\beta \\ \sqrt{2}m_W c_\beta & \mu \end{pmatrix}, \tag{2.51}$$

  where we used a short notation $s_\beta = \sin\beta$ and $c_\beta = \cos\beta$. The one-loop corrections to the mass matrix in this case can typically be safely neglected as they are often very small [114]. However, one important exception is the pure Wino case, where the radiative corrections due to custodial symmetry breaking introduce a mass shift of lighter chargino by about 0.17 GeV [115]. This is an important point in the computation of the Sommerfeld effect in the MSSM, see Sec. 4.3.

- The neutralinos are a combination of gauginos and higgsions with the mass matrix in the basis $(\tilde{B},\tilde{W}^3,\tilde{h}_1^0,\tilde{h}_2^0)$:

$$M_{\tilde{\chi}^0} = \begin{pmatrix} M_1 & 0 & -c_\beta s_W m_Z & s_\beta s_W m_Z \\ 0 & M_2 & c_\beta c_W m_Z & -s_\beta c_W m_Z \\ -c_\beta s_W m_Z & c_\beta c_W m_Z & \delta_{33} & -\mu \\ s_\beta s_W m_Z & -s_\beta c_W m_Z & -\mu & \delta_{44} \end{pmatrix}. \tag{2.52}$$

  They can be diagonalized to form four states $\tilde{\chi}_i^0$

$$\tilde{\chi}_i^0 = N_{i1}\tilde{B} + N_{i2}\tilde{W}^3 + N_{i3}\tilde{h}_1^0 + N_{i4}\tilde{h}_2^0,$$

  lightest of which, $\tilde{\chi}_1^0$, is called *the* neutralino. A useful parameter is a gaugino fraction defined as

$$Z_g^i = |N_{i1}|^2 + |N_{i2}|^2. \tag{2.53}$$

Typically one calls the neutralino Higgsino-like whenever $Z_g^1 < 0.01$ and gaugino like for $Z_g^1 < 0.99$.

In the mass matrix we introduced also two one-loop contributions, δ_{33} and δ_{44}. They are the most important ones in the case of Higgsino-like neutralino and come from dominantly quark-squark loops. The full expressions for these corrections are rather lengthy and not particularly illuminating. They can be found in [114] and are included in the DarkSUSY code.

- The gluinos, the superpartners of the gluon, are an octet fermion and therefore cannot mix with any other particle of the MSSM, even if R-parity is broken. Hence, they are not affected by the EWSB and are their own mass eigenstate. In models with minimal supergravity or gauge mediation, the gluino mass parameter is related to the Bino and Wino by:

$$M_3 = \frac{\alpha_s}{\alpha} s_W^2 M_2 = \frac{3}{5}\frac{\alpha_s}{\alpha} c_W^2 M_1. \tag{2.54}$$

This implies that at a TeV scale $M_3 : M_2 : M_1 \sim 6 : 2 : 1$, and hence that it is reasonable to suspect that in most of the situations the gluino is considerably heavier than lightes neutralinos and charginos.

The Higgs sector

As we already mentioned, in the MSSM there are five physical Higgs bosons: neutral scalars h, H^0, complex scalar $H^\pm$ and a pseudoscalar A. The Higgs sector has two free parameters, one of which is the $\tan\beta$ and the second one is conveniently chosen to be the pseudoscalar mass m_A. Then the remaining masses are expressed as:

$$m^2_{h,H^0} = \frac{1}{2}\left[m_A^2 + m_Z^2 \mp \sqrt{(m_A^2 + m_Z^2)^2 - 4m_Z^2 m_A^2 \cos^2 2\beta}\right], \tag{2.55}$$

$$m^2_{H^\pm} = m_A^2 + m_W^2 \,. \tag{2.56}$$

This expressions show a famous tree-level bound for the lighter neutral Higgs h mass, being:

$$m_h \leqslant m_Z |\cos 2\beta|, \tag{2.57}$$

which is already excluded by experiment. Fortunately, the loop corrections give large contributions and depending on the model parameters one can relax considerably this upper bound. Nevertheless, one can see that supersymmetry favours light Higgs, which is also desirable in the light of EWPT [30].

2.4 Supersymmetric dark matter

In the Section 1.2 we presented the necessary conditions that a particle have to satisfy in order to be considered a dark matter candidate. The most important of these were stability and no (or nearly no) coupling to the photons. In the supersymmetric extensions

to the SM several particles can satisfy these criteria, depending on the precise model for the SUSY breaking and the values of the parameters. In particular, stability of the LSP is ensured by the conservation of R-parity. Therefore, potential candidates could be those neutral particles which at least in some realizations of the model can be the LSP. In the MSSM these are: neutralinos or sneutrinos. When supersymmetry is made local and we consider supergravity theories one also has gravitinos (spin 3/2 superpartners of gravitons) as a viable, and interesting possibility. Finally, if the Peccei-Quinn extension of the SM is promoted to a supersymmetric theory, a fermionic superpartner of an axion, called *axino*, can be additional supersymmetric candidate.

Below we briefly describe all these possibilities paying most attention on the most promising and widely studied one, the neutralino.

2.4.1 Neutralino

In the most regions of the allowed parameter space of the MSSM the LSP is the neutralino. Therefore, it is the most natural dark mater candidate within supersymmetric theories.

Indeed, from a theoretical point of view it is rather difficult to describe and classify all its possible realizations. Even constraining ourselves to the MSSM, without invoking any of its extensions or effective approaches, we are left with far too large parameter space to probe. Therefore, the philosophy is rather to concentrate on the simpler (motivated theoretically) scenarios and simultaneously hope for positive signals from the experiments, giving hints about the dark matter properties.

One of such scenarios is the so-called Constrained MSSM (CMSSM). It is based on a SUSY breaking scenario inspired by supergravity theories where SUSY breaking is mediated via gravitational interactions [116, 117, 118, 119]. It relies on several assumptions constraining the parameter space of the general MSSM, steeming from requirements of gauge coupling unification at the GUT scale and the flavour puzzle. One then imposes the conditions at a GUT scale:

- gaugino masses universality

$$M_1 = M_2 = M_3 \equiv m_{1/2} \ , \tag{2.58}$$

- scalar (sfermion and Higgs) masses universality

$$m^2_{\tilde{Q}} = m^2_{\tilde{U}} = m^2_{\tilde{D}} = m^2_{\tilde{L}} = m^2_{\tilde{E}} = m_0^2 \mathbf{1} \qquad m_{h_u} = m_{h_d} \equiv m_0 \ , \tag{2.59}$$

- trilinear couplings universality

$$A_U = A_D = A_E \equiv A_0 \mathbf{1} \ . \tag{2.60}$$

All these conditions hold at a GUT scale and are then broken by the RGE evolution, so that at low energies one obtains a phenomenologically viable spectrum. Nevertheless, imposing relations of this kind will result in some specific patterns in the low energy

spectrum. In particular, in the CMSSM the Bino and Wino mass parameters at EW scale are related by:

$$M_1 = \frac{5}{3}\tan^2\theta_W M_2 \approx 0.5 M_2, \tag{2.61}$$

which leads to the conclusion that the Wino component of the lightest neutralino is always subdominant in this model.

After imposing these conditions we are left with only five free parameters: $m_{1/2}$, A_0, m_0, $\tan\beta$ and $\mathrm{sign}(\mu)$. The absolute value of μ is determined from the conditions for EWSB. Indeed, demanding radiative electroweak symmetry breaking, minimization of the Higgs potential gives the relations:

$$b = \frac{1}{2}\left[(m_{h_u}^2 - m_{h_d}^2)\tan 2\beta + M_Z^2 \sin 2\beta\right], \tag{2.62}$$

$$\mu^2 = \frac{m_{h_d}^2 \sin^2\beta - m_{h_u}^2 \cos^2\beta}{\cos 2\beta} - \frac{M_Z^2}{2}, \tag{2.63}$$

which means that the absolute value of μ is fixed, but the sign can be either plus or minus. However, μ is often chosen to be positive as favoured by the constraint from the anomalous magnetic moment of the muon.[10]

The model can be simplified even more, if one further assumes a relation between the bilinear and trilinear soft breaking terms and additionally a relation between the gravitino and scalar masses. Then the resulting model is called minimal supergravity (mSUGRA) since a minimal choice for the Kähler potential is used [118]. The main difference between it and CMSSM concerns the gravitino mass, which is not relevant in the scenarios of the neutralino being the LSP.

In this framework the properties of the neutralino can be studied in some more detail. In particular, as we mentioned above in the CMSSM the neutralino is mostly Bino, therefore couples very weakly to both the Z and the Higgs bosons. In the early Universe it annihilates mainly into SM fermions via sfermion t-channel exchange. This process is however not efficient enough, for the reason that it is helicity suppressed (see Sec. 3.1.1), leading typically to overproduction of the Bino dark matter. To avoid this one needs to choose the regions of parameter space in which the annihilations are particularly effective. This can happen in three distinctive cases: *i)* neutralino has significant Higgsino or Wino component, opening a much more effective annihilation channel into gauge bosons, *ii)* annihilations proceed via a resonance or *iii)* relic density is strongly affected by co-annihilations.

This translates to five distinct regions of the parameter space giving a correct thermal relic density (see also Fig. 2.2 borrowed from [122]):

- The *bulk region*: small $(m_{1/2}, m_0)$, annihilation goes mainly through t-channel sfermion exchange. This region is now mostly excluded by the LHC slepton searches and the measured value of the Higgs boson mass.

[10] The Standard Model predictions for the value of the anomalous magnetic moment of the muon are lower from the experimentally obtained value, with a statistical significance of about 3σ, but subject to considerable theoretical uncertainties [120]. The additional contributions from SUSY have are typically proportional to $\mathrm{sign}(\mu)$ and therefore $\mu > 0$ is generically favoured. For a review of the muon magnetic moment and supersymmetry see e.g. [121].

- The *stau co-annihilation region* [123]: still at low m_0, but slightly larger $m_{1/2}$, the neutralino is close in mass to the $\tilde{\tau}$ and co-annihilations are driving the relic density to observed value.

- The *funnel region* [124, 125]: relies on the resonance with one of the Higgs bosons. One possibility is for low $m_{1/2}$ when $2m_\chi \approx m_h$, so that the neutralinos have an enhanced annihilation rate through the narrow s-channel light Higgs resonance. Essentially excluded by the LHC results. Second, still allowed, is at large values of $\tan\beta$ where the mass of the pseudoscalar Higgs boson A is unsuppressed, when $2m_\chi \approx m_A$, so that the neutralino has an enhanced annihilation rate through the s-channel A-resonance.

- The *hyperbolic branch/focus point region* [126, 127]: at large m_0, where the neutralino obtains a significant Higgsino fraction.

- The *stop co-annihilation region* [128, 129]: when the $m_\chi \approx m_{\tilde{t}}$ and the very effective co-annihilation with the $\tilde{t}$ are present. This needs very light stops and thus is not captured in the $(m_{1/2}, m_0)$ planes for $A_0 = 0$, but it rather needs large negative values of A_0, see Fig. 2.3. Although stringent constraints on light stop are put by the new LHC results, still the scenario when it is degenerated in mass with the netralino is allowed [130].

From this discussion it is quite clear, that although many possible realizations compatible with experimental data exists, they are also constrained to rather narrow slices of the parameter space. In fact, those regions are critically sensitive to some of the soft SUSY breaking parameters. Moreover, this conclusion persists also if we depart from the constrained models like CMSSM or mSUGRA and allow much wider parameter space.

This brings again fine tuning into the game and produces an naturalness issue. One way of (partially) resolving it is the so-called *well-tempered neutralino* [53]. The idea is the following. When one varies the values of the soft terms, one finds that Ω_χ is typically too large (Bino LSP) or too small (Higgsino or Wino LSP). However, since Ω_χ is a continuous function of parameters, one should obtain a correct relic density also somewhere in between these limiting cases. This does not eliminate the fine tuning issue, but at least makes it somewhat less severe.

On the other hand, the fine tuning related to the relic density constraint can be resolved in the scenarios of split-supersymmetry [132, 133], i.e. when SUSY does not solve the hierarchy problem and the spectrum posses light Higgs and possibly the LSP, while other particles are considerably heavier. In this case the values of μ and M_2 at a TeV scale are perfectly acceptable and one can obtain naturally the Higgsino or Wino LSP with correct relic abundance. The motivation for this scenario got recently stronger due to null results of sparticles searches in the LHC. In particular, the gluino masses are constrained (roughly, since very model-dependent) to be larger than 1 TeV, pushing up the allowed region for all the SUSY particles. This possibility, the TeV scale neutralino, is the one on which we are concentrating in the work described in this thesis: the impact of higher order effects onto the relic density computations and indirect detection searches, discussed in the following Chapters.

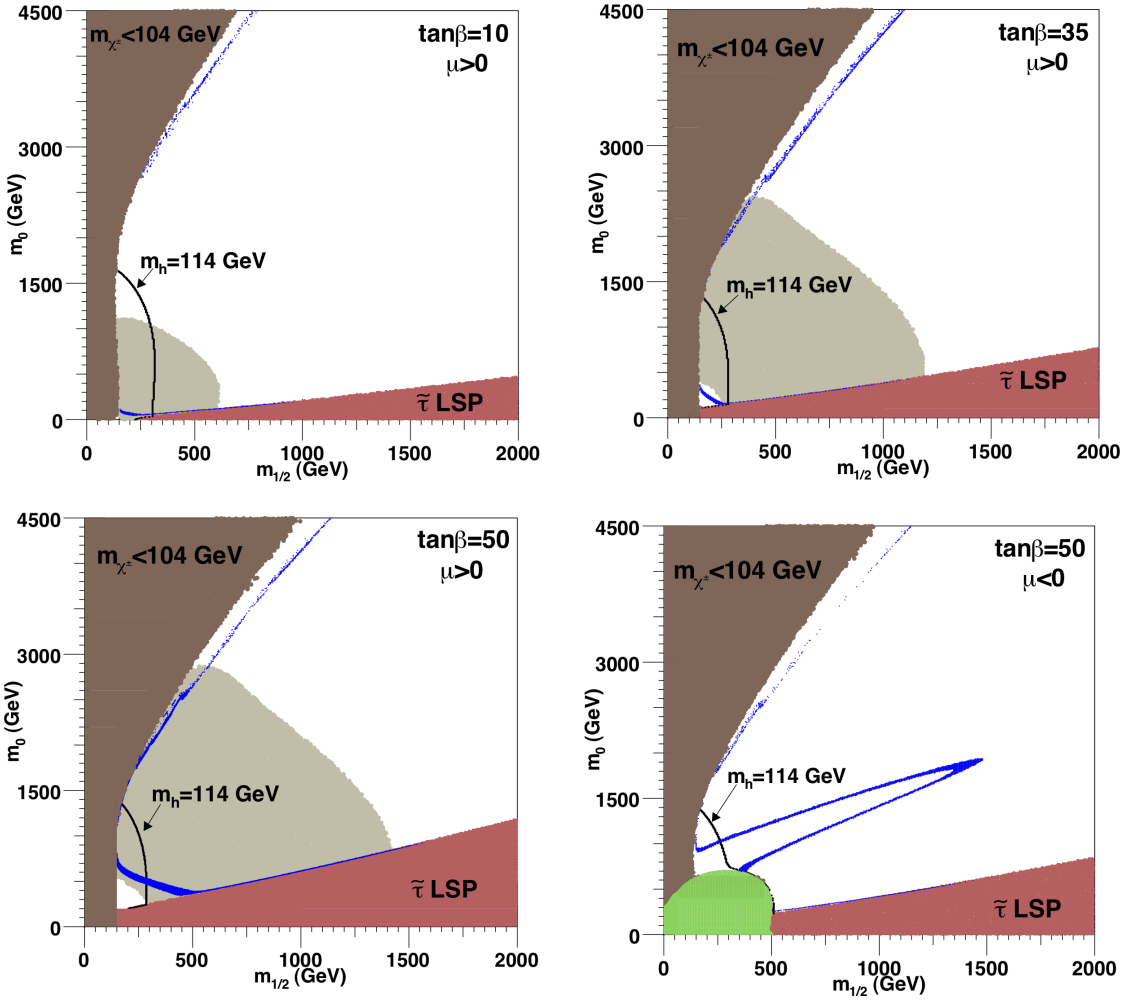

Figure 2.2: Illustrative regions of the CMSSM parameter space for $A_0 = 0$ with relevant cosmological constraints. The blue regions have a relic density consistent with the measured by WMAP. The shaded regions to the upper left and lower right are disfavoured by the LEP chargino bound and as a result of containing a (charged) stau LSP, respectively. The LEP bound on the light Higgs mass is shown as a solid line ($m_h = 114$ GeV). The region favored by measurements of the muon magnetic moment are shown as a light shaded region. Figure taken from a review [122]. With new Higgs searches results from LHC the m_h bounds are a bit more stringent.

Finally, let us comment on the recently revived possibility of a very light neutralino, with the mass of the order $\mathcal{O}(10\,\text{GeV})$. The models of this type are non-generic, since one has to ensure that they evade all the collider bounds, B-physics observables, precision measurements, as well as astrophysics constraints. Nevertheless, their interesting feature is that (at least in some cases) they can have the right scattering cross-section on the nuclei to potentially explain positive hints of detection signals obtained by DAMA, CoGeNT and CRESST (see Sec. 1.4.1). Recently several authors found that in the MSSM with non-universal gaugino masses a neutralino LSP with such a small mass can still be a viable

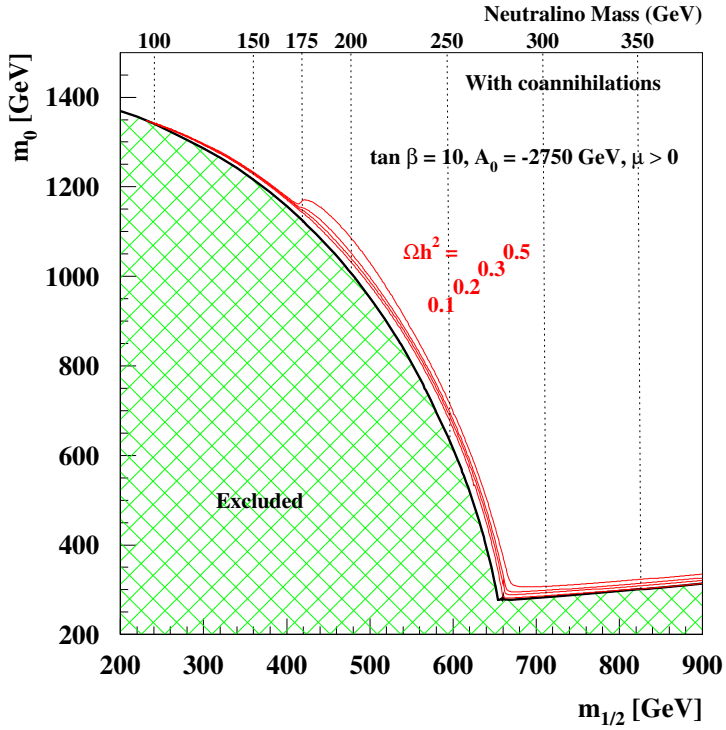

Figure 2.3: An example of relic density contours in the stop co-annihilation region in mSUGRA. Figure taken from [131].

possibility [134, 135, 136]. However, these models are not free from tension when the new LHC results are taken into account [137, 138].

2.4.2 Sneutrino

The sneutrino is a prototype of a scalar dark matter candidate. In 1994 Falk, Olive and Srednicki [139] showed that a heavy left-handed sneutrino can have an observed thermal relic density if it has a mass in the range of several hundreds GeV up to a few TeV. However, this original model is ruled out by the direct detection experiments: $\tilde{\nu}_L$ interacts with the nuclei via Z boson exchange with a cross-section, which is way too large for the cosmologically interesting masses.

The situation is different if we include in the model the neutrino masses. Then a right-handed neutrino requires a superpartner, $\tilde{\nu}_R$, which can then mix with the initial left-handed one. The latter do not couple to the Z boson, thus the $L-R$ mixed sneutrino may evade the direct detection bounds. It can be also a viable non-thermal or even thermal [140] dark matter candidate.

Another interesting feature of some sneutrino DM models is that it provides a possibility for light SUSY DM below 10 GeV. This is phenomenologically interesting in the light of direct detection anomalies (see Sec. 1.4.1), especially that one can naturally obtain scattering cross-section of the suggested order.

As an example of a recent model, in [141] a global Markov chain Monte Carlo analysis of a sneutrino DM model with Dirac neutrino masses originating from SUSY breaking was performed. The main distinctive feature of this model is a mainly right-handed mixed sneutrino as the LSP, which has a large coupling to the Higgs fields through non-suppressed weak-scale trilinear term. It was found that such a sneutrino can be an very good thermal cold dark matter candidate for masses around 3-6 GeV, as well as for masses larger than about 50 GeV. In particular, it was shown that it satisfies all experimantal constraints from direct detection and collider searches.

These kind of models, however, typically rely on fine-tunning between the left- and right-handed sneutrino components or need additional extension of the MSSM, e.g. by an additional $U(1)$ symmetry, see for example [142].

2.4.3 Gravitino

The gravitino $\tilde{G}$ appears when SUSY is promoted to a local symmetry leading to supergravity.[11] It is a prototypical superWIMP, i.e. super-weakly interacting massive particle, because it has only gravitational-strength[12] interactions. This is a feature with remarkable consequences for its aboundance and detection signals.

The gravitino mass $m_{\tilde{G}}$ depends strongly on the SUSY breaking scheme. It can range from the eV scale (typically for gauge mediation) up to scales around TeV (e.g. in gravity mediation). In order for it to be a dark matter candidate, it has to be the LSP, which can happen for large regions of the parameter space.

Because of its very weak interactions, gravitino is not expected to have been in thermal equilibrium in the early Universe. Therefore, it needs rather to be produced in high-energy particle collisions in the early Universe, or in the decays of next-to-lightest supersymmetric particle (NLSP), which typically is a charged slepton, sneutrino, chargino, or neutralino. In the latter case the relic aboundance is set by

$$\Omega_{\tilde{G}} = \frac{m_{\tilde{G}}}{m_{NLSP}} \Omega_{NLSP}. \tag{2.64}$$

This is independent of any cosmological parameters, like the reheating temperature, but needs a rather large gravitino mass, typically inconsistent with the BBN constraints (see e.g. [87]). For example, for a stable gravitino a very stringent constraints have been found if the Bino or the stau are the NLSP. Then, $m_{\tilde{G}} \geqslant 10\,\text{GeV}$ is excluded if the mass of the NLSP is smaller than about 1 TeV. It follows, that in such cases the decay of the NLSP alone cannot provide the correct amount of gravitino dark matter. More generally, BBN constraints on both unstable and stable gravitinos have been recently derived in [144].

An example of the former mechanism, is the $2 \to 2$ QCD inelastic scattering, which

[11] Since the SUSY algebra contains Poincaré generators, it can be seen that supergravity follows naturally from supersymmetry. Note, however, that this requires enlarging the field content by additional *gravity supermultiplet*, containing the spin-2 graviton and spin-3/2 gravitino. For a review of supergravity theories see e.g. [143].

[12] This include gravitational ones and after SUSY breaking also others, which are however suppressed by the Planck mass, and therefore of roughly the same order.

gives the gravitino relic density [145]:

$$\Omega_{\tilde{G}} h^2 \simeq 0.5 \left(\frac{T_{RH}}{10^{10}\,\mathrm{GeV}}\right)\left(\frac{100\,\mathrm{GeV}}{m_{\tilde{G}}}\right)\left(\frac{m_{\tilde{g}}}{1\,\mathrm{TeV}}\right), \tag{2.65}$$

which can give the correct relic density for typical parameters of supergravity and leptogenesis. These processes take place after inflation, therefore the resulting relic aboundance persists to present day, whenever gravitino is stable (or sufficiently long-lived).

As we can see, in the gravitino DM picture the dark matter, baryogenesis and BBN are strongly correlated in cosmological history. In fact, it may give rise to the so-called *gravitino problem* [146]: thermally produced gravitinos overclose the Universe, unless the reheating temperature is sufficiently low, which is however in conflict with thermal leptogenesis. Furthermore, one has to fine-tune the reheating temperature just below this upper bound to explain the required mass density of the dark matter.

The gravitino problem can be evaded for larger values of $m_{\tilde{G}}$ (like in gauge mediation) or even for light gravitinos in certain class of models, see e.g. [147]. Another possibility is to abandon the idea of thermal leptogenesis and rely on other baryogenesis mechanisms.

To summarize, gravitino's strong theoretical motivation coming from supergravity theories and rich phenomenology make it a very interesting topic to study. It plays an important role in many cosmological scenarios and in some cases can also be a dark matter candidate. For a short review see e.g. [148] and references therein.

2.4.4 Axino

The Peccei-Quinn solution of the strong-CP problem can be incorporated also an the level of a supersymmetric theory [149]. The axion needs then to be put in an additional chiral superfield, together with two additional particles: scalar saxion and Weyl fermion axino.

As long as SUSY is unbroken, the axion multiplet remains light, since it is protected by the $U(1)_{PQ}$ symmetry (for a review see [150]). It implies that no supersymmetric mass parameter is allowed for the axion multiplet since the axion does not have a potential. On the other hand if SUSY is broken, both saxion and axino get large mass contributions. For the saxion it is typically of the order of the soft scale, while for the axino it can be relaxed in both ways. If it is lighter, it provides a dark matter candidate.

If axinos are light, in the range MeV-GeV, they can be produced in the early Universe in the scatterings of thermal bath particles (linearly dependent on the temperature, thus most effective near the reheating T_{RH}) or from a decay of the lightest supersymmetric particle in the MSSM (LSPSM)[13]. In the second case, in the same way as for gravitinos, exists a strong connection of the axino relic density and the LSPSM would-be-relic density:

$$\Omega_{\tilde{a}} = \frac{m_{\tilde{a}}}{m_{LSPSM}} \Omega_{LSPSM}, \ . \tag{2.66}$$

It gives a connection with the classical WIMP mechanism in case the LSPSM is a neutralino. The thermal relic density was recently carefully analysed in [151], still however

[13] This can happen both in the case of R-parity violating and conserving theories.

with large uncertainties due to the strong interactions. It is also worth noting, that another axino production mechanism may also come form the Q-ball decay [152].

On the other hand, if axinos are heavier, they do not constitute the dark matter, but may decay into LSP and still give an important contribution to the neutralino abundance.

To summarize, axino is another reasonably motivated supersymmetric candidate. It is also an useful one, since its presence relaxes many of the bounds on the SUSY parameters, because the right number density of axinos can be obtained in a wider region of the parameter space.

Chapter 3

Electroweak corrections to DM annihilation

The most natural way to accommodate a WIMP into any BSM scenario is to make it charged under the electroweak group of the Standard Model. This is a generic situation in supersymmetric models, where the dark matter is composed typically of the superpartners of the $SU(2)_L \times U(1)_Y$ gauge and Higgs bosons. The models of this type are sometimes referred as EWIMP models.[1]

In Section 1.3.1 we demonstrated that the annihilation cross-section leading to a correct thermal relic density is easily achievable in this type of models, although sometimes giving strong constraints on the parameters.[2] This analysis was performed using the tree level value of the cross-section and assuming two-body annihilations as the dominant processes. However, in the case of EWIMP, the presence of the electroweak interactions may lead to important "corrections", coming from higher-order effects. In fact, as we will discuss, even when the DM itself is not charged under the weak interactions (like e.g. the Kaluza-Klein DM) the corrections to the final and virtual SM states often cannot be neglected.

In recent years a lot of effort was devoted to study the role of electroweak corrections in the DM physics, giving some insight on the general picture and providing more accurate results for several concrete models. Therefore, we start this Chapter with an introduction to the topic and a short review of existing results. Then in Section 3.2 we present and discuss our computation of the full radiative corrections at the level $\mathcal{O}(g^6)$ including virtual and real processes for a particular model, corresponding to the Wino DM case. In this way we explicitly show the interplay of the various contributions and obtain results which are not only self-consistent at a give order of the perturbation theory, but also as we show in Section 5 crucial in the phenomenology of this model.

[1] The same applies also to the sneutrino DM. Instead, if the LSP is the gravitino, it interacts only gravitationally and the situation is of course different.

[2] From another perspective, it means that treating this as a constraint allows to narrow, or for some simpler models even pin down, the predicted dark matter properties.

3.1 The importance of the electroweak corrections

Weak interactions are weak and thus one typically expects them to generate only per cent higher level corrections. Those are important for the collider experiments where such an accuracy is desirable and sometimes even necessary. On the other hand, in the dark matter searches the astrophysical and cosmological uncertainties are considerably larger and it may seem to be premature to study in detail these corrections at this stage. In many dark matter scenarios this is indeed the case. However, there are classes of models in which this simple expectation is not true. The most important and most widely studied examples are the effect of lifting the helicity suppression and the generic case of the heavy dark matter, at the scale of TeV or higher.

3.1.1 The helicity suppression and its lifting by gauge boson emission

The annihilation cross-section of a non-relativistic particle can be expanded in the relative velocity v of the incoming pair:

$$\sigma v_{ann} = a + bv^2 + \mathcal{O}(v^4), \tag{3.1}$$

where the a and b coefficients do not depend on the velocity. The velocity independent first term contains only the $L = 0$ partial wave, i.e. the S-wave, while second gets contributions from both S- and P-wave processes.[3] In the present day annihilations in the dark matter halos the relative velocity is $v \sim 10^{-3}$ which makes the second term very small.[4] Therefore, in the absence of any mechanism suppressing the S-wave annihilation the higher partial waves can be safely neglected.

On the other hand, if $a \approx 0$ then a careful computation of both terms is needed. This situation happens e.g. when there is some (approximate) symmetry forbidding the two-body S-wave final state. This is in fact a very common case in the SUSY extensions of the SM, when the dark matter is composed of Majorana particles and annihilates predominantly to two fermions, due to the well known helicity suppression.[5] The reason for this suppression is that the type of interaction favours the final fermions to be in a state forbidden from the conservation of the total angular momentum.

To see why this is the case it is useful to recap on some properties of two-body fermion states. The only possible spin states are the symmetric triplet $S = 1$ and antisymmetric singlet $S = 0$. The parity is $P = (-)^{L+1}$ where L is the total angular momentum of the pair and the intristic parity is always equal to -1. All of these hold for both Dirac and Majorana fermions, while the reason for the latter is different in those two cases. The intristic parity of a Majorana fermion is $\pm i$ which gives $(\pm i)^2 = -1$ for the pair. On the

[3] In general the L^{th} partial wave contribution to the annihilation cross-section is proportional to v^{2L}.

[4] For the relic density calculations, where at the freeze-out $v \sim 0.3$ the P-wave can introduce a non-negligible, but still sub-dominant contribution.

[5] Note however, that this is not always the case in any general Majorana DM model: if there exists a pseudoscalar particle mediating an s-channel annihilation process the S-wave is not suppressed in any way, see the discussion below and also appendix of [153] for more details.

other hand Dirac fermion and antifermion need to have opposite parities, since u and v spinors have opposite sign eigenvalues under the action of γ_0.

Additionally, fermion-antifermion pair under charge conjugation has $C = (-)^{L+S}$, which for the Majorana pair has to be equal to $+1$ (since it is it's own antiparticle). Therefore, for a Majorana pair L and S have to be both even or both odd.

It follows then, that for two Majoranas $CP = (-)^{L+S}(-)^{L+1} = (-)^{S+1}$ and thus the CP invariance forces the final fermions to be in the same spin state as the initial ones. In an S-wave, i.e. in the $v \to 0$ limit, the initial Majorana two-body state has to be antisymmetric due to the Pauli principle, hence it has to form a spin singlet state. This forces the final state also to have $S = 0$ and means that the only allowed s-channel interaction is the one mediated by a pseudoscalar, while all others are suppressed by v^{2L}.

The t- and u-channels annihilation can be rearranged with the help of the Fiertz identities, obtaining separate bilinears for the initial and final state fermions. In general this gives a sum of different "s-channel" contributions. However, if the t- or u-channel process is mediated by a scalar (as in the MSSM with sfermion exchange), then after the Fiertz transformation there is no pseudoscalar current contribution and the final cross-section contains only terms proportional to v^{2L} or $(m_f/m_\chi)^2$ (i.e. so-called helicity suppressed terms).[6]

The bottom line of the above discussion is that in such scenarios the S-wave contribution to the *two-body* annihilation cross-section is roughly of the same order as the P-wave one. However, in [154] it was noticed that in such a situation *three-body* final state may lift the helicity suppression, introducing instead two powers of the coupling constant, which effectively leads to an enhancement of the cross-section. The reason is that emission of a gauge boson changes the spin structure of the final state and hence there is no longer need for the fermions to form a singlet. This effect is most prominent if the gauge boson is emitted from the virtual leg, the so-called Virtual Internal Bremsstrahlung (VIB) or the Initial State Radiation (ISR).[7] On the contrary, Final State Radiation (FSR) is much less effective, since in this case the cross-section is dominated by the region of phase space where the gauge boson is emitted collinearly with one of the final fermions. This is purely kinematical effect, coming from the structure of the propagator of the outgoing particle,

$$D(p) \propto \frac{1}{(p+k)^2 - m_\chi^2}, \tag{3.2}$$

where p is the outgoing fermion momentum and k the gauge boson momentum. One immediately sees, that for a collinear photon emission the propagator diverges, while when emitting massive gauge boson it is inversely proportional to its mass squared. However, collinear gauge boson emission does not change the spin structure significantly and therefore does not lift the helicity suppression, in contrary to both ISR and VIB.

First studies of this topic where concentrated on the helicity suppression lifting by the photon emission and also its importance for the indirect detection signals. In particular,

[6] The only contribution which might have been non-suppressed is the s-channel exchange of Higgs pseudoscalar, but the coupling is then itself proportional to $m_f/v_{\rm EW}$ giving a suppression nearly of the same order.

[7] Internal Bremsstrahlung (IB) stands for emission of a gauge boson, accompanying some scattering process, without any external field.

existence of spectral features due to the IB was observed and studied on the example of heavy neutralino in [155] and in more model-independent way in [156]. Full scan of the relevance of this effect in general MSSM was performed in [157].

Interestingly, very recent works claim to find such a signal in the FERMI data [158, 159]. The authors of these works performed a dedicated analysis of the FERMI-LAT data to search for the internal bremsstrahlung and gamma ray line signals. The observed excess over the background is on the level of 4.6σ (or if one includes the look-elsewhere-effect 3.3σ) at the photons energy of about 130 GeV. If interpreted in terms of the dark matter signal from IB this gives its mass of about 150 GeV [158], while if the signal comes from a monochromatic gamma line then the best fit mass is $m_\chi = (129.8 \pm 2.4^{+7}_{-13})$ GeV and a partial annihilation cross-section $\langle \sigma v \rangle_{\chi\chi\to\gamma\gamma} = (1.27 \pm 0.32^{+0.18}_{-0.28}) \times 10^{-27}\mathrm{cm}^3\mathrm{s}^{-1}$ [159]. This tentative signal is based on about 50 photons and it most probably will take a few years of additional data to clarify its presence and maybe nature.

Apart from potential signals in gamma rays the IB has also other important phenomenological consequences. In [160] it was found that by enhancing the $e^+e^-\gamma$ annihilation, new spectral features in positron spectra should be expected. Moreover, since the collinear photons are dominant, the resulting positron spectrum is rather hard and posses a sharp cut-off.

Also other final states may obtain relevant "corrections" from internal Bremsstrahlung. Authors of [161] find a conservative, model independent upper bound on the cross-section, studying the electroweak bosons IB impact on the neutrino signals. They find it to be comparable to the original neutrino bound [162], but with some room for improvement from better spatial distribution of sources (studied recently by FERMI). This analysis was then extended in the following works [153, 163, 164, 165].

It is also interesting to mention another case when gauge boson emission introduces a significant correction, i.e. when the dark matter is a boson degenerated in mass with a particle mediating t-channel annihilation [157]. This is an effect related to the t-channel propagator for a non-relativistic initial state, which leads to enhancement for large energies of the emitted photon. Finally, a related effect was also observed in the Kaluza-Klein dark matter models [166, 167] and in the Inert Dark Matter (IDM) model [168].

3.1.2 TeV scale dark matter

If the dark matter mass is at $\mathcal{O}(1\text{–}100)$ GeV scale, than electroweak corrections are relevant typically only in some classes of models, like the ones described in previous subsection. However, for heavier dark matter the effect becomes not only stronger but also more generic.

This follows directly from the fact that electroweak part of the Standard Model is a spontaneously broken non-abelian gauge theory. This leads to large "IR-type" logarithms which do not cancel, even at the inclusive level. This is substantially different than e.g. QED where the Bloch-Nordesick theorem [169] states that the IR divergence from the virtual corrections is cancelled by the real emission of a soft photon. It is a very crucial fact ensuring that the QED is free from IR divergence and thus infrared safe.

In the non-abelian theory an analogue of this is the Lee, Nauenberg and Kinoshita

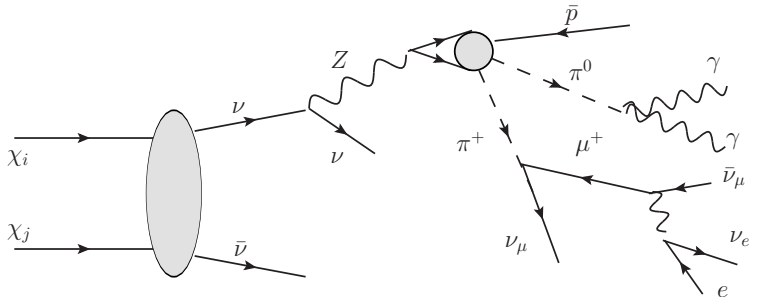

Figure 3.1: An example of a process including the FSR and its consequences on the apperance of all possible SM final states, even when primary annihilation channel is e.g. neutrinos.

theorem [170, 171], stating that soft singularities cancel after summing over initial and final soft states. This theorem is however not useful directly, because it involves the sum over the initial non-abelian charge, which of course is not available in the initial state (e.g. to obtain the cancellation for the e^+e^- scattering one needs to consider not only the inclusive level, but also sum over initial e^+e^- and $e^+\nu_e$).[8] This was noticed in the seminal works of Ciafaloni et al. [174, 175] and then explored in the context of dark matter indirect detection in [176].[9]

There are three main phenomenological consequences of this observation:

1. Electroweak corrections at the TeV scale are numerically important due to non-cancellation of the corrections containing the (double) Sudakov-type logarithms. For instance, for $m_\chi = 1$ TeV and electroweak coupling $\alpha_2 \approx 1/30$, one gets corrections of the typical size:

$$\alpha_2 \log\left(\frac{m_\chi^2}{m_W^2}\right) \approx 0.17, \qquad \alpha_2 \log\left(\frac{m_\chi^2}{m_W^2}\right)^2 \approx 0.86, \tag{3.3}$$

   which are hardly small.

2. After including the emission of the weak bosons, whatever is the primary annihilation channel of the dark matter particle, all SM stable states will be produced in the final state. This is illustrated on Fig. 3.1. For instance, emitted Z boson from a neutrino final leg can split/decay into quarks which after hadronization decay, among others, into antiprotons.

   This has an important consequence for the indirect searches, which was explored in series of works ranging from connected to the UHECRs from a decay of super-heavy particle [177, 178] to the dark matter annihilation [179, 180, 181]. We will come back to this point in Chapter 5, when we will deal with the indirect detection signals.

[8] In fact, as it is well known, similar situation occurs also in QCD [172, 173], but there confinement forces a color averaging in the initial state and luckily no IR divergence survives.

[9] This paper corrects also quantitatively some previous claims of [153, 163, 164] where s/m_w^2 contributions were found, although in full result they should cancel. The reason why they appeared was that these papers were using an effective approach which was explicitly braking the $SU(2) \times U(1)$ gauge symmetry.

3. Three-body annihilation has softer spectrum than the two-body one, which translates to much softer spectra of final stable particles after the whole showering and cascade evolution. Moreover, although the energy is conserved, the total number of particles is not and the FSR can in addition enhance the low energy part of the spectrum. This is indeed what was found in [179].

Those logarithmically enhanced terms arise form the FSR in the soft/collinear regime and therefore can be treated in a model independent way, whenever the approximation of the factorisation from the two-body annihilation can be applied. This was studied in detail in [179] where all the EW corrected splitting functions were computed. Those splitting functions, replacing the ones without electroweak corrections, can be used to get an approximated model-independent predictions for the indirect detection of dark matter. This was done in an important paper [182], where a comprehensive study of production and propagation of dark matter annihilation products were studied and the results given in the form of a ready to use *Mathematica* code, called *Poor Particle Physicist Cookbook For Dark Matter Indirect Detection* (PPPC 4 DM ID) [183]. As the name suggests, it is a very user-friendly code aiming in giving reliable (approximate) indirect detection signals for a given particle physics model, i.e. the user needs only to supply the mass and annihilation channels of the dark matter particle. This approach is of course very useful in the view of the fact that the true model of dark matter is unknown and detailed study of every single candidate is infeasible. Nevertheless, it has some considerable drawbacks, e.g. it cannot capture well the spectral features (depending on the VIB and not FSR, see Sec. 3.1.1) or the sharp edge (related to the $x \approx 1$ region, in which the collinear approximation fails). It also neglects non-logarithmically enhanced contributions, which can be also important and in some cases even dominant (see Sec. 3.2 below).

Finally, let us mention two recent works using effective field theory approach, capturing in a partially model independent fashion also some of the corrections beyond only FSR. In [180] annihilation of a Majorana particle to two fermions was studied and then [181] within similar setup deals with the initial state radiation, both showing that the helicity suppression is lifted at the level of dim-6 operators.

3.2 One-loop computation for the Wino dark matter

Most of the results discussed above include only real emission of the gauge bosons. They do not contain the full computation of virtual corrections being of the same order in perturbation theory, or include them only on the level needed to cancel the IR divergence. In the related literature only some loop computations exist, mostly for processes which do not occur at the tree level. In recent years there were some attempts to compute the one-loop corrections in a more systematic way. In particular, a project called SloopS [184] was initiated with the aim of fully implement all the one-loop corrections relevant for the supersymmetric dark matter in the MSSM in a numerical package, compatibile with micrOMEGAs code [185, 186]. However, up to now only partial results exist covering self-annihilation of the neutralino dark matter into two photons or a Z and a photon [187] and few examples of the corrections to the thermal relic density [188, 189] (see also [190]).

In our work [191] we took a different approach: we considered one particular model and computed full annihilation cross-section at the $\mathcal{O}(g^6)$ level, making analytical calculation as far as it was possible. This, first of all, allowed us to obtain better physical insight on the considered processes and secondly gave the full result with all the non-enhanced terms (which as we found are not negligible). Moreover, anticipating what will be discussed in Chapter 4, this computation is needed for consistent incorporation of the electroweak Sommerfeld effect.

The model we chose to study is a fermion dark matter living in the adjoint representation of $SU(2)_W$. This is the case of the pure Wino neutralino, but it is also interesting case per se (see e.g. the Minimal Dark Matter model [192]). It is also a good starting point for possible extensions because its relative simplicity makes more clear the description of the various effects. Another, more phenomenological reason to study this case is that it is precisely the one in which the Sommerfeld effect in the MSSM is the most important (see Chapter 4).

Similar physical scenario was later also studied in [193] with the idea of checking what is not captured in the effective approach discussed above. Indeed, they find a large impact on the total annihilation cross-section, but only if the lightest sfermion is degenerated in mass with the neutralino.

The model

We consider a Majorana fermion χ^0 and assume that it belongs to the adjoint representation of the $SU(2)$ subgroup of the electroweak $SU(2) \times U(1)$. The other two members of the triplet can be combined together and be described as a charged Dirac fermion and its anti-fermion which we call $\chi^\pm$. We assume that this triplet of fermions is massive due to an explicit mass term, that is present independently of the Higgs mechanism that might give mass to the weak vector bosons, and in fact we assume that these fermions do not interact with the Higgs field. Within this set-up, χ^0 interacts only with the charged weak-interaction vector bosons $W^\pm$ and its charged partners only interact with the $W^\pm$, and with the Z and γ.

We will be interested in the mass m_χ of the Wino up to a few TeV. For the computation of the radiative corrections we also assume that the charged fermions of the multiplet are degenerated in mass with the neutral ones.[10]

In our model, at the tree level there is only one possible annihilation channel:[11]

$$\chi^0\chi^0 \to W^+W^-. \tag{3.4}$$

However, at a higher order it is possible that the $\chi^0\chi^0$ pair becomes a (real or virtual) $\chi^+\chi^-$ pair which subsequently annihilates:

$$\chi^+\chi^- \to W^+W^- \qquad \text{or} \qquad \chi^+\chi^- \to ZZ, Z\gamma, \gamma\gamma. \tag{3.5}$$

[10] The mass difference comes from radiative corrections and is of the order of $\delta m = 0.17$ GeV [115], which is negligible with respect to the TeV scale.

[11] In the pure Wino scenario in the MSSM there are additional annihilation channels. However, in the case in which we are most interested in, i.e. χ^0 having a mass in the TeV range, this channel is by the far dominant one.

This sequential process is formally of higher order, but it can be enhanced by the two-channel version of the Sommerfeld effect (see Section 4.3). In this case it can be effectively of the same order as the tree level process and has to be included.

Moreover, since we consider the radiative corrections which provide an order $\mathcal{O}(g^4)$ correction to the amplitude and corresponding to an order $\mathcal{O}(g^6)$ term to the cross-section, we have also to include the annihilation in three final particles, i.e.

$$\chi^0\chi^0 \to W^+W^-Z,\ W^+W^-\gamma \tag{3.6}$$

and, by Sommerfeld effect, also

$$\chi^0\chi^0 \to \chi^+\chi^- \to W^+W^-Z,\ W^+W^-\gamma\,. \tag{3.7}$$

We are interested in the case when annihilating particles are non-relativistic, therefore, we can take σ_0 to be the nominal cross-section for the annihilation at rest within a negligible relative error $\mathcal{O}(v^2)$, that is the relative variation of the Mandelstam variables s and t averaged over the angles. In this case the two incoming neutralinos, being Majorana fermions, form an S-wave spin-singlet. This is a very good approximation for dark matter particles in the halo today, and it allows for a great simplifications of the computations. Firstly, because in this case the initial pair (being Majorana fermions) have to be in a S-wave spin singlet. Secondly, the kinematics simplifies, since the annihilation becomes like a decay of a particle with the mass $2m_\chi$.

To appreciate the consequences of the former observation note the identities, true for any Dirac matrix M:

$$\langle 0|\bar{\chi}^0 M\chi^0 a^\dagger_\downarrow a^\dagger_\uparrow|0\rangle = \frac{1}{(2\pi)^3}\mathrm{Tr}\left[M\frac{1+\gamma_0}{2}\gamma_5\right], \tag{3.8}$$

$$\langle 0|\bar{\chi}^+ M\chi^+\frac{a^\dagger_\downarrow b^\dagger_\uparrow - a^\dagger_\uparrow b^\dagger_\downarrow}{\sqrt{2}}|0\rangle = \frac{1}{\sqrt{2}(2\pi)^3}\mathrm{Tr}\left[M\frac{1+\gamma_0}{2}\gamma_5\right], \tag{3.9}$$

$a^\dagger_{\uparrow,\downarrow}(b^\dagger_{\uparrow,\downarrow})$ being particle (anti-particle) creation operators at rest, for a given spin-projection. As a result of this the spinor structure of the annihilation amplitude is greatly simplified, because after a projection on a given spin state we obtain a trace already at the amplitude level.

These approximations however set limits on the usage of the results for the relic density calculations. Although at freeze-out the dark matter particles are still non-relativistic, their velocity is about $v \sim 0.3$. On the other hand, in order to get accurate results in this case one needs not only to generalize this computations, but also include the P-wave, which is beyond the scope of this work.[12]

3.2.1 The scale of the coupling

Before presenting our computations, it is very important to understand at what energy scale the $SU(2)$ coupling g and of the Weinberg angle θ_W should be taken. We argue,

[12]For some results including one-loop corrections to relic density computations, however without the fully treated non-perturbative Sommerfeld effect see Refs. [188, 189].

that both in the radiative corrections and later for the Sommerfeld effect computations we should take them at the electroweak scale.

In the computation of the Sommerfeld factors $s_{0,\pm}$ one could wonder whether one should take g at the scale of the neutralino mass m_χ, since this sets the energy scale of the process. However, what matters in the Sommerfeld enhancement computation is in fact the scale of the momentum transfer between the incoming particles and this can be at most of the order of the vector boson mass.

The detailed computation, both analytical and numerical, shows [194] that the radiative corrections to the vertices $\chi\chi W$ (with χ on-shell as appropriate in the non-relativistic case) at zero momentum transfer exactly compensate the effect of the χ wave-function renormalization. Therefore, there is no dependence on m_χ once taking the renormalization scale to be m_W, and this compensation persists quite effectively up to momentum transfer $\mathcal{O}(m_W)$. What remains to be considered is the W wave-function renormalization, which is already included in the definition of the coupling at the scale m_W. Hence there are no appreciable corrections at all, if we take g at the scale m_W.

In fact, note that the use of the running coupling constant is appropriate for the processes which depend significantly on a *single* large scale. For instance it would be appropriate to take the coupling at the scale m_χ for processes in which the momentum transfer to χ is also of the order of m_χ.

In the case of the radiative corrections to the *annihilation amplitude*, there is no precise compensation of the radiative correction of the vertices $\chi\chi W$ with the χ wave-function renormalization. The reason is that the internal χ lines are off-shell, and therefore we take into account these loops that give a further radiative correction not included into taking g at the scale m_W.

Note that, by computing the Feynman diagrams giving the vertex corrections and the wave function renormalization and fixing the renormalization at the EW scale, we are evaluating perturbatively how the coupling "runs" from its EW value.

This is like expanding at the one-loop order the formula for the running coupling constant. The only difference is that we do not have to include the W wave-function renormalization, because it only depends on the square W-four-momentum which is equal to m_W^2 and therefore it is already inside the definition of the coupling at the scale m_W.

Let us also recall that the standard use of the renormalization group techniques holds in the "deep euclidean region" in which the external lines are quite off-shell. In our case instead, the external particles are on-shell and therefore there occur not only the large log's related to the UV divergences but also large log's due to IR effects. As we will discuss in the following, we do not attempt a re-summation of the large log's of various origin. This is indeed another reason why we do not attempt to use a kind of non-perturbative formula for the running coupling, suitably modified to take off the W-wave function renormalization, which would correspond to some partial re-summation of one subset only.

3.2.2 Wino-Wino annihilation

We start the discussion from the one-loop corrections to $\chi^0\chi^0$ annihilation. Firstly we will discuss the method of doing the computations and in the next subsections we will give the results. The way we present them is in terms of the correction to the tree level amplitude:

$$A = A_{\text{tree}} \left(1 + \frac{g^2}{(4\pi)^2} C_i(m_\chi)\right), \tag{3.10}$$

where $C_i(m_\chi)$ are the coefficients corresponding to the diagram i.

The UV divergent diagrams

The UV divergent one-loop diagrams come from the vertex corrections and the fermion wave-function renormalization, as presented on Fig. 3.2.

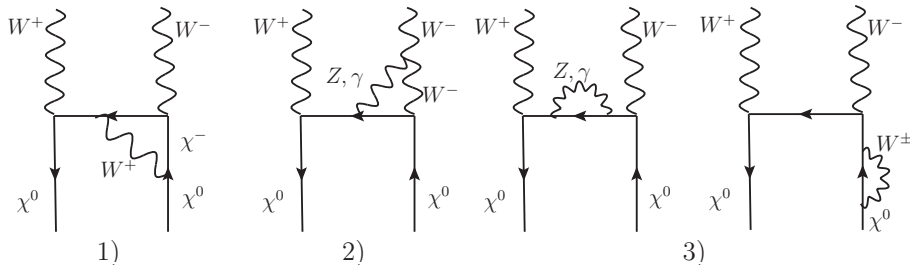

Figure 3.2: The UV divergent diagrams for $\chi^0\chi^0 \to W^+W^-$ process. The vertex corrections (diagrams 1 and 2) and the fermion wave-function renormalization (both diagrams are included in 3).

For all these diagrams, we have done the computations using full analytical expressions with Feynman parameters and integrated analytically (using *Mathematica*) over the first one and numerically over the second one.[13] We took the Feynman-'t Hooft gauge for the W propagator, which simplifies the computations, noting that χ is not coupled to the Higgs bosons and that there is no vertex with two W's and one neutral unphysical Higgs. We used dimensional regularization and dropped the terms $\mathcal{O}(1/\epsilon)$ because they are taken into account in the renormalization at the scale m_W. In fact, the loop corrections to the coupling g evaluated at the m_W scale do contain the same $\mathcal{O}(1/\epsilon)$ terms, which therefore are part of the definition of the coupling at that scale. We also did not include the W wave-function renormalization of the final W's for the same reason.[14]

[13] In the approximation of annihilation at rest all the diagrams can be expressed as a linear combination of integrals with only two Feynman parameters, because in this case there are only two independent external momenta.

[14] Except that we have to include the IR divergence of the W wave-function renormalization due to the photon exchange, which is cancelled by a real photon emission, see Fig. 3.5.

The UV finite diagrams and the IR divergence

Besides the loops giving the radiative correction of the vertices and the χ wave-function renormalization, there are two other loops, which are not UV divergent.[15]

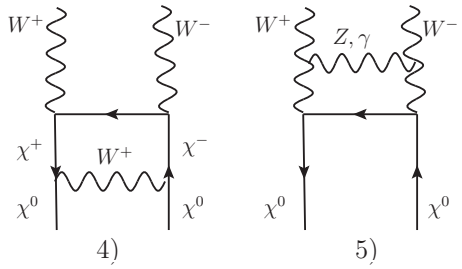

Figure 3.3: The UV finite diagrams for $\chi^0\chi^0 \to W^+W^-$ process.

Diagram 4 represents a process in which the incoming χ^0 pair goes to a virtual $\chi^\pm$ pair (which then annihilates in $W^\pm$) by $W^\pm$ exchange (see Fig. 3.3, diagram 4). The contribution of this loop is very large when $m_\chi \gg m_W$. In fact, the correction to the amplitude grows like m_χ/m_W, i.e. much faster than even the double Sudakov logarithms from the FSR. This is one of the places where the full higher order computation is crucial for obtaining correct results.

This part of the correction comes from the region of the integration where the virtual χ^+ momentum is nearly on-shell, that is the non-relativistic part of the diagram. Because of that it can be actually treated more carefully and even re-summed, which leads precisely to the advocated Sommerfeld effect and will be discussed in the next Chapter.

For the time being however, we will put this part aside and write the contribution from the diagram 4 as:

$$D_4 \equiv A_{\text{tree}} \frac{g^2}{(4\pi)^2} C_4 + A_{\text{tree}} \frac{g^2}{4\pi} \frac{m_\chi}{m_W}, \tag{3.11}$$

where the A_{tree} is the tree-level amplitude. Therefore the $\propto m_\chi/m_W$ part, which we will call the one-loop Sommerfeld one, is not included in any of the C coefficients and we will treat it separately.

Diagram 5 represents the exchange of Z or γ between the final $W^\pm$ (see Fig. 3.3). This loop is IR divergent in the part in which there is a photon exchange. This is the only IR divergence in the radiative corrections of σ_0, because the initial χ^0 does not couple to the photon and there is no photon contribution to the χ^0 wave-function renormalization. Moreover, in the other loops at least one of the χ line is off-shell thus avoiding IR divergences.

[15] The propagators and vertices of these diagrams give three powers of momentum in the numerator and eight powers in the denominator therefore the integration in four dimensions is convergent by power counting. In the case of diagram 5 the analytic integration on one parameter has been done using the PrincipalValue prescription, in order to discard the absorptive part, due to intermediate W's being possibly on-shell. This part does not interfere with the tree diagram and thus would give a higher order contribution.

The diagram containing the four vector boson vertex gives a vanishing contribution for the Wino annihilation at rest in a spin-singlet state.

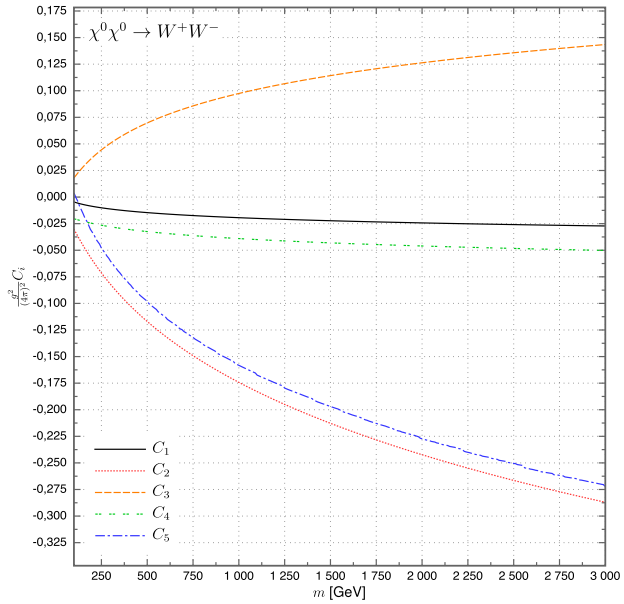

Figure 3.4: The results for the one-loop correction to the amplitude of the $\chi^0\chi^0 \to W^+W^-$ annihilation. The total correction is obtained by summing all those contributions and including the real production. The C_5 contribution is made finite due to adding a small mass to the photon $m_\gamma = 0.1$ GeV. In these result all the multiplicities of the diagrams were taken into account.

The total result for the radiative corrections due to the loops

On Fig. 3.4 we present the results for the one-loop corrections coming from all the diagrams separately, in function of the DM mass being in range of 100 GeV–3 TeV. One can see, that the largest contributions come from diagrams 2, 3 and 5, all containing photon exchange. Although the C_5 is IR divergent, we get a finite result by giving (in all the numerical calculations) a small (with respect to the TeV scale) mass $m_\gamma = 0.1$ GeV to the photon. In reality it is of course massless, and indeed as we shall see the dependence on m_γ will drop out in the final result. We will come back to this point later, where we discuss the cancellation of the IR divergence by the inclusion of a real production.

Actually, in order for the cancellation to be exact, we have also to take into account the IR divergent part of the virtual photon contribution to the W wave-function renormalization, that is not included in the renormalization of g at the scale m_W (see Fig. 3.5). It gives a further contribution to C which is: $s_W^2\, 4 \log\left(\frac{m_\chi}{m_\gamma}\right)$. Including it in one-loop corrections gives finally

$$C_{1-loop} = \sum_{i=1}^{5} C_i + s_W^2 4 \log\left(\frac{m_\chi}{m_\gamma}\right). \tag{3.12}$$

From the computation we get that $C_{1-loop} < 0$ and also that it diverges for $m_\gamma \to 0$. The divergence is due to the graph 5 described above and to IR divergent part of the W wave-function renormalization.

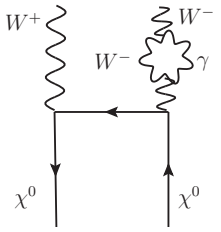

Figure 3.5: The IR divergent diagram present in the gauge boson wave-function renormalization.

The radiative correction due to the real production and the cancellation of the IR divergences

As we already mentioned, doing the computation of σ_0 at the order $\mathcal{O}(g^6)$, we have also to add to σ_0 the production cross-section of W^+W^-Z and $W^+W^-\gamma$, which are of the same order (see Fig. 3.6). This has to be done on the level of the cross-section. Hence, we start from a short review of the cross-section computation. If we call the amplitude $\mathcal{M}$, then the formula for the differential cross-section in our case reads:

$$d\sigma = \frac{1}{4m_\chi^2 v_r}\left(\prod_i \frac{d^3k_i}{(2\pi)^3 2\omega_i}\right)\sum_{\text{pol}}|\mathcal{M}|^2(2\pi)^4\delta^4(P-\sum_i k_i), \tag{3.13}$$

where $v_r = 2v$ is the relative velocity, $P = (2m_\chi, 0, 0, 0)$ and m_χ is the mass of annihilating DM particle. The sum over polarizations gives:

$$\sum_{\text{pol}}\epsilon_\mu\epsilon_\nu^* = -g_{\mu\nu} + \frac{k_\mu k_\nu}{m_{W,Z}^2}\ , \tag{3.14}$$

for massive gauge bosons and

$$\sum_{\text{pol}}\epsilon_i\epsilon_j^* = \delta_{ij} - \frac{k_i k_j}{\vec{k}^2}, \tag{3.15}$$

for the photon.

In the annihilation into two particles with the same mass m_g the integration over the phase space gives:

$$\sigma_2 v = \frac{1}{64\pi}\sqrt{1-\frac{m_g^2}{m_\chi^2}}\sum_{\text{pol}}|\mathcal{M}|^2. \tag{3.16}$$

For the annihilation into three body final state, in the limit in which initial particles are in rest, the cross-section can be computed in a convenient parametrization with the use of Dalitz variables[16], $m_{ij}^2 = (k_i + k_j)^2$:

$$d\sigma_3 = \frac{1}{(2\pi)^3}\frac{1}{16(2m_\chi)^4}\frac{1}{v_r}\sum_{\text{pol}}|\mathcal{M}|^2 dm_{12}^2 dm_{23}^2. \tag{3.17}$$

[16]In actual numerical computations we follow a more direct approach by integrating over the final energies, which we check to be equivalent; this is numerically more convenient but the formulae are too long and we don't write them here.

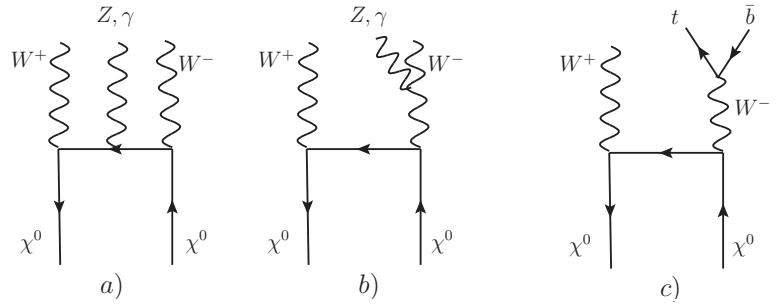

Figure 3.6: The diagrams for real production of the gauge bosons and the production of the $t\bar{b}$ quark pair.

The integration limits on these variables depend only on the masses and can be conveniently presented as [195]:

$$4m_1^2 \leqslant m_{12}^2 \leqslant (2m_\chi - m_3)^2 \qquad (m_{23}^2)_{min} \leqslant m_{23}^2 \leqslant (m_{23}^2)_{max}, \tag{3.18}$$

with

$$(m_{23}^2)_{min} = (E_2 + E_3)^2 - \left(\sqrt{E_2^2 - m_1^2} + \sqrt{E_3^2 - m_3^2}\right)^2, \tag{3.19}$$

$$(m_{23}^2)_{max} = (E_2 + E_3)^2 - \left(\sqrt{E_2^2 - m_1^2} - \sqrt{E_3^2 - m_3^2}\right)^2. \tag{3.20}$$

Here $E_2 = m_{12}/2$ and $E_3 = (4m_\chi^2 - m_3^2 - m_{12}^2)/2m_{12}$ are the energies of particles 2 and 3 in the m_{12} rest-frame.

In order to add these contributions to the one-loop corrections we define the coefficients C_Z^{rp} and C_γ^{rp} as:

$$2\frac{g^2}{(4\pi)^2} c_W^2 \, C_Z^{rp} \equiv \frac{\sigma_{W^+W^-Z}}{\sigma_2^{\text{tree}}}, \qquad 2\frac{g^2}{(4\pi)^2} s_W^2 \, C_\gamma^{rp} \equiv \frac{\sigma_{W^+W^-\gamma}}{\sigma_2^{\text{tree}}}. \tag{3.21}$$

Note the factor 2 in the definitions, which makes these coefficients to be the *corrections to the amplitude* coming from the real production. Using this we can write that the production cross-section provides a further correction:

$$C_{1-loop+rp} = C_{1-loop} + c_W^2 C_Z^{rp} + s_W^2 C_\gamma^{rp}. \tag{3.22}$$

The full $C_{1-loop+rp}$ coefficient should go to a finite constant for $m_\gamma \to 0$, which we find it is indeed the case. On the right plot of Fig. 3.7 we show the separate contributions from one-loop corrections and the real production to show that their sum is independent of m_γ.

Three body production involving t quark. There is a further, though very small, contribution to the production cross-section at the order $\mathcal{O}(g^6)$: the processes involving the t quark in the final state

$$\begin{aligned} &\chi^0\chi^0 \to W^- t\bar{d}, \qquad \chi^0\chi^0 \to W^- t\bar{s}, \qquad \chi^0\chi^0 \to W^- t\bar{b}\,, \\ &\chi^0\chi^0 \to W^+ \bar{t}d, \qquad \chi^0\chi^0 \to W^+ \bar{t}s, \qquad \chi^0\chi^0 \to W^+ \bar{t}b\,. \end{aligned}$$

These processes are due to the couplings $W^+ \to t\bar{d}, t\bar{s}, t\bar{b}$ and their conjugates.

Notice that the other processes with a charged W and either a charged $l_i\bar{l}_j$ or a lighter charged $q_i\bar{q}_j$ pair in the final state must not be included. They sum up to the total width of the charged W, and therefore are implicitly taken into account by unitarity when one takes the approximation of considering W as a stable particle. But the *top* is more massive than the W and therefore the $q_i\bar{q}_j$ pairs with the t as one of them are not included in in the total width of the W and have to be added to the correction.

Since the square of the coupling $W^+ \to t\bar{d}$ is negligible with respect to the sum of the square of $W^+ \to t\bar{b}$ and $W^+ \to t\bar{s}$ (which all together add up to g^2), and the masses of b and s are negligible at our energy scale, by defining as before

$$2\frac{g^2}{(4\pi)^2}C_t \equiv \frac{\sigma_{W^-t\bar{b}} + \sigma_{W^+\bar{t}b}}{\sigma_2^{\text{tree}}}, \tag{3.23}$$

we get final result for the total correction to the tree amplitude

$$C_{1-loop+rp+t} = \sum_{i=1}^{5} C_i + s_W^2\left(4\log\left(\frac{m_\chi}{m_\gamma}\right) + C_\gamma^{rp}\right) + c_W^2 C_Z^{rp} + C_t\,. \tag{3.24}$$

In the numerical results, as we will see, the relative contribution of C_t is very small. The reason is that it does not contain any large logarithms, which are present in the case of the production of three gauge bosons.

Note, that since the unphysical neutral Higgs is not coupled to $W^\pm$ we can use the Feynman-'t Hooft gauge for the vector bosons forgetting the unphysical Higgs. As for the physical Higgs, its coupling to $W^\pm$ is proportional to gm_W and therefore the (virtual or real) processes involving it will be suppressed by a factor m_W^2/m_χ^2 and we can neglect them.

The total result for the annihilation of $\chi^0\chi^0$

We show the results for the full radiative corrections to the $\chi^0\chi^0$ annihilation *amplitude* on the left panel of Fig. 3.7. One can see, that subtracting the one-loop Sommerfeld effect (that will be non-perturbatively treated, see Chapter 4), the total corrections (the solid black line) are significant, reaching over 15% for the $m_\chi = 3$ TeV, but still in the perturbative regime. Indeed, the perturbative evaluation of the correction to σ_0 looks like to be border-line-reliable up to values of m_χ of a few TeV.

This fact is not surprising: when m_χ and therefore the overall scale of the process gets large as compared to m_W, the vector bosons resemble more and more massless would-be gluons of an unbroken $SU(2)$, like an $SU(2)$ version of QCD. There occur large log's of the ratio m_χ/m_W, and powers of them, which are not related to the UV divergences (and therefore cannot be included in a standard renormalization group treatment). Therefore, for higher values of m_χ, one would need to borrow from QCD sophisticate techniques of re-summation of powers of large log's or semi-empirical formulae. All that is beyond the scope of this work.

We also see that at a TeV scale the one-loop perturbative evaluation of the Sommerfeld effect is quite large and this is one of the reasons why the full non-perturbative treatment of this effect is needed.

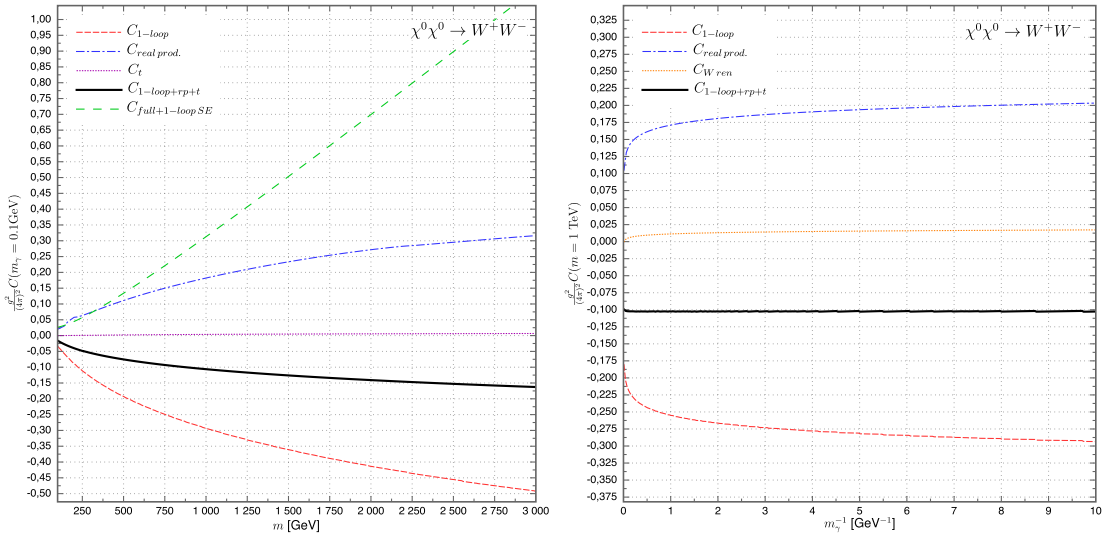

Figure 3.7: *Left plot:* the correction to the tree level $\chi^0\chi^0 \to W^+W^-$ amplitude coming from loop corrections (dashed red line), real production (chain blue) and the t quark (dotted violet). The full result is given by the solid black and sparse green lines (without and with the one-loop Sommerfeld correction, respectively). *Right plot:* the dependence of the full result on the photon mass, for fixed $m = 1$ TeV. A complete cancellation of the IR divergent terms can be seen, and that the full result is independent of m_γ.

3.2.3 Chargino-Chargino annihilation

The $\chi^+\chi^-$ annihilation gives a higher order, but still non-negligible contribution to the $\chi^0\chi^0$ annihilation process. In fact, it can be of the same order as the direct process, due to the $\propto m_\chi/m_W$ part, which is even more pronounced after the re-summation. Therefore, it is also important to compute the radiative correction to the annihilation with $\chi^+\chi^-$ in the initial state. Because the computations are very similar to the $\chi^0\chi^0$ case, we do not discuss them in detail, but rather stress the differences and present the final results.

In this case, in the Feynman-'t Hooft gauge it occurs also the vertex of the charged unphysical Higgs with the vector bosons. However, in the same way as for the physical Higgs, its coupling is proportional to gm_W. Therefore, the process involving it will be suppressed by a factor m_W^2/m_χ^2 and we neglect it.

One-loop corrections to $\chi^+\chi^- \to W^+W^-$

In the case of the annihilation of $\chi^+\chi^-$, since they are charged, there are more diagrams to be computed, see Fig. 3.8. The technique is however exactly the same.

Note however the difference in the normalization of the initial states. The spin-singlet $\chi^0\chi^0$ state is described by

$$\varphi^0(x)a_\uparrow^\dagger a_\downarrow^\dagger|0\rangle, \tag{3.25}$$

and the spin-singlet $\chi^+\chi^-$ state by

$$\varphi^\pm(x)\frac{a_\uparrow^\dagger b_\downarrow^\dagger - a_\downarrow^\dagger b_\uparrow^\dagger}{\sqrt{2}}|0\rangle, \tag{3.26}$$

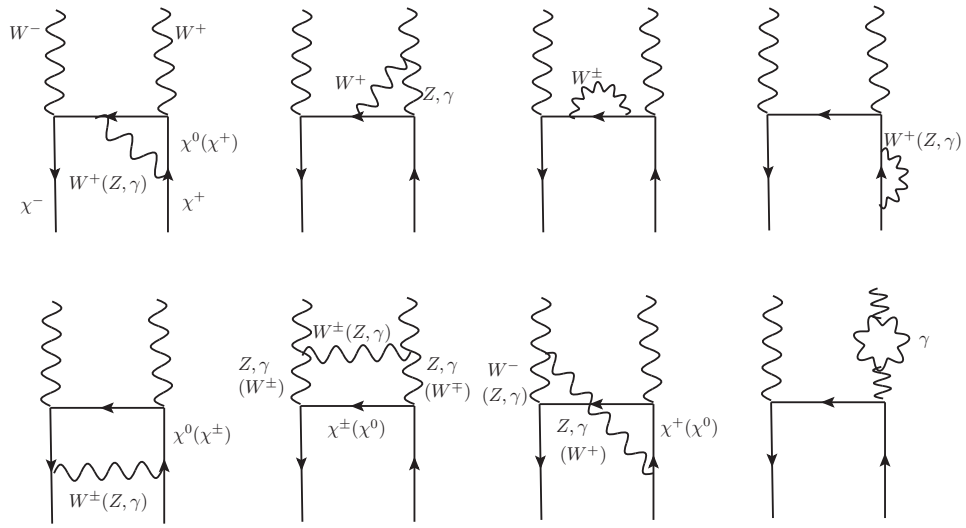

Figure 3.8: The diagrams for the one-loop corrections to $\chi^+\chi^- \to W^+W^-$ annihilation.

where $\varphi^0(x)$ and $\varphi^\pm(x)$ are the S-wave reduced wave functions. Hence, at the tree level we have $A^{\text{tree}}_{\chi^+\chi^-\to W^+W^-} = \frac{1}{\sqrt{2}} A^{\text{tree}}_{\chi^0\chi^0\to W^+W^-}$.

The radiative correction due to the real production

Also in this case the computations go in the same way, except that now the initial state particles are coupled to Z and γ, which gives the initial state Bremsstrahlung process (instead of internal one as in the $\chi^0\chi^0$ case). The diagrams to be computed are those on Fig. 3.9.

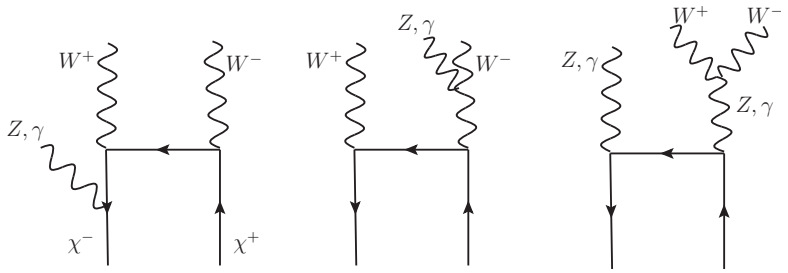

Figure 3.9: The diagrams for the correction to the process $\chi^+\chi^- \to W^+W^-$ coming from the real production of Z, γ.

The total result for the annihilation of $\chi^+\chi^- \to W^+W^-$

On Fig. 3.10 we show the full radiative correction to the amplitude of the process $\chi^+\chi^- \to W^+W^-$. When compared to the case of nuetralino annihilations, one immediately sees that although results are qualitatively similar, quantitatively are considerably smaller. In fact, the full one-loop result without the one-loop Sommerfeld effect is within -10% range even up to 3 TeV.

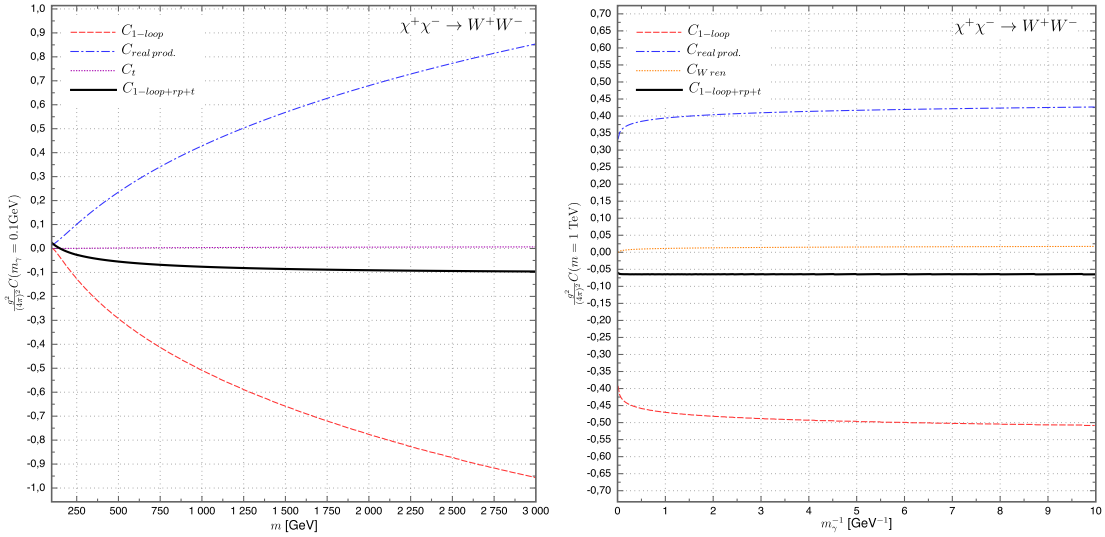

Figure 3.10: The correction to the $\chi^+\chi^- \to W^+W^-$ amplitude *(left plot)* and dependence on the photon mass *(right plot)*. The notation is the same as in Fig. 3.7.

For completeness, also in this case we show the IR cancellation and that our results are independent of m_γ.

3.2.4 The one-loop corrections to $\chi^+\chi^- \to ZZ, Z\gamma, \gamma\gamma$

The diagrams to be computed are given on Fig. 3.11. In this case there is no wave-function renormalization of the final states, because they do not couple to the photon and thus do not exhibit IR divergences. Moreover, in this case there are no IR divergences in the total one-loop corrections, since the fermion wave-function renormalization cancels precisely the IR divergence coming from the correction to the initial states (the bottom left diagram).

Here, there is also no three body production, since the emission of three W^3 (a mixture of Z and γ) is forbidden by the CP conservation: the initial state being spin singlet has an even CP, while both Z and γ are CP-odd.[17]

The results for the radiative correction to these processes are presented on Fig. 3.12. The corrections are very similar to each other, as could be expected from the fact that since m_χ is much larger than m_Z, the differences in masses of the final states are not very important. On the other hand, the differences in couplings are taken into account in the tree level amplitudes for these processes (i.e. every of these three corrections is normalized to its own tree level amplitude).

One can also see that the absolute value of these corrections is quite large. In fact, considerably larger than for the annihilation into charged final states. This might look surprising, since there are less diagrams and none is IR divergent, but actually it can be

[17]The processes involving two neutral gauge bosons where one of them subsequently decays into quark or lepton pairs are allowed, but similarly to what was said for the t quark production they are very suppressed and therefore we neglect them.

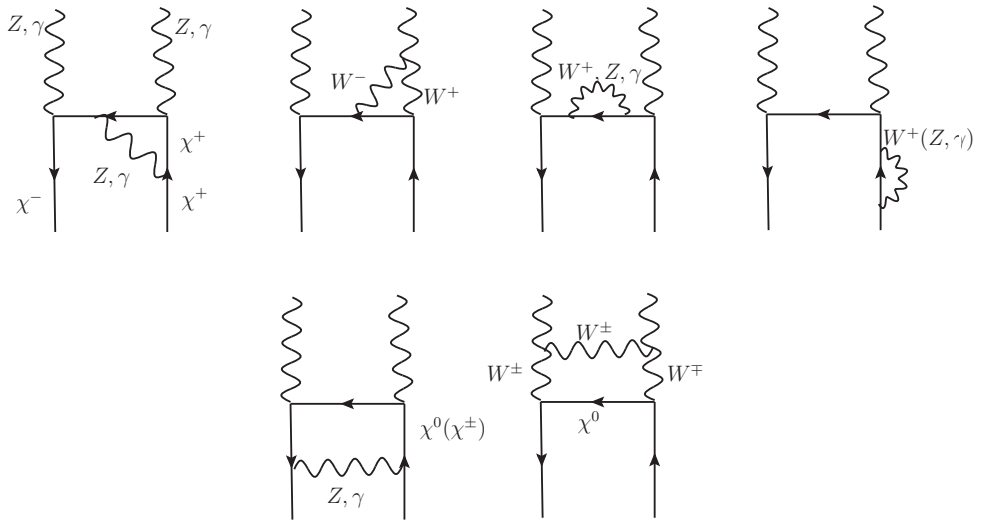

Figure 3.11: The diagrams for the one-loop corrections to $\chi^+\chi^-$ annihilation to neutral gauge bosons.

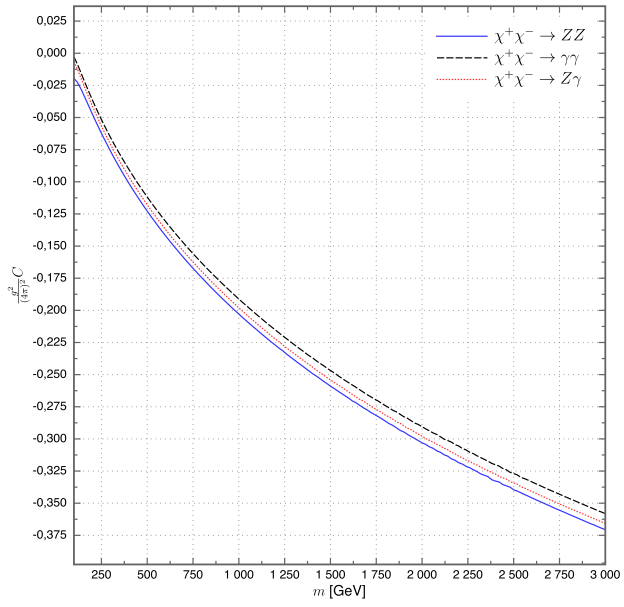

Figure 3.12: The full one-loop corrections to the annihilation of $\chi^+\chi^-$ into $ZZ, Z\gamma, \gamma\gamma$. These corrections come only from the loop diagrams, because there is no real production in this case (see the text).

easily understood by the fact that in this case there is no compensating effect of the real production.

With all those results we are ready to compute the total annihilation cross-section at the $\mathcal{O}(g^6)$ level. However, without proper treatment of the m_χ/m_W terms the result would be meaningless and for that reason, we leave the discussion of the final cross-section for the Sec. 5.1, after the Sommerfeld effect is presented in detail.

Chapter 4

The Sommerfeld effect

In the previous Chapter we have seen that electroweak corrections for the EWIMP in general cannot be neglected, especially at the TeV scale. We also observed a worrisome one-loop correction coming from the W boson exchange, when the states of $SU(2)_L$ multiplet are degenerated in mass. It was found to be of the order $\mathcal{O}(\alpha_2 m_\chi/m_W)$, which implies a breakdown of perturbation theory at the scale of a few TeV. This calls for resummation of higher orders, which leads to an effect known in the particle physics literature as the Sommerfeld enhancement. This chapter deals with the derivation and applications of this effect to the dark matter physics.

4.1 The origin of the Sommerfeld enhancement

In 1997 Bergström and Ullio [196], and independently using different method, Bern et al. [197] computed the annihilation of neutralinos to two photons at the full one-loop level. These results were in agreement with each other, both giving in the large dark matter mass limit result which was independent of m_χ. For example, in the pure Higgsino case [197] gives:

$$\sigma v_r \simeq \frac{\alpha_2^4 \pi}{4 m_W^2 s_W^4}. \tag{4.1}$$

This result was surprising. One would rather expect the cross-section to be proportional to m_χ^{-2}: for large m_χ the mass of the W boson can be neglected, hence the DM mass is the only dimensionful quantity and from dimensional analysis this is the only possible behaviour.

This becomes even more troublesome if one thinks about the unitarity bound [198]. For a given partial wave with angular momentum J, in two body scattering process:

$$\sigma_J \leqslant \frac{\pi(2J+1)}{p_i^2}, \tag{4.2}$$

where p_i is the center of mass three-momentum of the initial state. In the case of dark matter annihilation the initial state is non-relativistic $p_i^2 \approx m_\chi^2 v_r^2/4$, giving an upper bound:

$$\sigma v_r \lesssim \frac{4\pi(2J+1)}{v_r m_\chi^2}. \tag{4.3}$$

Clearly, for large enough m_χ, one-loop approximation of the cross section (4.1) is not sufficient and must be corrected by higher order terms. This was noticed very early [199], but since this happens for Higgsions with $m_\chi \gtrsim 100$ TeV, it seemed not to be of much practical interest. Nevertheless, it was clear that one should somehow revise the computations.

This has been done several years later by Hisano et al. [200] and subsequently in [201], where they computed the annihilation cross-section for pure Higgsino and Wino limits in the non-relativistic (NR) field theory. Indeed, they observed that the correct m_χ^{-2} behaviour is reproduced, and therefore the higher order contributions unitarize the cross-section. It was also shown that in this case the critical mass for which the perturbation theory breaks down, i.e. when the two-loop contribution is the same as the one-loop one, is about $m_{\text{crit}} \sim 10$ TeV.

Apart from saving consistency of the theory, another striking feature was discovered: leading higher order corrections in the NR limit can be resumed, and significantly alter the total cross-section. In particular, in the Wino case when the energy of the incoming neutralino is on the pole of the bound state of chargino, a resonance occurs. It can enhance the cross section by factor $\gg 1$. In fact, if zero energy resonance exists, then the corrected cross-section is proportional to $1/v^2$, where v is the DM velocity.[1] It leads to important phenomenological consequences for the possible indirect detection signals [202] and also for the thermal relic density [203]. Similar effect was found for the Bino dark matter in the case when it is nearly degenerated in mass with $\tilde{t}$ or $\tilde{\tau}$ and has CP violating interactions with those particles [204].

Later it was realized, that in 1931 Arnold Sommerfeld observed similar effect when calculating Bremsstrahlung in an external field and introduced a method based on solving the appropriate Schrödinger equation [205]. Therefore this effect was dubbed "the Sommerfeld enhancement".

The reason standing behind it is the existence of "long range" force, which distorts the incoming particles' wave functions. In the case of heavy Winos or Higgsinos (and also in the Minimal Dark Matter model [206]) the role of this force was played by the exchange of weak gauge bosons. It was, however, soon realized that in other physically interesting scenarios also electromagnetic or even strong interactions may have an analogous impact, e.g. in [207] radiative and Sommerfeld-type corrections to stop coannihilation were studied, where e.g. the $\tilde{t}\tilde{t}$ annihilation is greatly enhanced by the gluon exchange. Another application was the computation of the thermal relic density of a charged relic itself [208]. It is relevant e.g. for gravitino dark matter models, where its abundance depends on the abundance of NLSP, which can be a stop or stau.

In 2008 PAMELA satellite [209] observed rise in positron fraction $e^+/(e^+ + e^-)$ in cosmic rays with energies from 10–100 GeV. This built up over earlier findings of HEAT [210], AMS-01 [211] and also ATIC [212] experiments. Although these surprising results may be well explained by astrophysical sources, e.g. nearby yet undetected pulsars [213], there is an exciting possibility that it comes from dark matter annihilating predominantly into leptons. This explanation, however, needs an annihilation cross section larger by

[1] This does not violate unitarity, since for very low velocities σv is saturated by the finite width of the bound state, as is discussed below.

several orders of magnitude than the one giving correct thermal relic density.

To solve this issue Arkani-Hamed et al. [214] proposed, that dark matter can interact with a new "dark force". This implies, via the Sommerfeld effect, strong boost of the present-day NR annihilation cross-section, leaving untouched its value around the freeze-out, where the typical DM velocity is roughly $v \sim 0.3$. This idea started a second life for the Sommerfeld enhancement.

In our work we followed different direction: we studied what is the impact of this effect in the MSSM without adding any new interactions. For this we developed a formalism suitable for more complex scenarios, which we describe in Section 4.3. We implemented it numerically in the DarkSUSY code and in Section 4.4 we present the possible applications in the different regions of the parameter space of the MSSM. We start however the discussion from the "dark force" case, for two reasons. Firstly, because being more simple it is instructive for presenting main physical points. Secondly, it has grown to a separate topic on its own, which definitely is worth discussing, since it might give an explanation for several cosmic ray anomalies.

4.2 Enhancement due to a dark force

Imagine, that the dark matter particle χ interacts with some scalar or vector boson ϕ. In the non-relativistic limit its multiple exchange acts as a force with a range $\sim 1/m_\phi$. This force can be described by a Yukawa potential:

$$V(r) = \alpha \frac{e^{-m_\phi r}}{r}\,, \tag{4.4}$$

where $\alpha = g^2/(4\pi)$ and g is the coupling constant of the $\chi\chi\phi$ interaction.

The existence of this potential effects in distorting the initial wave function $\psi(\vec{r})$ of the incoming two-particle state. The whole effect can then be encoded into the ratio between the wave function of the incoming, free particle (at $r \to \infty$) and the distorted one at the point of annihilation (at $r = 0$). For that reason one usually defines the enhancement factor by

$$S = \frac{|\psi(\infty)|^2}{|\psi(0)|^2}\,, \tag{4.5}$$

which multiplies the cross-section

$$\sigma_{\text{full}} = S \cdot \sigma_0\,. \tag{4.6}$$

If one assumes one species of annihilating particle χ with mass much larger than the mass of force carrier, $m_\chi \gg m_\phi$, and a coupling strength of the order of the weak coupling or larger, then one gets a very large enhancement of the cross-section.

Interesting limiting case is when $m_\phi = 0$ and the potential is a Coulomb one, since then the Sommerfeld effect can be solved analytically, giving

$$S(v) = \frac{\pi\alpha/v}{1 - e^{-\pi\alpha/v}}. \tag{4.7}$$

The standard approach to compute the enhancement is to solve numerically the Schördinger equation for the incoming two-particle state to find the wave function distortion; some approximated solutions also exist [215, 216, 217], especially with the aim of studying resonances.

On the Fig. 4.1 value of the Sommerfeld factor is shown in the m_ϕ/m_χ vs. g plane in the case of typical DM halo velocities $v \sim 10^{-3}$. As expected from Eq. (4.4) it can be seen that the enhancement grows with the coupling and diminishes with the mediator mass. What is more interesting is the clearly visible resonance structure, leading to much larger enhancement factors. These resonances come from the formation of loosely bound states in the Yukawa potential. Whenever such a bound state can be formed, the annihilation cross-section grows rapidly. In fact, by following the method of solving the Schrödinger equation exactly at a resonance one obtains an infinite enhancement. This is of course unphysical, and is due to the fact that our quantum mechanical description does not take into account a bound state decay. Indeed, the finite lifetime of the bound state will make the enhancement saturate at $v \sim \alpha^3(m_\phi/m_\chi)$ [201].

To determine the paramterics of the resonances one can approximate the interaction potential by the Hulthén one:

$$V_H(r) = A\frac{\delta e^{-\delta r}}{1-e^{-\delta r}}, \tag{4.8}$$

which maintains the same both long and short distance behaviour as the Yukawa potential [215]. In this approximation the resonances occur whenever

$$\frac{m_\phi}{m_\chi} \approx \frac{6\alpha}{\pi^2 n^2}, \qquad n = 1, 2, 3, \ldots \tag{4.9}$$

which is in a reasonable agreement with the numerical solution. One can also deduce the magnitude of the Sommerfeld effect at the resonance, leading to

$$S(v) \approx \frac{\pi^2\alpha}{6v^2}\frac{m_\phi}{m_\chi}. \tag{4.10}$$

This shows that at the resonance the enhancement scales as v^{-2}, down to the velocities where the bound state decay becomes important.

Anticipating further application of this idea to the MSSM, on the same figure we indicate the value of the weak coupling at the electroweak scale, $g_2(m_Z) \approx 0.652$, and on the right axis we give the corresponding m_χ, putting $m_\phi = m_W$. This gives a rough estimate of the importance of the Sommerfeld effect for the neutralino. For a sizeable effect it has to be rather heavy, however for a mass of about several TeV one should observe a strong resonance. As we will show with detailed computation this is indeed the case.

Away from the resonance the velocity dependence is a bit different, but in general two features are present: strong suppression of the enhancement for $v \to 1$ and saturation at low v. On Fig. 4.2 full velocity dependence for four parameter choices is presented. The blue, violet and yellow lines correspond to a generic values of the mass ratio and strength of the coupling, while the green line shows the near resonance behaviour. In all cases the Sommerfeld factor falls rapidly with velocity and saturates at a value proportional

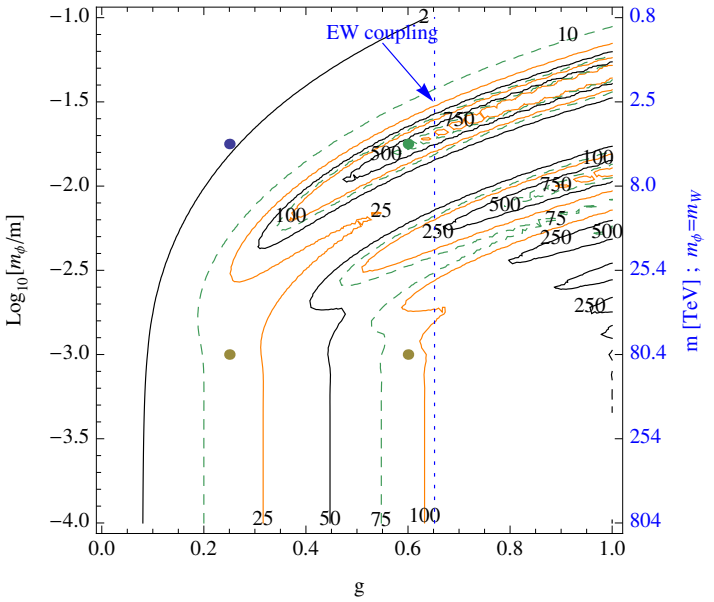

Figure 4.1: The Sommerfeld enhancement factor coming from exchange of a boson with mass m_ϕ between two DM particles with mass m and velocity $v = 10^{-3}$ in the function of the coupling constant g. Value of g_2 at the electroweak scale is highlighted and the corresponding mass of the neutralino in the case when $m_\phi = m_W$ is given on the right axis. Four points corresponding to the parameter choices of the Fig. 4.2 are also shown.

to $\alpha m_\chi/m_\phi$, with the precise value strongly depending on the DM mass. Away from resonance this happens when the de Broglie wavelength is comparable to the range of interaction, giving $v \sim m_\phi/m_\chi$, while close to the resonance the saturation occurs later.

In the intermediate regime, there is a strong v dependence. In the Coulomb case one has

$$S(v) \xrightarrow{\alpha \gg v} \frac{\pi\alpha}{v}, \tag{4.11}$$

which on Fig. 4.2 is shown as "$1/v$" enhancement. One can see that the off-resonance regimes follow approximately this solution before the saturation takes place (which is also apparent from the fact that Yukawa potential resembles the Coulomb one at distances shorter than $\sim 1/m_\phi$). On the resonance, the velocity dependence is indeed stronger, as advocated before.

Large Sommerfeld enhancements described above were studied by many authors, mostly in the context of model building for explaining cosmic ray anomalies. Its interplay with clumpiness of DM was proposed in [218] and later in [219, 220]. This may lead to enhanced production of gamma rays in the substructures: e.g. [221] shows that H.E.S.S. and MAGIC already constrain very large, resonant enhancements (and that the CTA will improve those limits, while FERMI data will not be able to tell us much on this issue).

The importance of the Sommerfeld effect for the thermal relic density was not appreciated at the very beginning. Only several years later, in [222] possible strong impact of the kinetic decoupling was observed in generic models with velocity-dependent interac-

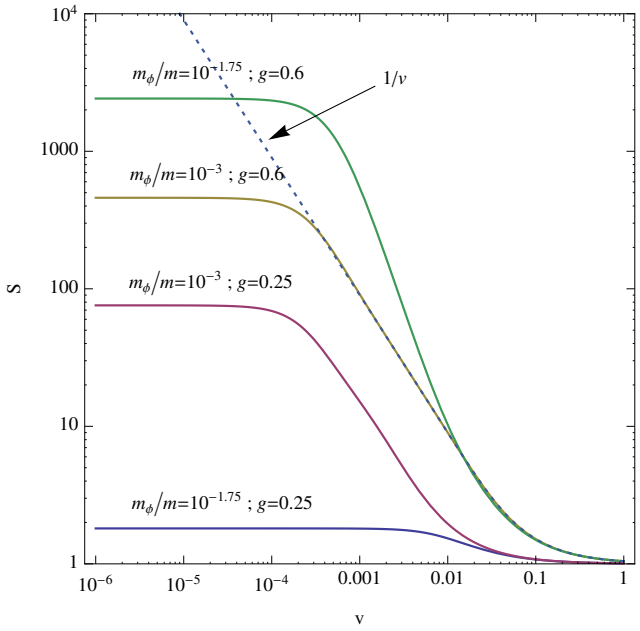

Figure 4.2: The Sommerfeld enhancement factor dependence on the velocity for several parameter choices. It grows rapidly for decreasing velocity, saturating roughly at $v \sim m_\phi/m_\chi$ with precise value depending on the parameters. For comparison Coulomb "$1/v$" enhancement is shown. The green line corresponds to parameters close to a resonance; in this case the dependence on velocity is even stronger than $1/v$ and saturation happens for lower v.

tions: after kinetic decoupling takes place the DM cools more rapidly and annihilation is enhanced stronger. This was confirmed and studied in detail in [223].

Such models with large enhancements are subject to many constraints coming from astrophysical observations as well as the history of the Universe. Among those are:

- the μ-type distorsion to the CMB power spectrum (already ruling out the proximity of the Yukawa resonance [224]),
- tension with obtaining correct thermal relic density [223],
- ellipticity of the halo, which puts constraints on the strength of DM self-interactions, ruling out $m_\phi \lesssim 100$ MeV [24],
- similar bounds are obtained from dissipation of sub-halos, growth rate of supermassive black holes and the Bullet cluster (conceptually clearest but numerically the weakest one); this rules out $m_\phi \lesssim 40$ MeV [225],
- direct detection due to mixing of the (scalar) force carrier with the Higgs; [226] finds strong constraints in this kind of models from the CDMS-II results [227], cutting part of the parameter space explaining PAMELA,
- however, one of the strongest constraints come from gamma-ray observations of the Galactic Center (GC) performed by H.E.S.S. [228].

An extensive summary of the possible consistent scenarios of the large Sommerfeld effect being able to take account for the PAMELA positron fraction data can be found in [229].

However, one should stress that most of the above constraints are weakened if local substructures exist [230]. The reason is that since SE is stronger in subhalos (because they are colder), the main signal explaining PAMELA comes from the substructures. This means that before they are formed one can accomodate for smaller Sommerfeld boost factors, thus one needs smaller coupling. This is especially relevant for the constraints coming from the GC, where one expects not to have any substructeres.

Other aspects of this topic were also studied, from which especially worth mentioning is the application of Sommerfeld corrections to leptogenesis [231] and studies of the WIMPonium, i.e. loosely bound states at the threshold (resonance) and its phenomenology [232, 233, 234].

4.3 Field theory derivation for general multi-state case

In the computations of the Sommerfeld effect there are however a few issues one should be careful about. First, the coefficient α in the potential depends on the nature of the incoming state and the possible type(s) of interaction. In particular, when the effect involves fermions, it is different if the interacting particles are Dirac or Majorana and whether they are identical or not. This is especially important when co-annihilations enter the computation of the relic density.

To stress other delicate points, it is useful to first recap on what are the conditions for the enhancement to be significant. As discussed above the Sommerfeld enhancement can be viewed as an consequence of forming a loosely bound state due to a long-range interaction. In order to have such a bound state the characteristic Bohr energy of the interaction need to be larger than the kinetic energy. In the limit $m_\phi \to 0$, this gives a condition $\alpha^2 m_\chi \gtrsim m_\chi v^2$, i.e.:

$$v \lesssim \alpha \,. \tag{4.12}$$

For a typical WIMP the coupling is of order $\alpha \sim 0.03$, so that there can be some sizeable enhancement only long after freeze-out (which happens for $v \sim 0.3$). However, if there exists a slightly heavier state, then it may happen that just after freeze-out DM particles have enough energy to produce it nearly on-shell. At threshold these heavier states are produced with, roughly speaking, zero velocity. As we will see later on, if the mass splitting between the DM and the heavier state is small enough, this may give rise to important changes in the relic density.

A second condition comes from the comparison of the range of the Yukawa potential with the Bohr radius. In order for the interaction to distort the wave function significantly, the range of the potential cannot be much smaller than the Bohr radius of the two-particle state,

$$\frac{1}{m_\phi} \gtrsim \frac{1}{\alpha m_\chi} \,. \tag{4.13}$$

In case of very large enhancements, this condition needs to be even stronger, i.e. the range of potential has to be much larger than the Bohr radius. However, even in case of enhancements of order unity one should treat carefully the regime when $m_\phi \approx \alpha m_\chi$.

When considering a system of two states with a small mass splitting δm interacting off-diagonally there is another important constraint [216]. If δm is significantly larger than the kinetic energy, it may seem that the heavier state cannot be produced, and hence there is no enhancement. However, if the potential is strong enough, there still may be an effect, coming from producing the heavier state at small distances, where the potential energy is large. Thus the condition reads:

$$2\delta m \lesssim \alpha^2 m_\chi + \mathcal{E}\,, \tag{4.14}$$

meaning that the characteristic Bohr energy of the potential plus the kinetic energy $\mathcal{E}$ is large enough to produce the heavier state. Moreover, when dealing with multi-state systems, the picture of the Sommerfeld enhancement as an effect of a static, long range force is in general no longer applicable. The reason is that exchange of ϕ leads to a momentum and energy transfer due to the mass splitting δm and one may need to take into account terms of order $O(\delta m/m)$ which modifies the interaction potential.

When dealing with a complex particle physics setup like, e.g., the MSSM, several such complications may intervene at the same time. A simple parametric description is not possible and for a proper estimate of the Sommerfeld effect and its impact on the relic density, a computation within a fully general formalism is needed. The approach we follow to address this problem is a generalization of the one developed in [235].[2]

4.3.1 Fermion initial state

We are interested in the general case with N two-particle fermionic states coupled together. They interact with "long-range forces" due to the exchange of some boson ϕ, denoting generically a vector, an axial vector or a scalar boson (in the MSSM those correspond to Z^0, $W^\pm$, γ, h, H^0 and $H^\pm$). The Sommerfeld enhancement corresponds to computing in the non-relativistic limit the sum of ladder diagrams as presented on the Fig. 4.3a.

The structure of those diagrams can be in general very complicated, since all states can appear in one diagram, through different interactions.

We start from writing the recurrence relation for the annihilation amplitudes as illustrated on Fig. 4.3b. Let's consider a process of the type

$$\chi_a\chi_b \to \chi_i\chi_j \to \chi_i'\chi_j' \to \ldots \to \text{SM final states}\,, \tag{4.15}$$

where the intermediate pairs $\chi_i\chi_j$ can be the same or different as the initial pair $\chi_a\chi_b$. The spin of the initial pair, which in the non-relativistic limit is a conserved quantity, can be in general either in the singlet ($S = 0$) or triplet ($S = 1$) state. For every possible $\chi_i\chi_j$

[2] In the literature one can find also other derivations of the Sommerfeld effect, which one might use [215, 236]

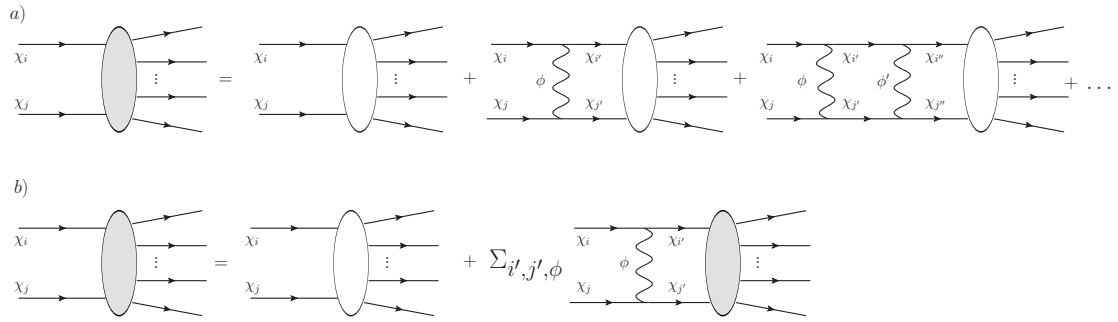

Figure 4.3: Ladder diagrams for the Sommerfeld enhancement. *a*) incoming $\chi_i\chi_j$ particles interact with exchange of ϕ's (in general different), which can be a scalar, vector or axial vector bosons. In the ladder a virtual states $\chi_{i'}\chi_{j'}$ can be produced and the final annihilation proceed in the channel which can be different than initial one. Filled blob represents full annihilation process with any number of SM particles in final state, while the empty one its tree level counterpart. *b*) the same but written in a recursive form; sum is over all possible intermediate states and exchanged bosons.

pair we get a recurrence relation for its annihilation amplitude. Denoting this amplitude by A_{ij} and its tree level value by A^0_{ij}, one obtains in the non-relativistic limit [235]:

$$A_{ij}(p) = A^0_{ij}(p) - \sum_{i'j'\phi} N_{ij,i'j'} \frac{g_{ii'\phi} g_{j'j\phi}}{(2\pi)^3} \int \frac{d^3k}{(\vec{p}-\vec{k})^2 + m_\phi^2} \frac{A_{i'j'}(k)}{\frac{\vec{k}^2}{2m_r^{i'j'}} - \mathcal{E} + 2\delta m_{i'j'}}\,, \tag{4.16}$$

where the sum is over different $\chi_{i'}\chi_{j'}$ intermediate states and different interactions. Here, $\mathcal{E} = \vec{p}^{\,2}/2m_r^{ab}$ is the kinetic energy of incoming pair (at infinity), with m_r^{ab} the reduced mass and $\vec{p}$ the CM three-momentum, $2\delta m_{ij} = m_i + m_j - (m_a + m_b)$ the mass splitting, $g_{ii'\phi}$ and $g_{j'j\phi}$ are the coupling constants and $N_{ij,i'j'}$ is the term containing normalization and combinatorial factors.

To rewrite the expression above in the form of the Schrödinger equations we make following redefinitions:

$$A_{ij}(\vec{p}) = \left(\frac{\vec{p}^{\,2}}{2m_r^{ij}} - \mathcal{E} + 2\delta m_{ij}\right) \tilde{\psi}_{ij}(\vec{p}), \tag{4.17}$$

$$U^0_{ij}(\vec{r}) = \int d^3\vec{p}\, e^{i\vec{p}\cdot\vec{r}} A^0_{ij}(\vec{p}, P_0), \tag{4.18}$$

$$\psi_{ij}(\vec{r}) = \int d\vec{p}\, e^{i\vec{p}\cdot\vec{r}} \tilde{\psi}_{ij}(\vec{p}), \tag{4.19}$$

which allows us to rewrite Eq. (4.16) as a differential equation:

$$-\frac{\partial^2}{2m_r^{ij}}\psi_{ij}(\vec{r}) = U^0_{ij}(\vec{r}) + (\mathcal{E} - 2\delta m_{ij})\,\psi_{ij}(\vec{r}) + \sum_{i'j'\phi} V^\phi_{ij,i'j'}\psi_{i'j'}(\vec{r}), \tag{4.20}$$

where ϕ refers to the type of the particle being exchanged (scalar, vector or axial vector boson).

The interaction potential

The form of the $V^{\phi}_{ij,i'j'}(r)$ for any two-particle states exchanging a boson ϕ is always of Yukawa- or Coulomb-type, but due to different couplings and multiplicities we can have different relative coefficients in front. Those numerical coefficients depend on the type of fermions present in the diagram. i.e are they Dirac or Majorana and distinguishable or not.

Therefore, we write in general:

$$V^{\phi}_{ij,i'j'}(r) = \frac{c_{ij,i'j'}(\phi)}{4\pi}\frac{e^{-m_\phi r}}{r}\,, \tag{4.21}$$

with $c_{ij,i'j'}(\phi)$ being coefficients depending on the couplings and states involved. An efficient way of computing them was developed in [237] and is explained below. The results in case of a system involving one spin 1/2 Dirac fermion and/or two different Majorana spin 1/2 fermions are summarized in Table 4.1. Whether the potential is attractive or repulsive is hidden in the sign of the coefficients c and depends on the interaction type. The exchange of scalars is always attractive in the spin singlet (i.e. overall plus sign), but can also be repulsive in the triplet. Vector and axial bosons can give attractive or repulsive forces, depending on the charges.

In [235] it was shown that the integration on the time component of the loop momentum of the Feynman graph expression of the Bethe-Salpeter equation for a four-point amplitude Ψ gives in non-relativistic limit:

$$\Psi = V_{int} * \frac{1}{H_0 - \mathcal{E}}\Psi\,. \tag{4.22}$$

From this expression, by redefining $\Psi \equiv (H_0 - \mathcal{E})\Phi$, we get the Schrödinger equation

$$H_0\Phi - V_{int} * \Phi = \mathcal{E}\Phi\,. \tag{4.23}$$

Here, Φ is in general a multicomponent state describing many possible pairs of particles that interact with each other. Hence this equation is just a compact form for a system of equations, and the symbol $*$ states for an operator acting on spins as well. For each pair ij:

$$H_0^{ij} = -\frac{\nabla^2}{2m_r^{ij}} + 2\delta m_{ij}\,, \tag{4.24}$$

where $m_r^{ij} = m_i m_j/(m_i + m_j)$ is the reduced mass of the pair ij.

In order to make explicit the action of the interaction V_{int} on a state, we express both the interaction and the state in terms of fields and then make the appropriate contractions. The relativistic Feynman diagram in the non-relativistic limit gives explicitly the result, but it is simpler to work directly with the form (4.23) by defining suitable non-relativistic contractions. This way of doing the computation has a virtue of easy bookkeeping of all multiplicative factors and signs appearing especially in the case involving Majorana particles. This formalism allows also to include easily the fact that we have initial and final state with defined total angular momentum and spin.

In the non-relativistic approximation the time delay is neglected and we can work in the time independent Schrödinger picture.

We introduce the state Φ describing a fermion-antifermion (Dirac or Majorana) pair expressed as[3]

$$|\Phi_\gamma^{ij}\rangle = N_{ij}\int d\vec{z}d\vec{w}\,\bar{\psi}_i(z)\mathcal{O}_\gamma\psi_j(w)|0\rangle\Phi_\gamma^{ij}(z,w). \tag{4.25}$$

For a (Dirac) fermion-fermion pair one needs to take $\psi(w)\to\psi^c(w)$. It is easy to see that the spin singlet $S=0$ and the spin triplet $S=1$ are encoded in the formula:[4]

$$S=0:\quad \mathcal{O}_\gamma\equiv\gamma_5\,,\qquad S=1:\quad \mathcal{O}_\gamma\equiv\vec{\gamma}\cdot\vec{S}\,, \tag{4.26}$$

where $\vec{S}$ is the spin of initial pair. The normalization is

$$\begin{aligned} N_{ij} &= 1/\sqrt{2} \qquad i\neq j\,,\\ N_{ij} &= 1/2 \qquad i=j\,. \end{aligned} \tag{4.27}$$

Take an interaction of the form (as usual by Γ we denote the gamma matrices structure)

$$V_{int} = g_\Gamma^2\int d\vec{x}d\vec{y}\,\bar{\psi}_k(x)\Gamma\psi_i(x)\bar{\psi}_j(y)\Gamma\psi_l(y)W^\phi_{kl,ij}(x-y), \tag{4.28}$$

where $W^\phi_{kl,ij}$ is the propagator of the boson exchanged between the two vertices. In the non-relativistic limit only $\Gamma=1,\gamma_0,\gamma_j\gamma_5$ can contribute. The transition $ij\to kl$ can be described in terms of operators acting on the initial state giving the final one:

$$\begin{aligned} &\frac{g_\phi^2}{2!}\int d\vec{x}d\vec{y}\,\left(\bar{\psi}_k(x)\Gamma\psi_i(x)+\bar{\psi}_l(x)\Gamma\psi_j(x)+h.c.\right)\left(\bar{\psi}_k(y)\Gamma\psi_i(y)+\bar{\psi}_l(y)\Gamma\psi_j(y)+h.c.\right)\times\\ &\times W^\phi_{kl,ij}(|\vec{x}-\vec{y}|)\int d\vec{z}d\vec{w}\,N_{ij}\bar{\psi}_i(z)\mathcal{O}_\gamma\psi_j(w)|0\rangle\Phi_\gamma^{ij}(z,w)=\\ &=\int d\vec{x}d\vec{y}\,N_{kl}\bar{\psi}_k(x)\mathcal{O}_\gamma\psi_l(y)|0\rangle V^\phi_{kl,ij}(|\vec{x}-\vec{y}|)\Phi_\gamma^{ij}(x,y). \end{aligned} \tag{4.29}$$

The interaction potential between two two-particle states ($ij\to kl$) arising due to vector, axial vector boson or scalar exchange with the mass m_ϕ has the Yukawa form (4.21). We are interested in computing the coefficients $c^\Gamma_{kl,ij(\gamma)}$ for all possible cases. Note that in the non-relativistic approximation spin-orbit interactions are suppressed. As a consequence, a spin-singlet(triplet) initial state gives a spin-singlet(triplet) final state, and also the parity of the wave function, that is whether $\Phi(\vec{r})=\pm\Phi(-\vec{r})$ (e.g. $+$ for the s-wave and $-$ for the p-wave) is the same in the initial and final state. As a result in general there are four independent systems of equations: the spin-singlet even, spin-singlet odd, spin-triplet even, spin-triplet odd. The coefficients $c^\Gamma_{kl,ij}$ and therefore the interaction potentials are in general different in the four cases.

[3] In the following we write x,y,z,w for $\vec{x},\vec{y},\vec{z},\vec{w}$, the time coordinate (not indicated) being everywhere the same.

[4] Here we extend the idea presented in [238] to include also the spin triplet.

To illustrate the method, consider first a (Dirac) fermion-antifermion pair. We make the possible contractions:

$$V_{int} * |\Phi^{ij}_\gamma\rangle = g^2 \int_{xyzw} \bar\psi_k(x)\Gamma\langle\psi_i(x)\bar\psi_i(z)\rangle\mathcal{O}_\gamma\langle\psi_j(w)\bar\psi_j(y)\rangle\Gamma\psi_l(y)W^\phi(x-y)\Phi^{ij}_\gamma(z,w).$$

By noting that only the creation operator part of both $\bar\psi_a(z)$ and $\psi_b(w)$ appear in the state $\bar\psi_i(z)\mathcal{O}_\gamma\psi_j(w)|0\rangle$, we get for $p \ll m$:

$$\langle\psi_i(x)\bar\psi_i(z)\rangle \equiv \langle 0|\psi_i(x)\bar\psi_i(z)|0\rangle = \int \frac{d\vec q}{2\omega(2\pi)^3} e^{i\vec p(\vec x-\vec z)} \sum_s u_s\bar u_s \to \delta(\vec x-\vec z)P_+\,, \qquad (4.30)$$

$$\langle\psi_l(w)\bar\psi_l(y)\rangle \equiv -\langle 0|\bar\psi_l(y)\psi_l(\vec w)|0\rangle^T = -\int \frac{d\vec q}{2\omega(2\pi)^3} e^{i\vec p(\vec w-\vec y)} \sum_s v_s\bar v_s \to \delta(\vec y-\vec w)P_-\,,$$

where $P_\pm = \frac{1\pm\gamma_0}{2}$ and $\omega = \sqrt{\vec q^2+m^2}$. Therefore

$$V_{int} * |\Phi^{ij}_\gamma\rangle = g^2 \int d\vec x d\vec y\, \bar\psi_k(x)\Gamma P_+\mathcal{O}_\gamma P_-\Gamma\psi_l(y)|0\rangle W^\phi_{kl,ij}(x-y)\Phi^{ij}_\gamma(x,y).$$

Note that $\bar\psi_k(x)P_+|0\rangle = \bar\psi_k(x)|0\rangle$ and that $P_-\psi_l(y)|0\rangle = \psi_l(y)|0\rangle$.

Keeping into account the sign difference between the vector and axial propagator with respect to scalar one and defining $W(\vec r) = e^{-m_\phi r}/4\pi r$, one can write $W_{\gamma_0} = -W$, $W_{1,\gamma_j\gamma_5} = +W$. Then by Dirac algebra we finally get

$$V_{int} * |\Phi^{ij}_\gamma\rangle = c^\Gamma_\gamma g^2 \int d\vec x d\vec y\, \bar\psi_k(x)\mathcal{O}_\gamma\psi_l(y)|0\rangle W(x-y)\Phi^{ij}_\gamma(x,y), \qquad (4.31)$$

with

$$c^1_{\gamma_5} = c^{\gamma_0}_{\gamma_5} = c^1_{\gamma_i} = c^{\gamma_0}_{\gamma_i} = 1, \qquad c^{\gamma_j\gamma_5}_{\gamma_5} = -3, \qquad c^{\gamma_j\gamma_5}_{\gamma_i} = 1.$$

This result gives a term in the equation for Φ^{kl}_γ:

$$H^{kl}_0\Phi^{kl}_\gamma - c^\Gamma_{kl,ij}\frac{e^{-m_\Gamma r}}{4\pi r}\Phi^{ij}_\gamma = \mathcal{E}\Phi^{kl}_\gamma\,, \qquad (4.32)$$

where $c^\Gamma_{kl,ij} = \frac{N^{ij}}{N^{kl}}c^\Gamma_\gamma g^2$.

The state may contain Majorana fermions $\chi = \chi^c = C\bar\chi^T$, like

$$\bar\psi(z)\mathcal{O}_\gamma\chi(w)|0\rangle\Phi(z,w),\ \bar\chi(z)\mathcal{O}_\gamma\psi(w)|0\rangle\Phi(z,w),\ \bar\chi_i(z)\mathcal{O}_\gamma\chi_j(w)|0\rangle\Phi(z,w).$$

Again $\mathcal{O}_\gamma = \gamma_5$ for the spin singlet and $\mathcal{O}_\gamma = \gamma_j$ for the spin triplet. Since $\bar\chi(z)$ and $\chi(w)$ contain only the creation operator part, the possible contractions between Majorana fermions are, in the non-relativistic limit,

$$\begin{aligned}
&\langle\chi(x)\bar\chi(z)\rangle \to \delta(\vec x-\vec z)P_+\,, \qquad \langle\chi(w)\bar\chi(y)\rangle \to \delta(\vec y-\vec w)P_-\,, \qquad (4.33)\\
&\langle\chi(x)\chi(w)^T\rangle = \langle\chi(x)\bar\chi(w)\rangle C^T \to -\delta(\vec x-\vec w)P_+C\,,\\
&\langle\bar\chi(y)^T\bar\chi(z)\rangle = C^T\langle\chi(y)\bar\chi(z)\rangle \to -\delta(\vec y-\vec z)CP_+\,.
\end{aligned}$$

The computations presented above are for the even orbital angular momentum, for instance $l = 0$ (s-wave). This means that the two-body wave function is symmetric. The results for these coefficients are summarized in Table 4.1. It is very easy to generalize it to higher partial waves.

These results cover all the possibilities of types of two-body to two-body interactions when we can have Dirac or Majorana states, i.e. every other case present in some model will have one of those forms (so the coefficient in Schrödinger equation for computing Sommerfeld enhancement will be the same) with possible different coupling constant.

Solving the Schrödinger equation

Notably in the approach outlined above we can split different interaction types (i.e. mediated by different bosons or with different couplings etc.) within a ladder diagram and consider them separately. The trade-off is that every possible intermediate two-particle state will lead to one equation, thus in such a general case we will need to consider a set of coupled Schrödinger equations. Although these equations are inhomogeneous, one can compute the Sommerfeld enhancement by solving the associated homogeneous ones, using the partial waves decomposition as described in [235]. The reason is that the Sommerfeld enhancement factorizes out from the annihilation matrix, as it does not depend on the final states but enters only as a distortion of the incoming wave function. We will be interested only in the s-wave, but it is straightforward (though not always easy numerically) to extend the analysis to higher partial waves.

To reduce these equations in a form more suitable for numerical calculations, after the partial wave decomposition we define the reduced radial wave function $\varphi(x)$ as

$$R^{ij}_{p,l}(r) = Np\frac{\varphi^{ij}_l(x)}{x}\,, \qquad x = pr\,, \tag{4.34}$$

where N is some normalization constant and p is the value of the CM three-momentum for one of the incoming particles (a or b). Since we restrict to the s-wave case $l = 0$, we will drop the l index from now on. From (4.20) one get then set of equations[5] for the $\varphi^{ij}(x)$:

$$\frac{d^2\varphi^{ij}(x)}{dx^2} + \frac{m^{ij}_r}{m^{ab}_r}\left[\left(1 - \frac{2\delta m_{ij}}{\mathcal{E}}\right)\varphi^{ij}(x) + \frac{1}{\mathcal{E}}\sum_{i'j'\phi} V^{\phi}_{ij,i'j'}(x)\varphi^{i'j'}(x)\right] = 0\,. \tag{4.35}$$

To obtain the enhancement we need to solve this set of equations with appropriate boundary conditions. In $x = 0$ they are set by the requirement that the solution is regular. In $x \to \infty$ the solution has to describe one incoming $\chi_a\chi_b$ state and all the possible $\chi_i\chi_j$ states that can be produced in the ladder. For the latter there can be two cases:

1. $2\delta m_{ij} < \mathcal{E}$ - there is enough energy to produce on-shell states $\chi_i\chi_j$,
2. $2\delta m_{ij} > \mathcal{E}$ - there is *not* enough energy; states $\chi_i\chi_j$ are off-shell.

[5] This form is most suitable for numerical solutions, while often it is presented not in terms of the CM momentum, but rather relative velocity of incoming particles, being equal to $v_r = p/m^{ab}_r$.

	Spin singlet		
ϕ :	scalar ($\Gamma = \mathbb{1}$)	vector ($\Gamma = \gamma_0$)	axial ($\Gamma = \gamma_i\gamma_5$)
$c_{+-,+-}$	g^2	g^2	$-3g^2$
$c_{++,++}$	g^2	$-g^2$	$-3g^2$
$c_{ii,+-}$	$\sqrt{2}\lvert g_{i+}\rvert^2$	$\sqrt{2}\lvert g_{i+}\rvert^2$	$-3\sqrt{2}\lvert g_{i+}\rvert^2$
$c_{ij,+-}$	$2\mathrm{Re}\,(g_{i+}g^*_{j+})$	$2\mathrm{Re}\,(g_{i+}g^*_{j+})$	$-6\mathrm{Re}\,(g_{i+}g^*_{j+})$
$c_{ii,jj}$	$2\lvert g_{ij}\rvert^2 + g_{ij}^2 + g_{ij}^{*2}$	$2\lvert g_{ij}\rvert^2 - g_{ij}^2 - g_{ij}^{*2}$	$-3(2\lvert g_{ij}\rvert^2 + g_{ij}^2 + g_{ij}^{*2})$
$c_{ij,ij}$	$2\lvert g_{ij}\rvert^2 + g_{ij}^2 + g_{ij}^{*2} + 4g_{ii}g_{jj}$	$-2\lvert g_{ij}\rvert^2 + g_{ij}^2 + g_{ij}^{*2}$	$-3(2\lvert g_{ij}\rvert^2 + g_{ij}^2 + g_{ij}^{*2}) - 12g_{ii}g_{jj}$
$c_{+i,+i}$	$\lvert g_{i+}\rvert^2 + 2g_{ii}g$	$-\lvert g_{i+}\rvert^2$	$-3\lvert g_{i+}\rvert^2 - 6g_{ii}g$
$c_{+i,+j}$	$g_{i+}g^*_{j+} + 2g\mathrm{Re}\,(g_{ij})$	$-g_{i+}g^*_{j+} - 2gi\mathrm{Im}\,(g_{ij})$	$-3g_{i+}g^*_{j+} - 6g\mathrm{Re}\,(g_{ij})$
$c_{ii,ii}$	$4g_{ii}^2$	0	$-12g_{ii}^2$
$c_{ij,ii}$	$4\sqrt{2}g_{ii}\mathrm{Re}\,(g_{ij})$	0	$-12\sqrt{2}g_{ii}\mathrm{Re}\,(g_{ij})$
	Spin triplet		
$c_{+-,+-}$	g^2	g^2	g^2
$c_{++,++}$	g^2	$-g^2$	g^2
$c_{ii,+-}$	0	0	0
$c_{ij,+-}$	$2i\mathrm{Im}\,(g^*_{i+}g_{j+})$	$2i\mathrm{Im}\,(g^*_{i+}g_{j+})$	$2i\mathrm{Im}\,(g^*_{i+}g_{j+})$
$c_{ii,jj}$	0	0	0
$c_{ij,ij}$	$-(2\lvert g_{ij}\rvert^2 + g_{ij}^2 + g_{ij}^{*2}) + 4g_{ii}g_{jj}$	$2\lvert g_{ij}\rvert^2 - g_{ij}^2 - g_{ij}^{*2}$	$-(2\lvert g_{ij}\rvert^2 + g_{ij}^2 + g_{ij}^{*2}) + 4g_{ii}g_{jj}$
$c_{+i,+i}$	$-\lvert g_{i+}\rvert^2 + 2gg_{ii}$	$\lvert g_{i+}\rvert^2$	$-\lvert g_{i+}\rvert^2 + 2gg_{ii}$
$c_{+i,+j}$	$-g_{i+}g^*_{j+} + 2g\mathrm{Re}\,(g_{ij})$	$g_{i+}g^*_{j+} - 2gi\mathrm{Im}\,(g_{ij})$	$-g_{i+}g^*_{j+} + 2g\mathrm{Re}\,(g_{ij})$
$c_{ii,ii}$	0	0	0
$c_{ij,ii}$	0	0	0
Couplings:	$g_{ij}^\Gamma\bar{\chi}_j\Gamma\chi_i\phi$ (+*h.c.* iff $i \neq j$),	$g_{i+}^\Gamma\bar{\psi}\Gamma\chi_i\phi$ + *h.c.*,	$g^\Gamma\bar{\psi}\Gamma\psi\phi$, where $\Gamma = \mathbb{1}, \gamma_0, \gamma_i\gamma_5$

Table 4.1: List of all possible coefficients in the potential $V^\phi_{ij,i'j'}(r)$ for the Sommerfeld effect computation. The table includes any annihilation process involving one spin 1/2 Dirac fermion (denoted by + or − depending on whether it is a particle or antiparticle) and/or two different Majorana spin 1/2 fermions (denoted by i and j), for an even partial wave. Couplings are defined in the last line for each Γ, where χ is a Majorana fermion, ψ a Dirac field, ϕ is the exchanged boson. When applied to the MSSM, where one needs to consider a chargino and one or two neutralinos, some of the coefficients vanish due to the CP conservation and couplings of type g_{ii} are negligible. The overall "+" sign refers to an attractive force while "−" to a repulsive force. Note also that $c_{ij,kl} = c^*_{kl,ij}$.

The radial wave functions behave at infinity as:

$$R^{ab}(r) \to \frac{C_1^{ab}}{2i}\frac{e^{ik_{ab}r}}{r} - \frac{1}{2i}\frac{e^{-ik_{ab}r}}{r}\,, \tag{4.36}$$

for the incoming pair and

$$R^{ij}(r) \to \begin{cases} \frac{C_2^{ij}}{2i}\frac{e^{ik_{ij}r}}{r} & \text{if on}-\text{shell}, \\ \frac{D_2^{ij}}{2i}\frac{e^{-|k_{ij}|r}}{r} & \text{if off}-\text{shell}, \end{cases} \tag{4.37}$$

for every other intermediate state $\chi_i\chi_j$. Our choice of normalization of the wave function is that for the non-interacting case $R_{ab} = \sin(k_{ab}r)/r$. After changing the variable to $x = k_{ab}\cdot r$ and defining $q_{ij} = m_r^{ij}/m_r^{ab}\,(1 - 2\delta m_{ij}/\mathcal{E})$ we get set of boundary conditions for the reduced wave functions at $x \to \infty$:

$$i\varphi^{ab} - \partial_x\varphi^{ab} = -e^{-ix}, \tag{4.38}$$

$$\begin{cases} i\sqrt{q_{ij}}\varphi^{ij} - \partial_x\varphi^{ij} = 0 & \text{if on}-\text{shell}, \\ \sqrt{-q_{ij}}\varphi^{ij} + \partial_x\varphi^{ij} = 0 & \text{if off}-\text{shell}. \end{cases} \tag{4.39}$$

To check our numerics we can use the unitarity condition, saying that:

$$1 = |C_1^{ab}|^2 + \sum_{ij}\sqrt{q_{ij}}|C_2^{ij}|^2. \tag{4.40}$$

Since the set of boundary conditions depends on the masses and energies of initial particles, the solutions to the Schrödinger equations, i.e. the wave-functions, depend on the initial conditions of the incoming pair $\chi_a\chi_b$: to be precise we should call them then $\varphi_{(ab)}^{ij}(x)$. After solving (4.35) the (co-)annihilation cross section of the pair $\chi_a\chi_b$ is determined, up to the kinematical factor, by

$$\sigma_{(ab)} \propto \sum_{ij} S_{(ab)}^{ij}\cdot|A_{ij}^0|^2, \tag{4.41}$$

where the enhancement factors with our normalization are

$$S_{(ab)}^{ij} = |\partial_x\varphi_{(ab)}^{ij}|^2_{x=0}\,. \tag{4.42}$$

It is important to note, that the computation of the enhancement depends on the spin state of the initial two-body state (see Table 4.1). This means that one needs to project each annihilation cross-section into two parts, one for the singlet and one for the triplet initial spin state, and multiply each of them by a different enhancement factor. The method we used to do so is described below.

Would one need to include higher partial waves, one has to compute $c_{ij,i'j'}(\phi)$ coefficients for odd partial waves, add a centrifugal term to the equations (4.20) and (4.35), and modify the expression for the enhancement, see [235].

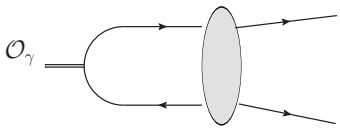

Figure 4.4: Diagram with explicit contraction of the initial spinors by $\mathcal{O}_\gamma$. The blob represents every possible annihilation process with all possible two-body final states - fermionic or bosonic.

Projection of the (co-)annihilation amplitudes into spin singlet and spin triplet initial states

We consider the annihilation of two fermionic dark matter particles into two bosonic or fermionic standard model particles. In our approximation we take the initial state to be at rest, and we neglect the dark matter mass differences and the masses of the particles resulting from the annihilation. Hence the kinematics of the annihilation process simplifies; by calling p_μ, p'_μ the momenta of the incoming dark matter particles and k_μ, k'_μ the momenta of the annihilation products we get in the CM frame:[6]

$$p_\mu \sim (m, \vec{0})\,, \qquad p'_\mu \sim (m, \vec{0})\,, \qquad k_\mu \sim (m, m\vec{n})\,, \qquad k'_\mu \sim (m, -m\vec{n})\,, \qquad \vec{n}^2 = 1\,. \tag{4.43}$$

The propagators of the virtual particles exchanged in the Feynman diagrams representing the amplitude will have denominators of the kind:

$$t - m^2 \sim -2m^2\,, \qquad u - m^2 \sim -2m^2\,, \qquad s - \mu^2 \sim 4m^2\,, \tag{4.44}$$

where $t \equiv (p-k)^2 \sim -m^2$, $u \equiv (p-k')^2 \sim -m^2$, $s \equiv (p+p')^2 \sim 4m^2$, and m is the appropriate mass of the particle mediating the annihilation.

With these simplifications one can decompose the rate to two factors, i.e. rate $\propto K \times \Phi$, where K is the amplitude squared summed over the final spin configurations and averaged over the initial one, and Φ is the phase space.

The phase space factor, apart from common factors, reads

$$\Phi = \left[\left(1 + \frac{m_1^2}{E_{cm}^2} - \frac{m_2^2}{E_{cm}^2} \right)^2 - 4\frac{m_1^2}{E_{cm}^2} \right]^{1/2}, \tag{4.45}$$

where m_1 and m_2 are masses of final particles and E_{cm}^2 is the energy in the CM frame.

The relative weights for singlet (triplet) will be computed by the ratio

$$\frac{Q(S=0,1)}{Q(S=0)+Q(S=1)}\,,$$

where $Q(S=0,1)$ is the sum of the singlet (triplet) squared amplitudes for the various annihilation channels:

$$Q(S=0,1) = \sum_j Q_{channel\ j}(S=0,1).$$

[6] It can be done without this simplification but in the case of interest it does not play any role, especially that we are interested only in the relative weights and so by doing this approximation we do not change the value of perturbative annihilation cross-section.

In conclusion, in our approximation the Sommerfeld enhanced total (i.e. summed over every channel) annihilation cross section σ_{enh} is related to the non-enhanced total annihilation cross section σ_0 by the formula

$$\sigma_{enh} = \left[\frac{Q(S=0)}{Q(S=0)+Q(S=1)} S(S=0) + \frac{Q(S=1)}{Q(S=0)+Q(S=1)} S(S=1) \right] \sigma_0 \,, \quad (4.46)$$

where $S(S=0,1)$ are the Sommerfeld enhancement factors for the spin singlet and triplet, respectively.

The computation of the weights follows closely the method previously seen. We compute the standard tree-level amplitude of annihilation to a given final state but with initial spinors contracted by $\mathcal{O}_\gamma$, as presented with a diagram on a Fig. 4.4. In a non-relativistic limit this gives precisely amplitudes $Q(S=0)$ for γ_5 and $Q(S=1)$ for $\vec{\gamma}\cdot\vec{S}$. From that point the computations proceed in a standard way.

4.3.2 Scalar and scalar-fermion initial state

We also extended the formalism presented above to the case of scalar-scalar and fermion-scalar initial pairs [239].

Again we consider an annihilation process of two particles, φ_i and φ_j, which are coupled to some light boson ϕ, leading to a long range interaction between them. In the case when this interaction is diagonal (i.e. the exchange of ϕ does not change the particles), in the non-relativistic limit the spin of initial particles does not matter - the static force is the same for both scalars and fermions. This is however not true if interactions can be off-diagonal and intermediate particles can have different masses. Then, due to the differences in the couplings and propagators between scalars and fermions, the computations of the Sommerfeld effect slightly differ.

Following the same steps as for the fermionic case, we write a recurrence relation for the annihilation amplitudes. Assuming that $\delta m_{ij}/m_i \ll 1$, in the non-relativistic limit we obtain the Schrödinger equation (4.20), obtaining automatically the coefficients $c_{ij,i'j'}(\phi)$ in the potential, Eq. (4.21).

Let's denote by a superscript S the case with two scalars and by F with one scalar and one fermion. In the second case let i and i' be fermions and j and j' scalars. Then we find:

$$c_{ij,i'j'} = g^\phi_{ii'} g^\phi_{jj'} N^{S,F}_{ij,i'j'} A^{S,F}_\phi(m_i, m_j, m_{i'}, m_{j'}) \,, \quad (4.47)$$

where $g^\phi_{ii'}$ is a coupling present in the $ii'\phi$ vertex. Tthe normalization and combinatorics gives

$$N^S_{ij,i'j'} = \begin{cases} 1 & i=j, i'=j' \text{ or } \mathrm{i}\neq\mathrm{j}, \mathrm{i}'\neq\mathrm{j}', \\ \sqrt{2} & i\neq j, i'=j' \text{ or } \mathrm{i}=\mathrm{j}, \mathrm{i}'\neq\mathrm{j}', \end{cases}$$
$$N^F_{ij,i'j'} = 1 \,,$$

and factors $A^{S,F}_\phi$ are, with $\phi = V, A, S$ indicating respectively a vector, an axial vector

and a scalar:

$$A_V^S = A_A^S = \frac{1}{2}\left(1 + \frac{m_i}{2m_{i'}} + \frac{m_j}{2m_{j'}}\right), \tag{4.48}$$

$$A_S^S = \frac{1}{4m_{i'}m_{j'}}, \tag{4.49}$$

$$A_V^F = \frac{m_{j'} + m_j}{2m_{j'}}, \tag{4.50}$$

$$A_A^F = 0, \tag{4.51}$$

$$A_S^F = \frac{1}{2m_{j'}}. \tag{4.52}$$

In the limit when all the masses are equal coefficients A_V^S, A_A^S reduce to the ones which were used in Refs. [207, 206, 208]. However, in general case when the masses of intermediate scalars differ, Eqs. (4.48) and (4.49) have to be used. Neglecting this fact can give rise to several per cent difference in the $c_{ij,i'j'}(\phi)$ coefficients.[7] We stress once again that those results are valid in the non-relativistic limit and when mass splitting is much smaller than all of the masses involved.

All the considerations above implicitly assumed that the interaction strength is sufficiently weak, so that the higher loop corrections do not alter the potential significantly. This is true for the weak and electromagnetic interactions, as well as for the Higgs exchange. However, in the case of strong interactions, corrections to the gluon exchange coming from gluon self-interactions and fermion loops may become important. To take this into account, following [207], instead of the potential (4.21) one should use one computed in [240], which in the configuration space is:[8]

$$V(\vec{r}) = -C_F\frac{\alpha_s}{r} - C_F\frac{\alpha_s^2}{4\pi}\frac{1}{r}\left[\frac{31}{9}C_A - \frac{20}{9}T_F n_f + \beta_0\big(2\gamma_E + \log(\mu^2 r^2)\big)\right] + \mathcal{O}(\alpha_s^3), \tag{4.53}$$

where $\beta_0 = \frac{11}{3}C_A - \frac{4}{3}T_F n_f$, n_f is the number of massless quarks[9] and Euler gamma is $\gamma_E \approx 0.5772$. For the case of SU(3) we have $C_F = 4/3$, $T_F = 1/2$, $C_A = 3$. For the QCD scale one can take $\mu^2 = 2m_t^2$.

4.4 Applications to the MSSM

The MSSM has a huge parameter space. It is then conceivable that in some its regions the Sommerfeld effect may be relevant and has to be included for the computations of supersymmetric dark matter relic density and indirect detections signals. In fact, as we

[7] Some of these coefficients are divergent in the limit when one of the masses vanish. However, in this case the non-relativistic approximation does not hold and hence these results are not valid.

[8] Note that here the interaction is diagonal and one does not need to use coefficients (4.48-4.52).

[9] In the numerical computations we will choose it to be 5, since the physically relevant application is in the stop co-annihilation regime, which is most important in the $\mathcal{O}$(100 GeV) region, where the top mass m_t is non-negligible

discussed at the beginning of this Chapter, the pure Wino and Higgsino case [200] was the point in which its importance was first appreciated.

Our goal is to identify all regions of the parameter space in the MSSM where the Sommerfeld effect can be important and study those cases in detail. Here we will be interested in the implications for the thermal relic density computations, while the indirect detections signals will be discussed in Chapter 5.

For the numerical computations of the relic density we have developed a package for DarkSUSY, which we called DarkSE. It is able to compute the Sommerfeld effect and its impact on the neutralino relic density for a general MSSM setup. We provide it as a publicly available tool to be used together with DarkSUSY for obtaining reliable relic density predictions in all possible cases where this effect is relevant.[10]

4.4.1 Sommerfeld enhanced scenarios of the MSSM

To have an idea when the Sommerfeld effect can have a non-negligible impact on the relic density it is useful to rephrase some approximate general conditions, which have to be satisfied by the dark matter particle or the co-annihilating one: *i)* coupling to the boson with much lower mass ("long range force"), *ii)* the coupling strength at least of the order of the weak coupling and *iii)* if the effect comes from the co-annihilating particle, small mass splitting between it and the DM.

Those conditions are not easy to satisfy without invoking some new interactions. The reason is that since the DM has to be electromagnetically neutral, it can couple only to Z, $W^{\pm}$ and Higgs bosons, all of which are heavy.[11] This pushes up to large masses the region where the Sommerfeld effect may be important. Hence, without additional interactions, the only possibility is the impact of co-annihilating particles, which can have very different quantum numbers, i.e. they can even have both electromagnetic and color charge. In this case their annihilation cross-sections can be altered significantly by the Sommerfeld effect coming from the exchange of photons and/or gluons. If such co-annihilating particle is degenerate with the DM, the total effective annihilation cross-section can get large corrections.

The co-annihilation regime is typically the only place where Sommerfeld effect can be significant in any theory beyond the Standard Model without new interactions. In the MSSM, as discussed in Section 2.4, particles which can efficiently annihilate with the neutralino are: the lightest chargino χ_1^+, stop $\tilde{t}$, stau $\tilde{\tau}$ or the second lightest neutralino $\tilde{\chi}_2^0$. The latter case is not very important from the point of view of studying the Sommerfeld effect, since $\tilde{\chi}_2^0$ is electromagnetically neutral and typically is a little to heavy with respect to the neutralino.

Therefore, we can identify three regimes with potential sizeable impact of the Sommerfeld effect: *i)* chargino co-annihilation, i.e. the Wino dark matter, *ii)* stau co-annihilation and *iii)* stop co-annihilation.[12]

[10] The package is available for download from the webpage: http://people.sissa.it/~hryczuk

[11] The last MSSM scalar, the CP-odd neutral Higgs A, does not give rise to any contribution for s-wave annihilations in the non-relativistic regime.

[12] Another well motivated case could be the sneutrino DM scenario. Possibly some small effect could

Wino-Higgsino dark matter

In this case we will focus on cases in which the sfermion sector is not playing any relevant role. To simplify the discussion and underline better which are the key parameters, we thus choose actually to refer to the SUSY framework usually dubbed "Split Supersymmetry" [132, 133]. This indicates a generic realization of the SUSY extension to the SM where fermionic superpartners feature a low mass spectrum (say at the TeV scale or lower), while scalar superpartners are heavy, with a mass scale which can in principle range from hundreds of TeV up to the GUT or the Planck scale [132]. This feature can occur in wide class of theories, see e.g. [241, 242, 243]. In this case we will also leave out of our discussion the gluino and the gravitino, supposing they are (moderately) heavy, focussing the analysis on neutralinos and charginos.

Since the $\tilde{B}$ is not charged under $SU(2)_L$, a large Bino component in the lightest neutralino drastically reduces the relevance of the Sommerfeld effect; we will then consider only the case of $M_1 \gg M_2$. Higgsinos and Winos have a pair annihilation cross-section into W and Z bosons which is fairly large, much larger than the standard reference value for thermal relics of $3 \cdot 10^{-26}$ cm^3 s^{-1} if their mass is at around 100 GeV. Going however for more massive neutralinos, namely around 1.1 TeV for Higgsinos and 2.2 TeV for Winos, the standard tree-level calculation of the thermal relic density gives a result which is compatible with the measured value for the energy density in CDM. This heavy mass regime is also the one in which the Sommerfeld enhancement condition of mass of the particle much heavier than mass of the force carrier is realized for weak interactions; hence relevant corrections to the tree-level estimate of the relic abundance may arise.[13]

Stau co-annihilation

The existence of the Sommerfeld effect in the stau case was first suggested by authors of Ref. [203] (a one-loop manifestation of this effect was also discussed in [188]). They pointed out that although $\tilde{\tau}^+\tilde{\tau}^-$ annihilation exhibits a strong enhancement, the $\tilde{\tau}^\pm\tilde{\tau}^\pm$ is strongly suppressed, thus the net result should not be very large. We will explicitly show below with full numerical calculations that this is indeed the case, and discuss its strong dependence on the value of $\tan\beta$ in the mSUGRA framework.

Stop co-annihilation

In the stop co-annihilation region one expects a large effect, due to the strong interactions for the co-annihilating scalars. This is indeed the case, as it was first discussed by Freitas [207]. In this work the QCD corrections to the Bino-stop co-annihilations were considered, among which the Sommerfeld one was dominant. Below we show our numerical results which were obtained with the DarkSE code. Although the physical setup we consider is

be seen in the "well tempered" neutralino [53] if the Higgs was lighter. Note, that in less motivated cases, e.g. when SUSY breaking scale is very high or when several states are degenerate with $\tilde{\chi}_1^0$, the Sommerfeld effect gives very large corrections and is essential for reliable relic density calculation.

[13] The Sommerfeld effect for the Wino dark matter was studied also in [244] with the goal to reconcile it with the PAMELA data, but this work assumed a oversimplified version of the SE leading to a different phenomenology.

slightly more general (we do not make any assumption on the neutralino composition), the results we obtain are in good agreement with those of Ref. [207].[14]

4.4.2 Relic density with the Sommerfeld effect

The appropriate way of computing the thermal relic density in the setup in which co-annihilations play an important role was described in Section 1.3.1. Including the Sommerfeld effect introduces important modification to the computation of the thermally averaged annihilation cross section Eq. (1.19). Usually this quantity is computed at the lowest order in perturbation theory taking tree-level amplitudes. We will include the Sommerfeld effect introducing the rescaling $|A_{ab}|^2 = \sum_{ij} S^{ij}_{(ab)} |A^0_{ij}|^2$, with $S^{ij}_{(ab)}$ computed in the way described in Section 4.3. Actually, since the effect can be interpreted as a rescaling in the wave function of the incoming pair, $S^{ij}_{(ab)}$ does not depend on the final state X and can be factorizes out of the total annihilation rate W_{ij}. Following the same steps of Ref. [48] and adopting an analogous notation, one finds:

$$\langle \sigma_{\rm eff} v \rangle = \frac{\int_0^\infty dp_{\rm eff} p_{\rm eff}^2 SW_{\rm eff}(p_{\rm eff}, T) K_1\left(\frac{\sqrt{s}}{T}\right)}{m_1^4 T \left[\sum_i \frac{h_i}{h_1}\frac{m_i^2}{m_1^2} K_2\left(\frac{m_i}{T}\right)\right]^2}, \tag{4.54}$$

where we have defined:

$$SW_{\rm eff}(p_{\rm eff}, T) = \sum_{ab}\sum_{ij} \frac{p_{ij}}{p_{\rm eff}} \frac{h_i h_j}{h_1^2} S^{ij}_{(ab)}(p_{\rm eff}, T) W_{ij}(p_{\rm eff}) \tag{4.55}$$

with:

$$W_{ij} = 4 p_{ij} \sqrt{s} \sigma_{ij} = 4 E_i E_j \sigma_{ij} v_{ij} , \tag{4.56}$$

and

$$p_{ij} = \frac{1}{2}\sqrt{\frac{[s-(m_i-m_j)^2][s-(m_i+m_j)^2]}{s}} \tag{4.57}$$

and $p_{\rm eff} = p_{11} = 1/2\sqrt{s-4m_1^2}$. The dependence on the relative velocity of the annihilating pairs has been rewritten instead in term of the integration variable, i.e. the effective momentum $p_{\rm eff}$.

The explicit dependence of $S^{ij}_{(ab)}$ on T stems from the fact that there may be an explicit dependence of the mass of the long-range force carriers on temperature, as already stressed in the analysis of Ref. [206]. There are two thermal effects which we need to include: first, we approximate the scaling of the VEV v with temperature as [245]:

$$v(T) = v \mathrm{Re}\left(1 - \frac{T^2}{T_c^2}\right)^{1/2}, \tag{4.58}$$

with the critical temperature T_c depending on the Higgs mass (as in Ref. [206], we will assume $T_c = 200$ GeV). Second, we consider the contribution to gauge boson masses, or

[14] The reason being that in the stop co-annihilation regime in mSUGRA the Wino and Higgsino component in the lightest neutralino are very small.

in more appropriate terms to their propagator poles, due to the screening by the thermal plasma. This effect can be approximated by adding the so-called Debye mass [246, 247], which in the SM and at $T \gg m_{W,Z}$ are:

$$\Delta m_\gamma^2 = \frac{11}{6} g_Y^2 T^2 \,, \qquad \Delta m_{W,Z}^2 = \frac{11}{6} g_2^2 T^2 \,.$$

For the gluon the screening of the plasma introduces at a leading order a contribution [248]:

$$\Delta m_g^2 = (N_c/3 + N_f/6) g_s^2 T^2 = \frac{3}{2} g_s^2 T^2 . \tag{4.59}$$

We will assume that these expressions are valid also for the MSSM and at lower temperatures; the first assumption is justified by the fact that the contributions from the additional states are small since these particles are heavy, the latter has a negligible impact on the relic density calculation. These two effects introduce a correction to the Sommerfeld factors which is non-negligible, but still quite small, since they are important mostly for high temperatures at which the Sommerfeld effect is anyway negligible.

The thermal corrections affects the interaction potentials as well as the mass splitting, which as we stressed in Section 4.3 is crucial in the analysis and therefore they cannot be neglected. The reason is that when calculating the mass spectrum we include also the radiative corrections to the neutralino and chargino masses due to gauge boson loops [249, 115] (tree-level neutralino and chargino masses are degenerate in the pure Higgsino or pure Wino limits) which is affected by the thermal dependence of the Higgs VEVs.

4.4.3 Results for the relic density

Having computed with high accuracy the mass spectra, we implement the procedure for the relic density, considering a system of coupled equations which includes all states with small mass splitting compared to the LSP.

In the case of co-annihilations with the chargino this in practice reduced to including two Majorana and one Dirac fermion when $\mu < M_2$ (i.e. two neutralinos and one chargino, mainly Higgsino-like) and one Majorana and one Dirac fermion when $\mu > M_2$ (i.e. one neutralino and one chargino, mainly Wino-like). For sfermion co-annihilation regions we needed to take into account neutralino and one scalar particle.

Additionally, since the Sommerfeld enhancements depend on the total spin of the initial pair, we considered each case separately if needed. Again, in practice this is important only if the incoming particles are one neutralino and one chargino: two identical Majoranas cannot form a s-wave spin triplet state, the triplet of two different Majoranas has suppressed annihilations (it cannot annihilate to W^+W^-), and for two charginos the effect comes dominantly via γ exchange, which is vector and both singlet and triplet computations coincide.

All the pair annihilation processes we needed to consider are dominated by their s-wave contribution (unlike e.g. the case of the pair annihilation of Binos into a fermion-antifermion). Moreover, the enhancement for the higher partial waves is smaller, due to

repulsive centrifugal term in the Schrödinger equation.[15] We can then safely assume that only the s-wave Sommerfeld effect is relevant.

Having introduced the method and particle physics framework, in this Section we present results for the Sommerfeld factors and the impact of the effect on the relic density of the neutralino in different scenarios.

As already explained, neutralino and co-annihilating particle masses are the critical parameters in this problem; we will consider an approach with these parameters set at the low energy scale (rather than at a GUT scale as often done) and let them vary freely.

Wino-Higgsino neutralino

For the chargino co-annihilation regime only two relevant parameters are M_2 and μ. Therefore, we can present results for the relic density scanning the two-dimensional plane. The other MSSM parameters are kept fixed: besides the sfermion sector which is assumed to be heavy, and the Bino which is also decoupled with the artifact of setting $M_1 = 100 M_2$, we assume $\tan\beta = 30$ and an Higgs sector with a light SM-like Higgs and all other states that are heavy, as expected in split SUSY. The value of $\tan\beta$ has a very modest impact on results and considering other values does not bring other information. In the same way, the other Higgs sector parameters have very little relevance.

For any given point in the MSSM parameter space leading to a lightest neutralino χ_1^0 which is heavy and has a large Wino or Higgsino fraction there are several Sommerfeld enhancement factors $S^{ij}_{(ab)}(v,T)$ needed for a relic density computation. The interplay between the different contributions to the thermal averaged effective cross-section is in most cases non-trivial. In Fig. 4.5 we give an example of $S^{ij}_{(ab)}(v,T)$ for the case when the neutralino is nearly purely $\tilde{W}^0$, just to give a intuition of what magnitude of enhancement factors we deal with. In this case in set of coupled equations (4.35) we have $N \leqslant 2$, i.e. only neutralino and chargino coupled together. One can see that the enhancements are of order $\mathcal{O}(1)$ and very quickly go to 1 or to 0 in higher momenta and that most channels are attractive while two are repulsive, namely $\chi^+\chi_1^0$ in the singlet spin state and $\chi^+\chi^+$. Also, as expected, one gets the highest enhancement factor for the $\chi^+\chi^-$ channel, since there is a long range nearly[16] Coulomb interaction present. For the cases with two coupled equations and lighter states incoming we see a resonance in the value of momentum corresponding to the mass splitting. This is easy to understand, since for this energy the heavier states are produced nearly at rest, so they feel large effect coming from, for instance, γ exchange. This is perfectly consistent with what was found in similar cases using analytical approximations [216].

We are now ready to compute σ_{eff} and solve the Boltzmann equation as discussed in Section 4.4.2. Values for the effective annihilation cross-section including the Sommerfeld

[15] This statement is not true in the case of resonances. In the Coulomb case, when analytical expressions can be derived, every partial wave is enhanced by the factor $\sim (\alpha/v)^{2l+1}$, so for higher l the resonant enhancement is higher and narrower. However, since one has to integrate over the thermal distributions, the resonances are smeared and net impact of the higher partial waves is very small.

[16] Due to the thermal corrections photon acquires small mass, which makes the potential to be Yukawa type, and the enhancement factor saturates at small p.

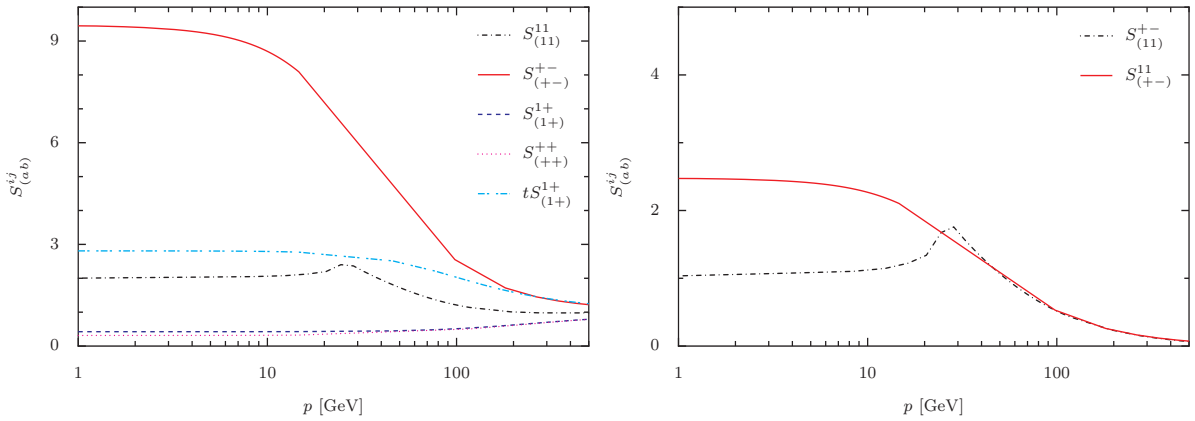

Figure 4.5: Example enhancement factors for $M_2 = 2.53$ TeV, $\mu = 5$ TeV and $x = 20$ (corresponding to $T \approx 126$ GeV). Subscripts refer to the incoming state with 1 - χ_1^0 and $\pm$ - $\chi^\pm$, while superscripts to the annihilating one. The left panel shows Sommerfeld factors when the annihilating pair is the same as the incoming one, while right panel when they are different. In the latter case these factors approach 0 because at high momenta there is no Sommerfeld enhancement and the annihilation amplitude is suppressed because it can only be obtained at one-loop level at least. All factors are computed for singlet spin state annihilation, except one indicated as tS being for triplet.

effect and without it are shown in Fig. 4.6 for sample cases of Wino- and Higgsino-like neutralino.

In the Higgsino-like case the effect is very mild. The Sommerfeld enhancement of the effective cross-section becomes relevant only in the small velocities regime, when the depletion term in the Boltzmann equation is marginally effective. This gives rise to a change in the relic density at the level of at most few per cent. In the Wino-like case the picture looks much more interesting. The net effect on the both yield and σ_{eff} is clearly visible and can become even very large in the parameter range where large resonance effects occur.

The reason for the difference in the behaviour of the Sommerfeld effect in the Wino- and Higgsino-like case comes mainly from the mass splitting between the lightest neutralino and chargino, which is typically much smaller in the Wino case. The Sommerfeld effect for the neutralinos relies mostly on a production of nearly on-shell charginos in the loop. Also the efficiency of co-annihilation, and subsequently the effect of the Sommerfeld enhancement coming from its impact on co-annihilating particles, strongly depends on the mass splitting. Hence, the larger the mass splitting the smaller the overall impact on the thermally averaged cross-section.[17]

In Figs. 4.7 and 4.8 we show results for the neutralino relic density in the plane M_2 versus μ, varying these parameters in the range 500 GeV to 5 TeV, a region in which the thermal relic density varies from values much below the cosmologically preferred one to much above it. In the left panel of Fig. 4.7, we are plotting results assuming the usual

[17]Note however, that in general Sommerfeld factors themselves are not monotonic functions of the mass splitting, see e.g. Ref. [216].

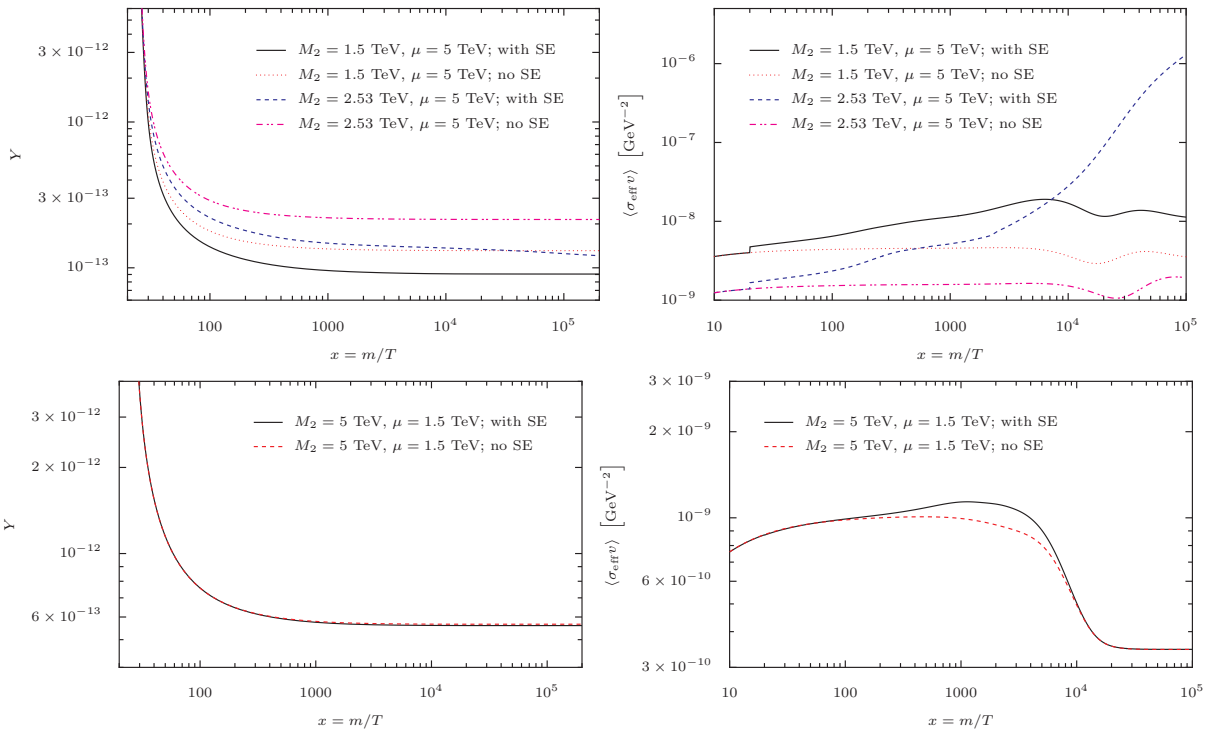

Figure 4.6: Number densities in units of entropy density Y and effective cross sections for the Wino-like *(top)* and Higgsino-like neutralino *(bottom)*. In the Wino case two set of parameters are presented - generic one and close to the resonance.

tree-level approximation for the pair annihilation amplitude, while in the right panel those including the full treatment of the Sommerfeld effect are shown. Most manifestly, there is a sharp shift in the Wino-like region consistent with the 7-year WMAP data to heavier masses; when including the Sommerfeld enhancement a pure Wino is found to have $\Omega h^2 = 0.11$ for a mass of about 3.2 TeV.[18] Much milder change takes place in the Higgsino-like region; the relic density is practically unchanged when considering models in the cosmologically interesting band. The relic density decrease is even larger in the ultra-heavy regime, with the Sommerfeld effect becoming larger and larger as the gauge boson masses are becoming less important. This regime would however be consistent with cosmology only invoking some extra ingredient, such as, e.g., a dilution effect via late entropy production or the decay of the neutralino into a lighter state, such as a gravitino or an axino, which is the true LSP (although viable, both scenario require large fine-tuning). The results found here for pure Winos and pure Higgsino are analogous to those of earlier works in Ref. [203] and Ref. [206] in the same limiting cases. There are small quantitative differences stemming from the fact that we have identified more annihilation channels that need to be treated separately, with the Sommerfeld factor depending on the

[18]Note that the values given in the paper [237] differ, pointing to a mass of about 2.8 TeV. This comes only as a result of using different value of the coupling constant, for which we then assumed the one at the m_χ scale. Only later we have studied the loop corrections and learnt that the proper choice is at the EW scale, as discussed in Sec. 3.2.1.

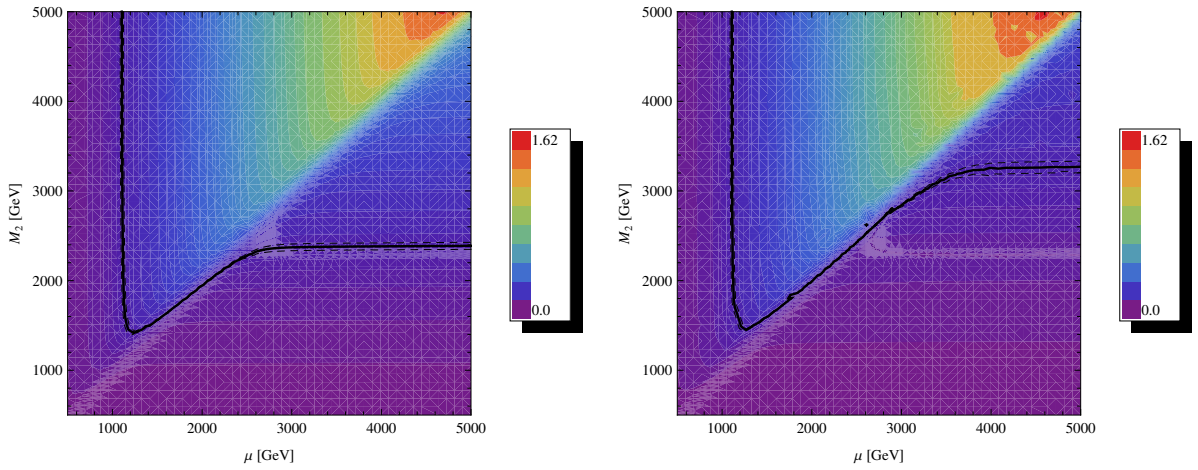

Figure 4.7: Relic density Ωh^2 in the μ-M_2 plane for perturbative case *(left panel)* and with Sommerfeld effect included *(right panel)*. The brighter the colour the higher Ωh^2 and the colour scale is linear. The solid line and dashed lines correspond to the central value and the 1σ error bar for relic density consistent with the 7-year WMAP data, $\Omega h^2 = 0.1123 \pm 0.0035$.

initial spin state of the annihilating particle pair. We have also found a different coefficient in the axial vector exchange, i.e. that the axial vector has an additional -3 factor with respect to the vector (in agreement with the result in Ref. [238]), and we have probably a better control of the numerical solution of the Boltzmann equation having implemented our full treatment in the DarkSUSY numerical package (the slight difference in numerical results between [203] and [206] are instead probably mainly due to the thermal corrections implemented here following [206]).

Another region showing interesting results is the band connecting the pure Higgsino to the pure Wino limit, towards $M_2 \sim \mu$ but still with a predominant Wino component. Features in this region are more clearly seen in Fig. 4.8 where we show the ratio between the relic density computed with tree-level amplitudes to the one with the full non-perturbative treatment. A thin "resonance" slice appears in the plane, starting for pure Winos with mass $m_\chi \approx 2.3$–2.4 TeV and extending to heavier masses into the region with a sizable Higgsino fraction, where the thermal relic density becomes consistent with observations. The value of the mass we find for a pure Wino is precisely the one saturating Eq. (4.13), i.e.:

$$\frac{1}{m_W} \approx \frac{1}{\alpha m_\chi}\,, \tag{4.60}$$

with α as computed in the vertex for pure Winos $\tilde{W}^0\,\tilde{W}^+\,W^-$. This means that the observed resonance is related to the possibility of creating the loosely bound state, occurring when the Bohr radius coincides with the interaction range. It also explains why, when we increase the Higgsino fraction, the resonance deviates to higher masses. A larger Higgsino fraction implies an increase in the mass splitting between lightest neutralino and chargino (since one goes from a mass splitting dominated by the radiative corrections, about 170 MeV, to the one induced by the mixing of interaction eigenstates), as well as a

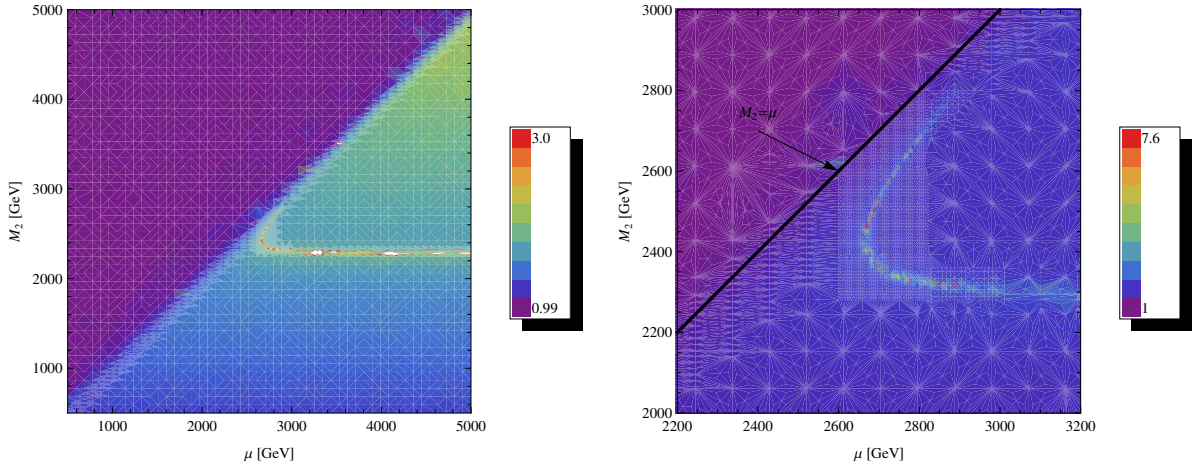

Figure 4.8: *Left panel*: ratio of relic densities without and with Sommerfeld effect, $(\Omega h^2)_0/(\Omega h^2)_{\rm SE}$. *Right panel*: the same ratio but focussing on the inner part of the resonant region. The colour scale is linear.

drop in the couplings (since the vertex $\tilde{H}^0\,\tilde{H}^+\,W^-$ as a coupling which is a factor of $\sqrt{2}$ smaller than for Winos) and hence a drop in α; this has to be compensated by a larger m_χ.

Stau co-annihilation

In this case the impact of the Sommerfeld effect is relatively mild. The reason is that, although at the freeze-out temperature the thermally averaged annihilation cross section $\langle\sigma_{\rm eff}v\rangle$ is dominated by the contribution coming from $\tilde{\tau}\tilde{\tau}$ annihilation, the net enhancement is rather small, since as can be seen in Fig. 4.9 there are both attractive and repulsive modes present.

Furthermore, if one enlarges the mass splitting, the co-annihilations become less effective and the total effect on the relic density gets even smaller. This has been shown in Fig. 4.10, from which one can see that the Sommerfeld effect introduces a several per cent correction to the relic density, but only in the region of a very degenerate $\tilde{\tau}$. This region in most of the parameter space does not give the relic density compatible with the WMAP data. However, the impact of the Sommerfeld enhancement become more important when m_χ grows, because then the WMAP contour approaches the region where $m_\chi \simeq m_{\tilde{\tau}}$: the $\tilde{\chi}^0_1\tilde{\chi}^0_1$ annihilation cross section scales as $\sim m_\chi^{-2}$ and to get the same $\langle\sigma_{\rm eff}v\rangle$ (and the same relic density) one has to compensate it with larger co-annihilation effects. This means, in particular, that the maximal $\tilde{\chi}^0_1$ mass that can give correct relic density gets shifted by a Sommerfeld effect by a sizeable amount. In mSUGRA the value of this shift depends strongly on $\tan\beta$. In Fig. 4.11 we show the dependence of Ωh^2 vs. the neutralino mass in the case where it is equal to the stau mass for its three different values. The maximal effect is seen for large $\tan\beta$ and drops down quite considerably when it is decreased. The reason for this is that for higher $\tan\beta$ the $\tilde{\tau}^+\tilde{\tau}^- \to h^0h^0$ annihilation

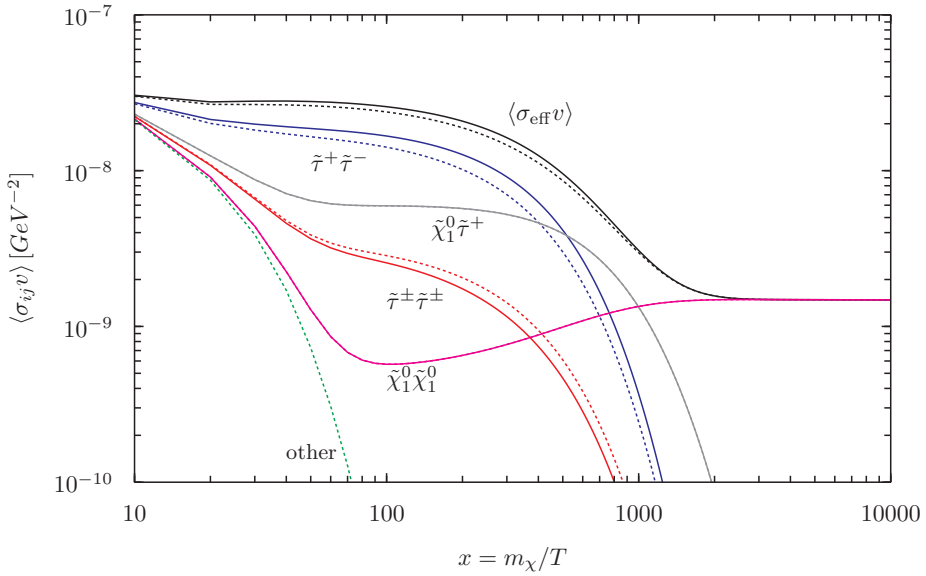

Figure 4.9: An example of the thermally averaged effective annihilation cross-section for the stau co-annihilation region. Contributions coming from different annihilation processes are indicated. The solid lines correspond to the case with Sommerfeld correction included, while dashed ones without it. In the $\tilde{\chi}_1^0\tilde{\chi}_1^0$ case the effect is too small to be visible. Parameters are: $m_\chi = 182.7$ GeV, $m_{\tilde{\tau}} = 183.2$ GeV, $\tan\beta = 50$, $A_0 = 0$ and $\mu > 0$.

becomes very efficient. On the other hand the annihilation cross sections of $\tilde{\tau}^\pm\tilde{\tau}^\pm$ to two leptons or quarks also grow with $\tan\beta$ but much slower. Hence, enlarging its value makes attractive channels dominant over repulsive ones (as in the case in Fig. 4.9).

Stop co-annihilation

In mSUGRA, in the region of parameter space where the large negative value of A_0 drives the lighter stop to be degenerate with the neutralino, the results of the relic density computations are significantly affected by the Sommerfeld effect.

Fig. 4.12 shows the change of the thermal averaged effective annihilation cross section due to the Sommerfeld effect for different mass splittings between $\tilde{\chi}_1^0$ and $\tilde{t}$. The correction is significantly larger than in the $\tilde{\tau}$ case, because of the strong force coming from the gluon exchange. When the mass splitting becomes larger two effects can be seen. Firstly, the $\tilde{t}\tilde{t}$ threshold occurs for higher temperature, which lowers the overall impact of the co-annihilating particle. Secondly, also the magnitude of the correction to $\langle\sigma_{\rm eff}v\rangle$ becomes smaller, since at higher T the typical velocities are higher and moreover, thermal corrections to the gluon mass are larger.

This change in $\langle\sigma_{\rm eff}v\rangle$ can affect considerably the relic density of the neutralino. The results for Ωh^2 with and without the Sommerfeld effect are presented in Fig. 4.13 for five different m_χ. One can see that the largest effect is obtained for parameters giving typically too small relic density. Nevertheless, in the region compatible with WMAP results, the correction can still be larger than the current observational uncertainty.

The importance of the Sommerfeld effect itself is more clearly seen in the Fig. 4.14,

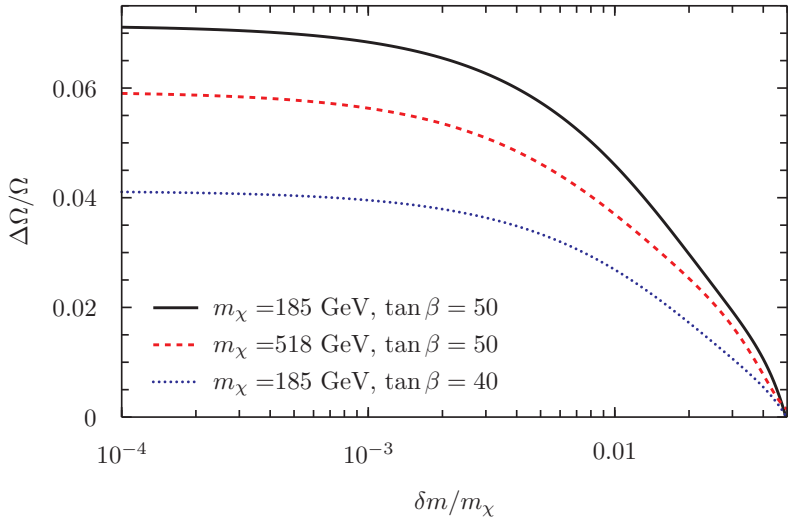

Figure 4.10: The correction to the relic density $\Delta\Omega = \Omega_0 - \Omega_{SE}$ coming from the Sommerfeld effect. Results for three different parameter points are given to show that the result is much more sensitive to $\tan\beta$ than m_χ. Note, that the accuracy of the relic density computation in DarkSUSY itself is about 1%.

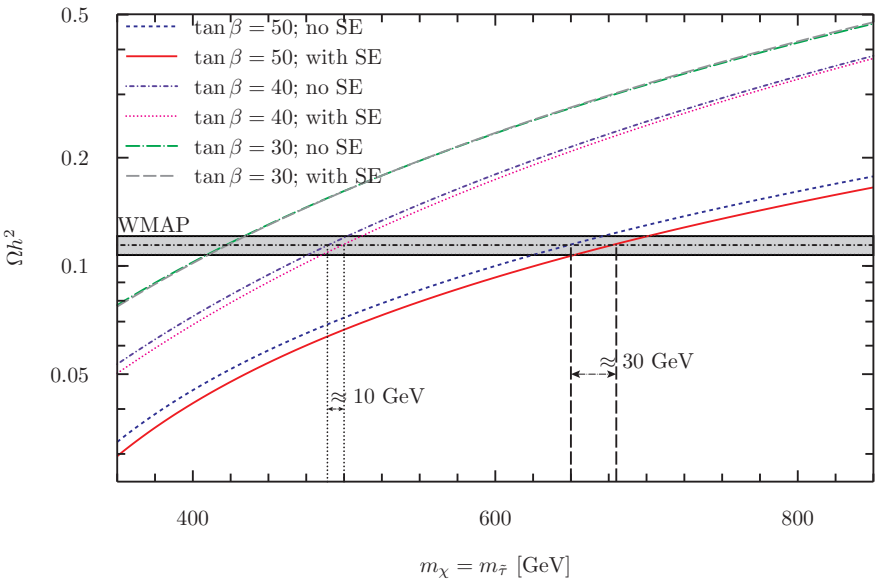

Figure 4.11: Effect of the Sommerfeld enhancement on the relic density for $m_\chi = m_{\tilde{\tau}}$. Maximal neutralino mass giving relic density compatible with data, and its shift due to the Sommerfeld effect are highlighted.

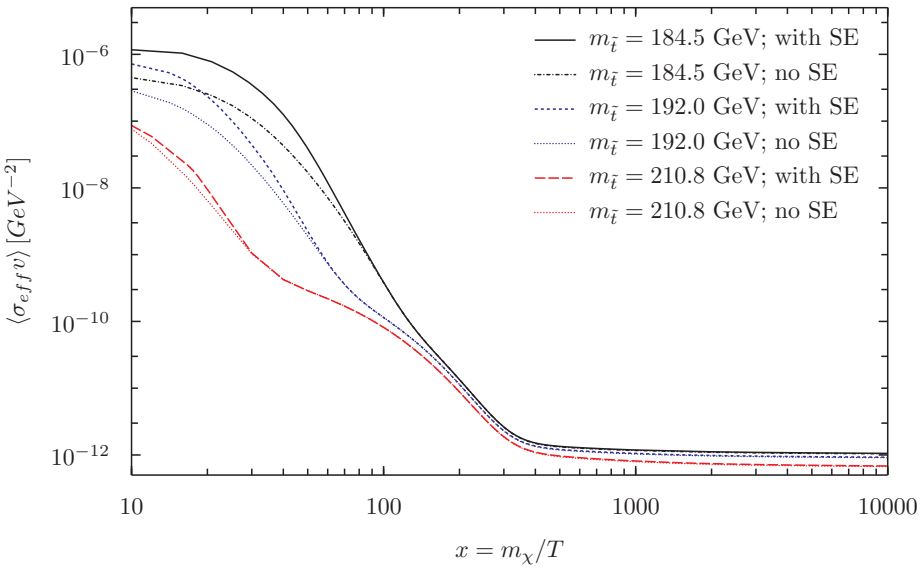

Figure 4.12: An example of the thermally averaged effective annihilation cross section for the stop co-annihilation region. Parameters are $m_\chi = 140.7$ GeV, $\tan\beta = 10$, $A_0 = -2750$ GeV and $\mu > 0$. Two thresholds are visible, smeared by the thermal average, $\tilde{\chi}_1^0 \tilde{t}$ and $\tilde{t}\tilde{t}$, but only the second one gets significant Sommerfeld correction.

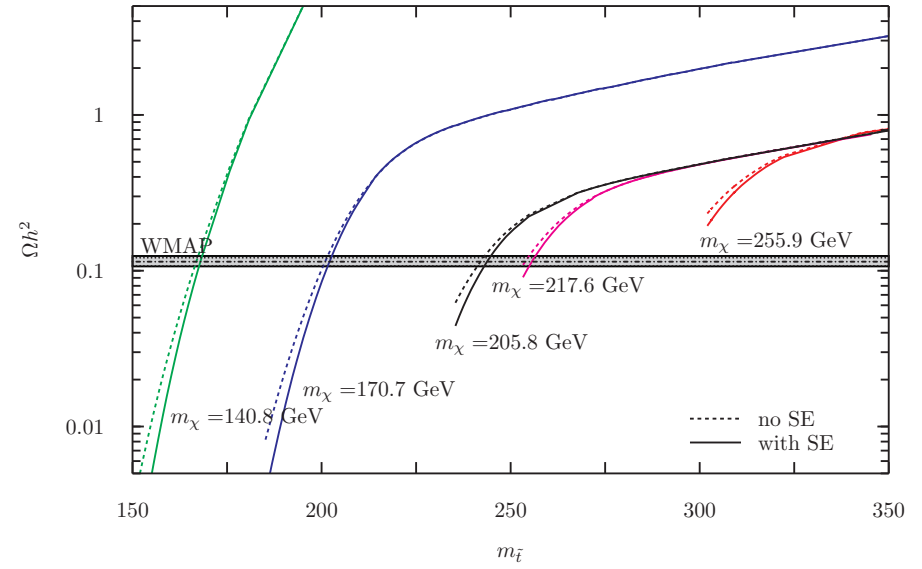

Figure 4.13: Effect of the Sommerfeld enhancement on the relic density for the stop co-annihilation region. For given m_χ there is a lower bound on $m_{\tilde{t}}$ due to the constraint on the lightest Higgs mass.

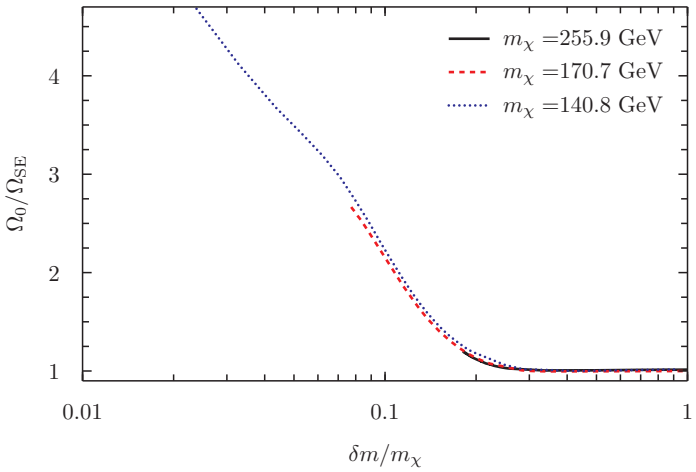

Figure 4.14: Sommerfeld effect on the relic density for $\tilde{t}$ very degenerate with $\tilde{\chi}_1^0$. As before, due to the bound on the lightest Higgs mass the degeneracy is limited; the more the larger m_χ.

where the ratio of relic densities without and with SE is presented. For very degenerate stops Ωh^2 can be suppressed by a factor of few.

The results we presented in this subsection are in qualitative agreement with those in [207]. However, there are slight quantitative differences, for several reasons. First of all, in this work we were interested in the Sommerfeld effect and we did not compute other QCD corrections. On the other hand, our treatment of the Sommerfeld enhancement is more accurate, since we include not only gluon exchange, but all possible interactions, and for all annihilation processes, not only for $\tilde{t}\tilde{t}$ one. We include also thermal corrections which modify the masses of exchanged bosons.

Finally, we would like to point out that the results in the stop co-annihilation region are subject to sizeable theoretical uncertainties. The reason is that since the coupling is relatively strong, Sommerfeld enhancement factors differ considerably from 1 even at high velocities. This cannot be however the true result, since the full quantum field theory initial state corrections in this case are not expected to be large. This discrepancy comes from the fact that the formalism used to compute the Sommerfeld enhancement is not valid in this regime. In our numerical calculations we used an approach to approximate the true corrections by the non-relativistic ones normalized in such a way that they vanish for $v \to 1$ (a better approximation would be to compute the NLO vertex correction, which is however beyond the scope of this work).[19] To obtain more reliable predictions for the intermediate regime of velocities $\mathcal{O}(10^{-1})$, which are very important for precise relic density computation, one should refine the theoretical calculations beyond the non-relativistic techniques used to derive the Sommerfeld enhancement.

[19]The normalization was done additively, i.e. the enhancement factors were shifted by a small constant value (always less than 1). Since for small velocities the enhancement is much larger than 1, in the non-relativistic regime this procedure does not introduce any significant change. This approach gives the relic density larger by at most 10% with respect to the case with the Sommerfeld factors simply extrapolated to the high velocities regime.

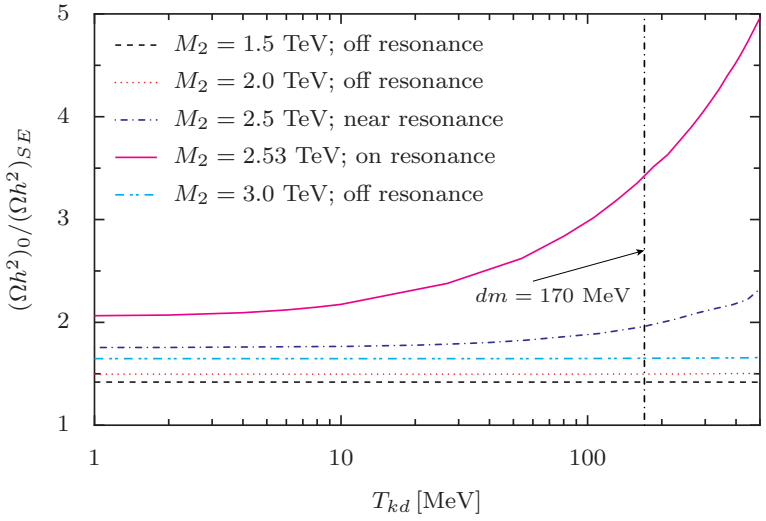

Figure 4.15: Influence of the kinetic decoupling on the relic density suppression by the Sommerfeld effect for Wino-like neutralinos. In all cases $\mu = 5$ TeV and other parameters are as for the mixed Wino-Higgsino scenario. There is a clear enhancement in the net effect within the resonance region, but no effect away from it.

4.5 Kinetic decouping and the SE

The results presented in previous subsections assume that the temperature of the neutralinos traces the thermal bath temperature. This is true as long as neutralinos are in kinetic equilibrium. After kinetic decoupling, at the temperature $T_{\rm kd}$, their temperature decreases with the scaling as appropriate for non-relativistic particles, i.e. $T_\chi \sim 1/a^2$, where a is the Universe scale factor, cooling much faster than thermal bath states for which $T \sim 1/a$. This does not have any influence on the relic density computation if interactions do not depend on velocity, as in the standard case of s-wave annihilations. When the Sommerfeld effect plays a major role, however, there is indeed a strong dependence on velocity and colder neutralino may have larger annihilation cross section. Hence, if the kinetic decoupling happened early enough, i.e. when the depletion term in the Boltzmann equation is still active, this might have given rise to stronger relic density suppression by the Sommerfeld enhancement.

We have just shown that, within the MSSM, the largest impact of the Sommerfeld effect occurs for Wino-like neutralino or the stop co-annihilation regime. In both these cases, since elastic scatterings are very strongly suppressed, the processes enforcing kinetic equilibrium are inelastic scatterings. For example, for the Wino-like neutralino there are of the type $\chi_1^0 e^- \leftrightarrow \chi^- \nu_e$; they are efficient up to the time when the temperature drops down below the mass splitting between neutralino and chargino. Hence, more accurately, we can estimate the kinetic decoupling temperature as $T_{\rm kd} \approx (2/3)\delta m = 133$ MeV [244].

The exact value of $T_{\rm kd}$ and shape of the distribution function after decoupling (since it is unlikely for the decoupling to be instantaneous) depend on the parameters in the model; it is in general rather involved to determine them (see e.g. [250, 251]) and this

goes beyond the purpose of this analysis. Here, to illustrate the possible effect of the kinetic decoupling on the relic density when the Sommerfeld enhancement is relevant, in Fig. 4.15 we plot the ratio between the value of the relic density as computed at the lowest order in perturbation theory $(\Omega h^2)_0$ and the full computation $(\Omega h^2)_{\rm SE}$, for a few points in the parameter space with Wino-like neutralinos, as a function of the value assumed for $T_{\rm kd}$ and assuming the neutralino distribution function as if decoupling is instantaneous. One can see that in general, the relic density is not sensitive to the kinetic decoupling temperature. The exception is the resonance case, when the Sommerfeld enhancement can be much larger and we find a sizable corrections depending on $T_{\rm kd}$. It follows that accurate predictions of the relic abundance in the resonance regime are possible only after determining the kinetic decoupling temperature with a certain accuracy. On the other hand the resonance region is rather tiny and the overall MSSM picture discussed in this work is not much affected.

This situation is qualitatively different then in the models with a "dark force". In those models, on contrary, large effects due to kinetic decoupling effect are expected [222, 223]. More recently a detailed study of the interplay of the solution of the Boltzmann equation with the proper treatment of the kinetic decoupling was performed in [252]. The authors developed a formalism appropriate for large Sommerfeld enhancement cases (or in general whenever the annihilation cross-section considerably increases for low DM velocities). Applying it to a toy model they observed, that on-resonance the DM annihilation can continue until well after matter-radiation equality. This can deplete the present-day DM abundance by more than two orders of magnitude due to annihilations that happen after the kinetic decoupling.

The natural question to ask is whether this more proper treatment is also needed to be applied in the MSSM. The answer is negative, for the reason that there is no "$1/v$" enhancement in this case: the Sommerfeld effect always comes from the interplay with the co-annihilating particle, which makes it ineffective when the neutralino energy is too small to produce on-shell heavier state. Therefore, the enhancement drops down and saturates below $v \sim \sqrt{2\delta m/m_\chi}$ (see e.g. Fig. 4.5).

As an illustration we show the effect of the kinetic decoupling for the on-resonance case for the Wino-like neutralino and its dependence on the $T_{\rm kd}$ on Fig. 4.16. On the left plot the ratio of the annihilation to the Hubble rates are shown, while on the right the evolution of the yield and the final effect on the relic density. The blue dashed line shows the result without the Sommerfeld effect included (obviously independent on the kinetic decoupling). Including the SE and assuming $T_{\rm kd} = 30$ MeV gives the red solid line, which differs from the one without the kinetic decoupling effect (green chain line) only at large x and gives the same relic density. If the kinetic decoupling could be much larger, which is not the case in reality, then some effect could be seen. This is shown by black solid line, where $T_{\rm kd} = 4$ GeV was assumed. Much bigger effect is visible for an "$1/v$" enhancement, given by dotted lines for those two kinetic decoupling temperatures.

The qualitative difference between our results and the "$1/v$" enhancement is clearly visible on the plot of Γ/H. While the full computation of the Sommerfeld effect in the MSSM shows that the expansion of the Universe is completely dominant for late times and the annihilations stop early, for the "$1/v$" enhancement they continue to be effective

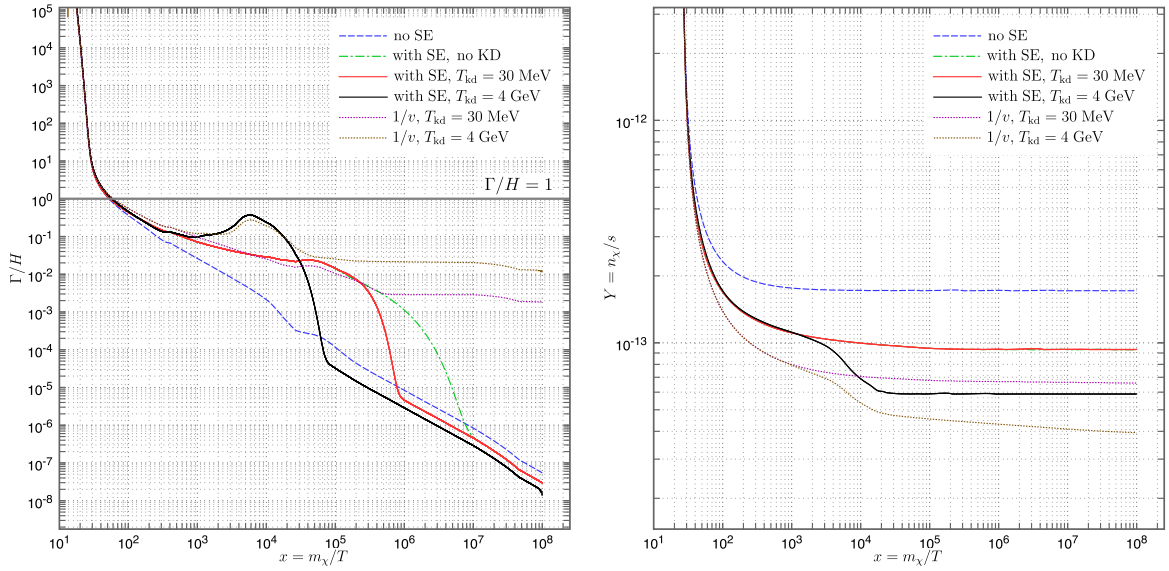

Figure 4.16: Effect of the kinetic decoupling for the relic density for the on-resonance pure Wino model with $m_\chi = 2.4$ TeV. *Left plot:* annihilation rate over the Hubble rate, *right plot:* comoving neutralino number density. For discussion see the text.

even for very large x. This is what was found in [252].

In summary, what we observe is that the lack of true "$1/v$" enhancement prevents the kinetic decoupling to be of very large impact on the relic density in the supersymmetric scenarios. In fact, the only dependence comes from the enhanced annihilations soon after the freeze-out (compare black and red solid lines on Fig. 4.16). Moreover, this is relevant only at the resonance and the effect is in reality much smaller than illustrated on the plot, since the true $T_{\rm kd}$ should be lower than the mass splitting.

Chapter 5

Indirect detection of Wino dark matter

The higher order effects discussed in the previous chapters are relevant not only for the relic density computations, but also for the indirect detection signals. In the latter case they are in fact of even greater importance, since especially the Sommerfeld effect is more pronounced for particles with lower velocities in the present-day halos, than at around the freeze-out. In this Chapter we will explore this observation in detail. In order to study the significance and consequences of the electroweak and Sommerfeld corrections for the dark matter searches one is forced to pick up a model first, as both these effects are (strongly) model-dependent. In our work [253] we have chosen to analyse the Wino dark matter model, for several reasons.

First of all, the Wino is a viable, well-motivated supersymmetric candidate. It is the LSP in most realizations of the anomaly mediated SUSY breaking (AMSB) models and its relic density can be naturally of the observed value in the thermal [203] and non-thermal scenarios, see e.g. [254, 255]. From our point of view the thermal case is especially interesting. If Wino has a mass larger than m_W, annihilation to W^+W^- is open and very efficient. Thus the thermal relic density is too low, unless one goes up to the TeV scale. As already mentioned, this regime was often considered less attractive, since it is a bit high for a low scale supersymmetry. However, in light of the lack of any hints for SUSY particles at the LHC by now, this scenario starts to get more attention. Secondly, as we discussed in detail in Chapter 3, at this energy scale the electroweak corrections are typically important. In fact, Wino DM is also the model for which we have under control the full one-loop computation and therefore can cross correlate various indirect detection channels. Thirdly, a pure Wino is always very degenerated in mass with the lighter chargino. This opens up an electroweak Sommerfeld enhancement, as described in detail in the previous Chapter, and the perturbative computations are not sufficient. Therefore, it is precisely the case in which both of these higher order effects intervene at the same time. Another virtue of this model is its relative simplicity and the fact that at least some of the results obtained here should be rather generic for a Majorana fermion in a adjoint of $SU(2)_L$, e.g. in the minimal dark matter model.

Finally, in this setup the higher order corrections are crucial for making robust predic-

tions for the indirect detection. It is especially important, because this is the only feasible way of excluding (or detecting) Wino DM, at least in the near future. The reason is that a TeV scale Wino evades all the direct detection and collider bounds put so far.[1] On the other hand, heavy Wino annihilations in the halo may give rise to observable cosmic ray signals, as we will show below.

Wino dark matter was studied from this point of view already in the past, see e.g. [258, 259, 257, 260]. Most of these works were interested in the low mass region, at most a few hundreds of GeV. The reason is that at a tree level such Wino can have large cross-sections possibly giving interesting signals. On the other hand, when one goes beyond tree level approximation, and in particular includes the Sommerfeld effect, also TeV scale Wino starts to have an interesting phenomenology. This was already noticed in [261], where positron and antiproton signals were discussed, especially inspired by the HEAT cosmic ray results. After PAMELA reported the positron fraction rise people were suggesting heavy DM as a possible explanation and this model was also advocated as one of the possibilities [262, 263]. However, none of these works considered electroweak corrections and all concentrated on only one or two detection channels. Below we will show that simultaneous study of all possible channels is essential for making robust claims on the exclusion or detection.

In the next section we discuss how to include the Sommerfeld effect and EW corrections simultaneously and give the results for the total and differential annihilation cross-sections of a non-relativistic Wino. Then in Sec. 5.1.2 we present the spectra of final stable SM sates per annihilation. These states are the γs and νs, which travel directly from the source and charged CRs like e^-/e^+, $p/\bar{p}$ and $d/\bar{d}$, which propagate in the interstellar magnetic fields. We review the propagation model used in this work in Sec. 5.2 and then discuss its uncertainties. Finally, in Sec. 5.3 we give the multi-channel indirect detections signals from the Wino DM model and discuss what are the prospects for each of them.

5.1 The EW and Sommerfeld corrections

In most of the literature the Sommerfeld effect is taken into account as an multiplicative factor to the tree level cross-section σ_{tree}. However, if one wants to incorporate loop corrections, the cross-section can be also computed at higher order in perturbation theory.[2] In our work we computed the cross-section up the order $\mathcal{O}(g^6)$. Whereas we considered the annihilation process at rest, we still keep into account the velocity in the Sommerfeld enhancement, since in this process the momentum transfer can depend on it substantially.

[1] At such high mass scale the direct detection lose sensitivity for a purely kinematical reasons: the nuclei mass, which sets the characteristic scale for sensitivity, is for all working DD experiments maximally of $\mathcal{O}(100\,\text{GeV})$. A substantial upgrade of the technology is needed, which might be provided by the new DARWIN project [256], or some of the other proposed ton-scale dark matter DD experiments. Note also that for a pure Wino the elastic scattering on a nucleus vanishes, because the coupling of nautralino to Z or Higgs bosons scales with gaugino-higgsino mixing. As far as collider searches are concerned, the reach of LHC even at 14 TeV is not enough for a discovery of 2–3 TeV weakly interacting particle like Wino, see e.g. [257].

[2] This can be done as long as the annihilation process is short distance one, when the long distance Sommerfeld effect is decoupled and can be treated separately with the full non-perturbative method.

The Sommerfeld enhancement factors are computed using a formalism explained in Sec. 4.3. In the case at hand, there are two possible channels through which the annihilation can take place: (χ^0, χ^0) and (χ^+, χ^-).

There are two important observations one needs to make in order to use this method to the one-loop computation. The first is that since SE comes from re-summation of ladder diagrams, the first in the series contributes also to the one-loop level cross-section. To avoid double counting one has to subtract its non-relativistic part from the loop computation. This is what was done in Sec. 3.2. Secondly, to be consistent in the order of the perturbation theory one needs to compute both the $\chi^0\chi^0$ and $\chi^+\chi^-$ annihilation amplitudes at the same order. This stems from the fact that the Sommerfeld effect is treated non-pertubatively and does not change the perturbation theory order.

Furthermore, one should note that the origin of the Sommerfeld effect is really on the level of amplitudes, not the cross-sections. This does not make any difference for the one channel version of the SE, but introduces a slight modification in more general cases. Indeed, let us call the *amplitude* Sommerfeld factors:

$$s_0 \equiv \partial_x \varphi^0(x)|_{x=0}, \qquad s_\pm \equiv \partial_x \varphi^\pm(x)|_{x=0}, \tag{5.1}$$

then the (Sommerfeld enhanced) amplitudes of the annihilation processes for any standard model final state are:

$$A_{\chi^0\chi^0\to \mathrm{SM}} = s_0 A^0_{\chi^0\chi^0\to \mathrm{SM}} + s_\pm A^0_{\chi^+\chi^-\to \mathrm{SM}}. \tag{5.2}$$

Note that by taking the modulus square of Eq. (5.2) there is also a cross term, which was first noticed in [191].

The result for these factors depends strongly on the mass-splitting between χ^0 and $\chi^\pm$; in fact, also the computation is somewhat different if the total energy of the χ^0 pair is greater or smaller than twice the $\chi^\pm$ mass. However, taking the mass splitting to be about 0.17 GeV, and the velocity of the order of present day dark matter velocity $v \sim 10^{-3}$, even for m_χ being a few TeV, the production of real $\chi^\pm$ from the χ^0 pair is not allowed. As we have seen, in this case (i.e. far below the $\chi^+\chi^-$ threshold) $s_{0,\pm}$ nearly does not depend on the velocity (see Fig. 4.5).

It is worth noting, that for small velocities the Sommerfeld effect at one-loop level (i.e. not summed over all orders), gives:

$$s_0 = 1, \qquad s_\pm = \sqrt{2}\frac{g^2}{4\pi}\frac{m_\chi}{m_W}. \tag{5.3}$$

This result is recovered from the full solution of the Schrödinger equations when one takes the limit of small $v\frac{m_\chi}{m_W}$ and small $\frac{g^2}{4\pi}\frac{m_\chi}{m_W}$. However, since for large enough m_χ this does not hold, the full numerical computation is needed.

Finally, let us make a comment about the perturbation theory orders are included in our computation. The resulting cross-section σ_2 can be written as (see Eq. (3.16)):

$$\begin{aligned}\sigma_2 v = \frac{1}{64\pi}\sqrt{1-\frac{m_g^2}{m_\chi^2}}\sum_{\mathrm{pol}} \Big\{ & |s_0|^2\left(|A_2^0|^2 + 2\,\mathrm{Re}\,A_2^{0*}A_4^0\right) + |s_\pm|^2\left(|A_2^\pm|^2 + 2\,\mathrm{Re}\,A_2^{\pm *}A_4^\pm\right) \\ & + 2\,\mathrm{Re}\left(s_0^* s_\pm\left(A_2^{0*}A_2^\pm + A_4^{0*}A_2^\pm + A_2^{0*}A_4^\pm\right)\right)\Big\},\end{aligned} \tag{5.4}$$

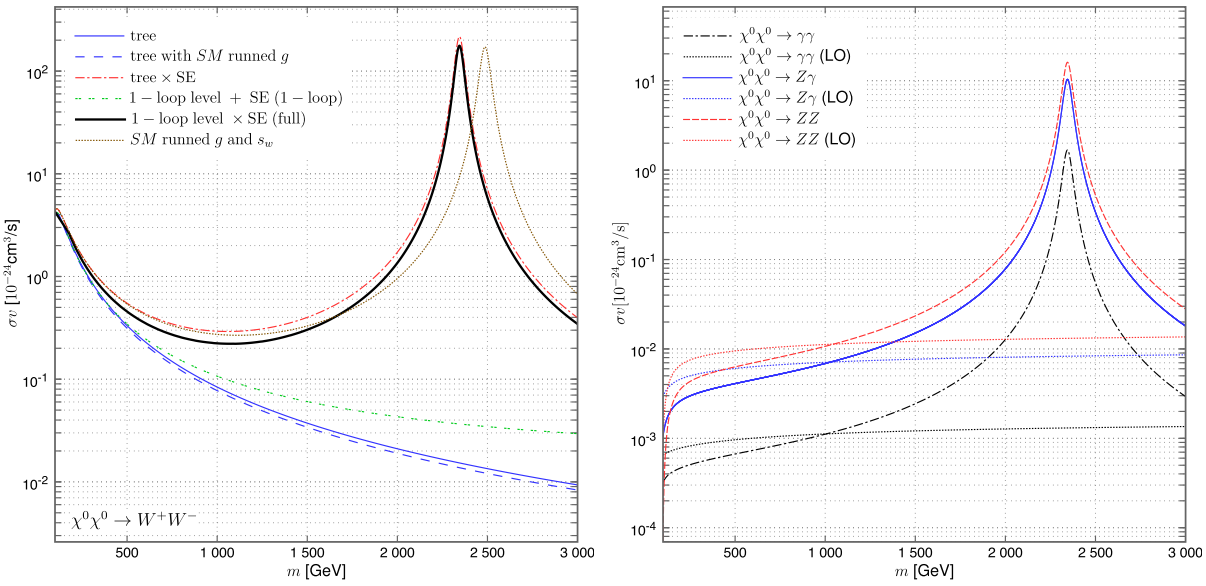

Figure 5.1: *Left plot*: the total cross-section for the annihilation of $\chi^0\chi^0$ to W^+W^- (including the three body production). Our final results including both the one-loop corrections and the Sommerfeld effect are given by the solid black line. For comparison we plot the tree result (solid blue), tree level with the full SE (chain red), full one-loop level results but without non-perturbative SE (twin green) and the tree level with (dotted brown) and without SE (sparse blue) but with runned couplings at the scale m. *Right plot*: the cross section for the annihilation to $ZZ, Z\gamma, \gamma\gamma$. The full one-loop results with the SE included are given and for comparison the leading order ones.

where $A^0_{(2,4)}$ and $A^\pm_{(2,4)}$ are the amplitudes of annihilation into two gauge bosons for initial $\chi^0\chi^0$ and $\chi^+\chi^-$, respectively. The subscript refers to the order of perturbation theory, i.e. A_2 is the $\mathcal{O}(g^2)$ part and A_4 the $\mathcal{O}(g^4)$ one.

One can see that we do not include any terms of the order $\mathcal{O}(g^8)$, say $|A^0_4|^2$, or higher. They are subdominant at the TeV scale, but may play a role in the low mass region (especially for the annihilation to ZZ, $\gamma\gamma$ and $Z\gamma$, where the tree level is not present). In order to incorporate them consistently with the Sommerfeld effect one would need to include also additional corrections, e.g. two-loop contribution to the $\chi^+\chi^-$ annihilation, which is beyond the scope of this work.

5.1.1 The results for the cross-sections

The results are presented on Fig. 5.1. Let us first concentrate on the plot in the left panel showing the $\chi^0\chi^0 \to W^+W^-$ (including the three body production) annihilation process. Our full results including the one-loop corrections and the Sommerfeld effect are given by the solid black line. There is a clear resonance visible[3], which is due to the creation of a loosely bound state of the incoming neutralino pair. As expected, the resonance occurs

[3]Note, that in contrast to what one typically calls a resonance, this is not a resonance in energy, but rather in the Wino mass.

approximately when the Bohr radius of the $\chi^0\chi^0$ pair matches the interaction range, i.e.: $1/(m_\chi \alpha) \approx 1/m_W$. For this reason, the position of the resonance depends strongly of the value of the coupling and this is why it is so important to use it at an appropriate scale. In Sec. 3.2.1 we have discussed that the proper value is the one at the electroweak scale. If one uses instead its value at the scale m_χ (and do not include the radiative corrections) then one get the result plotted by the brown dotted line. That is, if one used the running of the couplings instead of doing full one-loop computation, one would get the resonance peak displaced in m_χ from about 2.38 TeV to about 2.5 TeV.

In fact, the precise value of the g_2 affects also the result for the relic density. As we already discussed, see footnote 18 in Sec. 4.4.3, the Wino mass giving observed relic abundance shifts by about 400 GeV, if one uses its value at the scale m_χ and not the electroweak one.

On the same plot we show that including only the one-loop approximation of the Sommerfeld effect is a good approximation only up to about 200 GeV, beyond which it breaks down, mainly due to the presence of the resonance. However, it is of course still more accurate than just using the tree level value. What might seem surprising is that using the tree level formula but with a running coupling constant at a scale m_χ (blue sparse line) is even a worse approximation than simply taking the standard tree level cross-section. This comes from the fact that running of the couplings captures only the UV effects of re-summation of large log's (which gives a negative contribution), while in our setup the dominant correction to the annihilation amplitude is the Sommerfeld one, which is positive and (at a one-loop approximation) proportional to m_χ/m_W.

We also do a comparison with the results using the full Sommerfeld corrections, but this time applied only to the tree level annihilation amplitudes (red chained line). The largest difference occurs before the resonance, for the masses of about 1 TeV, where the inclusion of one-loop contributions makes the full cross-section smaller by as much as about 30%. In the resonance, although due to the logarithmic scale from the plot it seems that including the loop corrections do not change the result significantly, actually the radiative corrections make the value of σv in the peak is smaller by about 22%.

On the right panel of Fig. 5.1 we present the results of the annihilation cross section to ZZ, $Z\gamma$ and $\gamma\gamma$. Again a clear resonance is visible, for the same reason as before (in fact, by construction Sommerfeld effect is independent on the final states). However, the absolute value of the cross-section into $\gamma\gamma$ is about two orders of magnitude smaller than into W^+W^-. Since the annihilation of $\chi^0\chi^0$ into neutral gauge bosons cannot occur at the tree level, the Leading Order (LO) for those processes is computed by including only the one-loop contributions (from which the one-loop Sommerfeld is dominant for large masses, which makes the LO proportional to m_W^{-2}, rather than m_χ^{-2}, what explains the shape of the LO results).

Looking at the low mass region, one can see that the full cross-sections are smaller than the LO ones. There are two reasons for that, both relaying on the fact, that, as we discussed, the one-loop corrections are negative. This means that both annihilation amplitudes, to be combined with the Sommerfeld enhancement factors, are decreased with respect to their tree level values and, since the annihilation $\chi^0\chi^0$ to neutral gauge bosons do not occur at tree level, the two terms from which the Sommerfeld enhanced

amplitude is constructed (see Eq. (5.2)), have opposite signs. Thus, not only the one-loop contribution decrease the $\chi^+\chi^-$ annihilation, but also the Sommerfeld effect is suppressing the cross-section when $s_0 \gg s_\pm$, i.e. precisely in the low m_χ region. However, we want to emphasize once again, that in this regime one should extend our computation and include also order $\mathcal{O}(g^8)$ contributions.

Annihilation spectra

In the indirect detection the spectral shape of photons and cosmic rays is crucial, therefore not only the total cross-section, but also the differential one is needed. It can be obtained without any difficulty from what we have discussed so far. Indeed, the two-body W^+W^- annihilation give obviously a monochromatic line, while for the three-body processes it is enough to integrate only in one of the final energies in Eq. (3.17).

The total annihilation cross-section, as presented on Fig. 5.1, can be decomposed into:

$$\sigma_{tot} = \sigma_2^{tree} + \sigma_2^{loop} + \sigma_3^{WW\gamma} + \sigma_3^{WWZ}, \tag{5.5}$$

where, for clarity, we will always keep track of the perturbation order of various contributions: the tree level contribution is $\mathcal{O}(g^4)$, while loop and three-body are $\mathcal{O}(g^6)$. The differential cross-section with respect to the variable $x = E_k/m_\chi$ reads:

$$\frac{d\sigma_{tot}}{dx} = \underbrace{\sigma_{tree}\delta(1-x)}_{\mathcal{O}(g^4)} + \underbrace{\sigma_{loop}\delta(1-x) + \frac{d\sigma_{WW\gamma}}{dx} + \frac{d\sigma_{WWZ}}{dx}}_{\mathcal{O}(g^6)}. \tag{5.6}$$

Including the Sommerfeld effect has three implications:

- most importantly, the value of the cross-section gets enhanced; in the spectrum it is simply seen as a overall normalization shift,
- the annihilation channels ZZ, $Z\gamma$ and $\gamma\gamma$ open up; without the SE they are of higher order,
- and finally modifies the spectra, since the χ^0 annihilates differently than the $\chi^\pm$ and the Sommerled factors s_0, $s_\pm$ are also different.

The differential cross-section including the SE is thus given by:

$$\frac{d\sigma_{SE}}{dx} = \sigma_2^{tot}\delta(1-x) + |s_0|^2\frac{d\sigma^{00}_{WW\gamma,Z}}{dx} + |s_\pm|^2\frac{d\sigma^{+-}_{WW\gamma,Z}}{dx} + 2\mathrm{Re}\, s_0 s_\pm^* \frac{d\sigma^{mix}_{WW\gamma,Z}}{dx}, \tag{5.7}$$

where we used a short notation $d\sigma^{00}_{WW\gamma,Z}/dx = d\sigma^{00}_{WW\gamma}/dx + d\sigma^{00}_{WWZ}/dx$. The appearance of the last term is the result of computing the SE on an amplitude level and σ^{mix} denotes the "cross-section" obtained from integrating over phase space the mixed term with both $A_{\chi^0\chi^0}$ and $A_{\chi^+\chi^-}$.

The two-body enhanced cross-section is equal to:

$$\begin{aligned}\sigma_2^{tot} &= |s_0|^2\sigma_{tree}^{00\to WW} + |s_\pm|^2\sigma_{tree}^{+-\to WW} + 2\mathrm{Re}\, s_0 s_\pm^* \sigma_{tree}^{mix} \\ &+ |s_\pm|^2\left(\sigma_{tree}^{+-\to ZZ} + \sigma_{tree}^{+-\to Z\gamma} + \sigma_{tree}^{+-\to\gamma\gamma}\right) \\ &+ |s_0|^2\sigma_{loop}^{00\to WW} + |s_\pm|^2\sigma_{loop}^{+-\to WW} + 2\mathrm{Re}\, s_0 s_\pm^* \sigma_{loop}^{mix} \\ &+ |s_\pm|^2\left(\sigma_{loop}^{+-\to ZZ} + \sigma_{loop}^{+-\to Z\gamma} + \sigma_{loop}^{+-\to\gamma\gamma}\right) \\ &+ 2\mathrm{Re}\, s_0 s_\pm^*\left(\sigma_{loop}^{mix\to ZZ} + \sigma_{loop}^{mix\to Z\gamma} + \sigma_{loop}^{mix\to\gamma\gamma}\right). \end{aligned} \tag{5.8}$$

First two lines of the above expression give a contribution of the order $\mathcal{O}(g^4)$, while the rest $\mathcal{O}(g^6)$. Note, that the are no terms like $|s_0|^2\sigma_{loop}^{00\to\gamma\gamma}$, since this is of higher order.

Here, by writing only one delta function for all kind of final states we make an assumption that in the annihilation to $Z\gamma$ we can treat the resulting particles as having the same mass. It is a good approximation for the DM mass of several TeV. However, even for lower masses this approximation affects only the slight shift of the $Z\gamma$ line component.

On Fig. 5.2 we show the primary annihilation spectra for an example case of $m_\chi = 2.4$ TeV. It is chosen such to be near the resonance, where the impact of the Sommerfeld effect is most clearly visible. First of all note, that the perturbative result, given just by the standard three-body annihilation process (dotted lines), is normalized differently than the full Sommerfeld one (solid lines). The ploted spectra are *per annihilation*, i.e. normalized such that integrated over x give the total number of produced primary particles. Therefore,

$$\frac{dN_{tot}}{dx} = \frac{1}{\sigma_{tot}}\frac{d\sigma_{tot}}{dx}, \qquad \frac{dN_{SE}}{dx} = \frac{1}{\sigma_{SE}}\frac{d\sigma_{SE}}{dx}. \tag{5.9}$$

This is why these lines are close to each other, even though for this mass the SE enhances the cross-section by nearly four orders of magnitude.

For massive gauge bosons the spectrum posses a visible threshold at $x = m_{W,Z}/m_\chi$. Photons on the other hand are regulated by introducing an effective photon mass m_γ, which physically is en effect of the energy resolution below which one cannot distinguish the $W^+W^-\gamma$ state from W^+W^- one. In fact, this is a delicate point. In collider experiments the IR regulator is set by the known energy resolution of the detector. In our case however, it is not that simple, because of the effects of propagation before the signal actually reaches the detector. Having this in mind, we choose the energy resolution to be of 1%. To take it into account in the spectrum, we have followed the philosophy of [176]: one subtracts the part of the γ spectrum below E_{res} and adds it to the W one. This is done in such a way, that including the virtual corrections one obtains correct total cross-section after integrating over whole range of x. However, instead of flat distribution as in [176] we have chosen, a more physical Gaussian one. Moreover, we applied this procedure consistently to whole spectrum, by introducing a smearing, i.e. for every x we convolute the initial spectra with a Gaussian distribution

$$G(x_{\mathrm{obs}}, x) = \frac{1}{\sqrt{2\pi}x_{res}}\exp\left(\frac{(x_{obs}-x)^2}{2x_{res}^2}\right), \tag{5.10}$$

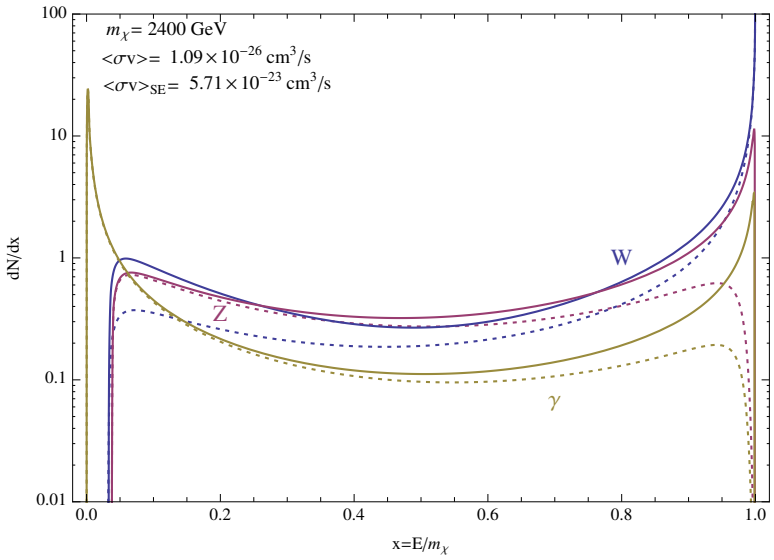

Figure 5.2: Initial annihilation spectra of $W^\pm$, Z and γ for the case near the resonance, with $m_\chi = 2.4$ TeV. The solid lines correspond to full Sommerfeld enhanced result, while dotted to the $\mathcal{O}(g^6)$ one. Notice the difference in normalization for dN/dx in these two cases, see Eq. (5.9).

where $x_{\rm res} = E_{\rm res}/m_\chi$ and $x_{\rm obs}$ is the observed value. This effectively makes the change:

$$D(x) \to D(x_{\rm obs}) = \int_0^1 dx D(x) G(x_{\rm obs}, x), \tag{5.11}$$

where $D(x)$ is the initial annihilation spectrum and $D(x_{\rm obs})$ the corrected one. Indeed, such a smearing simulates the physical process that makes the spectrum and cross-section finite in the IR. In our computations we used a small regulator, with $m_\gamma \ll E_{\rm res}$, and so after the smearing it is $E_{\rm res}$ who plays the role of a regulator, as if $m_\gamma = 0$. This smearing allows also to show on the plots the line component, which otherwise would be a Dirac delta function.

The impact of the Sommerfeld enhancement is most visible for large x, where in fact it starts to dominate and produces a strong signal. This comes mainly from the large enhancement of the two-body processes giving line components, but also from the amplification of the bump just below the upper threshold for γ and Z. This bump appears, because not only soft, but also the collinear (even hard) gauge boson emission is logarithmically enhanced.

5.1.2 Fluxes at production

The W and Z bosons produced in the annihilation process will subsequently decay into quarks and leptons. Quarks then undergo hadronization producing mesons and even baryons, which can be stable, like protons and antiprotons, or fragmentate into leptons and photons. We can see that a plethora of various final particles will be produced in even a single dark matter annihilation event. However, this is not the end of the story. The particles produced in these process can have very high invariant masses, i.e. the primary

particle can be off-shell with large vitruality. The resulting process is then not a decay, but a *splitting* and the whole process produces a shower of final particles. In particular, the primary gauge bosons produced in the annihilation are very energetic: their invariant mass is of the order of the mass of the neutralino, which in our case of interest is at the TeV scale.

All this processes can be described by the Dokshitzer-Gribov-Lipatov-Altarelli-Parisi (DGLAP) evolution [264, 265, 266], which relies on the fact that the branching probabilities in the soft/collinear approximation are universal. They depend only on the virtuality μ^2 and the so-called splitting functions, which one can derive given field content and interactions.

This approach is very well know and exploited a lot in collider physics, especially in the simulations of jets. Because of this, since many years robust numerical codes taking care of all the splitting/hadronization/fragemantation processes exist. Two most widely used are PYTHIA [267] and HERWIG [268], from which in our work we used the former one, as it is already implemented inside DarkSUSY. Unfortunately, they are optimized for the high energy collisions and not non-relativistic annihilations. Moreover, they concentrate mostly on the QCD jets and not EW processes. They have also some peculiarities, e.g. PYTHIA does include the photon Bremsstrahlung from fermion states, but not from $W^{\pm}$. One thus has to be careful when using them for the DM annihilation. Nevertheless, this can be done, which we will describe below. We follow the approach of [179] to include the additional electroweak splitting functions, which are missing in PYTHIA. However, in contrary to what was done there and then used in the PPPC 4 DM ID code, for the photon and W/Z Bremsstrahlung we use our full $\mathcal{O}(g^6)$ computation. In this way we take the advantage of our model specific treatment, for which we have computed the whole loop corrections, with the Sommerfeld effect included.

The first step is to compute the spectra of $f = \gamma, \nu, e^+, \bar{p}, \bar{d}$ at production per annihilation, i.e. the quantity:

$$\frac{dN^f_{tot}}{dx} = \frac{1}{\sigma_{tot}} \frac{d\sigma^{\chi\chi\to X\to f}_{tot}}{dx}, \tag{5.12}$$

where $x = E_f/m$, E_f is the kinetic energy of particle f, σ_{tot} is the total annihilation cross-section (summed over all possible annihilation channels), and $\sigma^{\chi\chi\to X\to f}_{tot}$ denotes the sum of cross-sections for all processes giving rise to particle f (with all multiplicities etc. included). This implicitly assumes, that:

$$\sigma_{tot} \approx \int_0^1 \frac{d\sigma^{\chi\chi\to X\to f}_{tot}}{dx} dx, \tag{5.13}$$

i.e. that the subsequent production of particle f from decay/fragmentation of primary annihilation products does not change the total cross-section. This is clearly justified, since all those additional contributions are of a higher order.

We start from the final spectra of $f = \gamma, \nu, e^+, \bar{p}$ (for antideuterons we will need a separate discussion). In the total spectrum, including the order $\mathcal{O}(g^6)$ terms, we have possible initial states $I = W, Z, \gamma$. To get final spectra one has to convolute the initial

ones with the fragmentation tables [179]:[4]

$$\frac{dN^f_{tot}}{dx}(M,x) = \sum_{I=W,Z,\gamma} \int_x^1 dz\, S_I\, D_I(z)\, \frac{dN^{\rm MC}_{I\to f}}{dx}\left(zM, \frac{x}{z}\right), \tag{5.14}$$

where

$$D_I(z) = BR_I \frac{dN_I}{dz} \tag{5.15}$$

is the spectrum of I (splitting function) and the symmetry factors are $S_W = 1$, $S_Z = S_\gamma = 1/2$. The splitting functions for gauge boson emission we obtain from our three-body initial spectra and the total annihilation cross-section, via:

$$\begin{aligned}
D_\gamma(z) &= \frac{\sigma_{WW\gamma}}{\sigma_{tot}} \frac{dN^\gamma_{WW\gamma}}{dx}, & (5.16)\\
D_Z(z) &= \frac{\sigma_{WWZ}}{\sigma_{tot}} \frac{dN^Z_{WWZ}}{dx}, & (5.17)\\
D^{tree}_W(z) &= \frac{\sigma^{WW}_{tree}}{\sigma_{tot}} \delta(1-x), & (5.18)\\
D^{loop+rp}_W(z) &= \frac{\sigma^{WW}_{loop}}{\sigma_{tot}} \delta(1-x) + \frac{\sigma_{WW\gamma}}{\sigma_{tot}} \frac{dN^W_{WW\gamma}}{dx} + \frac{\sigma_{WWZ}}{\sigma_{tot}} \frac{dN^W_{WWZ}}{dx}. & (5.19)
\end{aligned}$$

The final spectra we obtain then from:

$$\begin{aligned}
\frac{dN^f_{tot}}{dx}(M,x) &= \delta_{f\gamma} D_\gamma(x)\\
&+ \int_x^1 dz\, S_W \left(D^{tree}_W(z) + D^{loop+rp}_W(z)\right) \frac{dN^{\rm DS}_{W\to f}}{dx}\left(zM, \frac{x}{z}\right)\\
&+ \int_x^1 dz\, S_Z\, D_Z(z)\, \frac{dN^{\rm DS}_{Z\to f}}{dx}\left(zM, \frac{x}{z}\right).
\end{aligned}$$

In this way we include properly annihilation to gauge bosons with the radiative corrections. However, PYTHIA also does not include electroweak splitting of gauge bosons into fermions (it includes only the decay). We incorporate them by adding all the additional splitting functions, taken from [179], computed at the leading double log level.

The complete *Sommerfeld corrected* $D(z)$ functions, separated with respect to the perturbation theory order, are then:

$$\begin{aligned}
\sigma_{SE} D^{(4)}_\gamma(x) &= |s_\pm|^2 \left(2\sigma^{+-\to\gamma\gamma}_{tree} + \sigma^{+-\to Z\gamma}_{tree}\right) \delta(1-x) & (5.20)\\
\sigma_{SE} D^{(6)}_\gamma(x) &= |s_0|^2 \sigma^{00}_{WW\gamma} \frac{dN^\gamma_{WW\gamma}}{dx} + |s_\pm|^2 \sigma^{+-}_{WW\gamma} \frac{dN^\gamma_{WW\gamma}}{dx} + 2{\rm Re}\, s_0 s^*_\pm \sigma^{mix}_{WW\gamma} \frac{dN^\gamma_{WW\gamma}}{dx} & (5.21)\\
&+ |s_\pm|^2 \left(2\sigma^{+-\to\gamma\gamma}_{loop} + \sigma^{+-\to Z\gamma}_{loop}\right) \delta(1-x) + 2{\rm Re}\, s_0 s^*_\pm \left(2\sigma^{mix\to\gamma\gamma}_{loop} + \sigma^{mix\to Z\gamma}_{loop}\right) \delta(1-x)
\end{aligned}$$

[4] Note that the final f spectra are vs. the kinetic energy $x = E_k/m$, while in the formula z is the total energy fraction carried by a given primary channel particle (e.g. W); that is why $x \leqslant z \leqslant 1$. The same applies to the splitting functions, where $z = E/m$.

$$\sigma_{SE} D_Z^{(4)}(x) = |s_\pm|^2 \left(2\sigma_{tree}^{+-\to ZZ} + \sigma_{tree}^{+-\to Z\gamma}\right) \delta(1-x) \tag{5.22}$$

$$\begin{aligned}\sigma_{SE} D_Z^{(6)}(x) &= |s_0|^2 \sigma_{WWZ}^{00} \frac{dN_{WWZ}^Z}{dx} + |s_\pm|^2 \sigma_{WWZ}^{+-} \frac{dN_{WWZ}^Z}{dx} + 2\mathrm{Re}\, s_0 s_\pm^* \sigma_{WWZ}^{mix} \frac{dN_{WWZ}^Z}{dx} \\ &+ |s_\pm|^2 \left(2\sigma_{loop}^{+-\to ZZ} + \sigma_{loop}^{+-\to Z\gamma}\right) \delta(1-x) + 2\mathrm{Re}\, s_0 s_\pm^* \left(2\sigma_{loop}^{mix\to ZZ} + \sigma_{loop}^{mix\to Z\gamma}\right) \delta(1-x)\end{aligned} \tag{5.23}$$

$$\sigma_{SE} D_W^{(4)}(x) = \left(|s_0|^2 \sigma_{tree}^{00\to WW} + |s_\pm|^2 \sigma_{tree}^{+-\to WW} + 2\mathrm{Re}\, s_0 s_\pm^* \sigma_{tree}^{mix\to WW}\right) \delta(1-x) \tag{5.24}$$

$$\begin{aligned}\sigma_{SE} D_W^{(6)}(x) &= \left(|s_0|^2 \sigma_{loop}^{00\to WW} + |s_\pm|^2 \sigma_{loop}^{+-\to WW} + 2\mathrm{Re}\, s_0 s_\pm^* \sigma_{loop}^{mix\to WW}\right) \delta(1-x) \\ &+ |s_0|^2 \sigma_{WWZ}^{00} \frac{dN_{WWZ}^W}{dx} + |s_\pm|^2 \sigma_{WWZ}^{+-} \frac{dN_{WWZ}^W}{dx} + 2\mathrm{Re}\, s_0 s_\pm^* \sigma_{WWZ}^{mix} \frac{dN_{WWZ}^W}{dx} \\ &+ |s_0|^2 \sigma_{WW\gamma}^{00} \frac{dN_{WW\gamma}^W}{dx} + |s_\pm|^2 \sigma_{WW\gamma}^{+-} \frac{dN_{WW\gamma}^W}{dx} + 2\mathrm{Re}\, s_0 s_\pm^* \sigma_{WW\gamma}^{mix} \frac{dN_{WW\gamma}^W}{dx}\end{aligned} \tag{5.25}$$

Note the multiplicity factor of 2 in front of the terms with production of two identical gauge bosons.

In the same way as before, the final spectra we obtain then from:

$$\begin{aligned}\frac{dN_{SE}^f}{dx}(M,x) &= \delta_{f\gamma} D_\gamma^{(4)}(x) + \delta_{f\gamma} D_\gamma^{(6)}(x) \\ &+ \int_x^1 dz\, S_W \left(D_W^{(4)}(z) + D_W^{(4)}(z)\right) \frac{dN_{W\to f}^{\mathrm{DS}}}{dx}\left(zM, \frac{x}{z}\right) \\ &+ \int_x^1 dz\, S_Z \left(D_Z^{(4)}(z) + D_Z^{(4)}(z)\right) \frac{dN_{Z\to f}^{\mathrm{DS}}}{dx}\left(zM, \frac{x}{z}\right) .\end{aligned}$$

The results are given on Fig. 5.3 for several representative masses. In the left column we show the e^+, $\bar{p}$ and γ spectra, where on the right the neutrino ones.

Let us start the discussion from the charged CRs and photons. The chained line represents the result one would obtain for the tree level annihilation process. At the TeV scale it nearly does not change with the Wino mass, because we consider only one W^+W^- annihilation channel and thus m_χ affects only the total cross-section and not the spectrum. The dominant final state are soft photons, coming mainly from production and then decay of π^0s. Electrons are produced in direct W decay or splitting and also by charged pions. Finally, antiprotons are obviously much harder to produce and they are much less abundant, but nevertheless prove to be very useful in constraining many models (including this one).

The results do change considerably with the inclusion of electroweak and Sommerfeld corrections plotted as solid lines. For the soft part, when the Wino mass is relatively low the Sommerfeld effect is rather mild and nearly entire modification of the spectrum comes from radiative corrections. As advocated before, a clear enhancement of the very low energetic final states is visible. On the other hand in the higher end of the spectrum additional hard γ component arises, to which both radiative and Sommerfeld corrections

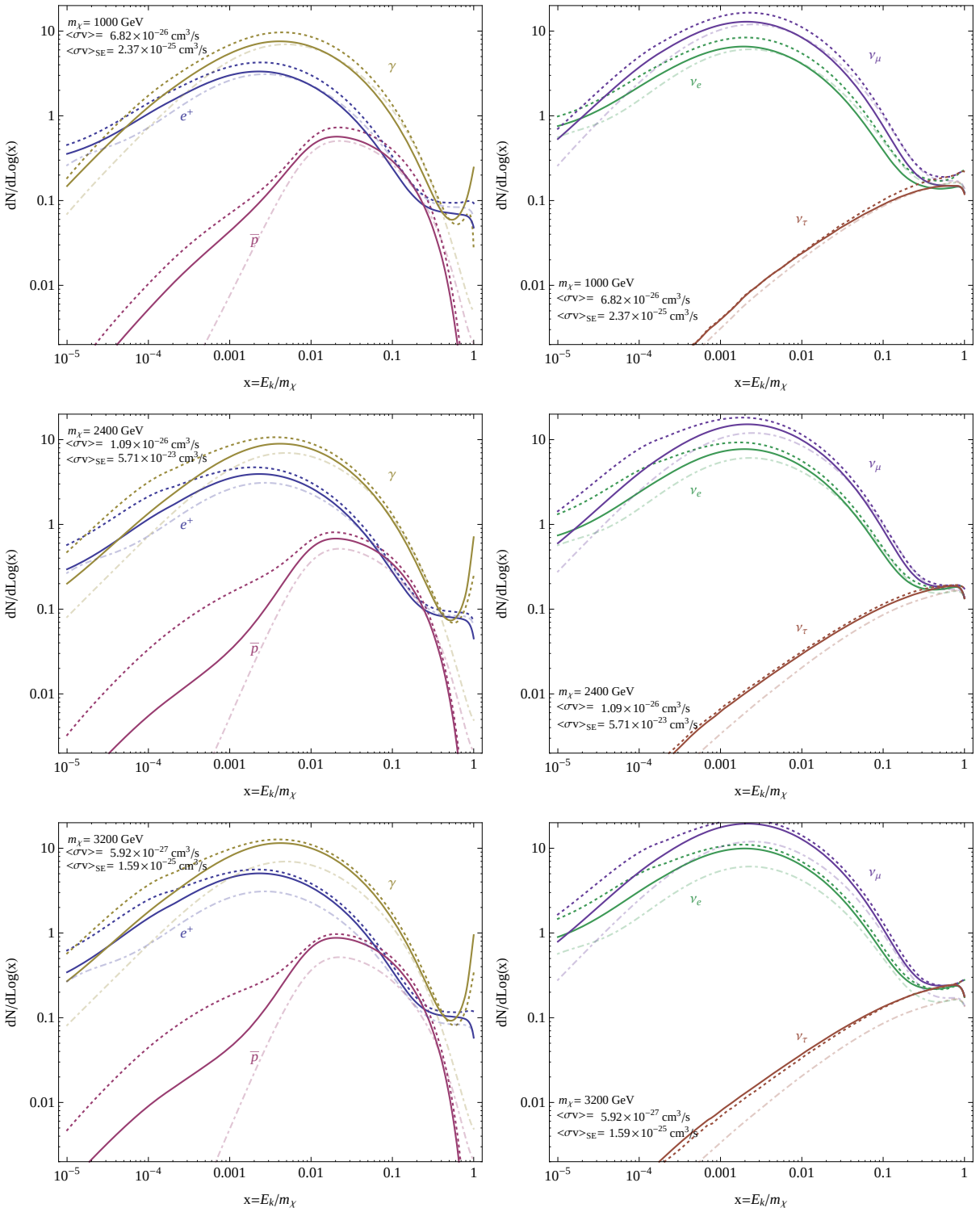

Figure 5.3: Number of final stable particles per annihilation for there representative Wino masses: typical $m = 1$ TeV (top), near resonance $m = 2.4$ TeV (middle) and giving correct thermal relic abundance $m = 3.2$ TeV (bottom). The chained lines show the tree-level result, dotted the EW corrected, while the solid the full Sommerfeld enhanced one.

contribute. The former mainly due to logarithmic enhancement of the collinear photon FSR, while the latter also amplifies a monochromatic gamma line.

When we look on higher masses, these effects are becoming slightly stronger. Notice however, that the near resonance case of $m_\chi = 2.4$ TeV does not introduce much stronger deformations of the spectra than the generic case of large m_χ. The reason is that the main effect of the Sommerfeld resonance is anyway the enhancement of the total cross-section, while the spectrum change is rather mild.

In total, the amplification of the signal is visible in both the very soft part (electroweak corrections) and the hard gamma component (Sommerfeld), while the total cross-sections is also strongly enhanced (Sommerfeld).

In the case of neutrinos the overall behaviour is similar. The tree level result gives weaker signals and is nearly mass independent. The ν_τ has a completely different spectrum than ν_e and ν_μ, because of difference in their production mechanisms. Neutrinos arise mostly due to pions' decays, through:

$$\pi^+ \to \mu^+\nu_\mu \to e^+\nu_e\bar{\nu}_\mu\nu_\mu \quad \text{and} \quad \pi^- \to \mu^-\bar{\nu}_\mu \to e^-\bar{\nu}_e\nu_\mu\bar{\nu}_\mu \,. \tag{5.26}$$

This is due to the helicity suppression of a pion decay, favoring muons as the heaviest kinematically allowed final states: the τ is heavier than $\pi^\pm$. Our full result again shows some enhancement, here mainly in the soft part. What is however most important phenomenologically in this case, is the effect on the total cross-section amplifying the dark matter component vs. background in very the high energetic neutrinos (see Sec. 5.3.5). Note also, that these are results at production, so no oscillation effects were included.

Antideuteron fluxes at production

Antideuterons are very interesting objects. Quite rare in Nature, their abundance in cosmic rays is also expected to be extremely low. They are produced in the high energy collision of a p, $\bar{p}$ or He impinging onto the interstellar gas (mainly H and He). The production cross-section is very low and has a relatively high threshold. For the anitdeuteron to be formed, an impinging particle needs to have an energy (in the rest frame of the gas) $E \geqslant 17m_p$. For the possible dark matter detection what is even more important is its low binding energy, $B_d \approx 2.2$ MeV. It means that they are easily destroyed and do not propagate long enough to loose most of their energy. This leads to very low background of astrophysical antideuterons with $E_k/n < 1$ GeV.

The downside of its rareness is that its cross-sections for production, elastic and inelastic scattering are not well known. It is an important source of uncertainty in the predictions of its signals coming from dark matter annihilation. In our work we adopted all these cross-sections from the work [269], based on fitting the experimental data under some reasonable assumptions.[5] We then implemented them into DRAGON code [271] for the production of secondary and tertiary antideuterons, as well as their propagation in the Galaxy.

[5]For all the details see the original work and also [270]. We would also like to thank David Maurin for sharing these cross-sections.

The standard treatment of how $\bar{d}$ is produced, the one which is also implemented in DarkSUSY, follows the "coalescence model", see e.g. [272, 270, 273]. This approach is based on an assumption that $\bar{p}$ and $\bar{n}$ will combine (coalesce) to an $\bar{d}$, if and only if:

$$|\vec{k}_{\bar{p}} - \vec{k}_{\bar{n}}| \leqslant p_0, \tag{5.27}$$

where p_0 is called *coalescence momentum*. As a rough estimate which gives some intuition, one can obtain this value from $p_0 \sim \sqrt{m_d B_d} \sim 60$ MeV, where the mass of deuteron is $m_d = 1.8756$ GeV.

The more precise values are derived from experimental data (e.g. formation of $\bar{d}$ from e^+e^- collisions or hadronic Z decays). Different works used a bit different values: in [272] $p_0 = 58$ MeV, which is also the default value DarkSUSY, then with the new data it was updated to a value $p_0 = 79$ MeV [270], while independently [274, 275] have found value $p_0 = 80$ MeV from their own fit to the ALEPH data.[6]

In the spherical approximation, in which the final $\bar{p}$ and $\bar{n}$ are distributed uniformly over all 4π, the dependence of the final result on p_0 is through an overall normalization factor, being the volume of 3-dim sphere in momentum space with radius p_0. The $\bar{d}$ yield is given by

$$\gamma_d \frac{dN_d}{d^3k_d} = \frac{4\pi p_0^3}{3} \gamma_n \frac{dN_n}{d^3k_n} \gamma_p \frac{dN_p}{d^3k_p}, \tag{5.28}$$

where the Lorenz factors are approximately equal $\gamma_d \approx \gamma_n \approx \gamma_p$. We have also

$$d^3k_X = 4\pi k_X^2 dk_X = 4\pi k_X^2 \frac{E_X}{\sqrt{E_X^2 - m_X^2}} dE_X, \tag{5.29}$$

where $k_X = \sqrt{E_X^2 - m_X^2}$. In order for $\bar{d}$ to form, the difference in momentum of $\bar{p}$ and $\bar{n}$ has to be less then $p_0 \ll k_n, k_p$. Thus, the momenta approximately satisfy relation:

$$\frac{k_d}{2} \approx k_p \approx k_n \equiv k \ , \tag{5.30}$$

and thus also $E_p \approx E_n \equiv E$. Finally, the antideuteron spectrum can be computed from the proton one via:

$$\frac{dN_d}{dE_d} = \frac{4p_0^3}{3} \frac{\gamma_p}{E\sqrt{E^2 - m_p^2}} \left(\frac{dN_p}{dE}\right)^2 \ . \tag{5.31}$$

Apart from the update in value of p_0 there is another, much more important difference in the newer works [274, 275] from the older ones: although they rely on the coalescence model they do not make the spherical approximation, but run a dedicated Monte Carlo codes to compute the $\bar{d}$ yields. The authors argue, that this is correct way to proceed, in contrary to previous works of [270, 272, 273], which they claim to be oversimplified. The important phenomenological difference is the behaviour of the flux for higher dark matter masses, where the spherical approximation gives m_χ^{-2} dependence, while Monte Carlo gives more flat distribution.

[6] In fact value used in the two latter works is 160 MeV, but they use a different definition of the normalization of the antideuteron yield by a factor of 2^3 coming from the change in p_0 by factor 2.

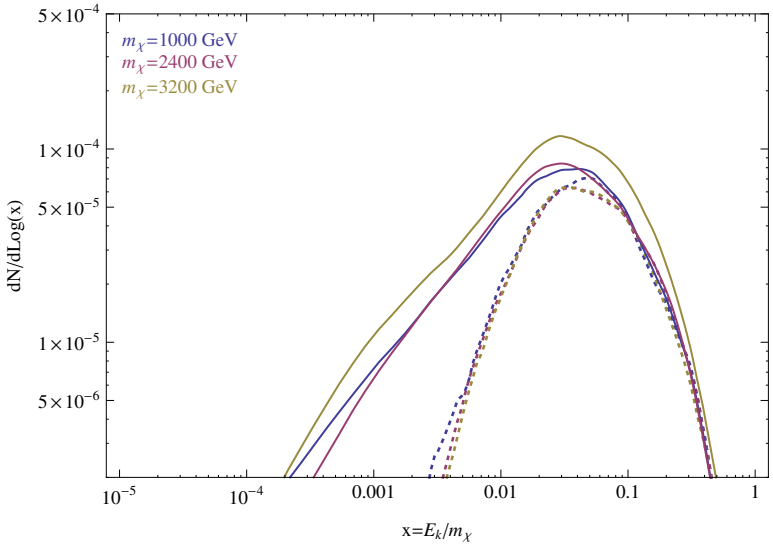

Figure 5.4: Antideuteron spectra from Wino annihilation for masses $m_\chi = 1, 2.4, 3.2$ TeV. Dotted lines show the tree level results, while solid the Sommerfeld enhanced ones.

The physical reason why the spherical coalescence model is not sufficient is that after dark matter annihilates, final states are very energetic and go in back-to-back jets, rather than distributed over all 4π. Therefore, the $\bar{p}$ and $\bar{n}$ are typically produced with much smaller separation angle. This is especially pronounced for high m_χ and explains why the in this regime the difference is the largest.

In our work we adopted the results from the Monte Carlo approach of Ref. [274], which is publicly available via the PPPC 4 DM ID code. However, as before, for the electroweak corrections we used our computation and also incorporated the Sommerfeld effect.

We show the antideuterons fluxes at production on Fig. 5.4 for the same set of masses as before. It is clearly visible that the spectra are very similar to each other. As discussed above, this is indeed on contrary to m_χ^{-2} scaling as found in pioneering works on this topic. The main effect of electroweak and Sommerfeld corrections is to increase the soft part of the spectrum, which seems promising for the detection prospects (see Sec. 5.3.6). Note also, that including the Sommerfeld effect makes the fluxes even larger for larger m_χ.

Before ending this section, let us comment on the normalization. In the literature the spectra are often given as $\frac{dN}{dx} = \frac{1}{\sigma_{tree}}\frac{d\sigma_{tot}}{dx}$. However, this does not give number of final states *per annihilation*, which should be rather $\frac{dN}{dx} = \frac{1}{\sigma_{tot}}\frac{d\sigma_{tot}}{dx}$, which is what we use. This difference has two implications. The first is obvious: when comparing the spectra among different works what matter is the shape, while the overall normalization can differ substantially. The second implication is that one has to be careful when combining the splitting functions of Ref. [179] with our full computation and use ones rescaled by $D^{EW}_{I\to J} \to \frac{\sigma_{tree}}{\sigma_{tot}} D^{EW}_{I\to J}$.

5.2 Cosmic ray propagation

Since the discovery of the cosmic rays (CRs) precisely 100 years ago by Victor Hess, we still don not fully understand their origin.[7] Nevertheless, we have been able to learn a lot about their composition, spectra and properties. The main basic observation is that CRs coming from various astrophysical sources (called primaries) are distinct from the ones produced by spallation of primary cosmic rays on interstellar gas (called secondaries). The latter are far less abundant and have different, more soft spectra.

This is indeed the key point for our understanding of how do CRs propagate in our Galaxy. The reason is that by measuring the primary nuclei we can make predictions for the production of secondary leptons and nuclei, based on cross-sections and the interstellar gas distribution. Obtained in this way secondary spectra can be propagated and compared with observations. This allows to test propagation models and fit their free parameters.

The propagation theory which is most widely accepted is the diffusion model with possible inclusion of convection [277]. It was tested to provide the most adequate description of CR transport in our Galaxy. Within this framework the general CR propagation equation can be written as:

$$\frac{\partial N^i}{\partial t} - \vec{\nabla}\cdot\left(D_{xx}\vec{\nabla} - \vec{v_c}\right)N^i + \frac{\partial}{\partial p}\left(\dot{p} - \frac{p}{3}\vec{\nabla}\cdot\vec{v_c}\right)N^i - \frac{\partial}{\partial p}p^2 D_{pp}\frac{\partial}{\partial p}\frac{N^i}{p^2} = \tag{5.32}$$
$$Q^i(p,r,z) + \sum_{j>i} c\beta n_{\rm gas}(r,z)\sigma_{ij}N^j - c\beta n_{\rm gas}\sigma_{\rm in}(E_k)N^i - \sum_{j<i}\frac{N^i}{\tau^{i\to j}} + \sum_{j>i}\frac{N^j}{\tau^{j\to i}}\,,$$

where $N^i(p,r,z)$ is the number density of the i-th particle species with momentum p and velocity $v = c\beta$. Below we describe in some more detail the physical meaning of various terms:

- **Spatial diffusion**: $-\vec{\nabla}\cdot D_{xx}\vec{\nabla}N^i$

  The observed high isotropy of low energy CRs and the relatively large number of secondary nuclei, suggest that cosmic rays travel long time in the Galaxy. This can be explained by the concept of spatial diffusion, caused by the galactic magnetic field that changes the trajectories of particles. On the microscopic level, the diffusion of CRs comes from scatterings on magnetic irregularities. Locally it is thus strongly anisotropic, but the particle density gets isotropised by the fluctuations of the magnetic field at scales of $\mathcal{O}(100\,\mathrm{pc})$.

  The typical values of the diffusion coefficient (found from fitting to CR data) are $D_{xx} = (3\text{–}5)\times 10^{28}\,\mathrm{cm^2 s^{-1}}$ at energy of about 1 GeV/n, and increase with energy (or more precisely magnetic rigidity R, defined as $R = pc/Ze$). Expressing the diffusion coefficient in rigidity, one finds a power-law scaling $D_{xx}\propto\beta R^\delta$, where δ is called the diffusion spectral index and its typical values are in the range $\delta \sim 0.2$–0.7.

[7] For a review of CR physics in general see e.g. [276] and references therein.

- **Convection**: $\vec{\nabla} \cdot \vec{v}_c N^i$ and $-\frac{\partial}{\partial p}\frac{p}{3}\vec{\nabla} \cdot \vec{v}_c N^i$

  In order for the convection processes to give an important contribution to the CR transport, some difference of pressure in the interstellar space is needed. In other words, one needs galactic winds. These have been found in many galaxies (see e.g. [278] and references therein), which suggests that in principle convection could play a role even in the Milky Way. In fact, apart from influencing the propagation (the first term), it can additionally produce adiabatic energy losses (the second term). Physically this is connected with the stretching out by the outgoing wind the volume into which CRs propagate.

  The convection rate is decreasing with energy, therefore it is important only for low energies. Typically it is considered to be linearly increasing with distance from the galactic disk, i.e. $\vec{v}_c \propto \vec{e}_z (dv_c/dz) z$, with the typical magnitude of $v_c \sim \mathcal{O}(10\,\mathrm{km/s})$.

- **Continuous energy losses**: $\frac{\partial}{\partial p}\dot{p}N^i$

  During the propagation CRs loose part of their energy. This happens in various ways. All types of CRs loose energy due to ionisation and Coulomb interactions. These are however important only at lower energies, roughly below a few GeV.

  For positrons and electrons other mechanisms are also efficient. Those are the Bremsstrahlung photon emission and, more importantly, synchrotron radiation and inverse Compton scattering (ICS) on interstellar radiation fields. Note that the synchrotron energy losses are proportional not to energy but rather to the Lorentz factor. Thus for a 100 GeV electron, they are much more efficient than for a proton with the same energy.

  Energy losses inflicted by these two processes are rather efficient. In the Thomson approximation[8] valid at lower energies they are proportional to E^2, while for higher energies they enter the Klein-Nishina regime. This leads to a suppression, with the energy losses in the extreme Klein-Nishina limit depending only logarithmically on E. Moreover, the physical picture of these processes is slightly different: while in every Thompson scattering an electron looses small fraction of its energy and the resulting losses are continuous, in the Klein-Nishina case the electron looses energy rather in discrete amounts, which are a sizeable fraction of its energy [279].

- **Reacceleration**: $-\frac{\partial}{\partial p} p^2 D_{pp} \frac{\partial}{\partial p}\frac{N^i}{p^2}$

  Reacceleration is a diffusive stochastic process in the turbulent galactic magnetic field. It is sometimes refereed to as a diffusion in momentum space, with a coefficient D_{pp}, related to the spatial diffusion via $D_{pp} D_{xx} = p^2 v_A^2/9$, where the Alfvén velocity v_A is introduced as a characteristic velocity of magnetohydrodynamic wave. Its typical value is around $v_A \sim 30\,\mathrm{km/s}$.

[8] The Thomson regime in electron-photon Compton scattering is defined by the condition $E_\gamma^{\mathrm{e.r.f.}} < m_e$, where the $E_\gamma^{\mathrm{e.r.f.}}$ is the energy of the photon in the electron rest-frame and m_e the electron mass. For the ICS on CMB photons this regime is valid even for electron energies up to about a few TeV, but for scatterings on starlight, which is significantly more energetic, the condition is satisfied only up to a few GeV.

- **Source term**: $Q^i(p, r, z)$

  This term includes primary astrophysical sources (with spectrum described by power law in energy with spectral index close to -2), as well as a possible dark matter component. The time dependence of Q is neglected in most of the cases.

- **Spallation**: $\sum_{j>1} c\beta n_{\rm gas}(r, z)\sigma_{ij}N^j - c\beta n_{\rm gas}\sigma_{\rm in}(E_k)N^i$

  Primary CRs are impinging on the ISM gas (with density $n_{\rm gas}$) and scatter both elastically and inelastically. Elastic processes do not change the number of CRs, but re-distribute their energies. On the other hand, inelastic scatterings lead additionally to depletion of primary CRs and production of secondaries. In the formula above $\sigma_{\rm in}$ is the total inelastic cross-section, while σ_{ij} is the production cross-section of a nuclear species j by the fragmentation of the i-th one. The spallation occurs predominantly on interstellar H and He (both atomic and molecular), since the remaining components of the gas have much lower densities.

- **Decays**: $-\sum_{j<i} \frac{N^i}{\tau^{i\to j}} + \sum_{j>i} \frac{N^j}{\tau^{j\to i}}$

  An i-th particle species can also decay into j (if is unstable, with a lifetime of $\tau^{i\to j}$) and/or be produced in the decays of other, heavier particles j.

The boundary conditions for solving the propagation Eq. (5.32) depend on the model. However, if one assumes that at the boundary of the diffusive zone particles escape into the intergalactic space (and never return, nor there are any extragalactic sources), then at this boundary $N^i = 0$. This is what us usually done together with putting also $\frac{\partial N^i}{\partial t} = 0$, i.e. solving only for the steady-state solution.[9]

There are two possible approaches to solving the Eq. (5.32): semi-analitycal and fully numerical. The first one was used much in the literature in the past years mainly because of its relative simplicity and was much easier to implement into numerical computations (and also considerably faster). In this case one typically considers the so-called two-zone diffusion model [280], where the Galaxy is decomposed on a thin disk and a thick diffusive halo. The interstellar gas is confined to the disk. The free parameters of the model are the halo thickness L, the diffusion coefficient D_0 and spectral index δ, the convection velocity v_c and Alfvén velocity v_A, where the reacceleration is typically assumed to take place in the thin disk only.

Nowadays, with much better computational power, fully numerical approaches seem to be more appropriate. They are far more accurate and can take into account much more realistic conditions of the gas and magnetic fields.

The most widely used numerical code for CR propagation is GALPROP [281, 282]. It is very well established c++ code, included by default e.g. in DarkSUSY. In our work we used instead the new code called DRAGON [283]. Although in many parts it is based on its predecessor, it has several advantages. From the physics point of view the main one is that DRAGON was especially designed to take into account spatially inhomogeneous

[9] In fact, many codes instead of neglecting this term, follow the time dependence until a steady-state is reached, which is found to be much faster numerically.

diffusion coefficient also in the direction perpendicular to the galactic plane, which is a much more realistic approach.

The set-up in which DRAGON solves the propagation equation is the following. It assumes cylindrical symmetry and looks for the solution in $2 + 1$ dimensions, with the galactocentric radius r, the height from the Galactic disk z and rigidity R. The diffusion coefficient is expressed by:

$$D(R, r, z) = D_0 \beta^\eta \left(\frac{R}{R_0} \right)^\delta e^{(|z|/z_d)} e^{((r-r_\odot)/r_d)}, \tag{5.33}$$

where the free parameters are the diffusion coefficient normalization D_0, spectral indices η and δ, parameters setting the thickness z_d and radial scale r_d of diffusion zone. The R_0 is the point in rigidity to which we fix the normalization. The diffusion coefficient grows with r, because it is proportional to the diffusion length which gets larger, since the magnetic fields are getting weaker the further we go from the galactic center.

The form of the source term is:

$$Q(R, r, z) = f(r, z) \left(\frac{R}{R_i} \right)^{-\gamma_i}, \tag{5.34}$$

where $f(r, z)$ is a function reflecting the spatial distribution of supernova remnants (SNRs) and γ_i is the injection spectral index for species i. For electrons and positrons one adds also an exponential cut-off with energy, e^{-E/E_c}, with E_c being set to a few TeV. The physical reason is that leptons loose energy very efficiently and thus very energetic ones need also to be very local. On the other hand we do not see nor expect many local sources of TeV scale leptons.

The gas distribution we used in our work is the one recently derived in [284]. It is a new, and arguably most accurate available model for three dimensional distribution of atomic hydrogen gas in our Galaxy, reproducing the global features of the gas distribution such as spiral arms. It was derived using the 21cm Leiden-Argentine-Bonn survey data [285], which is the most sensitive 21cm line survey up to date with the most extensive spatial and kinematic coverage.

5.2.1 The solar modulation

At energies below roughly 5 GeV, the new measurements of the positron fraction deviate significantly from the ones obtained in older experiments. There are two reasons for that. Firstly, for such low energies the systematics of the experiments are most likely not that well under control. The second reason is strictly physical: the fluxes of CR particles are modulated due to interactions with the solar wind when they arrive at the outskirts of the solar system. The modulation comes from the cyclic changes in the solar activity, which is known to change with a period of 11 years, after which the solar magnetic poles reverse. The effect on CRs is important only for low energies, because the solar magnetic fields on which CRs scatter are too weak to alter the trajectory of very energetic particles.

A standard way to describe the effect of solar modulation is by using the force field approximation [286], which is valid in the limit $B \gg 4\pi^2\rho$ (i.e. where the plasma in the solar

wind is completely dominated by the magnetic effects). This essentially means that the cosmic rays feel only the magnetic field: they are deflected by the continuous component and scattered on the irregularities of the solar magnetosphere. In this approximation for a given CR with mass m, atomic number Z and mass number A the modulated spectrum $\Phi_{mod}(E_k)$ is related to the unmodulated one $\Phi(E_k)$ by a formula:

$$\Phi_{mod}(E_k) = \frac{(E_k+m)^2 - m^2}{\left(E_k + m + \frac{Z|e|}{A}\phi\right)^2 - m^2}\Phi\left(E_k + \frac{Z|e|}{A}\phi\right), \tag{5.35}$$

where ϕ is the modulation potential. For electrons and positrons the same formula holds but with $Z/A = 1$. It captures effectively the effect of the scattering on the solar magnetic fields. The value of ϕ is typically determined by fitting the CR spectra at very low energies for a given propagation model. Note, that although theoretically the same value of this potential should be used for different CR species, in practise this is not the case. One always confront the model with the observational data, and these were taken by different experiments in different years. In particular, since now we are in the vicinity of the solar maximum, in the recent years the time dependence of the modulation was expected to be rather strong. This suggests, that what one should in fact do, is to not include the modulation as an effect on the propagation, but rather use it to "demodulate" the data. Effectively, however, this also boils down to using different values of ϕ in order to make the low energy CR data consistent, see e.g. [287].

Therefore, in the results discussed below we adopt a different values for the modulation potential, which we fix by fitting to the B/C, proton, electron and total $e^+ + e^-$ data.

5.3 Indirect detection signals

In the following we will discuss what are the indirect detection signals for the Wino dark matter simultaneously in several channels. The questions we are going to answer are: *i)* for what range of masses Wino is already excluded as a dark matter candidate, *ii)* what is the impact of various uncertainties and how can they affect the exclusion limits, and finally *iii)* does a configuration in which this model can explain the positron fraction rise and in the same time be consistent with the data from all other channels exist. In fact, in this way we not only give the electroweak and Sommerfeld corrected results for this particular model, but we also are able to quantify in a more systematic manner what are the impact of various astrophysical uncertainties. As a consequence, one can make more robust statements about exclusion or detection in this type of searches.

The strategy is the following. For the signals of annihilation to gauge bosons one expects the antiproton constraint to be one of the strongest. The biggest uncertainty in this channel is the diffusion of the DM originated antiprotons. The astrophysical background is fixed by the requirement of fitting the proton data and the data on a secondary to primary ratio in CRs such as boron over carbon (B/C), because essentially all observed antiprotons are secondaries generated by interaction of primary CR protons. The significance of the diffusion effect can be parametrized by the scale of the diffusion zone z_d, see Eq. (5.33). Therefore, we start from determining the propagation parameters

for a given value of z_d by fitting the obtained CR spectra to the data: the B/C, protons and afterwards electrons. For this set of models we compute the DM signal in antiprotons and confront with the observations, putting limits on the Wino model.

Having settled the propagation properties, we use them to determine the signals in leptons, due to experimental results chosen to be the total $e^+ + e^-$ flux and positron fraction defined as $e^+/(e^+ + e^-)$. In this case, diffusion is somewhat less relevant, since leptons loose energy much faster and the locally measured flux stems from much more local sources than for protons. What is then most uncertain is the production mechanism of secondary leptons and their exact energy losses during the propagation. However, as we will see, in our case the precise distinguishing between astrophysical and DM components in this channel is rather impossible. Nevertheless, determining the total fluxes is important for the determination of the total diffuse gamma ray spectrum, which partially comes from the inverse Compton scattering of leptons on the radiation fields and the Bremsstrahlung processes.

Therefore, after obtaining lepton spectra for all our propagation models and different Wino masses, we compute the gamma ray sky-map and compare with FERMI data. From this we *a posteriori* deduce which of our initial propagation models are the best ones, that is giving best fit to the data, and what are the uncertainties there. Having all this information we can already put some more robust bounds on the Wino model. Finally, we close the whole picture by discussing the signals coming from dwarf spheroidal galaxies (dSph), neutrinos and antideuterons.

To finish this introduction, let us comment about other assumptions that we make. In our work we have adopted the standard NFW profile Eq. (1.32), i.e. the generalized one with the parameters being fixed to $\alpha = \gamma = 1$ and $\beta = 3$, unless explicitly stated otherwise. As already mentioned, it is especially important for the GC, where the different profiles give very different predictions and has also some impact on the neutrino signals. For the leptons, antiprotons and antideuterons the precise shape of density distributions is only mildly affecting the final result, because it introduces much smaller uncertainty than the propagation itself.

We also did not include any effect coming from substructures. The reason is that although simulations tend to favor rather non-negligible amount of substructures in the Galaxy halo, they are still rather far from being conclusive [67]. On the other hand, overdensities would amplify the DM signal.[10] Therefore, in order to give conservative limits or prospects for DM searches, we decided not to include substructures.

The overall normalization of the density profile is obtained via the determination of the local dark matter density. This quantity is again not known exactly. We adopt a value from the recent work [289] giving for the NFW profile $\rho_{DM}(r_0) = (0.389 \pm 0.025)\,\mathrm{GeV/cm^3}$, which is much more accurate than the standard value of about $0.3\,\mathrm{GeV/cm^3}$ with an uncertainty of a factor of 2 to 3.

Furthermore, in the results below we always assume that the Wino accounts for the

[10] Additionally, substructures are colder, with much lower velocity dispersions, see e.g. [288]. Note however, that in contrast to the "dark force" Sommerfeld models, in our case this does not introduce any effect: recall that in the two channel version of the SE, below the threshold the effect is independent of the velocity.

whole dark matter. This in most of the choices of m_χ requires it to be of non-thermal origin, except for the masses of around 3.2 TeV, see Sec. 4.4.3. It is worth to emphasize that this is not at all an *ad hoc* scenario, as non-thermal Wino arises naturally in many well motivated theories, see e.g. [254, 255].

5.3.1 Propagation models and uncertainties

We identified 12 benchmark models with varying diffusion zone thickness, from $z_d = 0.5$ kpc to $z_d = 20$ kpc. The lower limiting value comes from the fact, that the galactic disk itself is extending to few hundreds of parsecs. The latter is chosen such, to be sure to enclose all the region with non-vanishing magnetic field, which is known to extend at least to few kpc. We also chose to fix spectral index $\delta = 0.5$ motivated by fit to the CR data and the radial scale of $r_d = 20$ kpc. The precise value of the latter do not introduce relevant effect and again comes from the radial scale of Milky Way. The convection was neglected, essentially because it is never a dominant effect in kpc scales and precisely for this reason it is not yet well understood on a quantitative level.

All the other parameters are fitted to the data. They are given in Table 5.1 together with the reduced χ^2 values of the fits to B/C, protons, antiprotons and electrons. In the latter one we chose to take into account only the data with $E > 5$ GeV, due to the lack of full understanding of the solar modulation and also the precise values of parameters for secondary production mechanisms at such low energies. Moreover, what seem to be more robust choice is to insist on good agreement with the FERMI diffuse gamma ray data and not the low energy electrons, since the backgrounds are much better understood in this case. Therefore, our prediction at energies below 5 GeV do not fit well the electron data, but gives much better agreement with the diffusive gamma rays. The modulation potential was treated as a free parameter of the fit, as advocated before.

All considered propagation models give a very good fit to the CR data and basing only on this it is impossible to single out the best models. This will be achieved later on, after calculating the gamma rays sky-maps. Note also, that our probing of the diffusive zone thickness is dense enough to be able to make an interpolation of the result for any $0.5 \text{ kpc} \leqslant z_d \leqslant 20$ kpc.

As an example of how our models match the observational data, on the Fig. 5.5 we show the fit of the thin $z_d = 1$ kpc, medium $z_d = 4$ kpc and thick $z_d = 10$ kpc cases. In the B/C and protons one can see the strong solar modulation effect at low energies (with doted lines everywhere corresponding to unmodulated result), even for rather moderate values of the potential ϕ.

In the case of electrons, the simple force field approximation is seen to be insufficient in predicting the correct spectra at energies below few GeV. The observed cut-off at large energies is due to already mentioned exponential suppression put in the injection spectrum, with energy $E_c = 5$ TeV. The dashed lines give the total spectrum including the background, dark matter (for a specific case of $m_\chi = 2.5$ TeV) and pulsar components. They are shown in order to convey that they are not very sensitive to variation of the propagation model and that they also improve the agreement with the electron data. For more discussion of these contributions see Sec. 5.3.3.

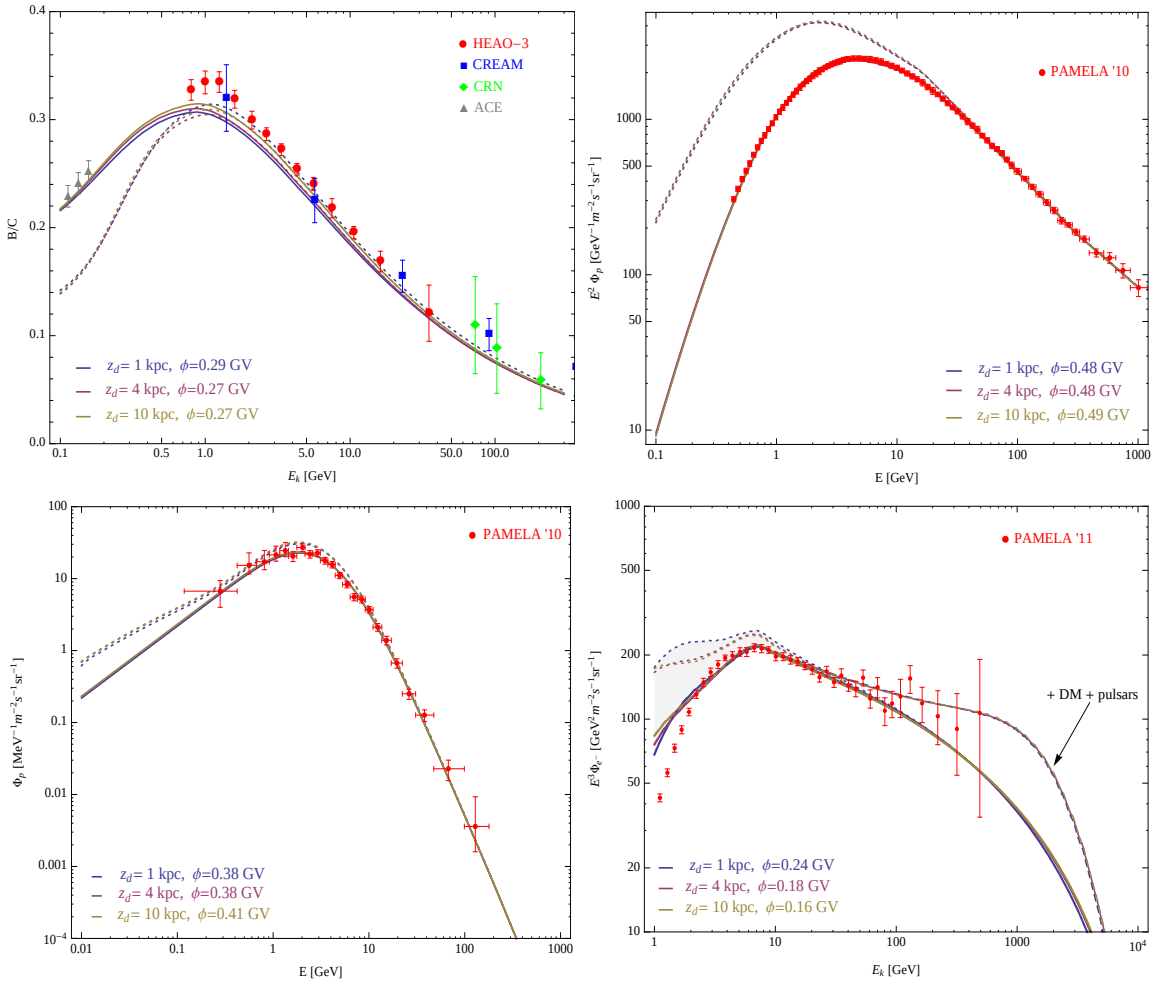

Figure 5.5: Comparison of propagation models. The solar modulated results are given by the solid, while for comparison also unmodulated spectrum is shown with dotted lines. *Top left:* B/C data, *top right*: protons, *bottom left*: antiprotons and *bottom right*: electrons. All the benchmark models give very good fit. In the case of electrons also dark matter for $m_\chi = 2.5$ TeV and pulsar component was included in the dashed lines, where the DM contribution is subdominant.

Benchmark			Fitted			Fitted		Goodness				
z_d [kpc]	δ	r_d [kpc]	$D_0 \times 10^{28}$ [cm^{2}s^{-1}]	v_A [km s^{-1}]	η	γ_1^p/γ_2^p	$R_{0,1}^p$ GV	$\chi^2_{B/C}$	χ^2_p	$\chi^2_{\bar{p}}$	χ^2_e $E_k > 5$ GeV	$\chi^2_{\rm tot}$
0.5	0.5	20	0.191	11.0	-0.60	2.11/2.36/2.18	16.9	0.69	0.67	0.37	0.68	0.65
1	0.5	20	0.53	16.3	-0.521	2.04/2.34/2.18	16.0	0.96	0.46	0.38	0.69	0.58
1.4	0.5	20	0.738	15.5	-0.499	2.11/2.36/2.18	16.1	0.51	0.62	0.36	0.71	0.60
1.7	0.5	20	0.932	16.2	-0.476	2.11/2.35/2.18	14.6	0.47	0.65	0.35	0.72	0.60
2	0.5	20	1.13	16.7	-0.458	2.11/2.35/2.18	14.6	0.48	0.59	0.35	0.72	0.58
3	0.5	20	1.75	18.5	-0.40	2.05/2.35/2.18	16.0	0.34	0.39	0.35	0.75	0.46
4	0.5	20	2.45	19.5	-0.363	2.05/2.35/2.18	16.0	0.79	0.33	0.36	0.75	0.49
6	0.5	20	3.17	19.2	-0.40	2.05/2.35/2.18	16.0	0.38	0.44	0.35	0.77	0.49
8	0.5	20	3.83	19.2	-0.370	2.05/2.35/2.18	15.2	0.39	0.53	0.35	0.77	0.54
10	0.5	20	4.36	19.1	-0.373	2.05/2.35/2.18	15.2	0.38	0.47	0.35	0.77	0.51
15	0.5	20	4.86	17.5	-0.448	2.11/2.36/2.18	14.8	0.46	0.89	0.34	0.77	0.74
20	0.5	20	5.19	17.1	-0.448	2.10/2.36/2.18	14.2	0.45	0.95	0.34	0.77	0.77

Table 5.1: Benchmark propagation models. Everywhere the convection is neglected $v_c = 0$. The second break in the proton injection spectra is always 300 GV. For primary electrons we use a broken power-law with spectral indices 1.6/2.62 and a break at 7 GV. For He and heavier nuclei we assumed one power-law with index 2.3 and 2.25, respectively. The parameters were obtained by fitting to B/C, proton and electron data. The antiproton $\chi^2_{\bar{p}}$ is then a predicted one. The total $\chi^2_{\rm tot}$ has been obtained by combining all the channels. See the text for more details.

Anticipating the discussion of the dark matter originated fluxes, on Fig. 5.6 we show how they are affected by varying the propagation model. The dotted lines correspond to our benchmark models, while solid ones single out the thin, medium and thick cases. As expected, the uncertainty associated with the propagation model is less important when going to higher energies, but even then it remains substantial.

Indeed, in the Wino model the phenomenologically most important effect of this uncertainty is the variation of high energy $\bar{p}$ fluxes originating from the dark matter, as we discuss below.

5.3.2 Antiprotons

In the cosmic rays antiprotons are far less abundant then the protons. They are believed not to be produced in astrophysical sources and hence the observed flux is secondary coming from interactions of protons (and to a certain extent also heavier nuclei) with the interstellar gas composing mostly of hydrogen (atomic and molecular) and helium. These produced antiprotons then propagate and interact with the gas by themselves, sometimes annihilating and sometimes scattering inelastically and loosing energy. The latter process introduces softening of the spectrum and is commonly taken into account by treating all the inelastic collisions as annihilating $\bar{p}$s and replacing them by the so-called *tertiary* source.

Note, that for all these processes, the gas distribution plays an important role. As discussed above, in all our computations we implemented the gas model derived in [284], based on the most precise observational surveys available up to date.

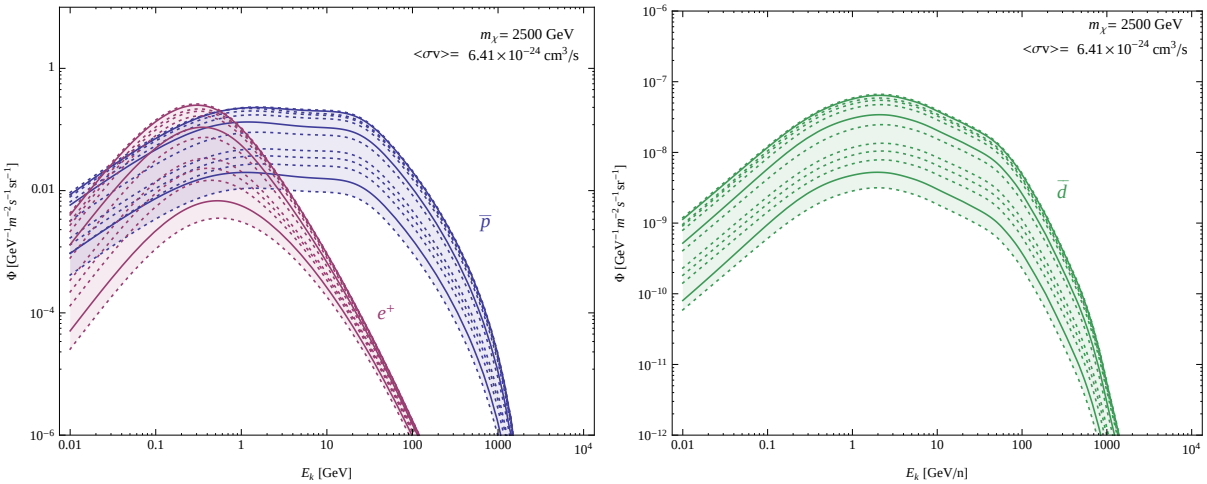

Figure 5.6: Effect of different propagation models onto indirect detection signal from Wino with $m_\chi = 2.5$ TeV. *Left:* antiproton (blue) and positron (violet) fluxes. *Right:* antideuteron flux. The dotted lines correspond to our benchmark models, while solid ones single out the $z_d = 10,\ 4,\ 1$ kpc cases (from top to bottom).

The propagation of antiprotons is governed mostly by diffusion. Energy losses, being proportional to the Loretnz gamma, are very small even for a kinetic energy of few hundreds GeV. On the other hand, diffusive reacceleration processes (and possibly convection) can have a strong impact on the low energy tail of the spectrum. For our purposes, however, only the energies larger than roughly 10 GeV matter, since at the TeV scale the Wino DM contribution affects mostly this part of the spectrum.

Indeed, on Fig. 5.7 we plot the predicted antiproton fluxes at Earth coming from the Wino with masses $m_\chi = 0.5,\ 2.4,\ 2.5,\ 3.2$ TeV. They were chosen in such a way, that the lowest is the generic "lighter" Wino case still in good agreement with the data. For lower masses the annihilation cross-section grows and generically (depending however on the propagation model) overshoots the data. The highest one $m_\chi = 3.2$ TeV gives correct thermal relic density and as can be seen does not produce any noticeable excess over the background. The two middle cases are close to the Sommerfeld resonance, where the total annihilation cross-section grows by several orders of magnitude. This can be seen by comparing the violet and green dashed lines on the plots, giving the dark matter contribution with and without Sommerfeld enhancement, respectively. Needless to say, it introduces a huge change in the predicted signal and therefore cannot be ignored.

The violet shaded region corresponds to the total DM plus background flux for all the range of z_d. It clearly shows the importance of the uncertainty of the propagation model in this search channel. The close to resonance case of $m_\chi = 2.4$ TeV is already excluded (in fact overshooting the data even without background) for thicker diffusion zones, but may be marginally consistent for very thin ones. Moving a bit away from the resonance eases the tension, but still the thickest cases give too much antiprotons.

Although, as we advocated at the beginning, the antiproton channel is expected to give one of the most stringent constraint for models with annihilations predominantly to weak gauge bosons, one can see that the obtained limits are not that severe. Indeed,

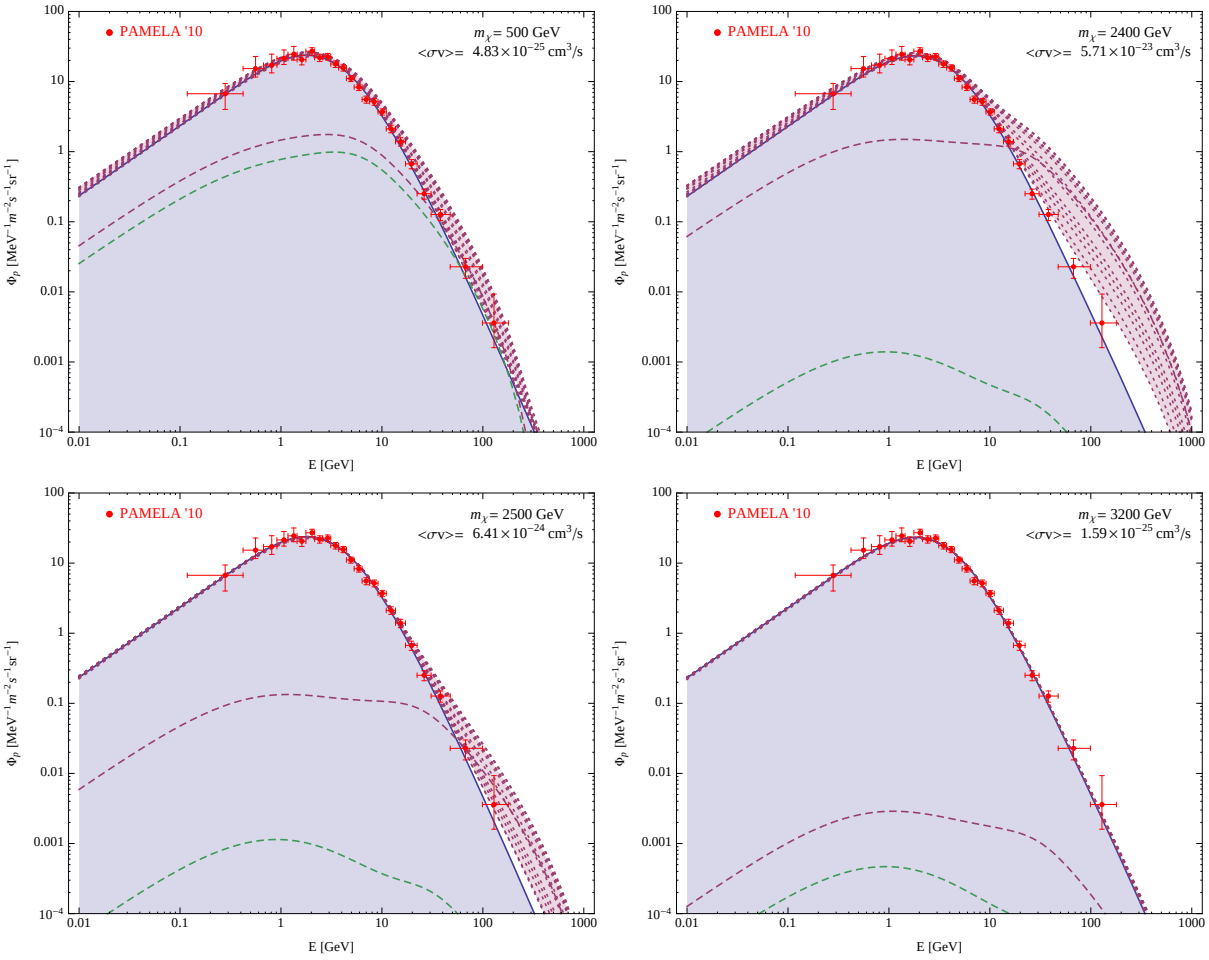

Figure 5.7: Antiproton fluxes for all the propagation models and $m_\chi = 0.5$, 2.4, 2.5, 3.2 TeV. The blue shaded region shows the expected background after solar modulation with $\phi = 0.46$ GV. The dashed lines represent the dark matter contribution without (green) and with Sommerfeld effect (violet) for the example case of $z_d = 4$ kpc model. The total spectrum including background and DM signal is given by the violet shaded regions where the dotted lines correspond to our benchmark models (the $z_d = 0.5$ kpc being the closest to the background and growing with the thickness). The strong boost of the signal for $m_\chi = 2.4$ and 2.5 TeV comes from the resonance in the Sommerfeld effect.

at this stage, when all the benchmark propagation models are allowed, the Wino dark matter can be excluded by the $\bar{p}$ channel only at low masses, i.e. $m_W \lesssim m_\chi \lesssim 300$ GeV[11] and in the very proximity of the resonance, i.e. in the range 2.35 TeV $\lesssim m_\chi \lesssim$ 2.4 TeV. We will come back to this point in the summary in Sec. 5.3.7, after discussing all the remaining channels.

5.3.3 Positrons

In the same way as antiprotons, positrons are typically produced as secondaries. They come mostly from the decay of charged mesons (π^+ and K^+) produced in the interactions of the nuclei with the gas. However, unlike antiprotons they can also be produced and accelerated in astrophysical objects, especially pulsars [290, 291, 292].

Pulsars are fast rotating magnetized neutron stars surrounded by a comoving plasma configuration called magnetosphere (see e.g. [293]). Electrons in the magnetosphere loose energy and emit photons, which are energetic enough to produce electron-positron pairs in the intense pulsar magnetic field. This leads to an potentially effective source of primary electrons and positrons, especially coming from the middle aged pulsars (about 10^5 years old) [294].

The contribution of pulsars can be effectively described by an injection spectrum with E^{-n} together with a high energy break related to the cooling time of the electrons and positrons during their propagation. We chose to fit the impact of the pulsars following the parametrization of [295]:

$$Q_{\rm pul}(r, z, E) = N_0 \left(\frac{E}{E_0}\right)^{-n} e^{-E/E_c} f_{\rm pul}(r, z), \tag{5.36}$$

where we will effectively assume that the $e^\pm$ reaching our location are isotropic and we can omit the spatial dependence. The injection index n, critical energy E_c introducing the cut-off and the normalisation N_0 will be treated as free parameters of the fit, while the normalization of the energy is fixed to $E_0 = 5$ GeV. It is important to bear in mind, that this is only an effective description, aiming in taking into account contribution of many nearby pulsars. However, as we will show below, the component of this kind added on top of the background (and of course dark matter contribution) can give a very good fit to the data.

In the propagation of leptons, the major role is played by the energy losses. Electrons and positrons loose energy by ICS on CMB photons and on infrared or optical galactic starlight. These mechanisms are very effective and growing with the kinetic energy and therefore the very energetic electrons and positrons measured locally by CR detectors have to come to us from nearby. Diffusion is the dominant process only at low energies, since only then leptons have time to diffuse before loosing most of their energy. It follows, that the main uncertainty in the signals coming from positrons is not attributed to the propagation, but rather the precise knowledge about the energy losses, the interstellar radiation field and the exact values of the primary injection spectra.

[11] The lower limit comes from the fact, that at the Wino masses below m_W, the W^+W^- annihilation channel is not allowed and the cross-section is considerably smaller.

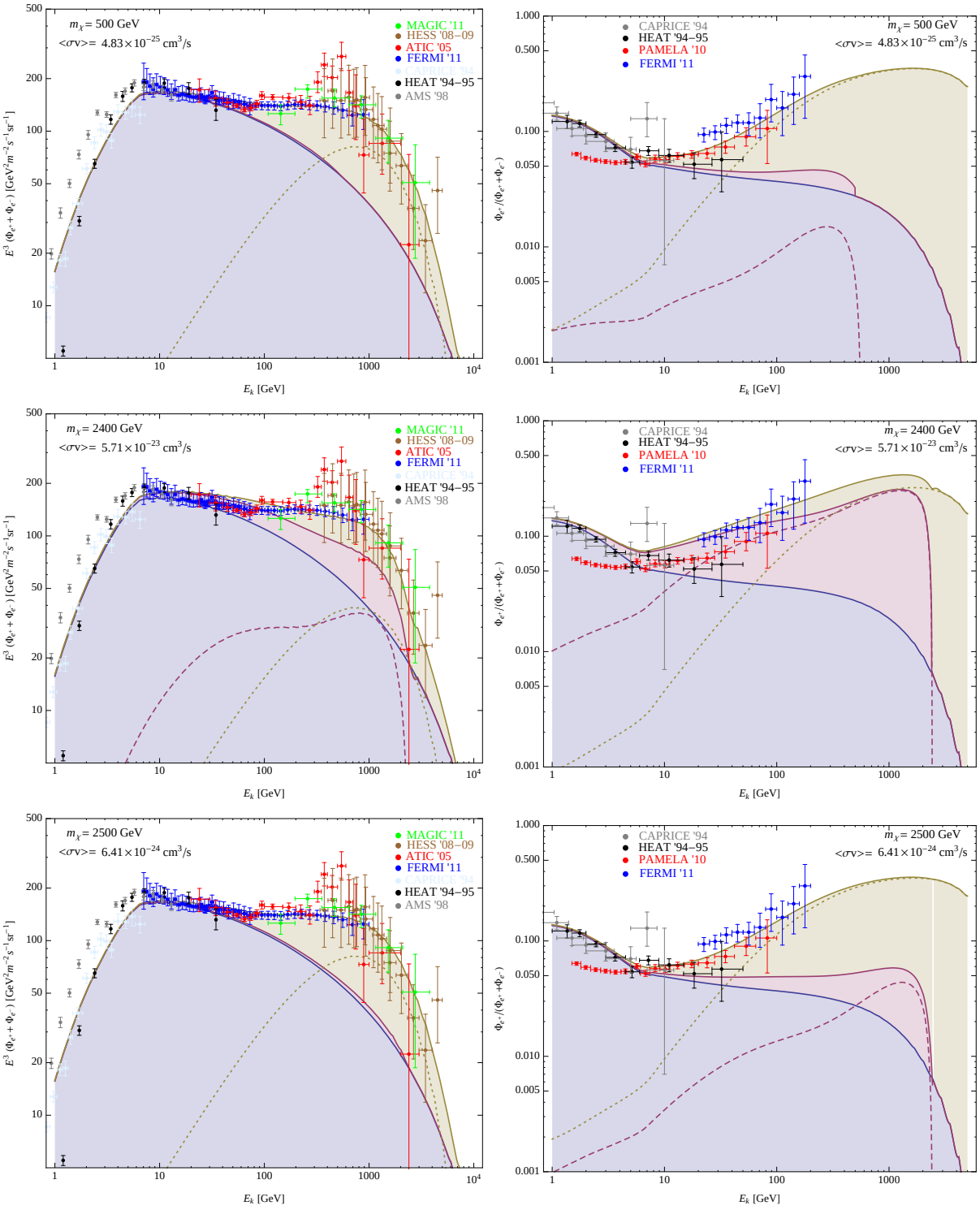

Figure 5.8: Total $e^- + e^+$ fluxes (*left column*) and positron fraction (*right column*) for the $z_d = 4$ kpc propagation model and $m_\chi = 0.5,\ 2.4,\ 2.5$ TeV. The blue shaded region represents the expected background with solar modulation. The DM component (violet dashed line) is typically not strong enough to fit the data and hence additional source of positrons from pulsars (yellow dotted) is needed. The solid yellow line gives total signal including all sources. The cases with larger masses outside of the presented range do not introduce nearly any significant lepton component.

m_χ [GeV]	n	E_c [GeV]	$\chi^2_{e^+ + e^-}$
500	1.4	1200	0.37
2400	1.2	1000	2.11
2500	1.4	1200	0.33

Table 5.2: The pulsar injection parameters used to fit the lepton data for $z_d = 4$ kpc propagation model, with the corresponding value of the reduced χ^2. The resonance case give a worse fit by overshooting the data at energies of few tens of GeV, due to large dark matter contribution.

As already mentioned several times in this thesis, in recent years a lot of effort was triggered by the measurements of the positron fraction rise ranging from about 10 GeV to nearly 200 GeV, where the last FERMI data point was obtained. Simultaneously, various experiments found an unexpectedly hard spectrum of total $e^+ + e^-$ flux. It is worth to note, that this particular way of presenting the experimental results, instead of just using separately electrons and positrons, comes form the difficulties of distinguishing one from another experimentally and also because ratios are subject to somewhat smaller measurement uncertainties.

Here we would like to first address the question, whether the Wino DM model by itself can solve this CR lepton puzzle. The starting observation is that to fit the positron fraction one needs large annihilation cross-section, of the order of $\mathcal{O}(10^{-22}$–10^{-23} cm^3/s). It is rather difficult to achieve for most models, especially if one insists on the thermal production mechanism, pointing to the cross-section of 3×10^{-26} cm^3/s. This is true also for the Wino case. However, the virtue of this particular model is that it posses and efficient mechanism of boosting the present-day cross-section to the needed values, i.e. the Sommerfeld effect coming from weak bosons exchange.[12] Is this sufficient to fit the lepton data?

The answer is negative, for the reason that can be already guessed from the Fig. 5.8. Whenever one is far from resonance, like in the top panel for $m_\chi = 500$ GeV, the dark matter contribution (given by violet dashed line) added to the expected background (blue region) gives total result (violet shaded region) much below the data. One needs a dominant pulsar contribution (the yellow dotted line) to add to the total flux and positron fraction (background+DM+pulsar, yellow region). The injection parameters used for the pulsar fit are given in the Tab. 5.2.

In fact, if one is only moderately off the resonance, like in the bottom panel, the dark matter contribution is too small. Therefore, only the proximity of the resonance could potentially fit the data with dark matter only, but also here one runs into troubles. The middle panel of Fig. 5.8 shows why. The $m_\chi = 2.4$ TeV case, close to the resonance (but not sitting precisely on it), produces typically to few total leptons and, more importantly, to much positrons with energies of around 10 GeV. Even if the former could be adjusted by varying the background, in particular the value of the exponential cut-off in primary electrons, the latter is very hard to evade.

Additionally, the full answer shows the importance of multi-channel studies. The

[12] We would like to stress once again that it is conceptually on a different footing than the Sommerfeld effect due to dark force, since the weak gauge bosons are known to exist!

$m_\chi = 2.4$ TeV (and clearly all the masses even closer to the resonance) was in fact already excluded by antiprotons constraints, unless very low value of z_d is adopted. But a very thin diffusion zone means also less electrons and positrons and higher positron fraction at very low energies, overshooting the data.

Before ending this subsection, let us just make a comment on the disagreement of the low energy positron fraction data with the predictions for the background, sometimes raised as a major issue, but much more often ignored. The reasons for the latter attitude is that, first of all, as already mentioned in Sec. 5.2.1, the systematic errors of the PAMELA experiment are quite likely to be underestimated for the energies of a few GeV, especially given the results of previous measurements. Moreover, the solar modulation is certainly not understood well enough. In particular, the widely adopted force field approximation is *charge independent*, which clearly should not be the case in reality. The more accurate approach distinguishing electrons from positrons may introduce a significant effect for this energy range.[13] And last but not least, the point we are making in our study concerns the high energy behaviour and is completely unaffected by the variation of the background predictions at GeV range.

To summarize, our detailed study show that the Wino model cannot explain the CR lepton puzzle. In fact, the lepton data can even rule out the very proximity of the resonance, independently of other channels, and not relying much on the propagation model. To fit the data one thus needs to have sources of positrons additional than the DM, at least in this model.

Finally, let us comment on the importance of the above results for the gamma-ray studies below. The low energy positron flux is comparable to the electron one and thus introduces a non-negligible contribution of the background positrons to the diffuse gamma ray emission in the MeV range. Moreover, the high energy leptons also may introduce some (smaller) contribution and for a robust prediction one should take them into account. This means that one needs also the dark matter and pulsar components to enter the calculation for the gamma-rays.

5.3.4 Gamma-rays

The search in γ-rays is a topic by its own. Although there is no propagation involved, the much more complex backgrounds are making this channel also rather demanding to study. On the other hand, it can give very good prospects and limits, in many cases even dominant of all the ID searches.

In the gamma-ray searches one can distinguish several approaches, depending on the target:

- diffusive galactic emission,
- extragalactic sources (in particular dwarf spheriodal galaxies),
- extragalactic diffusive emission,
- γ-ray lines.

[13] For more details on charged dependent solar modulation see e.g. [296].

Additionally, one typically looks on different regions of the sky and decides what regions maximize the signal to background ratio, which is by itself a non-trivial task.

In our work we concentrated on the first two approaches. The extragalactic diffuse emission comes dominantly from large scale objects and depends very strongly on the the concentration and scale of the dark matter substructures, whose inclusion is beyond the scope of this work. Additionally, this channel is typically more prospective for lighter DM masses, since the more energetic the photons coming from dark matter annihilation, the more effective is the attenuation process due to $\gamma\gamma \to e^+e^-$, acting effectively like an absorption (for details see e.g. [297] and references therein).

With the gamma line searches the situation is different. In principle, this is a very clean channel, especially if the line is rather strong. In fact, this is what is expected for Sommerfeld enhanced Wino at the TeV scale. However, the most pronounced effect, and indeed the one which would lead to a clear signal, happens on the resonance. But we have already seen that the proximity of the resonance is ruled out by both CR antiprotons and leptons, and shortly below we will see that also by gamma-ray searches. Away from the resonance, the total cross-section is much smaller and the line is not that easily distinguished from the background. Moreover, the energy resolution of a level of tens of per cent may not be enough to single out the line signal at a TeV scale. On Fig. 5.9 we show the total differential cross-section of Wino annihilation into photons for four benchmark masses. The line component was included assuming Gaussian distribution with a rather optimistic 1% energy resolution. Even with this assumption the line is often not distinguishable from the hard component coming from internal Bremsstrahlung. Whether such an effect could be observable in ongoing (MAGIC [298] and VERITAS [299]) or future (especially CTA [300]) experiments is unclear and needs a dedicated study.

Diffuse galactic gamma-rays

The FERMI gamma-ray background is mainly composed of the galactic diffuse background, the isotropic diffuse background (dominated by unresolved extragalactic sources) and the resolved galactic and extragalactic point sources. Also extended sources contribute mainly at lower latitudes. The galactic diffuse background arises from various astrophysical processes. These are, the inelastic pp collisions producing mainly π^0s which subsequently decay to 2 photons, Bremsstrahlung radiation from interactions of CR electrons with the ISM gas and also up-scattering of CMB and starlight photons. From the point of view of the dark matter searches in the diffuse gamma-rays channel, all these processes give rise to a very strong background. The DM contribution comes from two types of processes: direct emission (prompt γ-rays) during annihilation or decay process which includes the hadronization and decay processes that lead to stable SM particles and the secondary contribution coming from ICS and Bremsstrahlung from the produced stable electrons and positrons.

The dark matter prompt gamma-ray flux is given by:

$$\frac{d\Phi_\gamma}{dE} = \frac{1}{4\pi}\int \langle\sigma v\rangle \frac{\rho^2_{DM}(l,\Omega)}{2m^2_\chi}\frac{dN_\gamma}{dE}\, dl d\Omega \,, \tag{5.37}$$

where $d\Omega$ is the solid angle within which the observation is made, and l the length along

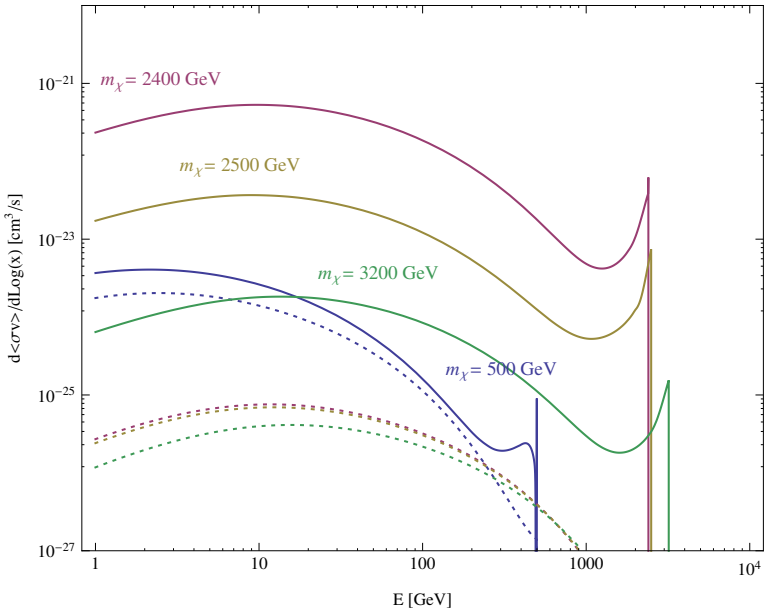

Figure 5.9: Differential cross-section into photons for several Wino masses. The full electroweak and SE corrected result is given by the solid lines, while the tree level with dotted ones. The difference in the total cross-section comes mostly from the Sommerfeld effect.

the line of sight. In the annihilation spectrum at production dN_γ/dE all the processes of prompt production of decay and radiative emission are taken into account. If the annihilation cross-section is homogeneous[14], then it simplifies to

$$\frac{d\Phi_\gamma}{dE} = \frac{1}{4\pi}\langle\sigma v\rangle\frac{1}{2m_\chi^2}\frac{dN_\gamma}{dE}\,J, \tag{5.38}$$

where all the factors depend on the particle physics properties of the dark matter, except the so-called J-factor:

$$J = \int \rho_{DM}^2(l,\Omega)\,dl d\Omega\ , \tag{5.39}$$

depending on the dark matter distribution in the halo. The ICS and Bremsstrahlung contributions form DM are evaluated from our codes in the same manner that the equivalent backgrounds are being calculated.

In order to obtain constraints on the DM component one needs to understand the astrophysical backgrounds first. We follow the approach of [301] and use DRAGON to compute the diffuse gamma-ray spectra coming from the CRs produced and accelerated in the astrophysical objects, for all our reference propagation models. For the low latitudes, the background coming from the sources in the galactic plane has to be modeled. This is done using DRAGON propagation code (see [301] for more details). Next we confront the results with the FERMI data to see how well the computed background fit the obtained

[14] A counterexample would be if $\langle\sigma v\rangle$ does significantly depend on the velocity dispersion and one includes substructures.

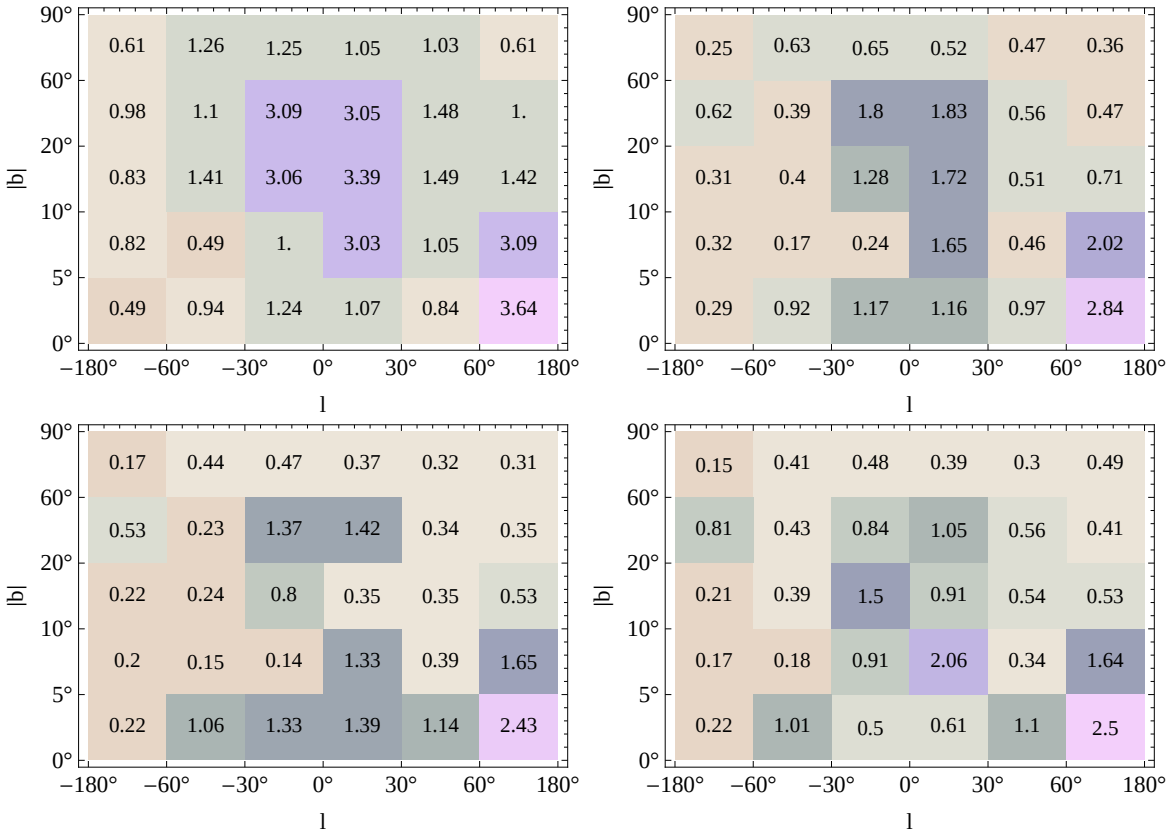

Figure 5.10: The values of reduced χ^2 of the computed gamma sky-maps confronted with the FERMI data for three propagation models $z_d = 1$ kpc *(top left)*, $z_d = 4$ kpc *(top right)* and $z_d = 10$ kpc *(bottom left)*, vs. the latitude b and longitude l. The predicted background fluxes typically underestimate the FERMI data, for thicker models giving however an overall good agreement. Additionally, the *bottom right* panel shows the $z_d = 10$ kpc model with included component of the Wino DM with $m_\chi = 2.5$ TeV.

gamma-ray fluxes in all regions of the sky. The obtained gamma ray sky-maps for three benchmark models $z_d = 1$, 4, 10 kpc are illustrated on Fig. 5.10.

At very high latitudes, an overall good agreement with the data is seen for all the propagation models, since there only very local regions are probed. When decreasing the latitude, one sees that the thicker the propagation model, the better fit. This is a consequence of the fact, that the observed disagreement with the data comes from underestimating the fluxes of diffuse γ-rays. Note that we do not include in our fits the contribution from the Fermi Bubbles/Haze [302, 303, 304]. Their contribution is constrained within about $|l| < 20^\circ$, $|b| < 50^\circ$. We thus allow for the dark matter annihilation in the main halo to contribute to that region of the sky. Similarly being more conservative in constraining the Wino DM annihilation contribution to gamma-rays we do not include the "dark gas" component which is most important at the $|b| < 10^\circ$ [305].

The thicker diffusion zones give higher ICS contribution up to about $|b| > 10^\circ$, because it allows for electrons to actually propagate far from the galactic disk. As a consequence, models with larger z_d are giving better agreement with the data. On the other hand,

towards the inner few degrees in $|b|$ thicker zones give smaller ICS contribution, since the larger diffusion coefficient D_0 (see Tab. 5.1) means that the electrons diffuse faster away from the disk and they contribute less to the gamma-ray flux. This also explains why at low latitudes, $|b| < 5^\circ$, the $z_d = 1$ kpc model gives the best fit. In the intermediate regime, the interplay of these both effects is difficult to resolve, but still on average the thicker zones are with better agreement with the data. In conclusion, the thin propagation models are disfavored, by under-predicting the diffuse flux especially at higher latitudes, while the thicker ones give a good agreement.

On the bottom right plot of Fig. 5.10 we additionally show how the fit changes when adding the dark matter contribution, chosen to be the $m_\chi = 2.5$ TeV case, with the $z_d = 10$ kpc model. Comparing it to the bottom left plot with background only, we observe that in most of the regions adding the DM does not alter the fit much. The biggest change is in lower latitudes, which stems from the fact that the main DM contribution comes from prompt gammas, while the ICS of DM origin is subdominant.[15] On average, including this particular dark matter model, makes the fits slightly worse. This can be however easily compensated by taking slightly thinner diffusion zone.

In order to check more systematically this effect, we concentrate on three windows: $0^\circ < |l| < 30^\circ$ and $5^\circ < |b| < 10^\circ$, $30^\circ < |l| < 60^\circ$ and $10^\circ < |b| < 60^\circ$, $0^\circ < |l| < 180^\circ$ and $60^\circ < |b| < 90^\circ$. They are chosen in such a way to cover low, intermediate and high latitudes. For these windows we compute diffusive gamma-ray fluxes for all the benchmark propagation models, including both the background and the dark matter contributions. The latter does not depend significantly on the propagation model, since as discussed above, the prompt gammas are the dominant ones. The total fluxes for $z_d = 1$ kpc model with highlighted all the contributions are presented on Fig. 5.11. Indeed, we see that predicted photon fluxes for this particular model are typically slightly below the data. For thicker diffusion zones these fluxes are getting larger and we observe a very good agreement with the data for $z_d \gtrsim 2$ kpc. This can be seen from the values of χ^2 for all the benchmark propagation models given in the Table 5.3.

These results have an important implication for the combined limits on the Wino DM model. The most straightforward one is that the Wino of $m_\chi = 2.5$ TeV gives a prediction consistent with all the search channels, if only the diffusion zone is in the range of about $2\,\mathrm{kpc} \lesssim z_d \lesssim 4\,\mathrm{kpc}$, where the upper bound comes from the antiproton constraints. Moreover, the thin propagation models, up to about $z_d = 2\,\mathrm{kpc}$, are disfavored by the FERMI data. It can be seen from both Fig. 5.10 and Tab. 5.3. This conclusion is true irrespectively of the Wino mass. Indeed, the thin propagation models under-predict the diffuse gamma-ray flux rather systematically at all energies (see Fig. 5.11). On the other hand, DM contribution has a spectrum peaked at $E \sim \mathcal{O}(100\ \mathrm{GeV})$. As a consequence, compensating the low energy part of the spectrum by larger DM component would lead to overshooting the data at higher energies.

This general result helps to put more stringent and robust limits on the Wino dark matter model. Recall, that in the resonance case it was marginally consistent with antiproton measurements, if and only if the diffusion zone was very thin. Including the

[15] This is because much less energy from the DM annihilations go to high energy electrons than to photons. The effect is seen mostly in lower latitudes, since there the J-factor is larger.

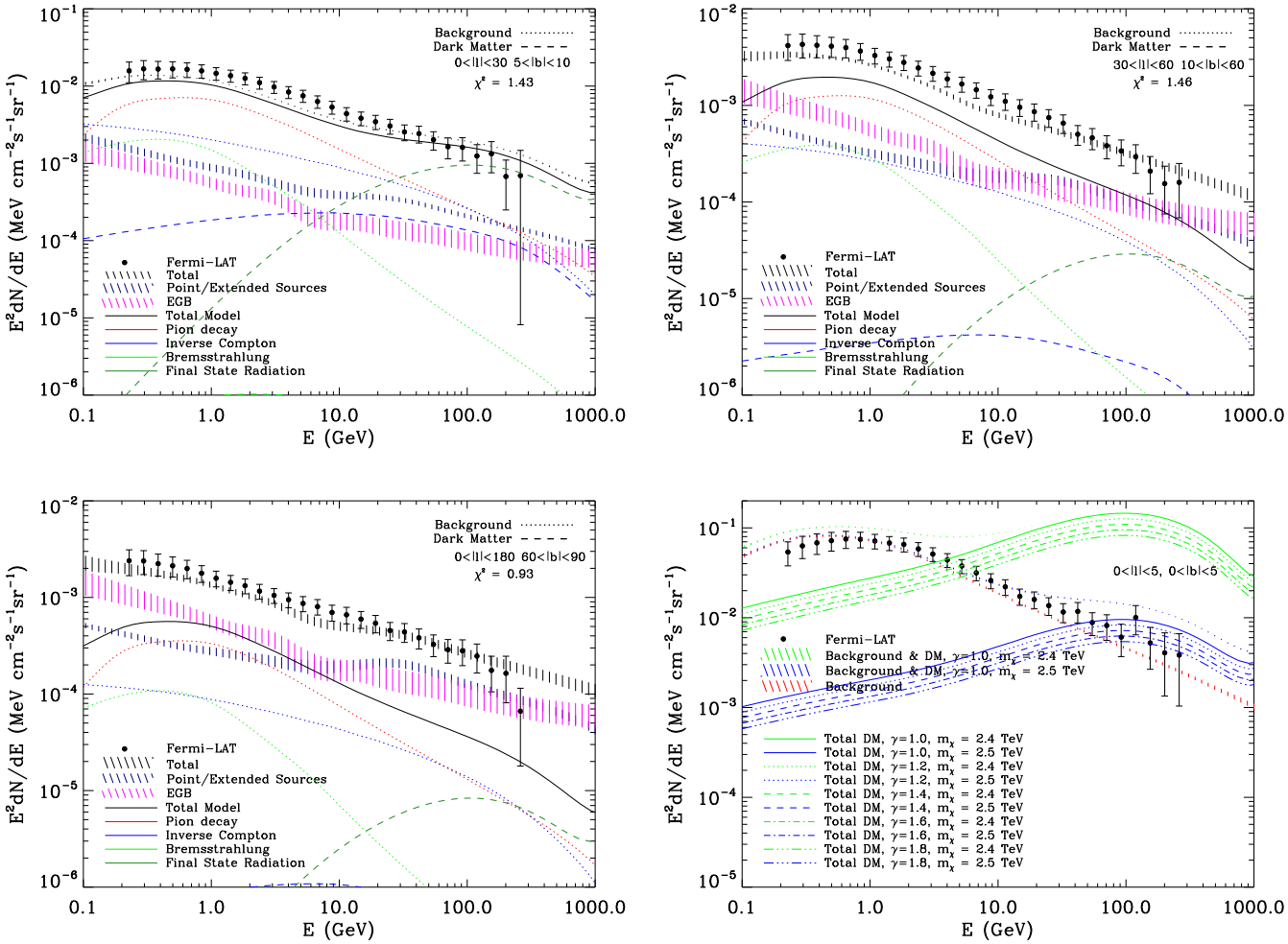

Figure 5.11: The γ-ray fluxes with highlighted all the included contributions, for three chosen windows $0^\circ < |l| < 30^\circ$ and $5^\circ < |b| < 10^\circ$ *(top left)*, $30^\circ < |l| < 60^\circ$ and $10^\circ < |b| < 60^\circ$ *(top right)*, $0^\circ < |l| < 180^\circ$ and $60^\circ < |b| < 90^\circ$ *(bottom left)*. The astrophysical background is typically slightly below the data, an effect which is more pronounced for thin diffusion zones. The Wino DM of $m_\chi = 2.5$ TeV contribution is given by a dashed green (prompt) and blue (ICS) lines. Everything, except the point/extended sources and extragalactic background (EGB), is computed with the DRAGON code. The sum of these contributions gives the solid black line (total model). The full γ-ray flux, dark matter plus all the background, is given by the black dashed region. *Bottom right:* results for the GC for $m_\chi = 2.4$ TeV (blue) and 2.5 TeV (green) with varying γ parameter of the generalized NFW profile.

z_d [kpc]	$0^\circ < \|l\| < 30^\circ$ $5^\circ < \|b\| < 10^\circ$	$30^\circ < \|l\| < 60^\circ$ $10^\circ < \|b\| < 60^\circ$	$0^\circ < \|l\| < 180^\circ$ $60^\circ < \|b\| < 90^\circ$
0.5	3.07	2.46	1.29
1	1.43	1.46	0.93
1.4	1.11	1.09	0.78
1.7	1.04	0.95	0.76
2	1.00	0.86	0.69
3	1.00	0.73	0.63
4	1.04	0.68	0.60
6	1.08	0.64	0.58
8	1.02	0.572	0.55
10	1.05	0.575	0.55
15	1.05	0.555	0.54
20	1.08	0.561	0.53

Table 5.3: The values of the reduced χ^2 for three selected windows. In all propagation models the Wino DM contribution of $m_\chi = 2.5$ TeV was included.

gamma-ray constraints this possibility is completely ruled out. Also the lower bound on the Wino DM mass becomes more stringent, as the thin diffusion models were giving less antiprotons and could ease the tension with observations.

On the bottom right plot of Fig. 5.11 we show also the results for the GC for the two Wino masses $m_\chi = 2.4$ TeV (blue) and 2.5 TeV (green) for several different choices of the DM distribution. We have used the generalized NFW profile and varied the value of γ parameter from 1 to 1.8. The resulting difference in the γ-ray fluxes reaches about 50%. This result suggest that predicted fluxes can be suppressed even more, if a cored profile, e.g. the Burkert one, is used instead. In such a case, the $m_\chi = 2.4$ TeV Wino would be still within the bounds from the GC, but then also the predicted fluxes at higher latitudes would inevitably change, leading possibly to tension with the data. Therefore, in order to make robust claims about the exclusion potential of the GC searches for the Wino model, one would need a dedicated study carefully taking into account different DM profiles [253]. Moreover, since the predicted γ-ray fluxes contain an ICS component of the order $\mathcal{O}(0.1)$, different assumptions on the interstellar radiation fields would lead to small uncertainties in the derived limits for the 2.4 and the 2.5 TeV Winos. However, we note again that the Wino masses for which such an analysis could be potentially useful, i.e. close to the resonance, are already ruled out by other channels.

Signals from dSphs

Dwarf spheroidal galaxies are small dark matter dominated galaxies with typical luminosities $O(10^7)$ $L_\odot$ (see e.g. [306] for a review). They have suppressed star formation rates and low gas densities and due to their smaller sizes the escape timescales of CRs produced in them are also significantly smaller than in the Milky Way. Therefore, the production of gamma-rays from point sources and interactions between CRs and the local medium is expected to be suppressed. Thanks to these properties, the dSphs provide some of the

	Ursa Minor			Sextans		
Mass [GeV]	68% CL	95% CL	99.9% CL	68% CL	95% CL	99.9% CL
500	1.65	2.58	3.76	3.77	5.33	7.38
2400	0.070	0.120	0.185	0.202	0.297	0.419
2500	1.15	1.97	3.02	3.28	4.81	6.78
3200	29.28	50.89	78.45	88.86	131.26	186.2

Table 5.4: The constraints on the boost factors coming from two dSphs: Ursa Minor and Sextans. The results come from confronting the gamma ray flux with the 3 years FERMI data for energies between 1 and 100 GeV. Values of BFs smaller than one suggest the model is excluded.

best targets to look for signals from DM annihilation [307]. Recent results from FERMI collaboration suggest that there is no clear excess of gamma-rays between 200 MeV and 100 GeV above the expected background towards all known dwarf spheroidal galaxies [308, 309]. Therefore, we can ask if from the data we can obtain limits on our DM model.

Here we will closely follow the approach of Ref. [310] and provide a limits coming from the two of the most background+foreground emission clean targets: the *Ursa Minor* and *Sextans*. The reason is that we adopt a conservative approach and for these two dwarf galaxies we have relatively large amount of kinematical data to extract the J-factor, which together with properly accounting for galactic foreground and extragalactic background γ-rays, is the main source of uncertainty in this channel.

The method for obtaining the limits is the same as in [310], from where we adopted also the values for the J-factors, definitions of regions of interest which are used for estimating the signal and the treatment of subtracting the galactic foreground and extragalactic background. Referring for all the details to this paper, here we will just give the results for the Wino model.

After computing the gamma ray flux for a given mass of the Wino, we confront it with the 3 years FERMI data for energies between 1 and 100 GeV. From this we compute what is the additional boost factor (BF) i.e. the multiplication factor on the cross-section for each model, that is allowed by the observed residual γ-ray spectrum at the given confidence levels (CL). Our results are summarized in Tab. 5.4, where three different confidence levels are presented. Again the results show that the close to resonance case, $m_\chi = 2.4$ TeV, is strongly ruled out. When moving a bit further from the resonance the allowed boost factors are getting close to 1, and effectively all other masses are not constrained in any way by this search channel.

Note, that the biggest uncertainty here comes from the evaluation of the J-factor. The FERMI collaboration itself following different assumptions on the uncertainties of the J-factors and the modeling of the background+foreground emission has provided limits on several "standard" channels of annihilation by doing a stacked and a source by source analysis [309]. For such an analysis our limits would be for the individual Ursa Minor dSph a factor of 3 weaker than those of Tab. 5.4. With a joint likelihood analysis though the limits are a factor of 3 stronger, thus confining also the cases of 0.5 and 2.5 TeV mass. Also authors of [311] using a different joint analysis strategy of Milky Way dSphs, have shown the significance in the uncertainties of the J-factors with their weaker limits still

being a factor of 5 stronger that those of Tab. 5.4.

5.3.5 Neutrinos

An alternative probe to search for indirect signals of DM annihilation without the uncertainties related to the propagation model is high energy neutrinos towards the GC. A signal to look for is a hardening or a "bump" in the spectrum of upward moving neutrino events in km^3 telescopes. Only muon (anti)neutrinos are considered here, because they are the ones giving the best signals in the existing types of experiments.[16] The background for such events is dominated by the isotropically distributed (over long observation time periods) atmospheric $\nu_\mu, \bar{\nu}_\mu$ flux. Its spectrum is known to be described by an almost featureless power-law with index of $dN_{\nu_\mu,\bar{\nu}_\mu}/dE \propto E^{-3.7}$.

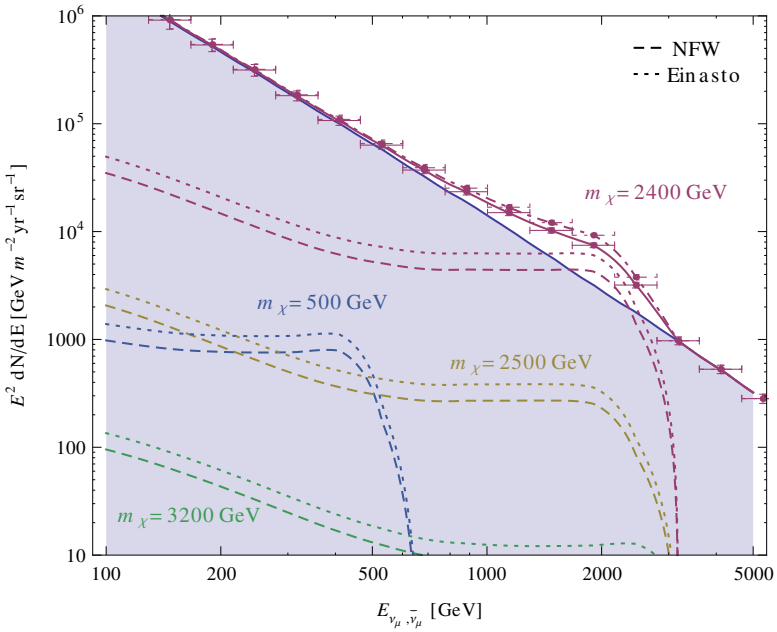

Figure 5.12: The KM3NeT simulated ν_μ upwards going/moving fluxes, from our benchmark Wino models. We consider 3 yrs of data taking and show the fluxes within the window of $|l| < 5°$, $5° < |b| < 15°$. *Continuous power-law line*: atmospheric background. *Dashed lines*: NFW DM profile, *dotted lines*: Einasto DM profile. The violet solid and chained lines show the total signal of background+DM for the resonance case $m_\chi = 2.4$ TeV, for the NFW and Einasto profiles, respectively.

We study only the upwards $\nu_\mu, \bar{\nu}_\mu$ from DM and backgrounds and use for the atmospheric one the parametrization of [312]. Additionally TeV neutrino point sources and

[16] The detection principle in high-energy neutrino telescopes relies on the measurement of the Čerenkov light coming from neutrino produced very energetic charged lepton travelling in a medium, typically water or ice. Electron neutrinos produce electrons, which normally scatter several times in the detector before loosing enough energy to fall below the Čerenkov threshold, making the signal more complicated to resolve. Tau leptons on the other hand are very short-lived and thus decay very fast also not leaving a clear signal.

diffuse neutrino flux from collisions of CR protons with the ISM contribute. These components peak on the disk, therefore to avoid having our results depending on predictions towards the inner few degrees in latitude, we choose to search for a signal in the region of $|l| < 5°$, $5° < |b| < 15°$, following [313].[17]

Situated at the south pole, the IceCube DeepCore experiment does not have the sensitivity towards the GC to look for a signal from DM annihilation. However, a km^3 telescope in the northern hemisphere, as the planned KM3NeT, will be able to probe such signals. Using the HOURS simulation [314], for the reconstruction of upward going $\nu_\mu, \bar{\nu}_\mu$ we show in Fig. 5.12 the expected fluxes from DM annihilation in the selected window. The error-bars refer to 3 years of collecting data. Given the uncertainties on the DM halo distribution we show results for both the NFW and the Einasto profiles.

These results show that among our four reference Wino models only the 2.4 TeV case where the cross-section is close to its resonance can be observed. After 3 years of data taking the calculated number of atmospheric background events[18] is 1025 between 600 GeV and 2.8 TeV, while the ones coming from dark matter are 926 for the Einasto profile and 627 for the NFW profile. This would mean a statistical significance for exclusion at the level of (17-25)σ. Nevertheless, given that all the other indirect detection channels strongly disfavor Wino being close to the Sommerfeld resonance, and that the expected number of neutrino events for the rest of the masses is strongly suppressed, we conclude that the neutrino channel does not give good prospects for testing the Wino DM model.

5.3.6 Antideuterons

Antideutrons have been proposed as a prospective, clean channel for DM searches already many years ago in [272]. In Sec. 5.1.2 we discussed how they can be produced in the dark matter annihilation. Although this mechanism is rather well understood, the precise computations are not that well under control. Indeed, very recently authors of [315] showed, that the result is very sensitive to the fragmentation model used in the Monte Carlo codes for the computation of the fluxes at production. In particular, PYTHIA which uses string fragmentation model gives results generically different by a factor of 2-3 than HERWIG, based on cluster hadronization model. Furthermore, close to the kinematical thresholds this discrepancy grows rapidly. Therefore, one still needs better understanding of the particle physics underlying the antideuteron production to make very robust claims.

Having all that said, it is nevertheless interesting to check what could be the potential signatures of our Wino model in this channel. The results for our four benchmark masses are plotted on Fig. 5.13. First of all note, that the overall values of the flux are very low, and that indeed the dark matter component can be dominant in some cases. This happens especially in low mass and resonance regions, i.e. whenever the annihilation cross-section is large enough. Secondly, the expected antidetueron flux can be of reach of not only the future planned experiment GAPS [316], but possibly also AMS-02 [317], which is already collecting data at the International Space Station. The bound set by BESS [318] and the

[17] For more on searches of DM signals from the GC with km^3 telescopes and the expected distribution of the $\nu_\mu, \bar{\nu}_\mu$ events on the sky see [313].

[18] Typically there is a 20-30 % uncertainty in the normalization of the atmospheric background [312].

Experiment	Energy/nucleon [GeV/n]	Upper bound/sensitivity [$m^{-2}s^{-1}sr^{-1}GeV^{-1}$]
BESS	$0.17 \leqslant E_k/n \leqslant 1.15$	0.95×10^{-4}
AMS-02	$0.2 \leqslant E_k/n \leqslant 0.8$	2.25×10^{-7}
	$2.2 \leqslant E_k/n \leqslant 4.2$	2.25×10^{-7}
GAPS (LDB)	$0.1 \leqslant E_k/n \leqslant 0.2$	1.5×10^{-7}
GAPS (ULDB)	$0.05 \leqslant E_k/n \leqslant 0.25$	3.0×10^{-8}
GAPS (SAT)	$0.1 \leqslant E_k/n \leqslant 0.4$	$\sim 2.6 \times 10^{-9}$

Table 5.5: Limits on antideuteron flux. The BESS limit is an only actual upper bound. The AMS-02 predicted sensitivity is given following [319] and refers to 3 years of data taking. For GAPS the three proposals are the Long Duration Balloon (LDB), the Ultra-Long Duration Balloon (ULDB), and a Satellite (SAT) mission. Limits taken from [275].

predicted sensitivities of AMS-02 and GAPS, plotted as a shaded regions, are summarized in Tab. 5.5. Unfortunately, the most clear signatures are expected in a models with cross-sections too large to be allowed by previous, more robust channels. For the still viable case $m_\chi = 2.5$ TeV the signal to background ratio at low energies is only about 2, which is way too small to be giving a clear signature, given the large uncertainties.

Indeed, in this case uncertainties are very large. Note, that on the plot the scale has ticks every two orders of magnitude, so that the propagation uncertainty introduces more than order of magnitude effect, especially in the experimentally interesting low energy window. Additionally, as we mentioned in the beginning it is hard to quantify our lack of full understanding of the production mechanisms. In fact, we also do not know very well the background, which comes from impinging of the cosmic ray protons and He on the interstellar gas. The reason is that not only there are no measurements of the CR antideuterons, but also the cross-sections of their secondary (and tertiary) production mechanisms are based on fitting to small sample of data and rely on some (reasonable) theoretical assumptions.[19] Nevertheless, at low energies the background is expected to be suppressed much more than in the case of antiprotons, what gives hope for exploiting this channel for dark matter detection.

In conclusion, the antidueteron channel may be very promising in the future, when some progress will be made on both experiential and theoretical sides. Then, it is conceivable that the Wino dark matter can be strongly constrained or maybe detected, by finding some $\bar{d}$s in the cosmic rays.

5.3.7 Summary

In this subsection we summarize all the constraints obtained for the Wino DM model from multi-channel searches. First of all note, that without electroweak corrections and even more importantly the Sommerfeld effect, the obtained results would be very different. The total cross-section would be significantly lower and no resonance would occur, but rather the cross-section would decrease monotonically with the Wino mass. Therefore, only low mass region could give potentially testable signals. In fact, in the range of m_χ

[19] For more details on the uncertainties and cross-sections see [270].

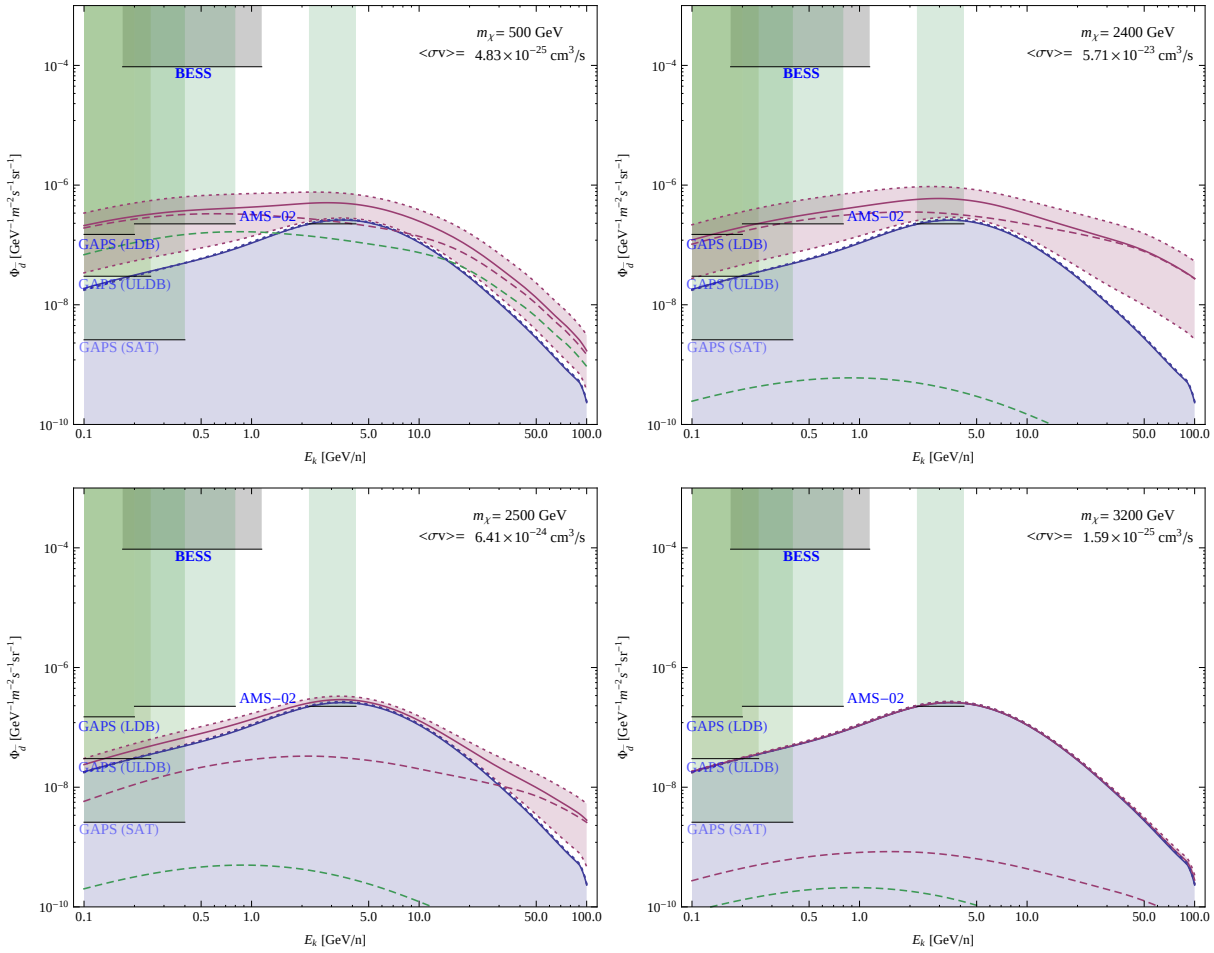

Figure 5.13: Antideutron fluxes for $m_\chi = 0.5, 2.4, 2.5, 3.2$ TeV. The blue shaded region shows the expected background after solar modulation with the modulation potentail assumed to be the same as for the antiprotons. Violet dashed line gives the DM component for $z_d = 4$ kpc model, while the solid line gives the total flux. The shaded violet region spans different propagation models, for the minimal and maximal denoted with dotted lines. For comparison, the dashed green line shows the DM contribution without the Sommerfeld effect. The shaded regions in the upper left give the exclusion by BESS experiment and projected sensitivity of GAPS and AMS-02.

of at most a few hundreds GeV the higher order effects are rather mild. What is more important, is the cross correlation between different channels. Indeed, by examining the antiproton constraints only, one cannot claim very strong exclusion limits: the DM contribution can be significantly suppressed if the diffusion zone is thin enough. Also other channels studied separately, total leptons, positron fraction or γ-rays from various targets do not put strong constraints. However, when one takes into account the correlation of diffuse galactic gamma-rays and antiprotons, then limits become more severe. This is a consequence of the fact that both indirect channels probe a significant part of the Galaxy and that the upper bound on the DM originated antiproton component favors thin diffusion zones, while the diffuse γ-rays favor thick ones. In the end, our analysis gives the combined lower bound on the mass of Wino dark matter annihilating into W^+W^- being $m_\chi \lesssim 450$ GeV.

When the cross-section is corrected by the higher order effects, the phenomenology at the TeV scale changes. The Sommerfeld effect can enlarge the annihilation cross-section by nearly four orders of magnitude in the narrow resonance with a peak at about $m_\chi = 2.35$ TeV. As a consequence, the cross-section in the proximity of the resonance is large enough to give a clear signatures much above the background, for the neutrino searches in KM3NeT and in the antideuteron channel in AMS-02 and GAPS experiments. This region is however strongly excluded by several other indirect channels: antiprotons, positron fraction, galactic gamma-rays and the ones from dSphs. The most stringent bounds come again from combined antiproton and diffuse gamma-ray channels, excluding the proximity of the resonance $2.2\,\text{TeV} \lesssim m_\chi \lesssim 2.5\,\text{TeV}$.

The value giving the correct thermal relic density evades all the indirect detection searches. The prospects for future observations using neutrino telescopes and satellite antideuteron searches are also unfavorable in this case, because the predicted signals lay far below the relevant astrophysical backgrounds.

Chapter 6

Conclusions

The nature of the dark matter is one of the most fascinating and challenging open issues in the modern particle and astroparticle physics. Its existence is considered to be well-established, with many evidences coming from observations on various scales ranging from galaxy and cluster up to cosmological ones. Up to the writing of this work most of its properties remain however unknown, as a consequence of the fact that all we could learn about it comes via gravitational effects.

From a particle physics perspective, a complete and fundamental theory should incorporate a dark matter candidate. Indeed, many promising extensions of the Standard Model do predict existence of stable, massive particles, which seem to have properties needed to accommodate for all the observations. The problem is therefore not only in finding a model that *potentially* can give a viable dark matter candidate, but also to be able to check robustly that it is really the case. In order to do that, one is forced to go beyond tree level computations, from the particle physics side, and carefully take into account various astrophysical effects and uncertainties, from the astroparticle side.

In this thesis, we examined how including electroweak corrections and non-perturbative Sommerfeld effect changes the phenomenology of large class of dark matter candidates, i.e. electroweak interacting WIMPs. In particular, we concentrated on the neutralino DM in the MSSM, being one of the best motivated candidates from the particle physics perspective. In order to study the importance of the electroweak corrections, we computed full $\mathcal{O}(g^6)$ corrections to the present-day annihilation processes for a particular model of a Wino-like neutralino. We chose this model for its interesting properties on one hand, and relative simplicity on the other. The former leads to an important phenomenological implications of EW corrections and the latter allowed to get better insight on the physics behind them. Indeed, we observed rather large electroweak one-loop effects, especially whenever the mass is at the TeV scale, diminishing the total annihilation cross-section by as much as 30%. The detailed computation shows, that using running coupling constant at the scale m_χ without threshold corrections can be a very inaccurate approximation and in fact, we found that at least in case at hand the IR-type logarithms are more important than UV-type ones.

Moreover, we explicitly observed a contribution to the one-loop corrections growing as m_χ/m_W, starting to give non-perturbative correction already at the TeV scale. It arises

due to non-relativistic part of the diagram with gauge boson exchange between incoming Winos and can be re-summed, by solving a set of appropriate Schrödinger equations. This re-summation leads to the Sommerfeld effect, which can strongly alter the cross-section, even by few orders of magnitude. This contribution and the existence of the Sommerfeld enhancement was already known in the literature. However, the existing formalism was not efficient for calculating its effect taking into account all contributing (off-)diagonal interactions. In order to change that, we have developed a general formalism for a multi-state system of fermions, in all possible spin configurations and with generic long-range interactions. This allowed us not only to compute the correct annihilation cross-section of the Wino, but also to study the general impact of the Sommerfeld effect on the neutralino dark matter phenomenology in a such complex scenario as generic MSSM setup.

In order to cover also other phenomenologically interesting regions, where it is the sfermion co-annihilations what drives the neutralino relic density to the observed value, we extended this formalism to the cases containing scalar particles. We derived and presented formulas for a general scenario with a set of particles with arbitrary masses and (off-)diagonal interactions, appropriate in this case. Using this general framework we extensively studied the impact of the electroweak Sommerfeld effect on the relic density of the neutralino for all well motivated cases of the MSSM. Firstly, we have shown how to include such effects in an accurate calculation of the thermal relic density for WIMP dark matter candidates and then applied the method to perform numerical computations.

We found non-negligible corrections in the whole sfermion co-annihilation regimes and a very strong effect for the heavy Wino-like neutralino. In particular, the Wino mass giving the correct thermal relic density was found to be shifted from about 2.3 TeV to roughly 3.2 TeV. Additionally, we explored a thin resonance region and especially its change with respect to the amount of the Higgsino fraction. In deriving these results the precise value of the coupling constant used has an important impact. Thanks to our previous computations of one-loop corrections, we were in position to argue that the value we should use in computing the Sommerfeld effect should be the one at the weak scale. This has an observable impact on the magnitude of the whole effect and the position of the resonance.

In order to perform all the numerical computations, we developed a numerical package for the DarkSUSY code, which we provide as a publicly available tool. It is able to calculate the Sommerfeld enhancement factors for all possible spectra in the MSSM and includes them into the accurate determination of the thermal relic density. In most of the parameter choices the observed corrections are at a % level, or even smaller. However, in broad class of scenarios, especially for relatively heavy neutralino, the Sommerfeld effect introduces a change of a factor of few. We conclude that to obtain accurate results for the relic density, the Sommerfeld effect needs to be included.

Next, we again turn to a specific scenario, where the dark matter is made of Wino-like particles. We study the indirect detection signals including both our full computation of one-loop level radiative electroweak corrections and the Sommerfeld effect. We discuss how to incorporate them simultaneously and present the results for the full present-day annihilation cross-section.

Having well under control the particle physics properties of the model, we concentrate

on what exclusion limits and detection prospects we can obtain for this model taking into account various astrophysical uncertainties. We have found that the most effective in constraining the Wino DM model are the combined data from antiprotons and diffuse γ-rays, allowing to exclude the whole resonance region and put lower limit on the allowed m_χ. In the positron channel we observed that the Wino DM model is not able to solve the CR lepton puzzle. In the low mass scenarios because of the antiproton constraints, while in the resonance case also due to problems in fitting both positron fraction and the total $e^+ + e^-$ data. We also studied indirect detection signals in neutrinos and antideuterons, which were found to be overwhelmed by the backgrounds everywhere, except already excluded resonance case. The Wino with a mass giving thermal relic abundance as observed by WMAP, $m_\chi = 3.2$ TeV, was shown to evade all the indirect detection searches and still remains a very hard to test, but viable possibility.

Bibliography

[1] **ATLAS Collaboration** Collaboration, G. Aad et al., *Observation of a new particle in the search for the Standard Model Higgs boson with the ATLAS detector at the LHC*, arXiv:1207.7214.

[2] **CMS Collaboration** Collaboration, S. Chatrchyan et al., *Observation of a new boson at a mass of 125 GeV with the CMS experiment at the LHC*, *Phys.Lett.B* (2012) [arXiv:1207.7235].

[3] F. Zwicky, *Spectral displacement of extra galactic nebulae*, *Helv.Phys.Acta* **6** (1933) 110–127.

[4] S. Smith, *The mass of the Virgo Cluster*, *Astrophys.J.* **83** (1936), no. 23.

[5] T. Clifton, P. G. Ferreira, A. Padilla, and C. Skordis, *Modified Gravity and Cosmology*, *Phys.Rept.* **513** (2012) 1–189, [arXiv:1106.2476].

[6] "http://hubblesite.org/newscenter/archive/releases/2003/01/image/a/."

[7] D. Clowe, M. Bradac, A. H. Gonzalez, M. Markevitch, S. W. Randall, et al., *A direct empirical proof of the existence of dark matter*, *Astrophys.J.* **648** (2006) L109–L113, [astro-ph/0608407].

[8] C. L. Sarazin, *X-ray emission from clusters of galaxies*, *Rev.Mod.Phys.* **58** (1986) 1–115.

[9] A. Dekel, F. Stoehr, G. Mamon, T. Cox, and J. Primack, *Dark-matter haloes in elliptical galaxies: Lost and found*, *Nature* **437** (2005) 707, [astro-ph/0501622].

[10] M. Mateo, *Dwarf galaxies of the Local Group*, *Ann.Rev.Astron.Astrophys.* **36** (1998) 435–506, [astro-ph/9810070].

[11] V. C. Rubin, W. K. J. Ford, and N. . Thonnard, *Rotational properties of 21 SC galaxies with a large range of luminosities and radii, from NGC 4605 R = 4kpc to UGC 2885 R = 122 kpc*, *APJ* **238** (June, 1980) 471–487.

[12] P. Salucci, *The mass distribution in spiral galaxies*, *IAU Symp.* (2007) [arXiv:0707.4370].

[13] K. Begeman, A. Broeils, and R. Sanders, *Extended rotation curves of spiral galaxies: Dark haloes and modified dynamics*, *Mon.Not.Roy.Astron.Soc.* **249** (1991) 523.

[14] D. Larson, J. Dunkley, G. Hinshaw, E. Komatsu, M. Nolta, et al., *Seven-Year Wilkinson Microwave Anisotropy Probe (WMAP) Observations: Power Spectra and WMAP-Derived Parameters*, *Astrophys.J.Suppl.* **192** (2011) 16, [arXiv:1001.4635].

[15] S. Dodelson, *Modern cosmology*. Academic Press, 1 edition ed., 2003.

[16] N. A. Bahcall, J. P. Ostriker, S. Perlmutter, and P. J. Steinhardt, *The Cosmic triangle: Assessing the state of the universe*, *Science* **284** (1999) 1481–1488, [astro-ph/9906463].

[17] N. Suzuki, D. Rubin, C. Lidman, G. Aldering, R. Amanullah, et al., *The Hubble Space Telescope Cluster Supernova Survey: V. Improving the Dark Energy Constraints Above $z > 1$ and Building an Early-Type-Hosted Supernova Sample*, *Astrophys.J.* **746** (2012) 85, [arXiv:1105.3470].

[18] **WMAP Collaboration** Collaboration, E. Komatsu et al., *Seven-Year Wilkinson Microwave Anisotropy Probe (WMAP) Observations: Cosmological Interpretation*, *Astrophys.J.Suppl.* **192** (2011) 18, [arXiv:1001.4538].

[19] G. Steigman, *Primordial nucleosynthesis: successes and challenges*, *Int.J.Mod.Phys.* **E15** (2006) 1–36, [astro-ph/0511534].

[20] "http://www.sdss.org/."

[21] A. A. Klypin, A. V. Kravtsov, O. Valenzuela, and F. Prada, *Where are the missing Galactic satellites?*, *Astrophys.J.* **522** (1999) 82–92, [astro-ph/9901240].

[22] W. de Blok, *The Core-Cusp Problem*, *Adv.Astron.* **2010** (2010) 789293, [arXiv:0910.3538].

[23] J. M. Overduin and P. Wesson, *Dark matter and background light*, *Phys.Rept.* **402** (2004) 267–406, [astro-ph/0407207].

[24] J. L. Feng, M. Kaplinghat, and H.-B. Yu, *Halo Shape and Relic Density Exclusions of Sommerfeld-Enhanced Dark Matter Explanations of Cosmic Ray Excesses*, *Phys.Rev.Lett.* **104** (2010) 151301, [arXiv:0911.0422].

[25] H.-W. Rix and G. Lake, *Can the dark matter be 10**6 solar mass objects?*, astro-ph/9308022.

[26] S. Tremaine and J. Gunn, *Dynamical Role of Light Neutral Leptons in Cosmology*, *Phys.Rev.Lett.* **42** (1979) 407–410.

[27] J. Bond and A. Szalay, *The Collisionless Damping of Density Fluctuations in an Expanding Universe*, *Astrophys.J.* **274** (1983) 443–468.

[28] K. Sigurdson, M. Doran, A. Kurylov, R. R. Caldwell, and M. Kamionkowski, *Dark-matter electric and magnetic dipole moments*, *Phys.Rev.* **D70** (2004) 083501, [astro-ph/0406355].

[29] P. Sikivie and Q. Yang, *Bose-Einstein Condensation of Dark Matter Axions*, *Phys.Rev.Lett.* **103** (2009) 111301, [arXiv:0901.1106].

[30] **Particle Data Group** Collaboration, K. Nakamura et al., *Review of particle physics*, *J.Phys.G* **G37** (2010) 075021.

[31] I. Antoniadis, *A Possible new dimension at a few TeV*, *Phys.Lett.* **B246** (1990) 377–384.

[32] K. R. Dienes, E. Dudas, and T. Gherghetta, *Extra space-time dimensions and unification*, *Phys.Lett.* **B436** (1998) 55–65, [hep-ph/9803466].

[33] L. Randall and R. Sundrum, *An Alternative to compactification*, *Phys.Rev.Lett.* **83** (1999) 4690–4693, [hep-th/9906064].

[34] G. Servant and T. M. Tait, *Is the lightest Kaluza-Klein particle a viable dark matter candidate?*, *Nucl.Phys.* **B650** (2003) 391–419, [hep-ph/0206071].

[35] M. Kakizaki, S. Matsumoto, Y. Sato, and M. Senami, *Significant effects of second KK particles on LKP dark matter physics*, *Phys.Rev.* **D71** (2005) 123522, [hep-ph/0502059].

[36] D. Hooper and S. Profumo, *Dark matter and collider phenomenology of universal extra dimensions*, *Phys.Rept.* **453** (2007) 29–115, [hep-ph/0701197].

[37] R. Peccei and H. R. Quinn, *CP Conservation in the Presence of Instantons*, *Phys.Rev.Lett.* **38** (1977) 1440–1443.

[38] F. Wilczek, *Problem of Strong p and t Invariance in the Presence of Instantons*, *Phys.Rev.Lett.* **40** (1978) 279–282.

[39] P. Sikivie, *Axions*, in *Particle dark matter* (G. e. Bertone, ed.), pp. 204–227. Cambridge University Press, 2010.

[40] S. R. Coleman, *Q Balls*, *Nucl.Phys.* **B262** (1985) 263.

[41] I. Affleck and M. Dine, *A New Mechanism for Baryogenesis*, *Nucl.Phys.* **B249** (1985) 361.

[42] S. Kasuya and M. Kawasaki, *Q ball formation through Affleck-Dine mechanism*, *Phys.Rev.* **D61** (2000) 041301, [hep-ph/9909509].

[43] A. Kusenko and M. E. Shaposhnikov, *Supersymmetric Q balls as dark matter*, *Phys.Lett.* **B418** (1998) 46–54, [hep-ph/9709492].

[44] O. Seto and M. Yamaguchi, *Axino warm dark matter and Omega(b) - Omega(DM) coincidence*, *Phys.Rev.* **D75** (2007) 123506, [arXiv:0704.0510].

[45] P. Ivanov, P. Naselsky, and I. Novikov, *Inflation and primordial black holes as dark matter*, *Phys.Rev.* **D50** (1994) 7173–7178.

[46] E. Kerins, *MACHOs and the clouds of uncertainty*, astro-ph/0007137.

[47] E. W. Kolb and M. S. Turner, *The Early universe*, *Front.Phys.* **69** (1990) 1–547.

[48] J. Edsjo and P. Gondolo, *Neutralino relic density including coannihilations*, *Phys.Rev.* **D56** (1997) 1879–1894, [hep-ph/9704361].

[49] P. Binetruy, G. Girardi, and P. Salati, *Constraints on a system of two neutral fermions from cosmology*, *Nucl.Phys.* **B237** (1984) 285.

[50] K. Griest and D. Seckel, *Three exceptions in the calculation of relic abundances*, *Phys.Rev.* **D43** (1991) 3191–3203.

[51] P. Gondolo, J. Edsjo, P. Ullio, L. Bergstrom, M. Schelke, et al., *DarkSUSY: Computing supersymmetric dark matter properties numerically*, *JCAP* **0407** (2004) 008, [astro-ph/0406204].

[52] G. Belanger, F. Boudjema, A. Pukhov, and A. Semenov, *MicrOMEGAs 2.0: A Program to calculate the relic density of dark matter in a generic model*, *Comput.Phys.Commun.* **176** (2007) 367–382, [hep-ph/0607059].

[53] N. Arkani-Hamed, A. Delgado, and G. Giudice, *The Well-tempered neutralino*, *Nucl.Phys.* **B741** (2006) 108–130, [hep-ph/0601041].

[54] R. Schnee, *Introduction to dark matter experiments*, arXiv:1101.5205.

[55] **XENON100 Collaboration** Collaboration, E. Aprile et al., *Dark Matter Results from 100 Live Days of XENON100 Data*, *Phys.Rev.Lett.* **107** (2011) 131302, [arXiv:1104.2549].

[56] **CDMS-II Collaboration** Collaboration, Z. Ahmed et al., *Results from a Low-Energy Analysis of the CDMS II Germanium Data*, *Phys.Rev.Lett.* **106** (2011) 131302, [arXiv:1011.2482].

[57] **XENON10 Collaboration** Collaboration, J. Angle et al., *A search for light dark matter in XENON10 data*, *Phys.Rev.Lett.* **107** (2011) 051301, [arXiv:1104.3088].

[58] E. Aprile, "New results from the xenon100 experiment." Talk at the Dark Attack Conference, July, 2012.

[59] **EDELWEISS Collaboration** Collaboration, E. Armengaud et al., *Final results of the EDELWEISS-II WIMP search using a 4-kg array of cryogenic germanium detectors with interleaved electrodes*, *Phys.Lett.* **B702** (2011) 329–335, [arXiv:1103.4070].

[60] D. Y. Akimov, H. Araujo, E. Barnes, V. Belov, A. Bewick, et al., *WIMP-nucleon cross-section results from the second science run of ZEPLIN-III*, *Phys.Lett.* **B709** (2012) 14–20, [arXiv:1110.4769].

[61] E. Behnke, J. Behnke, S. Brice, D. Broemmelsiek, J. Collar, et al., *First Dark Matter Search Results from a 4-kg CF_3I Bubble Chamber Operated in a Deep Underground Site*, arXiv:1204.3094.

[62] M. Felizardo, T. Girard, T. Morlat, A. Fernandes, A. Ramos, et al., *Final Analysis and Results of the Phase II SIMPLE Dark Matter Search*, *Phys.Rev.Lett.* **108** (2012) 201302, [arXiv:1106.3014].

[63] **DAMA Collaboration, LIBRA Collaboration** Collaboration, R. Bernabei et al., *New results from DAMA/LIBRA*, *Eur.Phys.J.* **C67** (2010) 39–49, [arXiv:1002.1028].

[64] **CoGeNT collaboration** Collaboration, C. Aalseth et al., *Results from a Search for Light-Mass Dark Matter with a P-type Point Contact Germanium Detector*, *Phys.Rev.Lett.* **106** (2011) 131301, [arXiv:1002.4703].

[65] C. Aalseth, P. Barbeau, J. Colaresi, J. Collar, J. Diaz Leon, et al., *Search for an Annual Modulation in a P-type Point Contact Germanium Dark Matter Detector*, *Phys.Rev.Lett.* **107** (2011) 141301, [arXiv:1106.0650].

[66] G. Angloher, M. Bauer, I. Bavykina, A. Bento, C. Bucci, et al., *Results from 730 kg days of the CRESST-II Dark Matter Search*, *Eur.Phys.J.* **C72** (2012) 1971, [arXiv:1109.0702].

[67] B. Moore and J. Diemand, *Simulation of cold dark matter haloes*, in *Particle dark matter* (G. e. Bertone, ed.), pp. 14–37. Cambridge University Press, 2010.

[68] J. F. Navarro, C. S. Frenk, and S. D. White, *A Universal density profile from hierarchical clustering*, *Astrophys.J.* **490** (1997) 493–508, [astro-ph/9611107].

[69] U. Haud and J. Einasto, *A Galactic Mass Model With Massive Corona*. Ac. of Sciences of the Estonian SSR, 1986.

[70] A. W. Graham, D. Merritt, B. Moore, J. Diemand, and B. Terzic, *Empirical Models for Dark Matter Halos. II. Inner profile slopes, dynamical profiles, and ρ/σ^3*, *Astron.J.* **132** (2006) 2701–2710, [astro-ph/0608613].

[71] A. Burkert, *The Structure of dark matter halos in dwarf galaxies*, *IAU Symp.* **171** (1996) 175, [astro-ph/9504041].

[72] T. Cheng and L. Li, *Gauge Theory of Elementary Particle Physics*. Oxford University Press, 1985.

[73] M. E. Peskin and D. V. Schroeder, *An Introduction to Quantum Field Theory*. Westview Press, 1995.

[74] S. Weinberg, *The Quantum Theory of Fields. Vol. 1: Foundations*. Cambridge University Press, 2005.

[75] S. Weinberg, *The Quantum Theory of Fields. Vol. 2: Modern Applications*. Cambridge University Press, 2005.

[76] M. Gell-Mann, *A Schematic Model of Baryons and Mesons*, *Phys.Lett.* **8** (1964) 214–215.

[77] D. Gross and F. Wilczek, *Ultraviolet Behavior of Nonabelian Gauge Theories*, *Phys.Rev.Lett.* **30** (1973) 1343–1346.

[78] H. D. Politzer, *Reliable Perturbative Results for Strong Interactions?*, *Phys.Rev.Lett.* **30** (1973) 1346–1349.

[79] S. Weinberg, *A Model of Leptons*, *Phys.Rev.Lett.* **19** (1967) 1264–1266.

[80] A. Salam, *Weak and Electromagnetic Interactions*, *Conf.Proc.* **C680519** (1968) 367–377.

[81] S. Glashow, *Partial Symmetries of Weak Interactions*, *Nucl.Phys.* **22** (1961) 579–588.

[82] P. W. Higgs, *Broken Symmetries and the Masses of Gauge Bosons*, *Phys.Rev.Lett.* **13** (1964) 508–509.

[83] P. W. Higgs, *Broken symmetries, massless particles and gauge fields*, *Phys.Lett.* **12** (1964) 132–133.

[84] F. Englert and R. Brout, *Broken Symmetry and the Mass of Gauge Vector Mesons*, *Phys.Rev.Lett.* **13** (1964) 321–323.

[85] G. Guralnik, C. Hagen, and T. Kibble, *Global Conservation Laws and Massless Particles*, *Phys.Rev.Lett.* **13** (1964) 585–587.

[86] M. S. Carena, P. M. Zerwas, E. Accomando, P. Bagnaia, A. Ballestrero, et al., *Higgs physics at LEP-2*, hep-ph/9602250.

[87] B. Fields and S. Sarkar, *Big-Bang nucleosynthesis (2006 Particle Data Group mini-review)*, astro-ph/0601514.

[88] A. Sakharov, *Violation of CP Invariance, c Asymmetry, and Baryon Asymmetry of the Universe*, *Pisma Zh.Eksp.Teor.Fiz.* **5** (1967) 32–35.

[89] N. Cabibbo, *Unitary Symmetry and Leptonic Decays*, *Phys.Rev.Lett.* **10** (1963) 531–533.

[90] M. Kobayashi and T. Maskawa, *CP Violation in the Renormalizable Theory of Weak Interaction*, *Prog.Theor.Phys.* **49** (1973) 652–657.

[91] C. Jarlskog, *Commutator of the Quark Mass Matrices in the Standard Electroweak Model and a Measure of Maximal CP Violation*, *Phys.Rev.Lett.* **55** (1985) 1039.

[92] K. Jansen, *Status of the finite temperature electroweak phase transition on the lattice*, *Nucl.Phys.Proc.Suppl.* **47** (1996) 196–211, [hep-lat/9509018].

[93] R. N. Mohapatra and G. Senjanovic, *Neutrino Masses and Mixings in Gauge Models with Spontaneous Parity Violation*, *Phys.Rev.* **D23** (1981) 165.

[94] M. Fukugita and T. Yanagida, *Baryogenesis Without Grand Unification*, *Phys.Lett.* **B174** (1986) 45.

[95] S. R. Coleman and J. Mandula, *All Possible Symmetries Of The S Matrix*, *Phys.Rev.* **159** (1967) 1251–1256.

[96] R. Haag, J. T. Lopuszanski, and M. Sohnius, *All Possible Generators of Supersymmetries of the s Matrix*, *Nucl.Phys.* **B88** (1975) 257.

[97] J. Wess and J. Bagger, *Supersymmetry and supergravity*. Princeton University Press, 1992.

[98] W. de Boer, *Grand unified theories and supersymmetry in particle physics and cosmology*, *Prog.Part.Nucl.Phys.* **33** (1994) 201–302, [hep-ph/9402266].

[99] J. Wess and B. Zumino, *Supergauge Transformations in Four-Dimensions*, *Nucl.Phys.* **B70** (1974) 39–50.

[100] R. K. Kaul and P. Majumdar, *Cancellation of Quadratically Divergent Mass Corrections in Globally Supersymmetric Spontaneously Broken Gauge Theories*, *Nucl.Phys.* **B199** (1982) 36.

[101] J. Wess and B. Zumino, *Supergauge Invariant Extension of Quantum Electrodynamics*, *Nucl.Phys.* **B78** (1974) 1.

[102] P. Fayet and J. Iliopoulos, *Spontaneously Broken Supergauge Symmetries and Goldstone Spinors*, *Phys.Lett.* **B51** (1974) 461–464.

[103] N. Sakai and T. Yanagida, *Proton Decay in a Class of Supersymmetric Grand Unified Models*, *Nucl.Phys.* **B197** (1982) 533.

[104] S. Weinberg, *Supersymmetry at Ordinary Energies. 1. Masses and Conservation Laws*, *Phys.Rev.* **D26** (1982) 287.

[105] A. Y. Smirnov and F. Vissani, *Upper bound on all products of R-parity violating couplings lambda-prime and lambda-prime-prime from proton decay*, *Phys.Lett.* **B380** (1996) 317–323, [hep-ph/9601387].

[106] R. Barbier, C. Berat, M. Besancon, M. Chemtob, A. Deandrea, et al., *R-parity violating supersymmetry*, *Phys.Rept.* **420** (2005) 1–202, [hep-ph/0406039].

[107] D. Z. Freedman, P. van Nieuwenhuizen, and S. Ferrara, *Progress Toward a Theory of Supergravity*, *Phys.Rev.* **D13** (1976) 3214–3218.

[108] G. Giudice and R. Rattazzi, *Theories with gauge mediated supersymmetry breaking*, *Phys.Rept.* **322** (1999) 419–499, [hep-ph/9801271].

[109] L. Randall and R. Sundrum, *Out of this world supersymmetry breaking*, *Nucl.Phys.* **B557** (1999) 79–118, [hep-th/9810155].

[110] M. Quiros, *New ideas in symmetry breaking*, hep-ph/0302189.

[111] L. J. Hall, J. D. Lykken, and S. Weinberg, *Supergravity as the Messenger of Supersymmetry Breaking*, *Phys.Rev.* **D27** (1983) 2359–2378.

[112] J. E. Kim and H. P. Nilles, *The mu Problem and the Strong CP Problem*, *Phys.Lett.* **B138** (1984) 150.

[113] F. Gabbiani, E. Gabrielli, A. Masiero, and L. Silvestrini, *A Complete analysis of FCNC and CP constraints in general SUSY extensions of the standard model*, *Nucl.Phys.* **B477** (1996) 321–352, [hep-ph/9604387].

[114] M. Drees, M. M. Nojiri, D. Roy, and Y. Yamada, *Light Higgsino dark matter*, *Phys.Rev.* **D56** (1997) 276–290, [hep-ph/9701219].

[115] H.-C. Cheng, B. A. Dobrescu, and K. T. Matchev, *Generic and chiral extensions of the supersymmetric standard model*, *Nucl.Phys.* **B543** (1999) 47–72, [hep-ph/9811316].

[116] H. P. Nilles, *Dynamically Broken Supergravity and the Hierarchy Problem*, *Phys.Lett.* **B115** (1982) 193.

[117] H. P. Nilles, *Supergravity Generates Hierarchies*, *Nucl.Phys.* **B217** (1983) 366.

[118] A. H. Chamseddine, R. L. Arnowitt, and P. Nath, *Locally Supersymmetric Grand Unification*, *Phys.Rev.Lett.* **49** (1982) 970.

[119] R. Barbieri, S. Ferrara, and C. A. Savoy, *Gauge Models with Spontaneously Broken Local Supersymmetry*, *Phys.Lett.* **B119** (1982) 343.

[120] **Particle Data Group** Collaboration, J. Beringer et al., *Review of particle physics*, *Phys. Rev. D* **86** (Jul, 2012) 010001.

[121] D. Stockinger, *The Muon Magnetic Moment and Supersymmetry*, *J.Phys.G* **G34** (2007) R45–R92, [hep-ph/0609168].

[122] D. Hooper, *TASI 2008 Lectures on Dark Matter*, arXiv:0901.4090.

[123] J. R. Ellis, T. Falk, and K. A. Olive, *Neutralino - Stau coannihilation and the cosmological upper limit on the mass of the lightest supersymmetric particle*, *Phys.Lett.* **B444** (1998) 367–372, [hep-ph/9810360].

[124] P. Nath and R. L. Arnowitt, *Predictions in SU(5) supergravity grand unification with proton stability and relic density constraints*, *Phys.Rev.Lett.* **70** (1993) 3696–3699, [hep-ph/9302318].

[125] M. Drees and M. M. Nojiri, *The Neutralino relic density in minimal $N = 1$ supergravity*, *Phys.Rev.* **D47** (1993) 376–408, [hep-ph/9207234].

[126] K. L. Chan, U. Chattopadhyay, and P. Nath, *Naturalness, weak scale supersymmetry and the prospect for the observation of supersymmetry at the Tevatron and at the CERN LHC*, *Phys.Rev.* **D58** (1998) 096004, [hep-ph/9710473].

[127] J. L. Feng, K. T. Matchev, and T. Moroi, *Focus points and naturalness in supersymmetry*, *Phys.Rev.* **D61** (2000) 075005, [hep-ph/9909334].

[128] C. Boehm, A. Djouadi, and M. Drees, *Light scalar top quarks and supersymmetric dark matter*, *Phys.Rev.* **D62** (2000) 035012, [hep-ph/9911496].

[129] J. R. Ellis, K. A. Olive, and Y. Santoso, *Calculations of neutralino stop coannihilation in the CMSSM*, *Astropart.Phys.* **18** (2003) 395–432, [hep-ph/0112113].

[130] M. A. Ajaib, T. Li, and Q. Shafi, *Stop-Neutralino Coannihilation in the Light of LHC*, *Phys.Rev.* **D85** (2012) 055021, [arXiv:1111.4467].

[131] J. Edsjo, M. Schelke, P. Ullio, and P. Gondolo, *Accurate relic densities with neutralino, chargino and sfermion coannihilations in msugra*, *JCAP* **0304** (2003) 001, [hep-ph/0301106].

[132] N. Arkani-Hamed and S. Dimopoulos, *Supersymmetric unification without low energy supersymmetry and signatures for fine-tuning at the LHC*, *JHEP* **0506** (2005) 073, [hep-th/0405159].

[133] G. Giudice and A. Romanino, *Split supersymmetry*, *Nucl.Phys.* **B699** (2004) 65–89, [hep-ph/0406088].

[134] D. A. Vasquez, G. Belanger, C. Boehm, A. Pukhov, and J. Silk, *Can neutralinos in the MSSM and NMSSM scenarios still be light?*, *Phys.Rev.* **D82** (2010) 115027, [arXiv:1009.4380].

[135] N. Fornengo, S. Scopel, and A. Bottino, *Discussing direct search of dark matter particles in the Minimal Supersymmetric extension of the Standard Model with light neutralinos*, *Phys.Rev.* **D83** (2011) 015001, [arXiv:1011.4743].

[136] G. Belanger, S. Biswas, C. Boehm, and B. Mukopadyaya, *Light neutralino dark matter in the MSSM and its implication for LHC searches for staus*, arXiv:1206.5404.

[137] D. T. Cumberbatch, D. E. Lopez-Fogliani, L. Roszkowski, R. R. de Austri, and Y.-L. S. Tsai, *Is light neutralino as dark matter still viable?*, arXiv:1107.1604.

[138] P. Grothaus, M. Lindner, and Y. Takanishi, *Naturalness of Neutralino Dark Matter*, arXiv:1207.4434.

[139] T. Falk, K. A. Olive, and M. Srednicki, *Heavy sneutrinos as dark matter*, *Phys.Lett.* **B339** (1994) 248–251, [hep-ph/9409270].

[140] C. Arina and N. Fornengo, *Sneutrino cold dark matter, a new analysis: Relic abundance and detection rates*, *JHEP* **0711** (2007) 029, [arXiv:0709.4477].

[141] B. Dumont, G. Belanger, S. Fichet, S. Kraml, and T. Schwetz, *Mixed sneutrino dark matter in light of the 2011 XENON and LHC results*, arXiv:1206.1521.

[142] H.-S. Lee, K. T. Matchev, and S. Nasri, *Revival of the thermal sneutrino dark matter*, *Phys.Rev.* **D76** (2007) 041302, [hep-ph/0702223].

[143] B. de Wit, *Supergravity*, hep-th/0212245.

[144] M. Kawasaki, K. Kohri, T. Moroi, and A. Yotsuyanagi, *Big-Bang Nucleosynthesis and Gravitino*, *Phys.Rev.* **D78** (2008) 065011, [arXiv:0804.3745].

[145] J. Pradler and F. D. Steffen, *Thermal gravitino production and collider tests of leptogenesis*, *Phys.Rev.* **D75** (2007) 023509, [hep-ph/0608344].

[146] S. Weinberg, *Cosmological Constraints on the Scale of Supersymmetry Breaking*, *Phys.Rev.Lett.* **48** (1982) 1303.

[147] M. Fujii and T. Yanagida, *Natural gravitino dark matter and thermal leptogenesis in gauge mediated supersymmetry breaking models*, *Phys.Lett.* **B549** (2002) 273–283, [hep-ph/0208191].

[148] F. D. Steffen, *Supersymmetric dark matter candidates: The Lightest neutralino, the gravitino, and the axino*, arXiv:0711.1240.

[149] H. P. Nilles and S. Raby, *Supersymmetry and the strong CP problem*, *Nucl.Phys.* **B198** (1982) 102–112.

[150] L. Covi and J. E. Kim, *Axinos as Dark Matter Particles*, *New J.Phys.* **11** (2009) 105003, [arXiv:0902.0769].

[151] K.-Y. Choi, L. Covi, J. E. Kim, and L. Roszkowski, *Axino Cold Dark Matter Revisited*, *JHEP* **1204** (2012) 106, [arXiv:1108.2282].

[152] L. Roszkowski and O. Seto, *Axino dark matter from Q-balls in Affleck-Dine baryogenesis and the Omega(b) - Omega(DM) coincidence problem*, *Phys.Rev.Lett.* **98** (2007) 161304, [hep-ph/0608013].

[153] N. F. Bell, J. B. Dent, T. D. Jacques, and T. J. Weiler, *Electroweak Bremsstrahlung in Dark Matter Annihilation*, *Phys.Rev.* **D78** (2008) 083540, [arXiv:0805.3423].

[154] L. Bergstrom, *Radiative Processes in Dark Matter Photino Annihilation*, *Phys. Lett.* **B225** (1989) 372.

[155] L. Bergstrom, T. Bringmann, M. Eriksson, and M. Gustafsson, *Gamma rays from heavy neutralino dark matter*, *Phys.Rev.Lett.* **95** (2005) 241301, [hep-ph/0507229].

[156] A. Birkedal, K. T. Matchev, M. Perelstein, and A. Spray, *Robust gamma ray signature of WIMP dark matter*, hep-ph/0507194.

[157] T. Bringmann, L. Bergstrom, and J. Edsjo, *New gamma-ray contributions to supersymmetric dark matter annihilation*, *JHEP* **0801** (2008) 049, [arXiv:0710.3169].

[158] T. Bringmann, F. Calore, G. Vertongen, and C. Weniger, *On the relevance of sharp gamma-ray features for indirect dark matter searches*, arXiv:1106.1874.

[159] C. Weniger, *A Tentative Gamma-Ray Line from Dark Matter Annihilation at the Fermi Large Area Telescope*, arXiv:1204.2797.

[160] L. Bergstrom, T. Bringmann, and J. Edsjo, *New positron spectral features from supersymmetric dark matter - a way to explain the pamela data?*, *Phys.Rev.D* **78** (2008) 103520, [arXiv:0808.3725].

[161] M. Kachelriess and P. Serpico, *Model-independent dark matter annihilation bound from the diffuse γ ray flux*, *Phys.Rev.* **D76** (2007) 063516, [arXiv:0707.0209].

[162] J. F. Beacom, N. F. Bell, and G. D. Mack, *General Upper Bound on the Dark Matter Total Annihilation Cross Section*, *Phys.Rev.Lett.* **99** (2007) 231301, [astro-ph/0608090]. 4 pages, 3 figures Report-no: KRL-MAP-322.

[163] J. B. Dent, R. J. Scherrer, and T. J. Weiler, *Toward a Minimum Branching Fraction for Dark Matter Annihilation into Electromagnetic Final States*, *Phys.Rev.* **D78** (2008) 063509, [arXiv:0806.0370].

[164] M. Kachelriess, P. Serpico, and M. A. Solberg, *On the role of electroweak bremsstrahlung for indirect dark matter signatures*, *Phys.Rev.* **D80** (2009) 123533, [arXiv:0911.0001].

[165] N. F. Bell, J. B. Dent, A. J. Galea, T. D. Jacques, L. M. Krauss, et al., *W/Z Bremsstrahlung as the Dominant Annihilation Channel for Dark Matter, Revisited*, *Phys.Lett.* **B706** (2011) 6–12, [arXiv:1104.3823].

[166] L. Bergstrom, T. Bringmann, M. Eriksson, and M. Gustafsson, *Two photon annihilation of Kaluza-Klein dark matter*, *JCAP* **0504** (2005) 004, [hep-ph/0412001]. 17 pages, 3 figures: slightly revised version Journal-ref: J. Cosmol. Astropart. Phys., JCAP 04 (2005) 004.

[167] L. Bergstrom, T. Bringmann, M. Eriksson, and M. Gustafsson, *Gamma rays from Kaluza-Klein dark matter*, *Phys.Rev.Lett.* **94** (2005) 131301, [astro-ph/0410359].

[168] M. Gustafsson, E. Lundstrom, L. Bergstrom, and J. Edsjo, *Significant Gamma Lines from Inert Higgs Dark Matter*, *Phys.Rev.Lett.* **99** (2007) 041301, [astro-ph/0703512].

[169] F. Bloch and A. Nordsieck, *Note on the Radiation Field of the electron*, *Phys.Rev.* **52** (1937) 54–59.

[170] T. Kinoshita, *Mass singularities of Feynman amplitudes*, *J.Math.Phys.* **3** (1962) 650–677.

[171] T. Lee and M. Nauenberg, *Degenerate Systems and Mass Singularities*, *Phys.Rev.* **133** (1964) B1549–B1562.

[172] R. Doria, J. Frenkel, and J. Taylor, *Counter Example to Nonabelian Bloch-Nordsieck Theorem*, *Nucl.Phys.* **B168** (1980) 93.

[173] G. T. Bodwin, S. J. Brodsky, and G. P. Lepage, *Initial State Interactions and the Drell-Yan Process*, *Phys.Rev.Lett.* **47** (1981) 1799.

[174] M. Ciafaloni, P. Ciafaloni, and D. Comelli, *Bloch-nordsieck violating electroweak corrections to inclusive tev scale hard processes*, *Phys.Rev.Lett.* **84** (2000) 4810–4813, [hep-ph/0001142].

[175] M. Ciafaloni, P. Ciafaloni, and D. Comelli, *Electroweak bloch-nordsieck violation at the tev scale: "strong" weak interactions ?*, *Nucl.Phys.* **B589** (2000) 359–380, [hep-ph/0004071].

[176] P. Ciafaloni and A. Urbano, *TeV scale Dark Matter and electroweak radiative corrections*, *Phys.Rev.* **D82** (2010) 043512, [arXiv:1001.3950].

[177] C. Barbot and M. Drees, *Production of ultraenergetic cosmic rays through the decay of superheavy X particles*, *Phys.Lett.* **B533** (2002) 107–115, [hep-ph/0202072].

[178] V. Berezinsky, M. Kachelriess, and S. Ostapchenko, *Electroweak jet cascading in the decay of superheavy particles*, *Phys.Rev.Lett.* **89** (2002) 171802, [hep-ph/0205218].

[179] P. Ciafaloni, D. Comelli, A. Riotto, F. Sala, A. Strumia, et al., *Weak Corrections are Relevant for Dark Matter Indirect Detection*, *JCAP* **1103** (2011) 019, [arXiv:1009.0224].

[180] P. Ciafaloni, M. Cirelli, D. Comelli, A. De Simone, A. Riotto, et al., *On the Importance of Electroweak Corrections for Majorana Dark Matter Indirect Detection*, *JCAP* **1106** (2011) 018, [arXiv:1104.2996].

[181] P. Ciafaloni, M. Cirelli, D. Comelli, A. De Simone, A. Riotto, et al., *Initial State Radiation in Majorana Dark Matter Annihilations*, *JCAP* **1110** (2011) 034, [arXiv:1107.4453].

[182] M. Cirelli, G. Corcella, A. Hektor, G. Hütsi, M. Kadastik, P. Panci, M. Raidal, F. Sala, and A. Strumia, *Pppc 4 dm id: A poor particle physicist cookbook for dark matter indirect detection*, *JCAP* **1103** (2011) 051, [arXiv:1012.4515].

[183] "http://www.marcocirelli.net/PPPC4DMID.html."

[184] "http://lapth.in2p3.fr/pg-nomin/boudjema/sloops/sloops.html."

[185] "http://lapth.in2p3.fr/micromegas/."

[186] G. Belanger, F. Boudjema, P. Brun, A. Pukhov, S. Rosier-Lees, et al., *Indirect search for dark matter with micrOMEGAs2.4*, *Comput.Phys.Commun.* **182** (2011) 842–856, [arXiv:1004.1092].

[187] F. Boudjema, A. Semenov, and D. Temes, *Self-annihilation of the neutralino dark matter into two photons or a Z and a photon in the MSSM*, *Phys.Rev.* **D72** (2005) 055024, [hep-ph/0507127].

[188] N. Baro, F. Boudjema, and A. Semenov, *Full one-loop corrections to the relic density in the MSSM: A Few examples*, *Phys.Lett.* **B660** (2008) 550–560, [arXiv:0710.1821].

[189] N. Baro, F. Boudjema, G. Chalons, and S. Hao, *Relic density at one-loop with gauge boson pair production*, *Phys.Rev.* **D81** (2010) 015005, [arXiv:0910.3293].

[190] F. Boudjema, G. Drieu La Rochelle, and S. Kulkarni, *One-loop corrections, uncertainties and approximations in neutralino annihilations: Examples*, *Phys.Rev.* **D84** (2011) 116001, [arXiv:1108.4291].

[191] A. Hryczuk and R. Iengo, *The one-loop and Sommerfeld electroweak corrections to the Wino dark matter annihilation*, *JHEP* **1201** (2012) 163, [arXiv:1111.2916].

[192] M. Cirelli, N. Fornengo, and A. Strumia, *Minimal dark matter*, *Nucl.Phys.* **B753** (2006) 178–194, [hep-ph/0512090].

[193] P. Ciafaloni, D. Comelli, A. D. Simone, A. Riotto, and A. Urbano, *Electroweak bremsstrahlung for wino-like dark matter annihilations*, arXiv:1202.0692.

[194] R. Iengo, "unpublished result."

[195] **Particle Data Group** Collaboration, C. Amsler et al., *Review of Particle Physics*, *Phys.Lett.* **B667** (2008) 1–1340.

[196] L. Bergstrom and P. Ullio, *Full one loop calculation of neutralino annihilation into two photons*, *Nucl.Phys.* **B504** (1997) 27–44, [hep-ph/9706232].

[197] Z. Bern, P. Gondolo, and M. Perelstein, *Neutralino annihilation into two photons*, *Phys.Lett.* **B411** (1997) 86–96, [hep-ph/9706538].

[198] K. Griest and M. Kamionkowski, *Unitarity Limits on the Mass and Radius of Dark Matter Particles*, *Phys.Rev.Lett.* **64** (1990) 615.

[199] M. Drees, *Particle dark matter physics: An Update*, *Pramana* **51** (1998) 87–106, [hep-ph/9804231].

[200] J. Hisano, S. Matsumoto, and M. M. Nojiri, *Unitarity and higher order corrections in neutralino dark matter annihilation into two photons*, *Phys.Rev.* **D67** (2003) 075014, [hep-ph/0212022].

[201] J. Hisano, S. Matsumoto, M. M. Nojiri, and O. Saito, *Non-perturbative effect on dark matter annihilation and gamma ray signature from galactic center*, *Phys.Rev.* **D71** (2005) 063528, [hep-ph/0412403].

[202] J. Hisano, S. Matsumoto, and M. M. Nojiri, *Explosive dark matter annihilation*, *Phys.Rev.Lett.* **92** (2004) 031303, [hep-ph/0307216].

[203] J. Hisano, S. Matsumoto, M. Nagai, O. Saito, and M. Senami, *Non-perturbative effect on thermal relic abundance of dark matter*, *Phys.Lett.* **B646** (2007) 34–38, [hep-ph/0610249].

[204] S. Matsumoto, J. Sato, and Y. Sato, *Enhancement of line gamma ray signature from Bino-like dark matter annihilation due to CP violation*, hep-ph/0505160.

[205] A. Sommerfeld, *Über die Beugung und Bremsung der Elektronen*, *Annalen der Physik* (1931), no. 403 257.

[206] M. Cirelli, A. Strumia, and M. Tamburini, *Cosmology and Astrophysics of Minimal Dark Matter*, *Nucl.Phys.* **B787** (2007) 152–175, [arXiv:0706.4071].

[207] A. Freitas, *Radiative corrections to co-annihilation processes*, *Phys.Lett.* **B652** (2007) 280–284, [arXiv:0705.4027].

[208] C. F. Berger, L. Covi, S. Kraml, and F. Palorini, *The Number density of a charged relic*, *JCAP* **0810** (2008) 005, [arXiv:0807.0211].

[209] **PAMELA Collaboration** Collaboration, O. Adriani et al., *An anomalous positron abundance in cosmic rays with energies 1.5-100 GeV*, *Nature* **458** (2009) 607–609, [arXiv:0810.4995].

[210] **HEAT Collaboration** Collaboration, S. Barwick et al., *Measurements of the cosmic ray positron fraction from 1-GeV to 50-GeV*, *Astrophys.J.* **482** (1997) L191–L194, [astro-ph/9703192].

[211] **AMS-01 Collaboration** Collaboration, M. Aguilar et al., *Cosmic-ray positron fraction measurement from 1 to 30-GeV with AMS-01*, *Phys.Lett.* **B646** (2007) 145–154, [astro-ph/0703154].

[212] J. Chang, J. Adams, H. Ahn, G. Bashindzhagyan, M. Christl, et al., *An excess of cosmic ray electrons at energies of 300-800 GeV*, *Nature* **456** (2008) 362–365.

[213] P. D. Serpico, *Astrophysical models for the origin of the positron 'excess'*, arXiv:1108.4827.

[214] N. Arkani-Hamed, D. P. Finkbeiner, T. R. Slatyer, and N. Weiner, *A theory of dark matter*, *Phys.Rev.D* **79** (2009) 015014, [arXiv:0810.0713].

[215] S. Cassel, *Sommerfeld factor for arbitrary partial wave processes*, *J.Phys.G* **G37** (2010) 105009, [arXiv:0903.5307].

[216] T. R. Slatyer, *The Sommerfeld enhancement for dark matter with an excited state*, *JCAP* **1002** (2010) 028, [arXiv:0910.5713].

[217] S. Hannestad and T. Tram, *Sommerfeld Enhancement of DM Annihilation: Resonance Structure, Freeze-Out and CMB Spectral Bound*, *JCAP* **1101** (2011) 016, [arXiv:1008.1511].

[218] M. Lattanzi and J. I. Silk, *Can the WIMP annihilation boost factor be boosted by the Sommerfeld enhancement?*, *Phys.Rev.* **D79** (2009) 083523, [arXiv:0812.0360].

[219] J. Bovy, *Substructure Boosts to Dark Matter Annihilation from Sommerfeld Enhancement*, *Phys.Rev.* **D79** (2009) 083539, [arXiv:0903.0413].

[220] Q. Yuan, X.-J. Bi, J. Liu, P.-F. Yin, J. Zhang, et al., *Clumpiness enhancement of charged cosmic rays from dark matter annihilation with Sommerfeld effect*, *JCAP* **0912** (2009) 011, [arXiv:0905.2736].

[221] L. Pieri, M. Lattanzi, and J. Silk, *Constraining the Sommerfeld enhancement with Cherenkov telescope observations of dwarf galaxies*, arXiv:0902.4330.

[222] J. B. Dent, S. Dutta, and R. J. Scherrer, *Thermal Relic Abundances of Particles with Velocity-Dependent Interactions*, *Phys.Lett.* **B687** (2010) 275–279, [arXiv:0909.4128].

[223] J. L. Feng, M. Kaplinghat, and H.-B. Yu, *Sommerfeld Enhancements for Thermal Relic Dark Matter*, *Phys.Rev.* **D82** (2010) 083525, [arXiv:1005.4678].

[224] J. Zavala, M. Vogelsberger, and S. D. White, *Relic density and CMB constraints on dark matter annihilation with Sommerfeld enhancement*, *Phys.Rev.* **D81** (2010) 083502, [arXiv:0910.5221].

[225] M. R. Buckley and P. J. Fox, *Dark Matter Self-Interactions and Light Force Carriers*, *Phys.Rev.* **D81** (2010) 083522, [arXiv:0911.3898].

[226] C. Arina, F.-X. Josse-Michaux, and N. Sahu, *Constraining Sommerfeld Enhanced Annihilation Cross-sections of Dark Matter via Direct Searches*, *Phys.Lett.* **B691** (2010) 219–224, [arXiv:1004.0645].

[227] **The CDMS-II Collaboration** Collaboration, Z. Ahmed et al., *Dark Matter Search Results from the CDMS II Experiment*, *Science* **327** (2010) 1619–1621, [arXiv:0912.3592].

[228] K. N. Abazajian and J. Harding, *Constraints on WIMP and Sommerfeld-Enhanced Dark Matter Annihilation from HESS Observations of the Galactic Center*, *JCAP* **1201** (2012) 041, [arXiv:1110.6151].

[229] D. P. Finkbeiner, L. Goodenough, T. R. Slatyer, M. Vogelsberger, and N. Weiner, *Consistent Scenarios for Cosmic-Ray Excesses from Sommerfeld-Enhanced Dark Matter Annihilation*, *JCAP* **1105** (2011) 002, [arXiv:1011.3082].

[230] T. R. Slatyer, N. Toro, and N. Weiner, *The Effect of Local Dark Matter Substructure on Constraints in Sommerfeld-Enhanced Models*, arXiv:1107.3546.

[231] A. Strumia, *Sommerfeld corrections to type-II and III leptogenesis*, *Nucl.Phys.* **B809** (2009) 308–317, [arXiv:0806.1630].

[232] M. Pospelov and A. Ritz, *Astrophysical Signatures of Secluded Dark Matter*, *Phys.Lett.* **B671** (2009) 391–397, [arXiv:0810.1502].

[233] J. D. March-Russell and S. M. West, *WIMPonium and Boost Factors for Indirect Dark Matter Detection*, *Phys.Lett.* **B676** (2009) 133–139, [arXiv:0812.0559].

[234] W. Shepherd, T. M. Tait, and G. Zaharijas, *Bound states of weakly interacting dark matter*, *Phys.Rev.* **D79** (2009) 055022, [arXiv:0901.2125].

[235] R. Iengo, *Sommerfeld enhancement: General results from field theory diagrams*, *JHEP* **0905** (2009) 024, [arXiv:0902.0688].

[236] L. Visinelli and P. Gondolo, *An integral equation for distorted wave amplitudes*, arXiv:1007.2903.

[237] A. Hryczuk, R. Iengo, and P. Ullio, *Relic densities including Sommerfeld enhancements in the MSSM*, *JHEP* **1103** (2011) 069, [arXiv:1010.2172].

[238] M. Drees, J. Kim, and K. Nagao, *Potentially Large One-loop Corrections to WIMP Annihilation*, *Phys.Rev.* **D81** (2010) 105004, [arXiv:0911.3795].

[239] A. Hryczuk, *The Sommerfeld enhancement for scalar particles and application to sfermion co-annihilation regions*, *Phys.Lett.* **B699** (2011) 271–275, [arXiv:1102.4295].

[240] Y. Schroder, *The Static potential in QCD to two loops*, *Phys.Lett.* **B447** (1999) 321–326, [hep-ph/9812205].

[241] N. Arkani-Hamed, S. Dimopoulos, G. Giudice, and A. Romanino, *Aspects of split supersymmetry*, *Nucl.Phys.* **B709** (2005) 3–46, [hep-ph/0409232].

[242] I. Antoniadis and S. Dimopoulos, *Splitting supersymmetry in string theory*, *Nucl.Phys.* **B715** (2005) 120–140, [hep-th/0411032].

[243] B. Kors and P. Nath, *Hierarchically split supersymmetry with Fayet-Iliopoulos D-terms in string theory*, *Nucl.Phys.* **B711** (2005) 112–132, [hep-th/0411201].

[244] S. Mohanty, S. Rao, and D. Roy, *Reconciling heavy wino dark matter model with the relic density and PAMELA data using Sommerfeld effect*, arXiv:1009.5058.

[245] M. Dine, R. G. Leigh, P. Y. Huet, A. D. Linde, and D. A. Linde, *Towards the theory of the electroweak phase transition*, *Phys.Rev.* **D46** (1992) 550–571, [hep-ph/9203203].

[246] D. J. Gross, R. D. Pisarski, and L. G. Yaffe, *QCD and Instantons at Finite Temperature*, *Rev.Mod.Phys.* **53** (1981) 43.

[247] H. A. Weldon, *Effective Fermion Masses of Order gT in High Temperature Gauge Theories with Exact Chiral Invariance*, *Phys.Rev.* **D26** (1982) 2789.

[248] K. Kajantie, M. Laine, J. Peisa, A. Rajantie, K. Rummukainen, et al., *Nonperturbative Debye mass in finite temperature QCD*, *Phys.Rev.Lett.* **79** (1997) 3130–3133, [hep-ph/9708207].

[249] D. Pierce and A. Papadopoulos, *The Complete radiative corrections to the gaugino and Higgsino masses in the minimal supersymmetric model*, *Nucl.Phys.* **B430** (1994) 278–294, [hep-ph/9403240].

[250] T. Bringmann and S. Hofmann, *Thermal decoupling of WIMPs from first principles*, *JCAP* **0407** (2007) 016, [hep-ph/0612238].

[251] T. Bringmann, *Particle Models and the Small-Scale Structure of Dark Matter*, *New J.Phys.* **11** (2009) 105027, [arXiv:0903.0189].

[252] L. G. van den Aarssen, T. Bringmann, and Y. C. Goedecke, *Thermal decoupling and the smallest subhalo mass in dark matter models with Sommerfeld-enhanced annihilation rates*, arXiv:1202.5456.

[253] A. Hryczuk, I. Cholis, R. Iengo, P. Ullio, and M. Tavakoli, *In preparation*, .

[254] T. Moroi and L. Randall, *Wino cold dark matter from anomaly mediated SUSY breaking*, *Nucl.Phys.* **B570** (2000) 455–472, [hep-ph/9906527].

[255] B. S. Acharya, K. Bobkov, G. L. Kane, P. Kumar, and J. Shao, *Explaining the Electroweak Scale and Stabilizing Moduli in M Theory*, *Phys.Rev.* **D76** (2007) 126010, [hep-th/0701034].

[256] **DARWIN Consortium** Collaboration, L. Baudis, *DARWIN: dark matter WIMP search with noble liquids*, arXiv:1201.2402.

[257] U. Chattopadhyay, D. Das, P. Konar, and D. Roy, *Looking for a heavy wino LSP in collider and dark matter experiments*, *Phys.Rev.* **D75** (2007) 073014, [hep-ph/0610077].

[258] P. Ullio, *Indirect detection of neutralino dark matter candidates in anomaly-mediated supersymmetry breaking scenarios*, *JHEP* **0106** (2001) 053, [hep-ph/0105052].

[259] H. Baer, A. Mustafayev, E.-K. Park, and S. Profumo, *Mixed wino dark matter: Consequences for direct, indirect and collider detection*, *JHEP* **0507** (2005) 046, [hep-ph/0505227].

[260] P. Grajek, G. Kane, D. J. Phalen, A. Pierce, and S. Watson, *Neutralino Dark Matter from Indirect Detection Revisited*, arXiv:0807.1508.

[261] J. Hisano, S. Matsumoto, O. Saito, and M. Senami, *Heavy wino-like neutralino dark matter annihilation into antiparticles*, *Phys.Rev.* **D73** (2006) 055004, [hep-ph/0511118].

[262] P. Grajek, G. Kane, D. Phalen, A. Pierce, and S. Watson, *Is the PAMELA Positron Excess Winos?*, *Phys.Rev.* **D79** (2009) 043506, [arXiv:0812.4555].

[263] G. Kane, R. Lu, and S. Watson, *PAMELA Satellite Data as a Signal of Non-Thermal Wino LSP Dark Matter*, *Phys.Lett.* **B681** (2009) 151–160, [arXiv:0906.4765].

[264] V. Gribov and L. Lipatov, *Deep inelastic e p scattering in perturbation theory*, *Sov.J.Nucl.Phys.* **15** (1972) 438–450.

[265] G. Altarelli and G. Parisi, *Asymptotic Freedom in Parton Language*, *Nucl.Phys.* **B126** (1977) 298.

[266] Y. L. Dokshitzer, *Calculation of the Structure Functions for Deep Inelastic Scattering and e+ e- Annihilation by Perturbation Theory in Quantum Chromodynamics.*, *Sov.Phys.JETP* **46** (1977) 641–653.

[267] T. Sjostrand, S. Mrenna, and P. Z. Skands, *PYTHIA 6.4 Physics and Manual*, *JHEP* **0605** (2006) 026, [hep-ph/0603175].

[268] G. Corcella, I. Knowles, G. Marchesini, S. Moretti, K. Odagiri, et al., *HERWIG 6.5 release note*, hep-ph/0210213.

[269] R. Duperray, B. Baret, D. Maurin, G. Boudoul, A. Barrau, et al., *Flux of light antimatter nuclei near Earth, induced by cosmic rays in the Galaxy and in the atmosphere*, *Phys.Rev.* **D71** (2005) 083013, [astro-ph/0503544].

[270] F. Donato, N. Fornengo, and D. Maurin, *Antideuteron fluxes from dark matter annihilation in diffusion models*, arXiv:0803.2640.

[271] C. Evoli, D. Gaggero, D. Grasso, and L. Maccione, *Cosmic-Ray Nuclei, Antiprotons and Gamma-rays in the Galaxy: a New Diffusion Model*, *JCAP* **0810** (2008) 018, [arXiv:0807.4730].

[272] F. Donato, N. Fornengo, and P. Salati, *Anti-deuterons as a signature of supersymmetric dark matter*, *Phys.Rev.* **D62** (2000) 043003, [hep-ph/9904481].

[273] C. B. Braeuninger and M. Cirelli, *Anti-deuterons from heavy dark matter*, arXiv:0904.1165.

[274] M. Kadastik, M. Raidal, and A. Strumia, *Enhanced anti-deuteron dark matter signal and the implications of pamela*, arXiv:0908.1578.

[275] Y. Cui, J. D. Mason, and L. Randall, *General Analysis of Antideuteron Searches for Dark Matter*, *JHEP* **1011** (2010) 017, [arXiv:1006.0983].

[276] A. W. Strong, I. V. Moskalenko, and V. S. Ptuskin, *Cosmic-ray propagation and interactions in the Galaxy*, *Ann.Rev.Nucl.Part.Sci.* **57** (2007) 285–327, [astro-ph/0701517].

[277] V. Ginzburg (ed.), V. Dogiel, V. Berezinsky, S. Bulanov, and V. Ptuskin, *Astrophysics of cosmic rays*. 1990.

[278] J. B. G. M. Bloemen, V. A. Dogiel, V. L. Dorman, and V. S. Ptuskin, *Galactic diffusion and wind models of cosmic-ray transport. I - Insight from CR composition studies and gamma-ray observations*, *Astron. Astrophys.* **267** (Jan., 1993) 372–387.

[279] G. Blumenthal and R. Gould, *Bremsstrahlung, synchrotron radiation, and compton scattering of high-energy electrons traversing dilute gases*, *Rev.Mod.Phys.* **42** (1970) 237–270.

[280] V. L. Ginzburg, Y. M. Khazan, and V. S. Ptuskin, *Origin of cosmic rays: Galactic models with halo*, *Astrophysics and Space Science* **68** (1980), no. 2 295–314.

[281] A. Strong and I. Moskalenko, *Propagation of cosmic-ray nucleons in the galaxy*, *Astrophys.J.* **509** (1998) 212–228, [astro-ph/9807150].

[282] "http://galprop.stanford.edu/webgalprop/galprophome.html."

[283] "http://www.desy.de/~maccione/DRAGON/."

[284] M. Tavakoli, *Three Dimensional Distribution of Atomic Hydrogen in the Milky Way*, arXiv:1207.6150.

[285] P. M. Kalberla, W. Burton, D. Hartmann, E. Arnal, E. Bajaja, et al., *The Leiden/Argentine/Bonn (LAB) survey of Galactic HI: Final data release of the combined LDS and IAR surveys with improved stray-radiation corrections*, *Astron.Astrophys.* **440** (2005) 775–782, [astro-ph/0504140].

[286] L. Gleeson and W. Axford, *Solar Modulation of Galactic Cosmic Rays*, *Astrophys.J.* **154** (1968) 1011.

[287] A. Putze, D. Maurin, and F. Donato, *p, He, and C to Fe cosmic-ray primary fluxes in diffusion models: Source and transport signatures on fluxes and ratios*, *Astron.Astrophys.* **526** (2011) A101, [arXiv:1011.0989].

[288] L. E. Strigari, S. M. Koushiappas, J. S. Bullock, and M. Kaplinghat, *Precise constraints on the dark matter content of Milky Way dwarf galaxies for gamma-ray experiments*, *Phys.Rev.* **D75** (2007) 083526, [astro-ph/0611925].

[289] R. Catena and P. Ullio, *A novel determination of the local dark matter density*, *JCAP* **1008** (2010) 004, [arXiv:0907.0018].

[290] T. Kobayashi, Y. Komori, K. Yoshida, and J. Nishimura, *The most likely sources of high energy cosmic-ray electrons in supernova remnants*, *Astrophys.J.* **601** (2004) 340–351, [astro-ph/0308470].

[291] D. Hooper, P. Blasi, and P. D. Serpico, *Pulsars as the Sources of High Energy Cosmic Ray Positrons*, *JCAP* **0901** (2009) 025, [arXiv:0810.1527].

[292] S. Profumo, *Dissecting cosmic-ray electron-positron data with Occam's Razor: the role of known Pulsars*, *Central Eur.J.Phys.* **10** (2011) 1–31, [arXiv:0812.4457].

[293] M. Longair, *High-energy astrophysics. Vol. 2: Stars, the galaxy and the interstellar medium*, .

[294] **FERMI-LAT Collaboration** Collaboration, D. Grasso et al., *On possible interpretations of the high energy electron-positron spectrum measured by the Fermi Large Area Telescope*, *Astropart.Phys.* **32** (2009) 140–151, [arXiv:0905.0636].

[295] D. Malyshev, I. Cholis, and J. Gelfand, *Pulsars versus Dark Matter Interpretation of ATIC/PAMELA*, *Phys.Rev.* **D80** (2009) 063005, [arXiv:0903.1310].

[296] V. D. Felice, *Low energy electron and positron measure- ments in space with the PAMELA experiment*. PhD thesis, Univ. of Rome "Tor Vergata", 2010.

[297] J. R. Primack, A. Dominguez, R. C. Gilmore, and R. S. Somerville, *Extragalactic Background Light and Gamma-Ray Attenuation*, *AIP Conf.Proc.* **1381** (2011) 72–83, [arXiv:1107.2566].

[298] "http://magic.mppmu.mpg.de/collaboration/index.html."

[299] "http://veritas.sao.arizona.edu/."

[300] "http://www.cta-observatory.org/."

[301] I. Cholis, M. Tavakoli, C. Evoli, L. Maccione, and P. Ullio, *Diffuse Galactic Gamma Rays at intermediate and high latitudes. I. Constraints on the ISM properties*, arXiv:1106.5073.

[302] G. Dobler, D. P. Finkbeiner, I. Cholis, T. R. Slatyer, and N. Weiner, *The Fermi Haze: A Gamma-Ray Counterpart to the Microwave Haze*, *Astrophys.J.* **717** (2010) 825–842, [arXiv:0910.4583].

[303] M. Su, T. R. Slatyer, and D. P. Finkbeiner, *Giant Gamma-ray Bubbles from Fermi-LAT: AGN Activity or Bipolar Galactic Wind?*, *Astrophys.J.* **724** (2010) 1044–1082, [arXiv:1005.5480].

[304] G. Dobler, I. Cholis, and N. Weiner, *The Fermi Gamma-Ray Haze from Dark Matter Annihilations and Anisotropic Diffusion*, *Astrophys.J.* **741** (2011) 25, [arXiv:1102.5095].

[305] M. Tavakoli, I. Cholis, C. Evoli, and P. Ullio Diffuse Galactic Gamma Rays at intermediate and high latitudes. II. Constraints on the DM properties.

[306] M. G. Walker, *Dark Matter in the Milky Way's Dwarf Spheroidal Satellites*, arXiv:1205.0311.

[307] S. Colafrancesco, S. Profumo, and P. Ullio, *Detecting dark matter WIMPs in the Draco dwarf: A multi-wavelength perspective*, *Phys.Rev.* **D75** (2007) 023513, [astro-ph/0607073].

[308] A. Abdo, M. Ackermann, M. Ajello, W. Atwood, L. Baldini, et al., *Observations of Milky Way Dwarf Spheroidal galaxies with the Fermi-LAT detector and constraints on Dark Matter models*, *Astrophys.J.* **712** (2010) 147–158, [arXiv:1001.4531].

[309] **Fermi-LAT collaboration** Collaboration, M. Ackermann et al., *Constraining Dark Matter Models from a Combined Analysis of Milky Way Satellites with the Fermi Large Area Telescope*, *Phys.Rev.Lett.* **107** (2011) 241302, [arXiv:1108.3546].

[310] I. Cholis and P. Salucci, *Extracting limits on dark matter annihilation from dwarf spheroidal galaxies at gamma-rays*, arXiv:1203.2954.

[311] A. Geringer-Sameth and S. M. Koushiappas, *Exclusion of canonical WIMPs by the joint analysis of Milky Way dwarfs with Fermi*, *Phys.Rev.Lett.* **107** (2011) 241303, [arXiv:1108.2914].

[312] M. Honda, T. Kajita, K. Kasahara, S. Midorikawa, and T. Sanuki, *Calculation of atmospheric neutrino flux using the interaction model calibrated with atmospheric muon data* , *Phys.Rev.* **D75** (2007) 043006, [astro-ph/0611418].

[313] I. Cholis, *Searching for the High Energy Neutrino counterpart of the Fermi Bubbles signal or from Dark Matter annihilation*, arXiv:1206.1607.

[314] A. Tsirigotis, A. Leisos, S. Tzamarias, and o. b. o. t. K. Consortium, *Reconstruction efficiency and discovery potential of a Mediterranean neutrino telescope: A simulation study using the Hellenic Open University Simulation; Reconstruction (HOURS) package*, arXiv:1201.5079.

[315] L. Dal and M. Kachelriess, *Antideuterons from dark matter annihilations and hadronization model dependence*, arXiv:1207.4560.

[316] "http://gamma1.astro.ucla.edu/gaps/index.html."

[317] "http://ams.cern.ch/AMS/ams_homepage.html."

[318] H. Fuke, T. Maeno, K. Abe, S. Haino, Y. Makida, et al., *Search for cosmic-ray antideuterons*, *Phys.Rev.Lett.* **95** (2005) 081101, [astro-ph/0504361].

[319] V. Choutko and F. Giovacchini, *Cosmic rays antideuteron sensitivity for ams-02 experiment*, 2007.